

Georgia State University

ScholarWorks @ Georgia State University

Chemistry Dissertations

Department of Chemistry

8-6-2007

Capillary Electrochromatography-Mass Spectrometry (CEC-MS) of Surfactants

Dean Stephen Norton

Follow this and additional works at: https://scholarworks.gsu.edu/chemistry_diss

 Part of the [Chemistry Commons](#)

Recommended Citation

Norton, Dean Stephen, "Capillary Electrochromatography-Mass Spectrometry (CEC-MS) of Surfactants." Dissertation, Georgia State University, 2007.
doi: <https://doi.org/10.57709/1059256>

This Dissertation is brought to you for free and open access by the Department of Chemistry at ScholarWorks @ Georgia State University. It has been accepted for inclusion in Chemistry Dissertations by an authorized administrator of ScholarWorks @ Georgia State University. For more information, please contact scholarworks@gsu.edu.

Capillary Electrochromatography-Mass Spectrometry (CEC-MS) of Surfactants

by

Dean Norton

Under the Direction of Shahab A. Shamsi

ABSTRACT

This research presents advancements in the coupling of capillary electrochromatography (CEC) to mass spectrometry (MS) for the analysis of different chemical classes of surfactants. Chapter 1 provides a brief introduction that summarizes the mechanics and fundamentals of CEC, including instrumentation and applications for CEC-MS. Chapter 2 describes the on-line hyphenation of a packed CEC column with an internally tapered tip coupled to electrospray ionization-mass spectrometry (ESI-MS) and atmospheric pressure chemical ionization-mass spectrometry (APCI-MS) for the analysis of betaine-type amphoteric or zwitterionic surfactants (Zwittergent®). The interesting aspects include CEC-MS column manufacture and characterization, as well as a comparison between the CEC-APCI-MS and CEC-ESI-MS ionization pattern of zwittergents. In Chapter 3, the CEC-MS of alkyltrimethyl-ammonium ions (ATMA⁺) with chain length ranging from C₁-C₁₈ is optimized using an internally tapered CEC-MS column packed with mixed mode C₆/strong cation exchange stationary phase and coupled

to an ESI source. In addition, the optimized CEC-ESI-MS protocol is applied for the challenging analysis of commercial sample Arquad S-50 ATMA⁺ containing *cis-trans* unsaturated and saturated soyabean fatty acid derivatives. In Chapter 4, a novel CEC-UV method for separation of the various Triton X-100 oligomers is presented. A systematic mobile phase tuning and comparison of monomeric vs. polymeric stationary phases was conducted. In Chapter 5, we present the first application of CEC coupled to MS for analysis of Triton X (TX-) series surfactants. A characterization from the viewpoint of the ion and adduct formation for TX-series nonionic surfactants with a variable number of ethoxy units (n=1-16) in the scan mode are first discussed. Next, utilizing the TX-series as model alkylphenolpolyethoxylates (APEOs), a detailed investigation of the chromatographic separation and MS detection are performed followed by analysis of very long chain TX series with n=30-70. In Chapter 6, CEC-MS utilizing full scan positive ion mode of ESI was employed to study the effect of fragmentor voltage on the in-source collision induced dissociation (IS-CID) of several APEO nonionic surfactants. Finally, in Chapter 7, the preparation and characterization of a novel liquid crystalline stationary phase suitable for separation of neutral and charged compounds in packed column CEC is evaluated.

INDEX WORDS: Capillary Electrochromatography-Mass Spectrometry (CEC-MS), Amphoteric, Zwitterionic, Cationic, Nonionic, Surfactants, Internal Taper, Triton X-Series, Lithocholic Acid Stationary Phase.

**CAPILLARY ELECTROCHROMATOGRAPHY-MASS
SPECTROMETRY (CEC-MS) OF SURFACTANTS**

by

DEAN NORTON

A Dissertation

Presented in Partial Fulfillment of Requirements for the Degree of

Doctor of Philosophy

in the College of Arts and Sciences

Georgia State University

2007

**Copyright by
Dean Stephen Norton
2007**

**CAPILLARY ELECTROCHROMATOGRAPHY-MASS
SPECTROMETRY (CEC-MS) OF SURFACTANTS**

by

DEAN NORTON

Major Professor:
Committee:

Shahab A. Shamsi
Gabor Patonay
Stuart Allison

Electronic Version Approved:

Office of Graduate Studies
College of Arts and Sciences
Georgia State University
August 2007

Dedicated to my wife, my parents, and John Gullickson

Acknowledgments

I would like to thank God as he has given me the strength to pursue and fulfill my dreams. With his help, every day has been filled with a sense of purpose.

I would like to gratefully acknowledge the following people who have helped me through this endeavor. First I cannot express my gratitude enough to Dr. Shahab A. Shamsi who has spent so much time to teach me Analytical Chemistry and CE. I will always pursue Chemistry with the same passion he has instilled in his students. I am forever grateful for his guidance through my education. I would also like to thank all the faculty of GSU Chemistry. Dr. Al Baumstark who has always encouraged me and achieved the best of his students, it has been my honor to be part of your department. Dr. Mark Germann who has provided words of wisdom and excellence guidance. There are also many other GSU faculty who have meant much to me; Dr. David Hamilton and Chromotography Class. Dr. Don Harden, Dr. Giovanni Gadda, Dr. Doyle Barrow, Dr. Paul Franklin, Dr. Stuart Allison and Dr. Gabor Patonay and many others thank you. My loving wife Christine Lee has always supported me since the beginning, both in spirit and financially, thank you my love. In addition, I believe John will be proud of me, and Nancy and Jay. Also, my family has supported me for many years. Thanks to my Dad ,Steve, who encouraged me to pursue Chemistry years ago. I hope I have made him proud, and Kerry and Mom too. And Kath, Eric, Steve, Eileen, Jeff, Sharon, Kelly all my family in England. Thanks to all my lab mates, especially Jack Zheng who taught me CEC from his heart, and Asad, Rashid, Will, Jun and Chris. This has been the hardest choice of my life. I am grateful to Michael Bishop who shares my passion of Chromatography. And to Dr. Brian Crow my friend. And finally Joe George, Dr. Andy and Carolyn Bralley, thank you for your patience, you are very kind. Thank you.

Table of Contents

Dedication.....	iv
Acknowledgements.....	v
List of Tables.....	ix
List of Figures.....	xi
 Chapter 1: Introduction	1
Introduction to CEC	2
Basic Operating Principles in CEC. Generation of EOF in a Packed Column.	4
Flat Profile of the EOF in CEC.	6
Influence of the Operating Variables in CEC.	9
Mass Spectrometry. Theory of Electrospray Ionization.	12
Theory of Atmospheric Pressure Chemical Ionization.	15
The Coupling of CEC to Mass Spectrometry.	17
Applications of CEC-MS.	22
Analysis of Surfactants.	27
General Properties of Surfactants.	28
Development of a New CEC Stationary Phase.	32
 Chapter 2: Capillary Electrochromatography-Mass Spectrometry of Zwitterionic Surfactants	40
Introduction	43

Experimental Section	47
Results and Discussion	54
Conclusions	87

Chapter 3: Capillary Electrochromatography-Mass Spectrometry of Cationic

Surfactants	93
Introduction	96
Experimental Section	99
Results and Discussion	104
Conclusions	136

Chapter 4: Capillary Electrochromatography of Triton X-100 | | | |------------------------------|-----| | Introduction | 143 | | Experimental Section | 145 | | Results and Discussion | 147 | | Conclusions | 159 | **Chapter 5: Capillary Electrochromatography-Mass Spectrometry of Nonionic** | | | |------------------------------|-----| | Surfactants | 162 | | Introduction | 165 | | Experimental Section | 169 | | Results and Discussion | 174 |

Conclusions	203
-------------------	-----

**Chapter 6: Capillary Electrochromatography-Mass Spectrometry Characterization
of Nonionic Surfactants Using In-Source Collision Induced Dissociation (IS-CID)**

.....	208
Introduction	211
Experimental Section	215
Results and Discussion	217
Conclusions	251

**Chapter 7: Packed Column Capillary Electrochromatography (CEC) and CEC-MS
Using a Lithocholic Acid Stationary Phase**

.....	257
Introduction	260
Experimental Section	262
Results and Discussion	275
Conclusions	302

List of Tables

Table 1.1: Applications of CEC-MS. From a recent review in 2004. The references are re-stated in this work. IT=ion trap, Q=quadrupole, QqQ=triple quadrupole, TOF=time of flight, FT-ICR=fourier transform ion cyclone resonance.....	23
Table 2.1: Coded values of sheath liquid parameters.	64
Table 2.2: Experimental design for sheath liquid optimization.	65
Table 2.3: CEC-ESI-MS fragmentation pattern for zwittergents at varying fragment voltage.	70
Table 2.4: Coded values of spray chamber parameters.	71
Table 2.5: Structured experimental design for spray chamber optimization.	72
Table 3.1: Linearity, LOD and LOQ of C ₁₂ -C ₁₈ -TMA ⁺ surfactants.	125
Table 3.2: Intraday and interday precision of the migration time, peak area, normalized peak area (NPA), efficiency (N) and resolution (Rs).	127
Table 3.3: Composition of S-50 sample, experimental vs. manufacturer value.	130
Table 3.4: Comparison of the peak area percent for C ₁₈ cis/trans isomers in Arquad S-50 versus S-50 spiked with cis-C ₁₈ -TMA ⁺	134
Table 4.1: Commercial stationary phases utilized in the study.	148
Table 5.1: Triton X Surfactants used in the work.	170
Table 5.2: TX-15-165 SIM mode ions used for optimization of the CEC and MS detection.	172
Table 5.3: Reproducibility, linearity and sensitivity of TX-45.	202
Table 6.1: Triton X-Series surfactants used in this work.....	214
Table 6.2: Full Scan mass/charge (m/z) values for the protonated molecular ions, adducts and fragment ions used in the breakdown graphs of TX-15, TX-45, TX-100 and TX-165 nonionic surfactants.	218
Table 7.1: List of PCBs used and their log <i>P</i>	266

Table 7.2: Elemental analysis of the aminopropyl silica intermediate and the LCA bonded phase.	276
Table 7.3: Elution order, mass (m), charge (z), z/m ratio and $\log P$ of the 7 β -blockers.	281
Table 7.4: Elution order, mass (m), charge (z), z/m ratio and $\log P$ of the PEAs.	288
Table 7.5: Elution order and $\log P$ of the PAH test mixtures run on the LCA bonded phase.	294

List of Figures

Figure 1.1: (A) Silanol groups comprising the inner wall of a fused silica capillary. (B) Distribution of ions and formation of the electrical double layer adjacent to the silanol groups. The zeta potential shows the point at which the voltage begins to drop between the charged surface and the counter ions located in the stern layer.	4
Figure 1.2: Flow profile in HPLC (laminar flow) vs. CEC (EOF).	7
Figure 1.3: A schematic of an ESI source.	14
Figure 1.4: A schematic of the components of an APCI source.	16
Figure 1.5: A detailed view of the mechanism of APCI	17
Figure 1.6: Instrumentation for (A) CEC-UV utilizing pressure applied at both the inlet and outlet of the capillary column and (B) CEC-MS that applies pressure only at the inlet side.	18
Figure 1.7: Illustration of the (a) externally tapered and the (B) internally tapered CEC column.	20
Figure 1.8: Chemical structures of the alkyl betaines which are most common types of amphoteric or zwitterionic surfactants.	29
Figure 1.9: Different types of cationic surfactants.	30
Figure 1.10: Different types of nonionic surfactants including (A) alcohol and alkylphenol ethoxylates, (B) fatty acid diethanolamides, and (C) alkylpolyglucosides.	31
Figure 2.1: Chemical structure of the Zwittergent standards and the <i>Rewoteric AM-CAS</i> commercial sample.	44
Figure 2.2: Microscopic images (a-d) of internal taper for CEC-MS. Capillary: 360 μm o.d., 78 μm i.d. stationary phase: CEC-C18-3 μm -100 \AA . a) Calibration slide, manufacturer spec = 150 μm . b) Magnification at 100X showing the CEC-MS column packed with stationary phase and flushed with solvent. c) Same as b) except inverted color. d) Same as b) except 400X magnification. Diameters of internal tapered tips shown were measured using Motic Images Software (v.2.0).	50
Figure 2.3: Electrochromatograms (a-d) and bar plots (e-g) showing effects of %ACN (v/v) on separation of zwittergents Z8-Z16, (e) R_s , (f) N and (g) α . The error bar in each plot represents one standard deviation (SD) of 3 measurements. Conditions: Column 1:	

64 cm long, 22 cm packed bed length, 75 μm (I.D.) capillary tapered internally (ca. 8-10 μm) packed with 3 μm CEC C_{18} stationary phase; mobile phase, (a) 90% (v/v) ACN, (b) 80% (v/v) ACN, (c) 75% (v/v) ACN, (d) 70% (v/v) ACN, 5 mM Tris, pH 8.0. Sheath liquid, 1 mM HCO_2NH_4 in MeOH- H_2O (80:20, v/v), 7.5 $\mu\text{L}/\text{min}$. Spray chamber, dry gas flow 4 L/min, nebulizer pressure 5 psi, dry gas temp. 100 $^\circ\text{C}$, V_{cap} 4000 V, fragmentor 125 V. Electrokinetic injection: 6kv, 6 sec., 18 kV run voltage, ESI SIM positive ions (5 ions) monitored at m/z 280, 308, 336, 364, 392.57

Figure 2.4: Electrochromatograms (a-d) and bar plots (e-g) showing effects of mobile phase BGE content of Tris buffer on the separation of zwittergents Z8-Z16, (e) R_s , (f) N and (g) α . Conditions: mobile phase; 75% (v/v) ACN, pH = 8.0 containing (a) 2.5 mM Tris, (b) 5.0 mM Tris, (c) 7.5 mM Tris, and (d) 10.0 mM Tris. All other conditions same as Figure 2.3.60

Figure 2.5: Electrochromatograms (a-c) and bar plots (d-f) showing effects of mobile phase pH on separation of zwittergents Z8-Z16, (d) R_s , (e) N and (f) α . Conditions: mobile phase; 75% (v/v) ACN containing 5 mM Tris and pH (a) 9.0, (b) 8.0, (c) 7.0. All other conditions same as Figure 2.4.62

Figure 2.6: Effect of varying ESI fragmentor voltage in the range of 75-225 V. Electrochromatograms (a) and CEC-ESI mass spectral scan (50-1100 amu.) for (b) Z10 and (c) Z16 surfactant. Conditions: same as Figure 2.3 except Column 2 = 63 cm long, 18.5 cm packed bed, and sheath liquid was 3 $\mu\text{L}/\text{min}$, 1 mM A.F., and 80/20% MeOH/ H_2O68

Figure 2.7: Effect of sheath liquid flow rate on the detection of zwittergent in APCI-MS mode. Conditions: Column 2, 75% (v/v) ACN, 5 mM Tris, pH 8.0; sheath liquid: (a) 200 $\mu\text{L}/\text{min}$, 6 kV 6 sec. inj., (b) 50 $\mu\text{L}/\text{min}$, 6 kV 15 sec. inj., 1 mM A.F., and 80/20% MeOH/ H_2O . Spray chamber: dry gas flow 5 L/min, nebulizer pressure 2 psi, dry gas temp. 100 $^\circ\text{C}$, V_{cap} 4000 V, vaporizer temperature 400 $^\circ\text{C}$, corona current 4 μA , fragmentor voltage 100 V, 18 kV applied voltage. A mixture of five zwittergent homologues at a concentration of 5 mg/mL were monitored as positive ions in APCI SIM at m/z 158, 186, 214, 242, and 270.76

Figure 2.8: (a) CEC-APCI-MS scan (50-1500 amu.) electrochromatogram of a mixture of five zwittergent standards. (b) mass spectra of each zwittergent homologue and (c) expanded view of the mass spectra of Z10 zwittergent. Conditions: column 3, 64 cm total length, 23 packed bed; 10 kV 13 sec. injection. All other conditions are the same as Figure 2.7 except the concentration of each zwittergent homologue in the mixture was 25 mg/mL.79

Figure 2.9: Zwittergent limit of detection (LOD) electrochromatograms in (a) ESI positive ion scan mode, range 50-1500 amu. (b) ESI positive ion SIM, group 1 = 4 ions monitored at m/z 280, 308, 336, 364 and group = 1 ion monitored at m/z 392. (c) APCI

positive ion scan, range same as ESI. (d)) APCI positive ion SIM , group 1 = 4 ions monitored at m/z 158, 186, 214, 242 and group 2 = 1 ion monitored at m/z 270. Conditions for ESI same as Figure 2.3 except fragmentor voltage was 150 V and V_{cap} = 5000 V; APCI parameters same as Figure 2.8.80

Figure 2.10: *Rewoteric AM CAS* commercial sample analysis. (a) CEC-ESI-MS scan mode (50-1500 amu.) with corresponding mass spectra. Conditions: same as Figure 2.8 except sample concentration = 1 mg/mL. (b) CEC-APCI-MS scan mode (50-1500 amu.) with corresponding mass spectra. Conditions are same as Figure 2.8 except sample concentration was 40 mg/mL.....82

Figure 2.11: Summary of the fragment pattern observed for the commercial sample using (a-b) CEC-ESI-MS and (c-d) CEC-APCI-MS scan mode. Conditions are same as Figure 2.10.84

Figure 2.12: CEC-ESI-MS and CEC-APCI-MS SIM mode analysis of the commercial sample. Conditions for ESI are same as Figure 2.9 except 6 kV 12 sec. injection and ESI-SIM positive ions monitored in three groups. Group 1 = 4 ions monitored at m/z 367, 395, 423, 451; group 2 = 1 ion at m/z 479 and group 3 = 1 ion monitored at m/z 507. For APCI conditions, same as Figure 2.10 except ions are grouped as follows: group 1 = 4 ions monitored at m/z 229, 257, 285, 313; group 2 = 1 ion at m/z 341 and group 3 = 1 ion monitored at m/z 369.86

Figure 3.1: Generalized chemical structure of the alkyltrimethylammonium surfactant.98

Figure 3.2: Electrochromatograms showing the effect of ACN volume fraction on the separation of nine alkyltrimethylammonium cationic compounds. Inset shows the extract ion chromatogram (EIC) for short chain C_1 - and C_2 -TMA⁺ at (top) 90% ACN (v/v) and (bottom) 70% ACN (v/v). Conditions: Column 1: 64 cm long, 22 cm packed bed length, 75 μ m (I.D.) capillary tapered internally (ca. 8 μ m) packed with 3 μ m CEC C₆/SCX stationary phase; mobile phase: ACN% (v/v) varied, 10 mM NH₄OAc, pH 3.0. Sheath liquid; 70/30 MeOH/H₂O, 10 mM NH₄OAc, natural pH (6.7), pump flow = 5 μ L/min. Spray chamber: drying gas flow 6 L/min, nebulizer pressure 10 psi, drying gas temp. 300 °C, V_{cap} 4000 V, fragmentor 125 V. Electrokinetic injection: 10 kv, 10 sec., 16 kV run voltage, ESI SIM positive ions (9 ions) monitored as group SIM at m/z 74, 88, 144, 172, 200, 228, 256, 284, 312.106

Figure 3.3: Electrochromatograms showing the effect of TEA volume fraction on the separation. Conditions are the same as Fig. 3.2 except (a) % TEA varied at 90%ACN (v/v), (b) % TEA varied at 70% ACN (v/v) on Column 2 packed bed = 27 cm, total length 70 cm with 18 kV runs. Inset (c) shows the optimum separation achieved using 0.4% TEA. Spray chamber and sheath liquid conditions are same as Fig.3.2.108

Figure 3.4: Electrochromatograms showing the effect of buffer pH. Inset of pH 5.0 shows effect of thiourea retention as a function of pH, injected at 10 mg/mL in 65/35 ACN/H₂O with 12 kv, 13 sec injection. Conditions are the same as Fig. 3.3 (b) except TEA = 0.40% and Column 3 = 30 cm packed, 70 cm total length. Spray chamber drying and sheath liquid conditions are same as Fig.3.2.110

Figure 3.5: Plots of signal, signal/noise (S/N), resolution (R_s), and efficiency (N). Conditions are the same as Fig. 3.4 (b) except TEA = 0.40% and Column 3 = 30 cm packed, 70 cm total length. Spray chamber drying and sheath liquid conditions are same as Fig.3.2.113

Figure 3.6: Electrochromatograms (a) and plots (b-c) showing the effect of buffer NH₄OAc concentration (mM) on the separation, (b) thiourea retention trend (t_0) and (c) CEC capacity factor (k^*) vs. NH₄OAc concentration (mM) with correlation value (dashed line indicates 2.5 mM is omitted from R^2). CEC conditions are the same as Fig. 3.4. except the mobile phase pH = 3.0 and column 4=25 cm packed, 67 cm total length. Spray chamber and sheath liquid conditions are same as Fig.3.2.114

Figure 3.7: Sheath liquid tuning plots. Effects of (a) IPA volume fraction on (a) MS signal, (b) S/N, (c) MeOH volume fraction on (c) MS signal, (d) S/N. (e) NH₄OAc concentration effects on (e) MS signal (f) S/N using 50/50 MeOH/H₂O (g) pump flow effect on (g) MS Signal (h) S/N using 10 mM NH₄OAc. Conditions: same as Fig. 3.6. except CEC mobile phase contains 15 mM NH₄OAc and 15 kV runs using 3000 V_{cap}.118

Figure 3.8: ESI fragment voltage and capillary voltage (V_{cap}) optimization using two representative cationic surfactants C₆-TMA⁺ and C₈-TMA⁺. Effect of fragment voltage on (a) MS signal and (b) S/N. Effect of V_{cap} on (c) MS signal, (d) S/N. Conditions: (a-d) 50/50 MeOH/H₂O, 10 mM NH₄OAc, 7 μ L/min, (c-d) same as (a-b) except fragment voltage = 50 V.120

Figure 3.9: ESI spray chamber optimization. Structured experimental design calls for maintaining two of three spray chamber parameters constant for analysis of trends when varying the drying gas temperature, drying gas flow rate, and nebulizer pressure. For two representative surfactant C₆-TMA⁺ and C₈-TMA⁺, plots show effects on C₆-TMA⁺ (a) MS signal, (b) S/N and C₈-TMA⁺, (c) MS signal, (d) S/N. Conditions: same as Fig. 3.8 (c-d) except V_{cap} = 3000 V.122

Figure 3.10: CEC-ESI-MS analysis of Arquad S-50 industrial sample. Conditions same as Fig. 3.9 except sample concentration was 15 μ g/mL and injection was 6 kV for 8 sec. (a) top shows SIM group method monitoring m/z for C₁₂-C₁₈-TMA⁺, while the bottom shows EIC of each ion, (b) same as (a) four peaks in the region of 25-27 min (left circle) corresponding to separation of four cis-trans isomer for C₁₈-TMA⁺ with two

degrees of unsaturation; two peaks in the region of 28-30 min (right circle) corresponding to separation of two cis-trans isomer for C₁₈'-TMA⁺ with one degree of unsaturation.

.....129

Figure 3.11: Spiking study of the cis-trans C₁₈' component present in Arquad S-50 sample. Duplicate injections for each study are shown for reproducibility. Conditions are same as Fig. 3.10. (a) SIM analysis of S-50 sample. The inset EIC shows extracted *m/z* corresponding to C₁₈', (b) Analysis of synthetic cis-C₁₈'-TMA⁺ injected at 10 µg/mL with corresponding EIC (shown as inset) for C₁₈'-TMA⁺, (c) spiking of synthetic cis-C₁₈'-TMA⁺ into Arquad S-50 using two vial injections both 6 kV 8 sec. SIM ions and analyte concentrations are same as (a-b) above.133

Figure 4.1: The chemical structure of Triton X-100 (TX-100).144

Figure 4.2: Electrochromatograms showing the comparison between monomeric and polymeric stationary phase for separation of TX-100 oligomers. Conditions: 80% (v/v) ACN / 12.5 mM Tris buffer; pH 8.0; 20°C; separation voltage, 30 kV; electrokinetic sample injection 5 sec, 5 kV, followed by a 3 sec, 5 kV run buffer injection; UV detection at 214 nm.149

Figure 4.3: Electrochromatograms showing the effect of ACN volume fraction on the separation of TX-100. The numbered peaks represent the oligomers. The inset bar plots (A) and (B) shows *N* and *R_s* respectively over the same volume fraction of ACN. Mobile phase, 12.5 mM Tris buffer; pH 8.0, [% (v/v)] of ACN varied: (a) 65% ACN, (b) 70% ACN, (c) 75% ACN, (d) 80% ACN, (e) 90% ACN. Other conditions: capillary temperature 20°C; separation voltage, 30 kV; electrokinetic sample injection 5 sec, 5 kV, followed by a 3 sec, 5 kV run buffer injection; UV detection at 214 nm.152

Figure 4.4: Electrochromatograms showing the effect of Tris concentration on the separation of TX-100. The inset bar plots provide *N* (A) and *R_s* (B) for TX-100 oligomers. Conditions are the same as Fig. 4.3 except 90% (v/v) ACN in various Tris buffers, pH 8.0: (a) 3.12 mM, (b) 6.25 mM, (c) 12.5 mM, (d) 18.7 mM, (e) 25.0 mM.

.....154

Figure 4.5: Electrochromatograms showing the effect of pH on the separation of TX-100. The inset bar plots provide *N* (A) and *R_s* (B) for critical TX-100 oligomers. Conditions are the same as Fig. 4.4 except 12.5 mM Tris / 90% (v/v) ACN and pH was varied: (a) pH 9.0, (b) pH 8.0, (c) pH 7.0, (d) pH 6.0.156

Figure 4.6: Electrochromatograms showing the effect of voltage on the separation of TX-100. The inset bar plots provide *N* (A) and *R_s* (B) for critical TX-100 oligomers. Conditions are the same as Fig. 4.5 except 12.5 mM Tris / 90% (v/v) ACN, pH 7.0.

.....157

Figure 5.1: Full Scan CEC-MS of TX-15. In the legend, E=ethoxylate group. Conditions: Buffer 80/20 ACN/H₂O 5 mM Tris, pH 8. Sheath liquid: flow rate 5 μ L/min, 80/20 MeOH/H₂O, 1 mM HCO₂NH₄. MS spray chamber: Drying gas flow rate 10 L/min, Nebulizer pressure 10 psi, drying gas temperature 300 °C, Fragment voltage 125 V, Capillary voltage 4000 V, Gain 4. Full Scan 50-1500 amu. CEC 16 kV runs, column 20 cm packed bed, 60 cm total length and 75 μ m I.D. x 363 μ m O.D., 6 kV 6 sec injection. TX -15 injected at 10 mg/mL dissolved in 65/35 ACN/H₂O.175

Figure 5.2: Initial Full Scan CEC-MS of TX-45. Conditions are the same as Figure 5.1.177

Figure 5.3: Initial Full Scan CEC-MS of TX-100. Conditions are the same as Figure 5.1.179

Figure 5.4: Initial Full Scan CEC-MS of TX-165. Conditions are the same as Figure 5.1.181

Figure 5.5: Summary of the fragmentation, ion and adduct formation of the TX series surfactants (TX-45 used as example). Fragments, the protonated molecular ion, ammonium and sodium adducts were observed. (A) a loss of 3 ethoxylate groups to leave 2 degrees of ethoxylation, $m/z=277$ observed; (B) a loss of 4 ethoxylate groups to leave 1 degree of ethoxylation, $m/z=233$ observed; (C) loss of octyl chain $m/z=271$ observed.182

Figure 5.6: Effect of mobile phase ACN content (v/v) on the CEC-MS separation of Triton series (A) TX-15, (B) TX-45, (C) TX-100, (D) TX-165. Column dimensions are the same as Figure 5.1, packed with 3 μ m / 100 Å Reliasil ODS. Conditions: buffer ACN varied/5 mM Tris, pH 8.0. Sheath liquid: flow rate 5 μ L/min, 80/20 MeOH/H₂O, 1 mM HCO₂NH₄. MS spray chamber: drying gas flow 10 L/min, nebulizer pressure 10 psi, drying gas temperature 300 °C, fragmentor voltage 125 V, capillary voltage 4000 V, gain 4. SIM ions as described in Table 5.2, applied voltage 16 kV runs, 6 kV 6 sec injection. Analytes: 10 mg/mL 65/35 ACN/H₂O.185

Figure 5.7: Effect of BGE Tris concentration (mM) on the CEC-MS separation of Triton series (A) TX-15, (B) TX-45, (C) TX-100, (D) TX-165. Conditions are the same as Figure 5.6 except 90% (v/v) of ACN.187

Figure 5.8: Effect of mobile phase pH on the CEC-MS separation of Triton series (A) TX-15, (B) TX-45, (C) TX-100, (D) TX-165. Conditions are the same as Figure 5.7 except ACN = 90% (v/v), and Tris = 2.5 mM.189

Figure 5.9: Variation in sheath liquid MeOH composition in the range 50-90% (v/v) for effects on S/N (A) TX-15, (B) TX-45, (C) TX-100, (D) TX-165. Conditions are the same as Figure 5.8 except pH = 8.191

Figure 5.10: Variation in sheath liquid HCO_2NH_4 concentration in the range 1-50 mM for effects on S/N : (A) TX-15, (B) TX-45, (C) TX-100, (D) TX-165. Conditions are the same as Figure 5.9 except MeOH/ H_2O 50/50.193

Figure 5.11: Investigation of MS capillary voltage in the range of 2000-5000 V for effects on S/N . TX-100 was used as the model analyte. Conditions are the same as Figure 5.10 except HCO_2NH_4 = 10 mM, and spray chamber drying gas flow set to 6 mL/min, nebulizer pressure = 5 psi, and drying gas temperature set to 200 °C.196

Figure 5.12: Variation in MS fragmentor voltage range 25-200 V. TX-100 was used as a representative surfactant. Conditions are the same as Figure 5.11 except V_{cap} = 3000 V.198

Figure 5.13: CEC-MS of long chain nonionic surfactants (A) TX-305, (B) TX-405, (C) TX-705 and midlength (D) TX-165 combining small volume fractions of polar aprotic solvent THF with previously optimized mobile phase. Conditions are the same as Figure 5.12 except for substitution of 90% ACN with THF as follows: 1% THF/89% ACN/10% H_2O ; 2% THF/88% ACN/10% H_2O ; 3% THF/87% ACN/10% H_2O ; 4% THF/86% ACN/10% H_2O ; 5% THF/85% ACN/10% H_2O200

Figure 6.1: Full Scan CEC-MS chromatograms of TX-45 showing the effect of varying fragmentor voltage. Column dimensions 20 cm packed bed, 60 cm total length and 75 μm I.D. x 363 μm O.D., packed with 3 μm / 100 Å Reliasil ODS. Conditions: 90/10 ACN/2.5mM Tris, pH 8.0. Sheath liquid: flow rate 5 $\mu\text{L}/\text{min}$, 50/50 MeOH/ H_2O , 10 mM HCO_2NH_4 . MS spray chamber: drying gas flow 6 L/min, nebulizer pressure 10 psi, drying gas temperature 200 °C, fragmentor voltage varied, capillary voltage 3000 V, gain 4, applied voltage 16 kV runs, 6 kV 6 sec injection. Analyte: 10 mg/mL 65/35 ACN/ H_2O219

Figure 6.2: Mass spectra of TX-45 at varying fragmentor voltage. Conditions are the same as Figure 6.1.220

Figure 6.3: Breakdown curves showing the effects of varying fragmentation voltage on the mass spectral fractional abundance of molecular ion $[\text{M}+\text{H}]^+$ formation for individual degree of ethoxylation (n-value) for A) TX-15, B) TX-45, C) TX-100, and D) TX-165. The conditions and m/z are as listed in the experimental section.228

Figure 6.4: Breakdown curves showing the effects of varying fragmentation voltage on the mass spectral fractional abundance of ammonium adduct $[\text{M}+\text{NH}_4]^+$ formation for individual degree of ethoxylation (n-value) for A) TX-15, B) TX-45, C) TX-100, and D) TX-165.230

Figure 6.5: Breakdown curves showing the effects of varying fragmentation voltage on the mass spectral fractional abundance of sodium adduct $[M+Na]^+$ formation for individual degree of ethoxylation (n-value) for A) TX-15, B) TX-45, C) TX-100, and D) TX-165.234

Figure 6.6: Breakdown curves showing the effects of varying fragmentation voltage on the mass spectral fractional abundance of fragment ion $[M-C_8H_{17}+2H]^+$ formation for individual degree of ethoxylation (n-value) for A) TX-15, B) TX-45, C) TX-100, and D) TX-165.236

Figure 6.7: Breakdown curves overlaying the $[M+H]^+$, $[M+NH_4]^+$, $[M+Na]^+$ and $[M-C_8H_{17}+2H]^+$ ions at varying fragment voltage and individual n-value for TX-15.....238

Figure 6.8: Breakdown curves overlaying the $[M+H]^+$, $[M+NH_4]^+$, $[M+Na]^+$ and $[M-C_8H_{17}+2H]^+$ ions at varying fragment voltage and individual n-value for TX-45.241

Figure 6.9: Breakdown curves overlaying the $[M+H]^+$, $[M+NH_4]^+$, $[M+Na]^+$ and $[M-C_8H_{17}+2H]^+$ ions at varying fragment voltage and individual n-value for TX-100.244

Figure 6.10: Breakdown curves overlaying the $[M+H]^+$, $[M+NH_4]^+$, $[M+Na]^+$ and $[M-C_8H_{17}+2H]^+$ ions at varying fragment voltage and individual n-value for TX-165.248

Figure 7.1: Chemical structure of the β -blockers.263

Figure 7.2: Chemical structure of the PEAs with varying degree of hydroxyl substitution around the aromatic ring. Class I has 2 –OH groups, Class II has 1 –OH group, and Class III has no –OH substitution.264

Figure 7.3: Chemical structures of the PAH along with the log *P* value.265

Figure 7.4: Carbon-13 CP-MAS NMR spectrum of the aminopropyl bonded silica intermediate. Instrumentation: Bruker DSX400 solid state NMR spectrometer. Conditions: Data were recorded using a operating at a 1H frequency of 400 MHz. ^{13}C solid state NMR spectra were recorded using the CP-MAS technique. The 90 degree pulse length was 5 μs . The length of the contact pulse was 1 ms, and high power 1H decoupling was utilized during the acquisition of the FID. The spinning frequency was 10 kHz. 10,000- 20,000 averages were recorded in order to obtain spectra with sufficient signal to noise ratio.268

Figure 7.5: 1H -NMR comparison of the (A) LCA and the (B) LCA following conversion to the chloroformate. Instrumentation: 400 MHz Varian NMR. Conditions: Sample in $CDCl_3$ 271

Figure 7.6: Carbon-13 CP-MAS NMR spectrum of the LCA bonded phase. Instrumentation and conditions are same as Figure 7.4. Peaks observed at 176 and 157 ppm in the LCA spectra occur at about 10 kHz from peaks in the aliphatic region. It was confirmed that these peaks are “true peaks” and not spinning sidebands by recording an additional spectrum with a spinning speed of 8 kHz, which look essentially identical to the spectrum recorded with a spinning speed of 10 kHz.273

Figure 7.7: IR comparison of the (a) Kromasil 300Å bare silica, (b) Kromasil 300Å bare silica following reaction with aminopropyl silane, (c) attachment of LCA-CF to Si-C₃-NH₂. Instrumentation: GSU Spectrum One. Conditions: KBr was used as the background.277

Figure 7.8: CEC-MS Comparison of (A) Kromasil Si-C₃-NH₂ to (B) Kromasil Si-C₃-NH-LCA for separation of 7 component β -blockers. Conditions: Packed bed 25 cm, total length 58 cm, Buffer, 85/15 ACN/10mM NH₄OAc, pH 3, 0.05% TEA. Sheath liquid: 70/30 MeOH/10 mM NH₄OAc delivered at 500 μ l/min. ESI spray chamber: drying gas flow rate 6 L/min, nebulizer pressure 5 psi, drying gas temp. 200°C, Vcap 2700 V, Fragment V 80, CEC 12 kV runs, 4 kV 4 sec injection. Analytes 1 mg/mL in MeOH, injection sample 80/20 analyte/running buffer. Peak identification: 1=oxprenolol, 2= alprenolol, 3=pindolol, 4=propranolol, 5=metoprolol, 6=atenolol, 7=talinolol. The inset provides the EIC for each m/z monitored.280

Figure 7.9: CEC-MS Comparison of Kromasil Si-C₃-NH-LCA to Kromasil Si-C₃-NH₂ for (A) comparison of the current profile and (B) comparison of the thiourea dead time marker. Conditions are the same as Figure 7.8.283

Figure 7.10: Separation of a mixture of ten PEAs compounds on the (A) aminopropyl silica and (B) LCA bonded phase. Conditions are same as Figure 7.8. The protonated molecular ion $[M+H]^+$ was monitored for all analytes. Peak identification; 1=pseudoephedrine; 2=ephedrine; 3=norephedrine; 4=synephrine; 5=octopamine; 6=isoproterenol; 7=norphenylephrine; 8=terbutaline; 9=epinephrine, 10=norepinephrine. The inset provides the EIC for each m/z monitored, for both A) and B) a: [norephedrine $M+H]^+$, b: [isoproterenol $M+H-C_3H_8O]^+$, c: [terbutaline $M+H-C_4H_{10}O]^+$, d: [norepinephrine $M+H-H_2O]^+$, e: [octopamine $M+H]^+$, f: [norphenylephrine $M+H]^+$, g: [pseudoephedrine $M+H]^+$, h: [ephedrine $M+H]^+$, i: [epinephrine $M+H-H_2O]^+$, j: [synephrine $M+H]^+$, k: [terbutaline $M+H-C_4H_8]^+$, l: [norepinephrine $M+H]^+$, m: [epinephrine $[M+H]^+$, n: [isoproterenol $M+H]^+$, o: [terbutaline $M+H]^+$. Packed bed lengths 25 cm, total length 60 cm.285

Figure 7.11: Separation of a mixture of ten PEA compounds on the LCA bonded phase using a longer packed bed length of 55 cm. All other conditions are same as Figure 7.10.286

Figure 7.12: Proposed fragmentation pathway of PEAs, A) norepinerhrine by loss of H₂O, and B) terbutaline by loss of isobutyl alkyl group followed by loss of H₂O.287

Figure 7.13: Variation of the mobile phase pH for separation of 16 PAH test mixture on the LCA bonded phase. The inset shows the same separation achieved at pH 4.5 using the aminopropyl silica phase. Conditions: 85/15 ACN/15 mM NH₄OAc, packed length 30 cm, 10 kV runs, 10 kV 18 sec injection. Analytes 1mg/mL in 85% ACN, injection sample 85/15 analyte/running buffer Peak identification: peak 1=acenaphthylene; peak 2=naphthalene, acenaphthene, peak 3=phenanthrene; peak 4=fluoranthene; anthracene, fluorene; peak 5=chrysene, pyrene, 1,2-benzanthracene; peak 6=benzo[k]fluoranthene, benzo(b)fluoranthene; peak 7=1,2:5,6-ibenzanthracene; benzo[a]pyrene; peak 8=indeno(1.2.3-cd)pyrene; peak 9=benzo[ghi]perylene.291

Figure 7.14: Separation of different PAH on the LCA bonded phase. Conditions are the same as Figure 7.13 except for the mobile phase pH = 4.293

Figure 7.15. Variation in mobile phase pH in the range of pH 3.0-4.5 for analysis of 8 component PCB mixture on the LCA bonded phase. The inset shows the same separation at pH 4.5 on the aminopropyl silica phase. Conditions are same as Figure 7.14. Peak identification: peak 1=2 chlorobiphenyl; peak 2=2.3-dichlorobiphenyl; peak 3=2.4'.5-trichlorobiphenyl; peak 4,5=2.2'.4.4'-tetrachlorobiphenyl, 2.2'-3'-4.6-pentachlorobiphenyl; peak 6=2.2'.4.4'.5.6'-hexachlorobiphenyl; peak 7,8=2'.3.3'.4.4'.6-heptachlorobiphenyl, 2.2'-3.3'.4.5'.6.6'-octachlorobiphenyl.296

Figure 7.16: Separation of 4 PCB mixture on the LCA bonded phase. Conditions are the same as Figure 7.15.297

Figure 7.17: CEC-MS trend of thiourea used as a dead time marker for propyl amine silica compared to the LCA bonded phase. Conditions are as shown on the Figure.299

Figure 7.18: CEC-UV trend of thiourea used as a dead time marker for propyl amine silica compared to the LCA bonded phase. Conditions are as shown on the Figure.301

Chapter 1: Introduction

Introduction to CEC

Capillary electrochromatography (CEC) is a liquid phase analytical separation technique that combines the advantages of high selectivity inherent to high performance liquid chromatography (HPLC) along with high separation efficiency like that found in capillary electrophoresis (CE). The separation in CEC is typically conducted in fused silica capillary tubing (50-200 μm ID) which is packed with stationary phase (3-5 μm ID) like that of HPLC. However, instead of pressure driven mobile phase like that used in HPLC, the mobile phase in CEC is propelled by electroosmotic force (EOF) which is generated by high electric field applied across the length of the capillary. In the presence of electrolyte, positive ions migrate toward the cathode dragging the surrounding mobile phase with them which gives rise to the EOF. Although the EOF based mobility is useful for separation of charged compounds resulting from differences in mass to charge (m/z) ratio and electrophoretic mobility inherent to capillary zone electrophoresis (CZE), the neutral compounds are unable to be separated as they migrate with the EOF which has a flat profile moving through the column. Therefore, the employment of a fixed stationary phase in packed column CEC allows the added advantage of partitioning of neutral analytes back and forth between the mobile phase and the stationary phase. This allows retention and selective separation of both neutral type and charged type analytes which are able to interact with the stationary phase based upon ionic, hydrophilic and hydrophobic interactions. From this basis, CEC has become an attractive alternative to traditional HPLC techniques and has recently received growing attention.

The early development of CEC dates back to the 1950s in which the first demonstration of the use of EOF to drive a liquid in a thin-layer chromatographic system was conducted by Mould and Synge.^{1,2} However, it was Pretorius et al. in 1974 who actually showed the first applications of EOF to electrically pump or propel liquid mobile phase through a column packed with stationary phase or adsorbent.³ The results of this early work showed that band broadening inherent to pressure driven systems such as HPLC was substantially lower in EOF driven systems such as CEC. In 1981, Jorgenson and Lukacs demonstrated the reversed phase CEC separation of polyaromatic hydrocarbons (PAHs) on a 170 μm ID column packed with 10 μm C18 packing which can be considered the most similar to CEC as we know it today.⁴ It was not until the 1980s that Knox and Grant showed that the EOF was capable of being generated using particles as small as 1.5 μm in diameter.^{5,6} The achievement of extremely high theoretical plate numbers at that time (e.g., 69,000) resulted in the interest of the analytical community and the solidification of CEC as a capable and powerful micro-scale separation technique.

In this work, the introduction to the dissertation is comprised of three sections. The first section reviews the basic principles of CEC such as the generation of EOF and operating variables that affect the EOF. The second section describes the fundamentals of electrospray ionization mass spectrometry (ESI)-MS and atmospheric pressure chemical ionization (APCI)-MS followed by the discussion of current trends in the coupling of CEC columns to the MS instrumentation. The third and final section discusses the applications of CEC-MS and a discussion of the different chemical classes of surfactants.

Basic Operating Principles in CEC. Generation of EOF in a Packed Column.

The movement of liquid mobile phase through the capillary is accomplished by electroosmosis which can be defined as the movement of liquid relative to a stationary charged surface under the influence of an applied electric field. Under alkaline conditions, the silanol (e.g., Si-OH) groups located on the inner wall of the fused silica capillary and outer surface of stationary phase packing become negatively charged which lay the groundwork for the distribution of ions in the CEC system. In the presence of added electrolyte, cations become adsorbed to the anionic silanol groups (Figure 1.1A) while anions are repelled. A distribution of ions forms a double layer known as the inner Stern layer and the outer Gouy layer (Figure 1.1B).

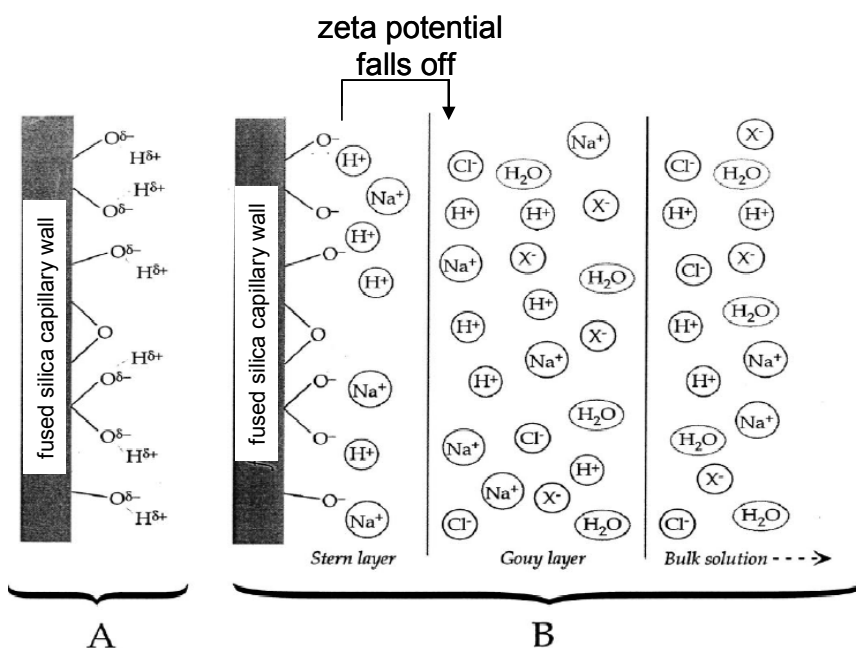


Figure 1.1: (A) Silanol groups comprising the inner wall of a fused silica capillary. (B) Distribution of ions and formation of the electrical double layer adjacent to the silanol groups. The zeta potential shows the point at which the voltage begins to drop between the charged surface and the counter ions located in the stern layer.⁷

The electrical double layer is a modified version of the Gouy-Chapman model⁸⁻¹⁰ in which the counter ions are configured in a fixed or moving diffuse layer, with a surface of shear located just beyond the interface.⁷ Between the silica wall and the surface of shear, the drop in electric potential is known as the zeta potential, ζ . This falls exponentially to zero in the diffuse layer and by a factor e^{-1} over a distance δ known as the double layer thickness.⁸ The ζ is dependent upon the product of δ and surface charge σ according to the equation 1:

$$\zeta = \sigma \delta / \varepsilon_o \varepsilon_r \quad (1)$$

where ε_o is the permittivity of a vacuum and ε_r is the dielectric constant of the electrolyte solution.⁷ The thickness of the double layer is dependent on ε_o and also on the ionic strength of electrolyte solution I as shown in equation 2:

$$\delta = (\varepsilon_o \varepsilon_r RT / 2F^2 I)^{0.5} \quad (2)$$

where R is the universal gas constant, T is the temperature in Kelvin, F is the Faraday constant. Upon the application of electric field a potential difference is generated over the column length, which in turn drags the solvated cations and solvent molecules towards the cathode thus giving rise to EOF.

The electroosmotic mobility μ_{eof} or linear flow is related to the zeta potential ζ and to the viscosity of solution η by equation 3:

$$\mu_{\text{eof}} = \varepsilon_o \varepsilon_r \zeta E / \eta \quad (3)$$

where E is the strength of the electric field. From this equation the factors influencing the strength of the EOF are surface charge properties of the stationary phase and silica wall, ionic strength of the buffer as well as viscosity, and finally the magnitude of the electric

field applied. Therefore, the optimization of these operational parameters is important to consider for method development in CEC. In addition, equation 3 shows that the linear velocity of the EOF is not dependent on the stationary phase particle size, as can be seen by the absence of this parameter in the equation. This means that very small particles can be used in CEC which has very important implication regarding the performance of the chromatographic separation. The only limitation to the use of extremely small particles is the possibility for overlap of the double layer which was suggested by Knox and Grant.^{5,6} In their work, they demonstrated the feasibility of utilizing particles down to 1.5 μm in diameter. Similarly, they also showed that when comparing the use of 3 and 5 μm particles sizes in CEC versus pressure driven HPLC systems, the efficiency of the CEC separation was superior to that of the HPLC.

Flat Profile of the EOF in CEC. One important advantage of CEC is the flat profile of the EOF as compared to the laminar flow profile like that of pressure driven HPLC. This is illustrated below in Figure 1.2 which shows the difference between the two.

As shown in the Figure 1.2 for pressure driven flow, the variation in distance between particles results in a flow profile with different velocities and more opportunity for peak band broadening. In contrast, the EOF driven CEC system provides a more uniform flow profile that reduces band broadening.

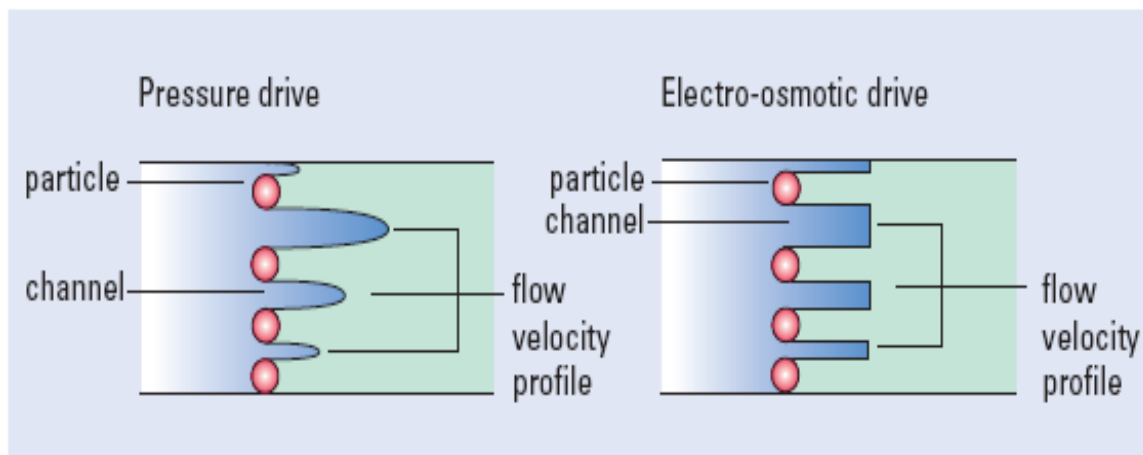


Figure 1.2: Flow profile in HPLC (laminar flow) vs. CEC (EOF).¹¹

A measure of Gaussian peakshape in a chromatographic separation is known as peak efficiency. The efficiency increases along with the sharpness of the peak. The determination of peak efficiency is controlled by factors described in the Van Deemter Equation, which relates kinetic and thermodynamic processes to efficiency by equation (4):

$$H = A + (B/u) + Cu \quad (4)$$

where H is the theoretical plate height, A is the eddy diffusion resulting from a poorly packed column, B is longitudinal diffusion, C is the resistance to mass transfer, and u is the mobile phase velocity in ml/min. Since a small theoretical plate height is desired, therefore the contribution from each factor must be as small as possible.

Within a packed stationary bed, there are several chromatographic processes that can contribute to solute band broadening which result in lower peak efficiency such as (a) eddy diffusion, which arises from the varying flow paths through the column; (b) axial

molecular diffusion or longitudinal diffusion; (c) resistance to mass transfer in both mobile and stationary phases; and (d) system effects such as those resulting from dead volumes inside the column.⁷ A smaller theoretical plate height (H) and higher plate numbers $N = (L / H)$ (where L is length of the column) in CEC as compared to pressure driven HPLC result from reduced contribution to H from factors (a) and (c) above.¹²

As CEC utilizes a uniform electric field to propel the mobile phase through the column, the flow velocity is independent of the channel width such that all analytes are propelled equally through all the channels, therefore, a flat velocity profile is observed. A significant reduction in the contribution due to eddy diffusion and multiple path lengths in CEC is achieved. This is contrary to HPLC, in which solutes take both fast and slow paths through the column and a non-uniform flow profile is observed which results in unequal propulsion of analytes through the column.

The size of the stationary phase particles affects both the Eddy diffusion and pathlengths of the analyte through the column. Hence, larger stationary phase particles will contribute more to these factors as a result of increased dead volumes located between the particles. As there are no pressure limitations in CEC as compared to HPLC, the utilization of very small particles down to 1 μm eliminates the unwanted contribution of aforementioned factors to H , consequently lowering the plate height and increasing overall peak efficiency.

The additional benefit of small particles in CEC is the minimization of the mass transfer contribution in the mobile phase, $C_m \mu$, which also decreases plate height H since the average linear velocity (μ) is proportional to particle diameter (d_p). This is also a

result of the flat flow velocity profile between the stationary phase particles. The inter-particle channels reduce C_m by a factor that can be estimated by considering an individual channel as an open tube of diameter, d_c , where C_m is given by the Golay equation.⁷

$$C_m = (f(k) d_c^2) / D_m \quad (5)$$

where D_m is the diffusion coefficient of the solute in the mobile phase.

For the parabolic flow of HPLC:

$$f(k) = (1 + 6k + 11k^2) / 96 (1 + k)^2 \quad (6)$$

In contrast, for the plug flow of CEC:

$$f(k) = (k^2) / 16 (1 + k)^2 \quad (7)$$

A comparison of equations (6) and (7) shows that for a given k , and same d_c and D_m , the contribution to H from CEC is roughly half of that in capillary HPLC.⁷ Overall, the possibility for chromatographic separations with higher efficiency are achievable in CEC as compared to HPLC.

Influence of the Operating Variables in CEC. The optimization of the operating variables in CEC is important to achieve the most efficient and selective separation in the shortest amount of time, as well as optimizing compatibility with sensitive detection techniques such as mass spectrometric (MS) analyzers. Some of the most important considerations are the composition of the mobile phase including ionic strength and type of ions that should be small and volatile, the pH of the mobile phase, and the influence of the organic solvent added to the mobile phase. Although, the additional factors including amount of voltage applied across the capillary column and column temperature are

important to consider during optimization, a moderate voltage approximately 15-20 kV and operating at room temperature (e.g., 25°C) typically provide suitable operating conditions. Therefore, the influence of more critical operating parameters such as mobile phase ionic strength, pH, and organic solvent composition are described.

First, it is important to select a suitable background electrolyte (BGE) for use in the CEC running buffer. The ionic strength of the BGE affects the double layer thickness and the zeta potential according to equation (2) shown previously. Therefore, the use of appropriate BGE will determine the magnitude of the EOF which ultimately can provide stable or unsuitable operating conditions. In addition, when coupled to MS detection, the BGE should be volatile to avoid contamination of the ion source. For method optimization, the ionic strength of the CEC is typically varied in the range of 1-50 mM. A moderate concentration of around 10 mM is typically considered as optimum for use in CEC-MS. Ammonium salts such as formate and acetate are typically well suited for CEC-MS, while BGE such as trihydroxyaminomethane (Tris) buffer is also well suited for CEC with UV or MS detection. As shown in this dissertation, in CEC-MS, a low concentration (i.e., lower than 10 mM) of Tris buffer can be used without contaminating the ionization source. At higher concentrations, the solubility of the BGE in organic solvent systems should be considered, although salting out of the BGE is rarely observed. Too low ionic strength can result in double layer overlap, while too high BGE strength can increase viscosity and dramatically increase retention time.

Second, the pH of the BGE is a critical operating variable that influences both the surface charge of the silica surfaces and also the ionization of the analyte if ionizable

groups are present. As CEC typically uses silica stationary phases and the fused silica wall of the capillary depends upon activation of the silanol groups to aid in generation of EOF, operating at too low pH approaching pH=2.0 usually results in detrimental effects on EOF. This is because the double layer will not be able to be maintained in stable configuration and break down of the EOF will occur. In addition, the pKa range of the buffer must be considered, where a positive charge is typically desired to aid in generation of EOF. In the case of Tris which has a natural pH of about pH=10 in aqueous solution, our results have shown that the most suitable operating conditions were achieved at pH=8, which is in fact very close to the pKa of this BGE. Therefore, for Tris solutions the pH must be lowered using additive such as HCl or increased using ammonium hydroxide. In the case where too much acid or base is added, the additional ionic strength results in increased viscosity and significant drop in EOF, which is similar to increased BGE strength mentioned previously. With the consideration of the pKa of the BGE, in the case for analysis of polar or charged analytes, the appropriate pH should be chosen to influence the electroosmotic mobility of the analyte. Hence, a positively charged analyte will migrate faster toward the cathode than negatively charged analyte which has retarded migration due to attraction to the anode. In general, negatively charged ions are usually separated in suppressed ion mode as neutral species as they are difficult to detect in CEC-UV or CEC-MS.

Finally, the selection of suitable mobile phase organic modifier and composition should be addressed. The polarity, viscosity, dielectric constant and proportion in the mobile phase are all important factors that contribute to the magnitude of EOF mobility

in the CEC column. In general the four solvents typically utilized in CEC are acetone, acetonitrile, methanol, and 2-propanol. Acetonitrile is by far the most popular solvent due to excellent balance of dielectric constant/ viscosity ratio and ability to maintain EOF typically when larger volume fractions (e.g., 80% v/v) are added to the mobile phase in reversed phase CEC systems (e.g., C_{18} stationary phase). Experimental results in our previous work have shown that acetone helps to generate EOF when combined in small volumes (e.g., 5-10% v/v) with acetonitrile. This was in cases where the EOF was unstable and hard to generate, however, the integrity of the packing and CEC column were found to break down after a short period of time. Methanol is also a suitable solvent for use in CEC, and is very compatible with ESI-MS detection. This solvent however provides lower EOF than acetonitrile which results in longer separation times, but may be also able to provide higher resolution as a trade off. Alternatively, the use of methanol is employed in the analysis of chiral compounds and polar molecules using specialized stationary phase such as teicoplanin, vancomycin and cellulose based phases. Finally, 2-propanol can be used in CEC although this solvent is far less popular due to low EOF. Acetonitrile is most often the best solvent choice in CEC. It is used in large volume fraction (e.g., 80%) and is sometimes combined with other solvents such as acetone or 2-propanol in small volumes to investigate changes in EOF mobility, and selectivity such as changes in resolution.

Mass Spectrometry. Theory of Electrospray Ionization. Although the mechanism of electrospray ionization (ESI) has been around for hundreds of years, it was not until the

early 20th century that its relevance to science was fully comprehended.¹³ Approximately 30 years later, Malcom Dole *et al* demonstrated the use of electrospray to ionize intact chemical species and the technique of ESI-MS was invented.¹⁴ An additional 20 years elapsed until work in the laboratory of John Fenn showed for the first time the use of electrospray for the ionization of high mass biologically important compounds followed by analysis using MS.¹⁵ This impressive work enabled John Fenn to share a part in the 2002 Nobel prize for chemistry, which was the 4th time a Nobel prize was awarded to MS pioneers.¹⁶ In the original manuscripts from the late 1980's, Fenn and his co-workers described the basic experimental principles and methodologies of ESI, such as soft ionization of non volatile and thermally labile compounds, multiple charging of proteins and intact ionization of complexes. As a result of Fenns groundbreaking discoveries, ESI-MS is now commonplace in many biochemical labs worldwide.

Throughout its history, the ESI source has received continued improvements since the early models, however the fundamental design has remained relatively unchanged (Figure 1.3). In ESI, a solution of analyte is introduced to the source directly using a syringe, or from the outlet of coupled hyphenated separation techniques. Flow rates are typically in the range of 1 $\mu\text{l}/\text{min}$.¹⁷ As the solution of analyte flows through the electrospray needle, a large potential difference typically in the range of 2.5 to 4 kV with respect to a counter electrode is applied to the needle.¹⁷ This results in a fine mist of spray containing charged droplets with a surface charge of identical polarity to the needle.

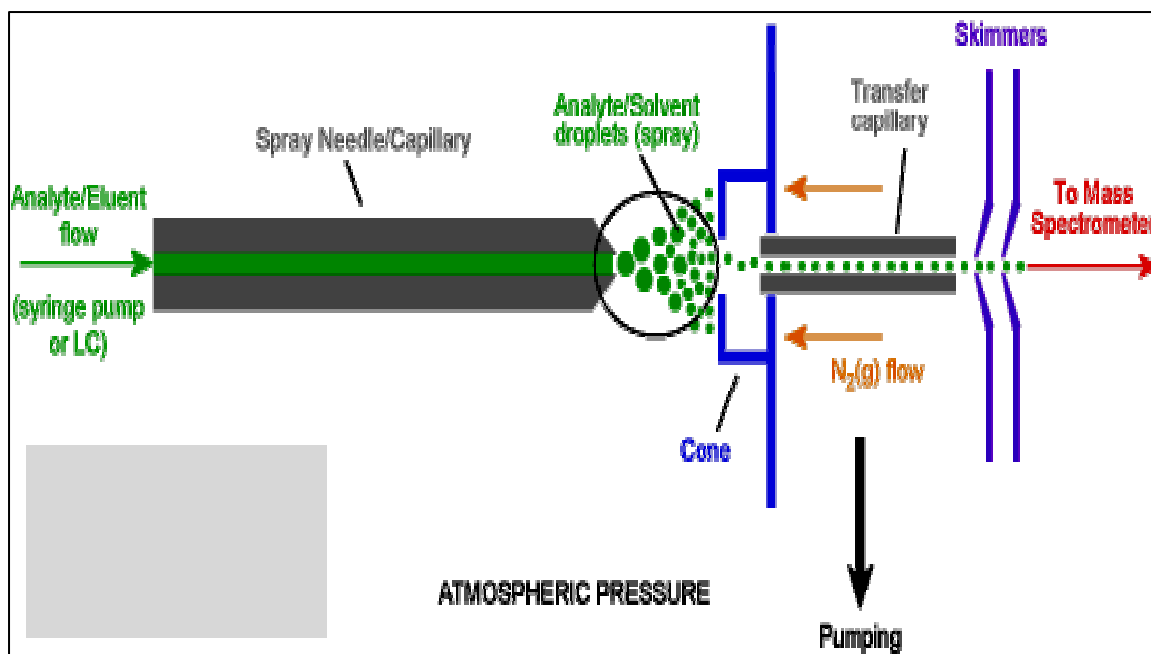


Figure 1.3: A schematic of an ESI source.¹⁷

Hence, they are repelled away from the needle and travel towards the source sampling cone located on the counter electrode (Figure 1.3). A steady stream of heated nitrogen gas enables solvent evaporation to take place as the mist of charged droplets travels between the needle tip and the cone.

As the evaporation of the solvent takes place, the droplet undergoes shrinkage until the surface tension of the droplet can no longer sustain the charge which is known as the Raleigh limit. At this time, a series of coulombic explosions causes the droplets to be ripped apart, which results in more droplets and more coulombic explosions until only naked analyte molecules are left. These molecules can have one or multiple charges

depending on the number of ionizable groups on the analyte. In general, the mechanism of ionization in ESI is deemed soft ionization as the analytes retain little residual energy during the process. As a result, it is possible to maintain the integrity of analyte species which is important in the analysis of biomolecules. For example, even the intact protein complexes can be subsequently transferred into the gas phase allowing the useful structural and important biochemical information to be obtained. Typically in ESI, analyte ionization takes place originally in solution phase and is carried through the ESI process into the gas phase.

Theory of Atmospheric Pressure Chemical Ionization. In atmospheric pressure chemical ionisation (APCI), the source configuration (Fig. 1.4) shares many similarities with that of ESI and is also used in conjunction with hyphenated separation techniques. However, the mechanism of ionization between ESI and APCI is quite different. In ESI, the analyte ionization is generated through the potential difference between the spray needle and the cone along with rapid but gentle desolvation.¹⁷ In APCI, the analyte solution is introduced into a pneumatic nebulizer and desolvated in a heated quartz tube before interacting with the corona discharge creating ions.¹⁷ Typically, neutral analytes containing carbon and hydrogen are the most suitable analytes because APCI ionizes in the gas phase unlike ESI which ionizes charged molecules formed previously in the solution phase (i.e., mobile phase).

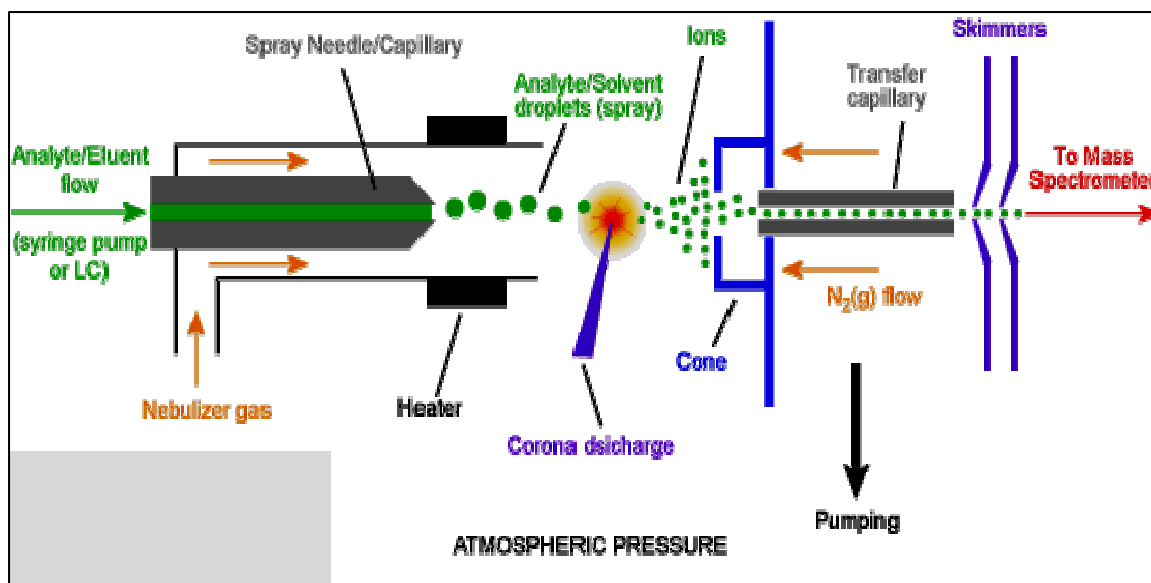


Figure 1.4: A schematic of the components of an APCI source.¹⁷

A corona discharge generates primary $\text{N}_2^{\circ+}$ and $\text{N}_4^{\circ+}$ by electron ionization. These primary ions collide with the vaporized solvent molecules to form secondary reactant gas ions - e.g. H_3O^+ and $(\text{H}_2\text{O})_n\text{H}^+$ (see Fig. 1.5).¹⁷ In turn, these reactant gas ions then collide repeatedly with the analyte which produces charged analyte ions. The high frequency of collisions results in a high ionization efficiency and thermalisation of the analyte ions.¹⁷ In the positive ion mode, either proton transfer or adducts of reactant gas ion can occur to produce the ions of molecular species, depending on the relative proton affinities of the

reactant ions and the gaseous analyte molecules. In the negative mode, the ions of the molecular species are produced either by proton abstraction or adduct formation.¹⁸

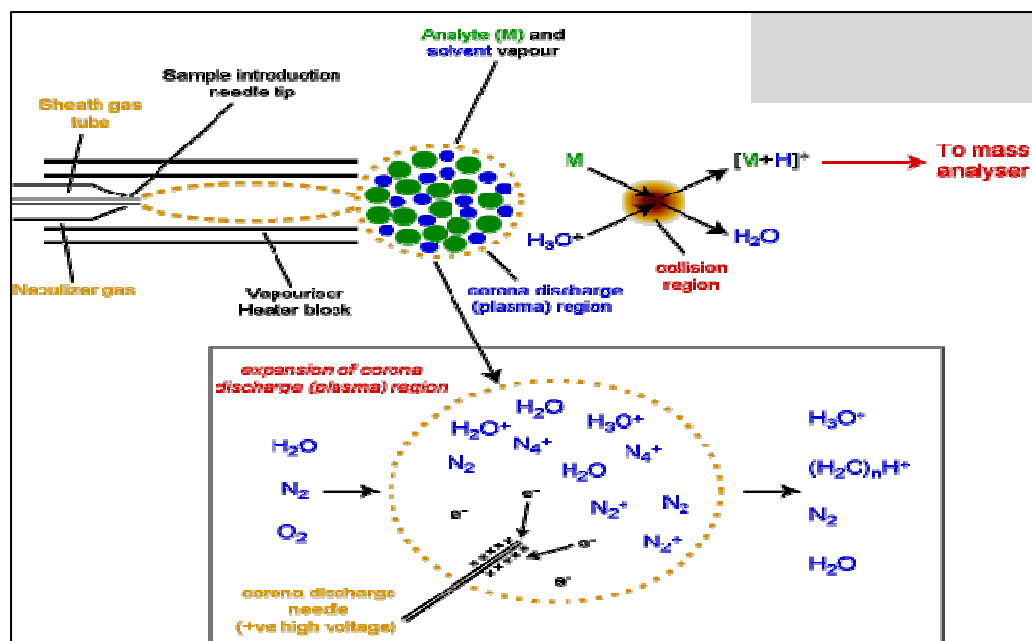


Figure 1.5: A detailed view of the mechanism of APCI.¹⁷

The Coupling of CEC to Mass Spectrometry. Although mass spectrometry utilizing ESI and APCI ionization sources provide arguably the best detection choice based on high sensitivity and the ability to provide structural information, the coupling of MS to external separation techniques such as CEC can be quite challenging. This is because the traditional means of retaining the packed stationary bed in a CEC-UV column relies on a sintered frit that is prone to form bubbles at the outlet end. To counteract unwanted bubble formation that can result in break down or failure of the EOF, a pressure of 12 bar is applied at both the inlet and outlet ends of the CEC column when using uv-detection or instrumentation that can apply pressure at the MS end. This is because the CEC-MS

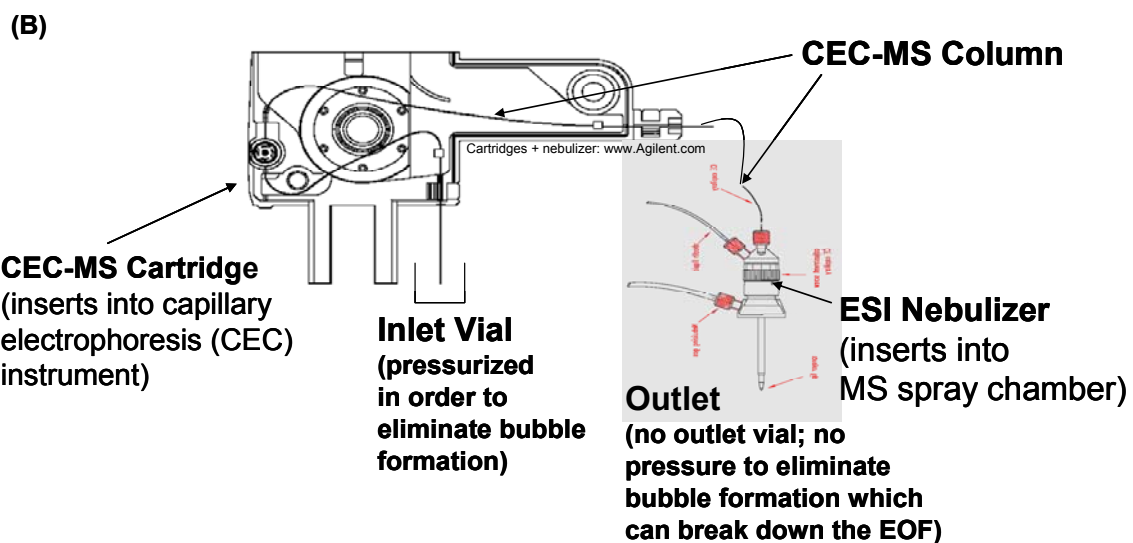
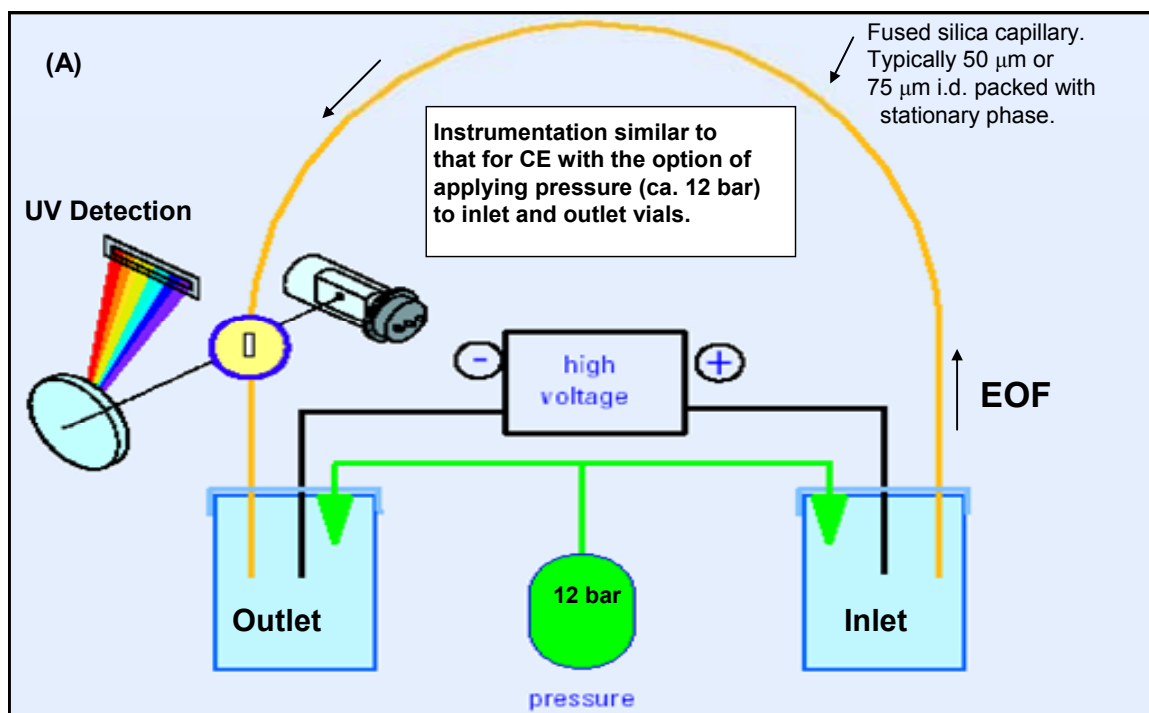


Figure 1.6: Instrumentation for (A) CEC-UV utilizing pressure applied at both the inlet and outlet of the capillary column and (B) CEC-MS that applies pressure only at the inlet side.

column is inserted through the ESI nebulizing sprayer that is set to atmospheric pressure inside the spray chamber (Fig.1.6B). It is also worth noting that the feasibility of performing simultaneous CEC-UV and CEC-MS detection is possible using the cartridge cassette configuration of Fig. 1.6B. Overall, the traditional sintered frit is an unsuitable means of retaining stationary phase in CEC-MS due to bubble formation at the outlet end. This has required the exploration and development of alternative means of CEC-MS column design for retention of the packed stationary bed that eliminates the use of sintered frits at the outlet end of the CEC-MS column.

As mentioned earlier, the use of sintered frit CEC-MS columns are prone to bubble formation causing unstable EOF, irreproducible retention times and peak areas, high baseline noise and poor signal to noise (S/N) ratio. To circumvent these problems the use of a tapered design for retention of the packing at the outlet of the CEC-MS has been first described by Lord et al.¹⁹ In their work, a capillary pulling apparatus utilizing a thumbwheel for rotation of the capillary, a micro-burner for heat, and springs for tension on the fused silica capillary were used to fabricate several types of external and internal tapered capillaries suitable for CEC-MS applications. Most importantly, they showed that tapering the internal channel down to $\sim 10\ \mu\text{m}$ I.D. was able to hold a $3\ \mu\text{m}$ particle size stationary phase firmly in place using the keystone effect. However, they only demonstrated the use of externally tapered CEC-MS columns for the analysis of steroids.¹⁹ These columns were the first application of external taper for CEC-MS, although a significant problem of durability associated with the fragile tapered tip prone to breakage was encountered.

Although the internally tapered column was presented by Lord et al¹⁹ as an alternative to fragile externally tapered columns, its use was not actually demonstrated or applied until Choudhary et al.²⁰ showed the use of internally tapered columns for the separation of PTH-amino acids. An illustration of the externally and internally tapered columns is shown in Figure 1.7.

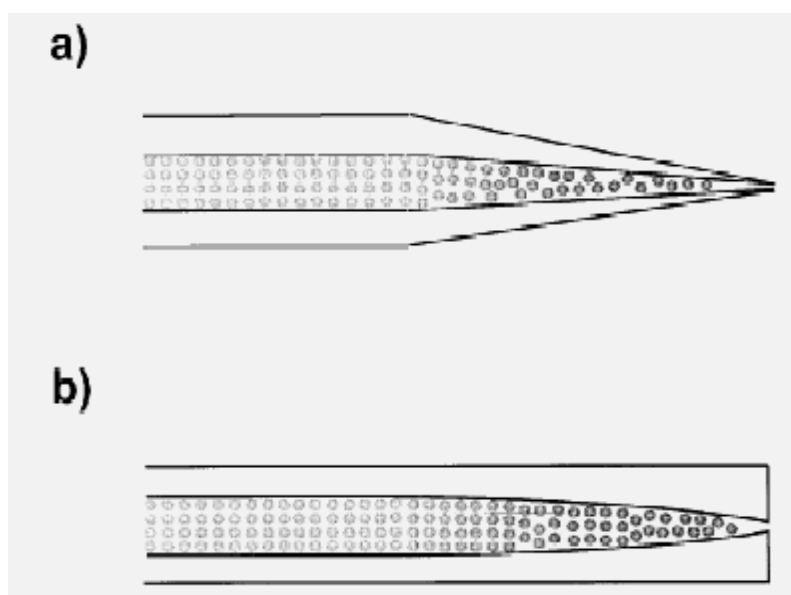


Figure 1.7: Illustration of the (a) externally tapered and the (B) internally tapered CEC column.²⁰

It is noted that in their work of fabricating the internal taper, Choudhary et al followed the design protocol of Lord et al where the fabrication required first tapering the capillary to a closed end or outlet, then using fine grit sand paper to re-open the channel. Considering the important contributions to CEC-MS column fabrication, technology and configuration by both Lord and Choudhary, in our laboratory we provide the first

demonstration of a rugged internally tapered CEC-MS columns suitable for coupling of CEC to both ESI and APCI MS which has never previously been shown before.

Our results showed not only that the columns are more durable than externally tapered columns,²¹ but the feasibility for the CEC-ESI-MS and CEC-APCI-MS analysis of environmentally and industrially relevant chemicals such as various class of surfactants.^{22,23} In addition, an important improvement over the column fabrication method reported by Choudhary and Lord has been implemented in our laboratory. Our initial investigations using the method of tapering the outlet of the CEC-MS column to closure using heat, then re-opening the channel using sandpaper was found to be irreproducible. Most importantly, the diameter of the inner channel was often created too wide using sandpaper whereupon the stationary phase particles were unable to be stabilized in place for extended period of use. Therefore, the step of tapering using sandpaper to widen and re-open the closed channel has been improved.

The fabrication of CEC-MS in our laboratory involves several modifications. For example, instead of re-opening the tapered channel using sandpaper, we have first finely squared the capillary tip using a marble capillary cutter and water for lubrication, then simply used the small micro-torch to create the internal taper of exact and precise dimension which is characterized and calibrated using a digital microscope. Our results compared to the two fabrication techniques has proved to be much easier and reproducible. Using this new design, we have demonstrated that the coupling of CEC with MS detection is now a capable and durable analytical technique that can be complimentary to traditional hyphenated methods such as HPLC-MS and GC-MS. In this

dissertation, several developed methods using the internally tapered CEC-MS column are described.

Applications of CEC-MS. Recently there has been growing interest in CEC-MS, and as a result the number of applications and publications has also increased. Due to the ability to analyze a wide range of analytes including pharmaceutical samples, biomolecules, environmentally relevant toxins, and natural products, CEC-MS is a capable and powerful analytical technique. Therefore, CEC-MS can be applied in the industry, universities, pharmaceutical companies and government regulatory settings for both qualitative and quantitative methodologies. Most of the applications of CEC-MS have been undertaken using packed columns, although monolithic columns where the packing is created in situ are becoming more popular. Several reviews of the state of the art in hyphenation of CEC with MS have been written in the last couple of years.^{24,25,26} A comprehensive review of the current applications has been summarized in Table 1.1 which was compiled by Barcelo-Barrachina et al in 2004.²⁴ They actually describe the type of column outlet which shows that packed column using frits comprises about 95% of the total configurations. In fact, only one internal taper configuration is listed as Choudhary et al which was discussed in the previous section.²⁰ Therefore, the methods described in this dissertation using internal taper CEC-MS columns lay groundwork for further development in the field.

Table 1.1: Applications of CEC-MS. From a recent review in 2004.²⁴ The references are re-stated in this work. IT=ion trap, Q=quadrupole, QqQ=triple quadrupole, TOF=time of flight, FT-ICR=fourier transform ion cyclone resonance.

Compound	Column and outlet end	Separation conditions	Ionization source	Mass analyzer	Ref.
Pharmaceutical compounds					
NSAIDs	Packed C ₁₈ Frits	Isocratic elution Formic acid/ammonia pH 2.5/ acetonitrile	ESI, sheath flow	IT	[27]
NSAIDs	Packed C ₁₈ Frits	Isocratic elution Ammonium formate pH 3.0/ acetonitrile	ESI, sheath flow	IT	[28,29]
Steroids	Packed C ₁₈ External tapered end	Isocratic elution Sodium tetraborate pH 8/ acetonitrile	ESI, sheath flow ESI, sheathless	Q	[19]
Steroids	Packed C ₁₈ /SCX, C ₈ /SCX Frits	Isocratic elution Ammonium acetate pH 4.2/ acetonitrile	Micro-ESI, sheath flow Nano-ESI, sheathless	IT	[30]
Corticosteroids	Packed C ₁₈ /SCX, C ₈ /SCX Frits	Isocratic elution Ammonium acetate pH 4.0/ acetonitrile	Micro-ESI, sheath flow	QqQ	[31]
Corticosteroids	Packed C ₈ /SCX, C ₁₈ , SCX Frits	Isocratic elution Ammonium acetate pH 4.0/ acetonitrile	Micro-ESI, sheath flow	QqQ	[32]
Corticosteroids, salbutamol, salmeterol, tricyclic antidepressants	Packed C ₁₈ /SCX Frits	Isocratic elution Ammonium acetate pH 4.0/ acetonitrile	Micro-ESI, sheath flow	QqQ	[33]

Table 1.3: Applications of CEC-MS continued:

Compound	Column and outlet end	Separation conditions	Ionization source	Mass analyzer	Ref.
Flunitrazepam and metabolites	Packed C ₁₈ Frits	Isocratic elution Formic acid/ammonia pH 8/ acetonitrile	Orthogonal ESI, sheath flow	Q	[34]
Neostigmine, salbutamol, fenoterol	Packed C ₁₈ Frits	Isocratic elution Ammonium acetate pH 5.0/ methanol/water	ESI, sheath flow	Q	[35]
Drug (GW1) and related compounds	Packed C ₁₈ /SCX Frits	Isocratic elution Ammonium acetate pH 3.5/ acetonitrile	ESI, sheath flow	Q	[36]
Salbutamol, nortriptyline, diphenhydramine	Pseudostationary phase with methacrylate nanoparticles	Isocratic elution Ammonium carbonate pH 8.2/ acetonitrile	Orthogonal ESI, sheath flow	IT	[37]
Benzodiazepines, thiazide diuretic drugs	Packed C ₁₈ Frits	Step-gradient elution Ammonium acetate/water/ acetonitrile	ESI, sheath flow	Q	[38]
Sulfonamides	Packed C ₈ Frits	Isocratic elution Ammonium acetate pH 5/ methanol	ESI, sheath flow	Q	[39]
Antiviral drug, nucleotides, alkaloids	Packed C ₁₈ Frits	Isocratic elution Ammonium acetate/aceto- nitrile, methanol/dibutylamine	FAB, liquid junction and sheath flow	Double focus- ing magnetic sector	[40]
Phenytoln, prednisolone, caffeine, thiourea, testosterone, amoxicillin, cefatrizine	Packed C ₈ /SCX Frits	Isocratic elution Sodium dihydrogenphosphate pH 3.5/acetonitrile	ESI	Q	[41]
Biomolecules					
Peptides	Packed C ₁₈ Frits	Isocratic elution Ammonium acetate pH 6.7/ acetonitrile	Nano-ESI, sheath flow	IT	[42]
Peptides	Packed C ₈ , C ₁₈ Frits	Isocratic elution Ammonium acetate pH 6.7/ acetonitrile	Nano-ESI, sheathless	IT	[43]
Peptides	Packed C ₁₈ Frits	Isocratic elution Trifluoroacetic/acetonitrile/ water	ESI, sheathless	QqQ	[44]
Peptides	Packed C ₁₈ Frits	Isocratic elution Ammonium acetate/ acetonitrile	Nano-ESI, sheath flow	IT	[45]
Peptides	Open tubular C ₈ / amino	Linear gradient and isocratic elution Ammonium acetate/ trifluoroacetic acid/ acetonitrile/water	Nano-ESI, sheathless	IT/TOF	[46]
Bovine protein (lactoglobulin A) digests	Packed C ₁₈ Frits	Linear gradient elution Trifluoroacetic acid/water/ acetonitrile	ESI	IT/TOF	[47]
Peptides and horse heart myoglobin	Packed C ₁₈ /NH ₂ Frits	Linear gradient elution Trifluoroacetic acid/acetic acid/water/acetonitrile	ESI	IT/TOF	[48]

Table 1.3: Applications of CEC-MS continued:

Compound	Column and outlet end	Separation conditions	Ionization source	Mass analyzer	Ref.
Peptides and bovine serum albumin digests	Monolithic, methacrylate-based, amino functional group	Linear gradient and isocratic elution Acetic acid/acetonitrile/water	ESI, sheathless	IT and TOF	[49]
Bovine hemoglobins digests	Microchip with a methacrylate-based monolith, and amino functional group	Isocratic elution Ammonium acetate pH 4.6/ methanol	Microchip ESI	TOF	[50]
Proteins	Packed with size-exclusion chromatography particles Frits	Isocratic elution Formic acid/acetonitrile/water	ESI	QqQ	[51]
Trypsin and chicken ovalbumin digests	Packed C ₁₈ Glass wool in column end-fittings	Linear gradient elution Trifluoroacetic acid/ acetonitrile/water	ESI	IT/TOF	[52]
Aromatic glucuronides	Packed with polymer Filters	Isocratic elution Ammonium acetate pH 7/ acetonitrile	ESI, sheath flow	QqQ	[53]
Phenylthiohydantoin amino acids	Packed C ₁₈ Internal tapered end	Linear gradient and isocratic elution Ammonium acetate/ acetonitrile	ESI, sheath flow	Linear TOF	[20]
Polycyclic aromatic hydrocarbons – DNA adducts	Packed C ₁₈ Frits	Isocratic elution Ammonium acetate/ acetonitrile	Micro-ESI, sheath flow	QqQ	[54,55]
Styrene oxide nucleoside adducts	Packed C ₁₈ Frits	Isocratic elution Ammonium acetate/ acetonitrile/methanol	Micro-ESI, liquid junction	QqQ	[56]
Steroids	Monolithic, acrylamide-based C ₁₂ functional group	Linear gradient elution Ammonium formate pH 3.0/ acetonitrile/water	Nano-ESI, sheath flow	IT	[57]
Bile acids	Monolithic, acrylamide-based C ₁₂ and amino functional groups	Isocratic elution Ammonium formate pH 3.0/ acetonitrile/water	Nano-ESI, sheath flow	IT	[58]
Saccharides	Monolithic, acrylamide-based cyano and amino functional groups	Isocratic elution Ammonium formate pH 3.0/ acetonitrile/water	Nano-ESI, sheath flow	IT	[59,60]
Saccharides	Monolithic, acrylamide-based cyano functional group	Isocratic elution Ammonium formate pH 3.0/ acetonitrile/water	Nano-ESI, sheath flow	FT-ICR	[61]
Natural products					
Whitanolides in plant extract	Packed C ₁₈ Frits	Isocratic elution Formic acid-ammonia pH 8/ acetonitrile	Orthogonal ESI, sheath flow	Q	[62]
Crude extract of ergot fungus	Packed C ₁₈ Frits	Linear gradient elution Acetonitrile/water	ESI	QqQ	[51]

Table 1.3: Applications of CEC-MS continued:

Compound	Column and outlet end	Separation conditions	Ionization source	Mass analyzer	Ref.
Enantiomers					
Hexobarbital	Open tubular, bonded cyclodextrin	Isocratic elution Ammonium acetate pH 7.2	ESI, sheath flow	Q	[64]
Barbiturates and chlorinated alkyl phenoxypropanoates	Packed with cyclodextrin Frits	Isocratic elution Ammonium acetate pH 6.6/ acetonitrile/water	CIS, orthogonal, sheath flow (Ag ⁺ , Co ²⁺ , Cu ²⁺ , Li ⁺)	QqQ	[65]
Miscellaneous					
Food colors	Packed C ₁₈ Filters	Isocratic elution Ammonium acetate pH 8.5/ methanol	ESI, sheath flow	QqQ	[53]
Textile dyes	Packed C ₁₈ No frits	Isocratic elution Sodium tetraborate pH 8/ acetonitrile	ESI, sheath flow	Q	[66]
Dansylated secondary amine tags	Packed C ₁₈ /SCX Frits	Isocratic elution Ammonium acetate pH 4.0/ acetonitrile	Micro-ESI, sheath flow	QqQ	[31]
Unsaturated fatty acid methyl esters, vitamins D ₂ and D ₃ , estrogens	Packed C ₁₈ Frits	Isocratic elution Ammonium acetate pH 9/ acetonitrile	CIS, orthogonal, sheath flow (Ag ⁺)	QqQ	[67]
Arsenic, chromium, and selenium species	Open tubular, bonded macrocyclic polyamine	Isocratic elution pyromellitate pH 6.0, phosphate pH 6.5, acetate pH 6.0	Cross-flow nebulizer, ICP	ICP, Q	[68]

Following this review in 2004, a more recent application of CEC-MS in the Journal of Chromatography A describes the utilization of both a tapered inlet and tapered outlet for analysis of eight triazines.⁶⁹ Also since 2004, applications of CEC-MS published in Analytical Chemistry on CEC-MS not including work from our laboratory entail peptide analysis using open tubular coated columns⁷⁰ and neutral compounds using nanoparticle full filling technique.⁷¹ Finally, in Electrophoresis since 2004 there are three additional articles that have applied CEC-MS in their investigations (not including work from our lab). The applications include 1) Analysis of triazines by capillary electrochromatography/electrospray ionization-mass spectrometry using a low-flow

sheath liquid interface⁷² which is also published in JCA mentioned above, 2) Speciation of selenium compounds by open tubular capillary electrochromatography-inductively coupled plasma mass spectrometry,⁷³ and 3) on-line concentration of proteins in pressurized capillary electrochromatography coupled with electrospray ionization mass spectrometry.⁷⁴ To date, there are no published reports on the analysis of surfactants which are environmental and industrially relevant compounds.

Analysis of Surfactants. Surfactants are common ingredients in many household and industrial cleaning agents. Typically, there can be several tens to hundreds or even thousand of structurally similar homologues, isomers, and oligomers comprising the detergent formulation. Therefore, the necessity for chromatographic separation is warranted if these compounds are to be characterized for environmental or industrial investigations. In addition, the need for sensitive and selective detection of these compounds is well suited for mass spectrometry which can provide low limit of detection along with the ability to provide important structural information. Although HPLC-MS is usually employed for the analysis of surfactant systems, there is a need for alternative analytical methodologies especially due to the large solvent consumption inherent to HPLC. Therefore, in this work the CEC-MS application to several different classes of surfactants is described.

General Properties of Surfactants. Surfactants are surface active compounds that contain both a hydrophilic head group and a hydrophobic alkyl chain of varying length.⁷⁵

As a result, these compounds have the natural tendency to form micelles in aqueous solutions. Surfactants can be classed according to the functionality of the hydrophilic head group either as anionic, cationic or a combination of both which are called zwitterionic, or neutral which are known as nonionic surfactants. The focus of the CEC-MS methods and applications in this work is on zwitterionic, cationic and nonionic surfactants.

Zwitterionic or amphoteric surfactants contain both acidic and alkaline functionalities. The most common type of zwitterionic surfactant are the alkyl betaines (Figure 1.8). The chemical structures typically contain a quaternized nitrogen functionality as well as an anionic group such as carboxylate, sulfate or oxide. Betaine type surfactants are characterized by a fully quaternized nitrogen atom and do not exhibit anionic properties in alkaline solutions, which means that betaines are present only as 'zwitterions'.⁷⁶ Uses of zwitterionic surfactants include personal care products (e.g. liquid soaps, hair shampoos and conditioners, and cleansing lotions) and in all-purpose and industrial cleaning agents. By volume, the most important groups of amphoteric surfactants today consist of alkylamido betaines and alkyl betaines.⁷⁶

Cationic surfactants are surface-active compounds with at least one hydrophobic alkyl chain and a hydrophilic group that is capable of possessing a positive charge. These surfactants maintain a positive charge in aqueous solutions. The quaternary ammonium cationic surfactants are one of the most popular type used in commercial products and formulations. These quaternary ammonium compounds maintain a positive charge at all times due to the quaternary nitrogen atom. Commercial raw materials are normally

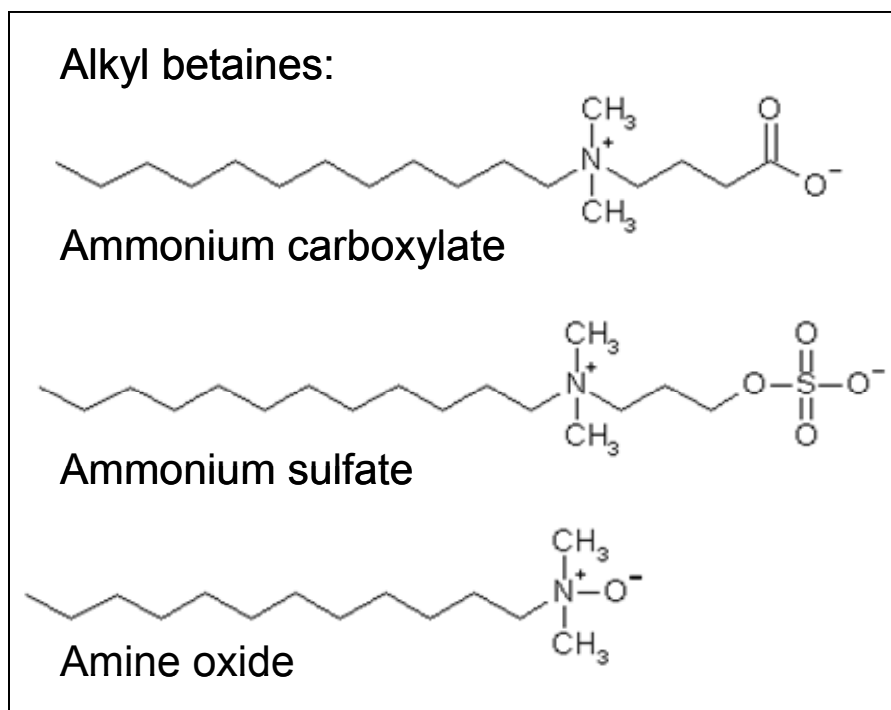


Figure 1.8: Chemical structures of the alkyl betaines which are most common types of amphoteric or zwitterionic surfactants.

derived from natural oils which implies that homologous mixtures of surfactants with different alkyl chain lengths are used in the products.⁷⁶ Additional applications of cationic surfactants include fabric softeners, hair conditioners, and other hair formulations. Disinfectants, biocides, emulsifiers, wetting agents, and processing additives also contain cationic surfactants. By volume, the most important cationic surfactants in household products are the alkyl ester ammonium salts that are used in fabric softeners.⁷⁶ Several different types of cationic surfactants are illustrated in Figure 1.9.

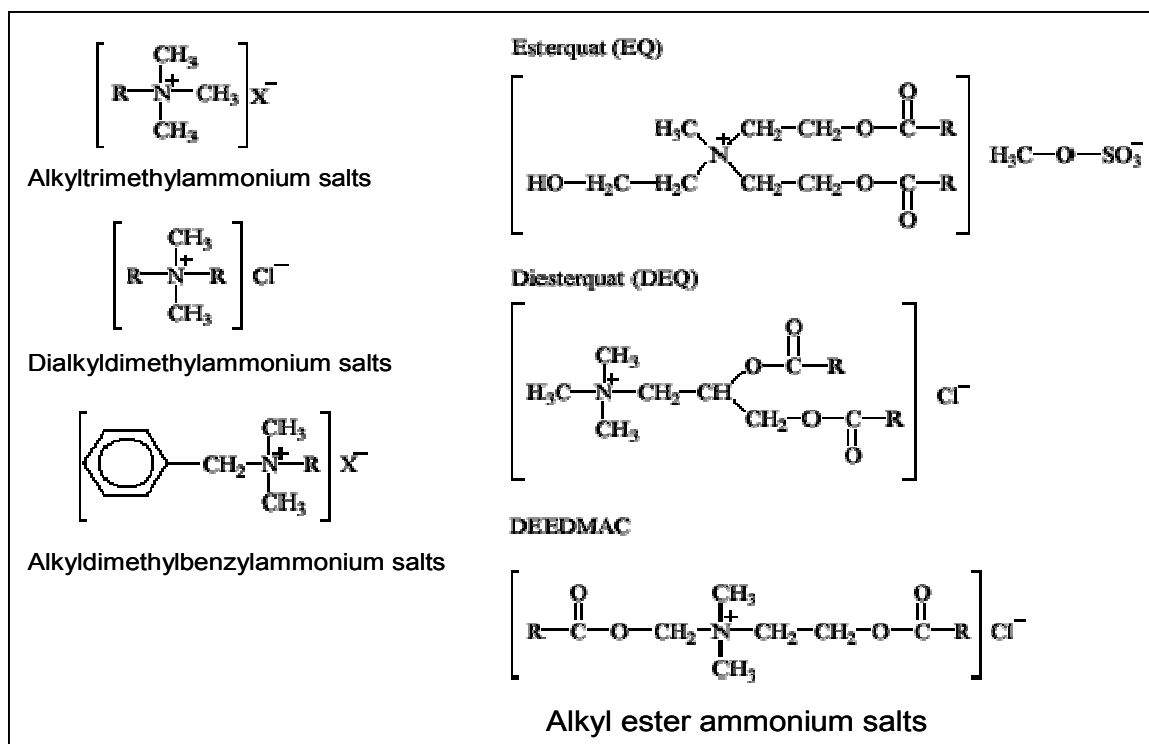


Figure 1.9: Different types of cationic surfactants.⁷⁶

Nonionic surfactants are surface-active compounds that contain both hydrophobic and hydrophilic moieties. However, these surfactants are not able to be ionized in aqueous solutions. Commercial nonionic surfactants are typically a mixture of homologous structures comprised of alkyl chains that vary in the number of carbons and with hydrophilic moieties that differ in the number of ethylene oxide (ethoxylate, EO), propylene oxide (propoxylate, PO) and butylene oxide (butoxylate, BO) units.⁷⁶ Uses of nonionic surfactants include consumer products such as laundry detergents, personal care products, and cleaning and dishwashing agents. Nonionic

surfactants are also used as ingredients in industrial formulations and as solubilizing agents in biotechnological applications. By volume, the most important nonionic surfactants are included in the very versatile group of alcohol ethoxylates and alcohol alkoxyates.⁷⁶ The most common types of nonionic surfactants are shown below in Figure 1.10.

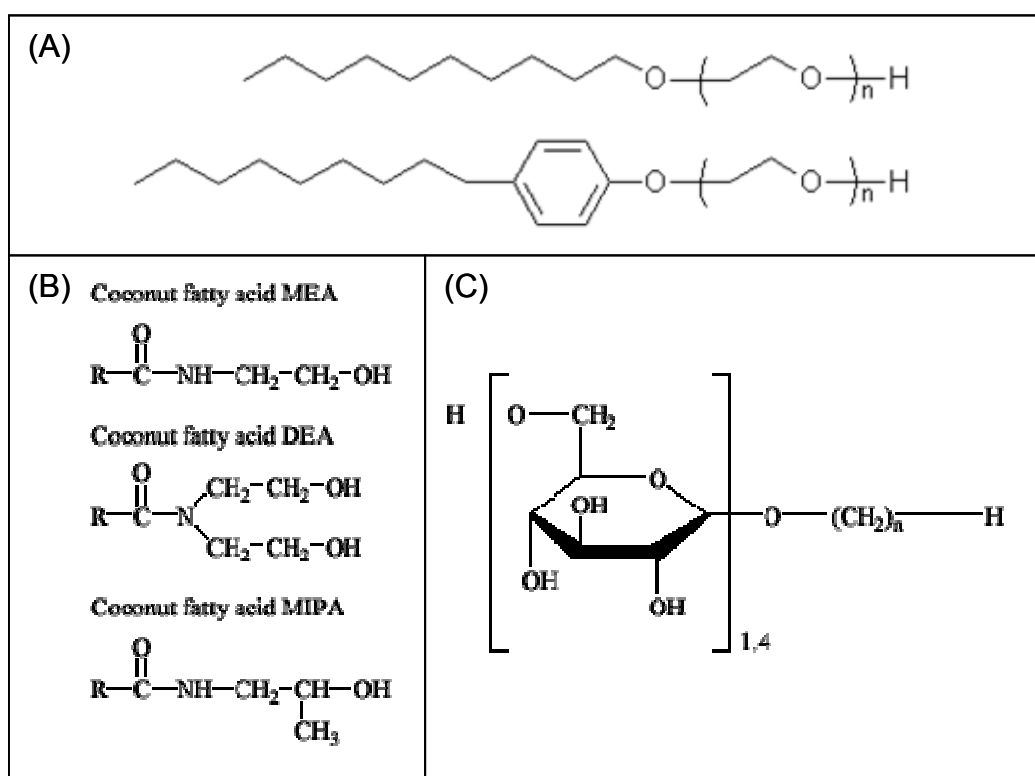


Figure 1.10: Different types of nonionic surfactants including (A) alcohol and alkylphenol ethoxylates, (B) fatty acid diethanolamides, and (C) alkylpolyglucosides.⁷⁵

Development of a New CEC Stationary Phase. As CEC is still a relatively new technique compared to traditional techniques such as HPLC or gas chromatography (GC), there are few stationary phases commercially available that are dedicated to CEC.

In order to broaden the scope and applications of CEC, it is important to develop new stationary phases accordingly that are capable of improved molecular recognition. This in turn will provide fundamental insight into separation mechanics of CEC, and promote further understanding for the separation of a broad class of analytes using the powerful and capable technique. For these reasons, the synthesis of a novel stationary phase for CEC is undertaken.

Recently, the application of cholesteric liquid crystalline stationary phases have been applied in HPLC.⁷⁷⁻⁹⁴ Interestingly, an extensive literature search shows that these liquid crystalline stationary phases are only applied in CEC using the open tubular approach to coat the inside of the capillary.^{83, 95-97} Therefore, an alternative approach of bonding these molecules to silica for use in packed column CEC can be considered novel in this field. The results of this work will therefore contribute better scientific understanding for application of liquid crystalline stationary phases applied to packed column CEC.

There are several features of these specialized cholesteric phases that are attractive for use in chromatography including CEC. Most importantly, an extensive cyclic ring network that maintains specific order provide the possibility for separations based on cyclic ring interaction with planar molecules such as PAH (of environmental importance). In the final chapter of this dissertation, lithocholic acid was chosen as a representative steroidal ligand to attach to silica as it possesses a carboxylic functional group at the terminal end which was expected to aid in generating electroosmotic flow (EOF) in the CEC system. It is also noted that a literature search resulted in no

applications of this phase in CEC, thus this work can be considered a novel approach. A survey of the properties and separation capabilities of a cholesteric liquid crystalline steroidal lithocholic acid stationary phase is reported. The surface properties of the stationary phases before and after modification have been carefully characterized using several physiochemical techniques such as nuclear magnetic resonance (NMR), elemental analysis and finally chromatography using several different classes of analytes.

To our knowledge, this dissertation is the first presentation of CEC-MS applications for analysis of different classes of surfactants. In addition, there is one novel CEC-UV method for analysis of nonionic surfactants that is included as part of the study, as well as the application of liquid crystalline stationary phase in CEC and CEC-MS.

References:

- (1) Mould, D.L., Synge, R.L.M. *Analyst* **1952**, 77, 964.
- (2) Mould, D.L., Synge, R.L.M. *J. Biochem.* **1954**, 58, 571.
- (3) Pretorius, V., Hopkins, B.J., Schieke, J.D., *J. Chromatogr.* **1974**, 99, 23.
- (4) Jorgenson, J.W., Lukacs, K.D. *J. Chromatogr.* **1981**, 218, 209.
- (5) Knox, J.H., Grant, I.H. *Chromatographia* **1987**, 24, 135.
- (6) Knox, J.H., Grant, I.H. *Chromatographia* **1991**, 32, 317.
- (7) Bartle, K.D., Meyers, P. *J. Chromatogr. A* **2001**, 916, 3-23.
- (8) Shaw, D.J. *Electrophoresis*, Academic Press, London, **1969**.
- (9) Foret, F., Bocek, P. *Adv. Electrophoresis* **1990**, 3, 272.
- (10) Solomon, K., Burgi, D.S., Helmer, J.C. *J. Chromatog. A* **1991**, 559, 69.
- (11) Ross, G.A., Rozing, G.P. (Eds.), *Capillary Electrochromatography-Technology and Applications, CEC-Guidebook*, Publ. Num. 5968-9892E, Agilent Technologies, Germany, **2000**.
- (12) Bartle, K.D., Meyers, P. (Eds.), *Capillary Electrochromatography*, The Royal Socieity of Chemistry, Cambridge, UK, **2001**, pp.7-8.
- (13) Chapman, S. *Physical Review* **1937**, 10, 184.
- (14) Dole, M. *Journal of Chemical Physics* **1968**, 49, 2240.
- (15) Fenn, J.B. *Journal of Physical Chemistry* **1984**, 88, 4451.
- (16) Fenn, J.B. *Agewandte Chemie - International Edition* **2003**, 42, 3871.
- (17) www.chm.bris.ac.uk. Bristol University.
- (18) Hoffman, E.de, Stroobant, V., Eds. In: *Mass Spectrometry, Principles and*

Applications, Second Edition, John Wiley and Sons, West Sussex, England, **2002**, p.45.

- (19) Lord, G.A., Gordon, D.B., Myers, P., King, B.W. *J. Chromatogr. A* **1997**, 768, 9.
- (20) Choudhary, G., Horváth, C., Fred Banks, J. *J. Chromatogr. A* **1998**, 828, 469.
- (21) Zheng, J., Norton, D., Shamsi, S.A. *Anal. Chem.* **2006**, 78, 1323.
- (22) Norton, D., Zheng, J., Danielson, N.D., Shamsi, S.A. *Anal. Chem.* **2005**, 77, 6874.
- (23) Norton, D., Rizvi, S.A.A., Shamsi, S.A. *Electrophoresis* **2006**, 27, 4273.
- (24) Barceló-Barrachina, E., Moyano, E., Galceran, M.T. *Electrophoresis* **2004**, 25, 1927.
- (25) Klampfl, C.W. *J. Chromatogr. A* **2004**, 1044, 131.
- (26) Shamsi, S.A., Miller, B. E. *Electrophoresis* **2004**, 25, 3927.
- (27) Desiderio, C., Fanali, S. *J. Chromatogr. A* **2000**, 895, 123.
- (28) Strickman, D.B., Chankvetadze, B., Blaschke, G., Desiderio, C., Fanali, S. *J. Chromatogr. A* **2000**, 887, 393.
- (29) Strickman, D.B., Blaschke, G. *J. Chromatogr. B* **2000**, 748, 213.
- (30) Warriner, R.N., Craze, A.S., Games, D.E., Lane, S.J. *Rapid Commun Mass Spectrom.* **1998**, 12, 1143.
- (31) Lane, S.J., Tucker, M.G. *Rapid Commun. Mass Spectrom.* **1998**, 12, 947.
- (32) Spikmans, V., Lane, S.J., Tjaden, U.R., van der Greef, J. *Rapid Commun. Mass Spectrom.* **1999**, 13, 141.
- (33) Spikmans, V., Lane, S.J., Smith, N.M. *Chromatographia* **2000**, 51, 18.

- (34) Cahours, X., Cherkaoui, S., Rozing, G., Veuthey, J.L. *Electrophoresis* **2002**, 23, 2320.
- (35) Mazereeuw, M., Spikmans, V., Tjaden, U.R., van der Greef, J. *J. Chromatogr. A* **2000**, 879, 219.
- (36) Paterson, C.J., Boughtflower, R.J., Higton, D., Palmer, E. *Chromatographia* **1997**, 46, 599.
- (37) Viberg, P., Jorntenkarlsson, M., Petersson, P., Spegel, P., Nilsson, S. *Anal Chem* **2002**, 74, 4595.
- (38) Taylor, M.R., Teale, P. *J. Chromatogr. A* **1997**, 768, 89.
- (39) Dekkers, S.E.G., Tjaden, U.R., van der Greef, J. *J. Chromatogr. A* **1995**, 712, 201.
- (40) Verheij, E.R., Tjaden, U.R., Niessen, V.M.A., van der Greef, J. *J. Chromatogr.* **1991**, 554, 339.
- (41) Boughtflower, R.J., Paterson, C.J., Knox, J. *J. Chromatogr. A* **2000**, 887, 409.
- (42) Gaspari, M., Guček, M., Walhagen, K., Vreeken, R.J., Verheij, E.R., van der Greef, J. *J. Microcol. Sep.* **2001**, 13, 243.
- (43) Guček, M., Gaspari, M., Walhagen, K., Vreeken, R.J., Verheij, E.R., van der Greef, J. *Rapid Commun Mass Spectrom* **2000**, 14, 1448.
- (44) Schmeer, K., Behnke, B., Bayer, E. *Anal. Chem.* **1995**, 67, 3656.
- (45) Walhagen, K., Gaspari, M., Tjaden, U.R., Rozing, G.P., van der Greef, J. *Rapid Commun. Mass Spectrom.* **2001**, 15, 878.
- (46) Wu, J.T., Huang, P.Q., Li, M.X., Qian, M.G., Lubman, D.M. *Anal. Chem.* **1997**, 69,

320.

- (47) Huang, P.Q., Wu, J.T., Lubman, D.M. *Anal. Chem.* **1998**, 70, 3003.
- (48) Huang, P.Q., Jin, X.Y., Chen, Y.J., Srinivasan, J.R., Lubman, D.M. *Anal. Chem* \ **1999**, 71, 1786.
- (49) Ivanov, A.R., Horváth, C., Karger, B.L. *Electrophoresis* **2003**, 24, 3663.
- (50) Lazar, I.M, Li, L., Yang, Y., Karger, B.L. *Electrophoresis* **2003**, 24, 3655.
- (51) Stahl, M., Jakob, A., von Brocke, A., Nicholson, G., Bayer, R. *Electrophoresis* **2002**, 23, 2949.
- (52) Wu, J.T., Huang, P.Q., Li, M.X., Lubman, D.M. *Anal. Chem.* **1997**, 69, 2908.
- (53) Hugener, M., Tinke, A.P., Niessen, W.M.A., Tjaden, U.R., van der Greef, J. *J. Chromatogr.* **1993**, 647, 375.
- (54) Ding, J.M, Vouros, P. *Anal. Chem.* **1997**, 69, 379.
- (55) Ding, J.M, Vouros, P. *J. Chromatogr. A* **2000**, 887, 103.
- (56) Ding, J.M., Barlow, T., Dipple, A., Vouros, P. *J. Am. Soc. Mass Spectrom.* **1998**, 9, 823.
- (57) Que, A.H., Palm, A., Baker, A.G., Novotny, M.V. *J. Chromatogr. A* **2000**, 887, 379.
- (58) Que, A.H., Konse, T., Baker, A.G., Novotny, M.V. *Anal. Chem.* **2000**, 72, 2703.
- (59) Que, A.H., Novotny, M.V. *Anal. Chem.* **2002**, 74, 5184.
- (60) Que, A.H., Novotny, M.V. *Anal. Bioanal. Chem.* **2003**, 375, 599.
- (61) Que, A.H., Mechref, Y., Huang, Y.P., Taraszka, J.A., Clemmer, D.E., Novotny, M.V. *Anal. Chem.* **2003**, 75, 1684.

- (62) Cherkaoui, S., Cahours, X., Veuthey, J.L. *Electrophoresis* **2003**, 24, 336.
- (63) M. Stahl, A. Jakob, A. von Brocke, G. Nicholson, R. Bayer, *Electrophoresis* 23 (2002) 2949.
- (64) Schurig, V., Mayer, S. *J.Biochem. Biophys. Methods* **2001**, 48, 117.
- (65) von Brocke, A., Wistuba, D., Gfroerer, P., Stahl, M., Schurig, V., Bayer, E. *Electrophoresis* **2002**, 23, 2963.
- (66) Lord, G.A., Gordon, D.B., Tetler, L.W., Carr, C.M. *J. Chromatogr. A* **1995**, 700, 27.
- (67) Rentel, C., Gfroerer, P., Bayer, E. *Electrophoresis* **1999**, 20, 2329.
- (68) Chen, W.H., Lin, S.Y., Liu, C.Y. *Anal. Chim. Acta* **2000**, 410, 25.
- (69) Chen, C.J., Chang, C-H, Her, G-R *J. Chromatogr. A*, in press (**2007**).
- (70) Yang, Y., Boysen, R.I., Matyska, M.T., Pesek, J.J., Hearn, M.T.W. *Anal. Chem.* ASAP article, **2007**.
- (71) Wilsson, C., Viberg, P., Spegel, P., Jornten- Carlsson, M., Peterson, P., Nilsson, S. *Anal. Chem.* **2006**, 78, 6088.
- (72) Chang, C-H, Chen, C.J., Chuang, Y-C. *Electrophoresis* **2006**, 27, 4303.
- (73) Lin, S-Y, Wang, G-R, Huang, Q-P, Liu, C-Y *Electrophoresis* **2006**, 27, 4257.
- (74) Liang, Z., Zhang, L., Duan, J., Yan, C., Zhang, W., Zhang, Y. *Electrophoresis* **2005**, 26, 1398.
- (75) Eichhorn, P. in: Knepper, T.P.; Barceló, D.; de Voogt, P. , (Eds.) *Comprehensive Analytical Chemistry: Analysis and Fate of Surfactants in the Environment*, 1st ed.; Elsevier Science: Amsterdam, (**2003**).

- (76) Danish EPA project 615, (2001).
- (77) B.Buszewski et al. *J Chromatogr. B* **2003**, 792, 279.
- (78) B.Buszewski et al. *J Chromatogr. A* **1999**, 845, 433.
- (79) B.Buszewski et al. Review: *J. High Resol. Chromatogr.* **1998**, 21, 267.
- (80) B.Buszewski et al. *Chromatographia* **1998**, 48, No.9/10
- (81) Al-Haj et al *J Pharm and Biomed Analysis* **1998**, 18, 721.
- (82) Matyska et al. *Chromatographia* **2005**, 61, N0. 7/8.
- (83) Wleerowicz et al. *Biomed.l Chromatogr* **2005**, 19, 725.
- (84) Engelhardt et al *J Chromatogr* **1991**, 544, 371.
- (85) Kohler et al *J Chromatogr* **1987**, 385, 125.
- (86) B. Buszewski et al *J ChromatogrA.* **1994**, 673, 11.
- (87) B. Buszewski et al *J Chromatogr* **1991**, 552, 415.
- (88) Albert et al. B. *J Chromatogr* **1991**, 544, 345.
- (89) B. Buszewski et al *J Chromatogr* **1990**, 520, 237.
- (90) B. Buszewski et al *J Chromatogr* **1990**, 499, 305.
- (91) Nawrocki J. *J Chromatog. A* **1997**, 779, 29.
- (92) Pesek et al *J ChromatogrA* **2003**, 986, 253.
- (93) B. Buszewski et al *Anal Chem* **1997**, 69, 3277.
- (94) Matyska et al. *Anal Chem* **2001**, 73, 5116-5125.
- (95) Pesek et al *Electrophoresis* **2004**, 25, 1211-1218.
- (96) Matyska et al. *Anal Chem* **1999**, 71, 5508-5514.

Chapter 2:
Capillary Electrophoresis- Mass Spectrometry (CEC- MS)
of Zwitterionic Surfactants

Abstract

This work describes the on-line hyphenation of a packed capillary electrochromatography (CEC) column with an internally tapered tip coupled to electrospray ionization-mass spectrometry (ESI-MS) and atmospheric pressure chemical ionization-mass spectrometry (APCI-MS) for the analysis of betaine-type amphoteric or zwitterionic surfactants (Zwittergent®). A systematic investigation of the CEC separation and MS detection parameters comparing ESI and APCI is shown. First, a detailed and optimized manufacturing procedure for fabrication of the CEC-MS column with a reproducible internally tapered tip (7-9 μm) is presented. Next, the optimization of the separation parameters by varying the C_{18} stationary phase particle size (3 μm versus 1.5 μm), as well as mobile phase composition including acetonitrile (ACN) volume fraction, ionic strength and pH is described. The optimized separation is achieved using 3 μm C_{18} packing with 75% ACN (v/v), 5 mM Tris at pH 8.0. Optimization for on-line CEC-ESI-MS detection is then done varying both the sheath liquid and spray chamber parameters while evaluating the use of random versus structured factorial table experimental designs. The more structured approach allows fundamental analysis of individual ESI-MS parameters while minimizing CEC and MS equilibration time between settings. A comparison of CEC-ESI-MS to CEC-APCI-MS using similar sheath and spray chamber conditions presents new insight for coupling of CEC to APCI-MS. The sheath liquid flow rate required to maintain adequate sensitivity is much higher in APCI source (50 $\mu\text{L}/\text{min}$) as compared to ESI source (3 $\mu\text{L}/\text{min}$). The on-line mass spectra obtained in the full scan-mode show that fragmentation in the two sources occur at different positions on the Zwittergent® molecules. For ESI-MS, the protonated molecular ion is always highest

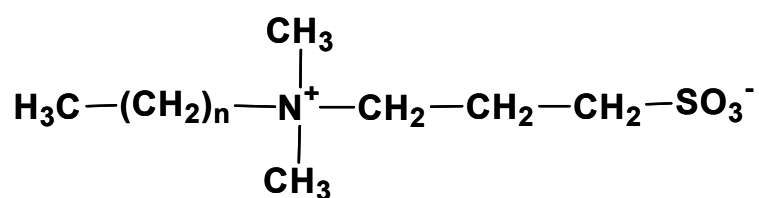
in abundance with minor fragmentation occurring due to the loss of the alkyl chain. In contrast, the APCI-MS spectra show that the highest abundant ion resulted by elimination of propane sulfonate from the Zwittergent® molecule. A comparison of the sensitivity between the two sources in positive ionization SIM mode shows that CEC-ESI-MS provides an impressive limit of detection (LOD) of 5 ng/mL, which is at least 3-orders of magnitude lower than CEC-APCI-MS (LOD 100 µg/mL). Finally, the optimized CEC-MS methods comparing ESI and APCI are applied for separation and structural characterization of a real industrial zwittergent sample, *Rewoteric AM CAS*.

Introduction

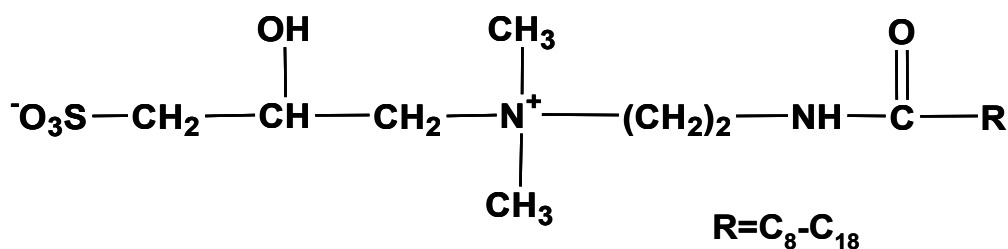
Surfactants are an important class of chemical compounds that are utilized in large quantity for a variety of domestic and industrial manufacturing applications. Of the four classes including anionic, cationic, amphoteric, and nonionic, the amphoteric or zwitterionic type are considered to be specialty surfactants because they account for typically 5% of the total surfactant trade.¹ However, this demand is expected to grow significantly in the coming years due to their unique ability to impart a milder and softer feel to the end product. Zwitterionic surfactants are often used as ingredients in personal care products such as shampoos, conditioners, liquid soaps, and cosmetics, as well as in industrial all purpose cleaning agents. In addition, the ionic charge balance of zwitterionic surfactant makes them well suited as detergents for cell membrane solubilization due to a decreased potential for irreversible binding to charged compounds. Therefore, it is important to develop improved analytical techniques for characterization of these surfactants.

The separation and analysis of zwitterionic surfactants into the various homologues comprising these complex mixtures is of importance for two reasons. First, during the manufacturing process it is necessary to monitor their purity and composition as small imperfections or batch-to-batch variation can adversely affect the performance. Second, since the vast majority of these surfactants ultimately find their way into the matrices of environmental origin and wastewater facilities, it is of utmost concern to evaluate the persistence and degradation of these compounds. There are several inherent properties of betaine zwitterionic surfactants which pose a significant challenge to the

analytical chemist. First, in the case of amidosulfobetaines detergents (aka, Zwittergent®, Figure 2.1), the presence of both a strongly basic quaternary ammonium ion and an acidic sulfonate of equal strength creates a strong intermolecular balance of charge over a wide pH range. This results in no net net charge, conductivity, or electrophoretic mobility, as well as insensitivity for the most part to variation in separation conditions including pH, ionic strength, and temperature. Second, the majority of zwitterionic surfactants including Zwittergent® possess no chromophore which renders ultraviolet (UV) detection not feasible.



Zwittergent® 3-08 $n=7$
Zwittergent® 3-10 $n=9$
Zwittergent® 3-12 $n=11$
Zwittergent® 3-14 $n=13$
Zwittergent® 3-16 $n=15$



Rewoteric AM CAS
Commercial Sample

Figure 2.1: Chemical structure of the Zwittergent standards and the *Rewoteric AM-CAS* commercial sample.

To date, the vast majority of methods developed for separation of surfactant formulations containing various homologues of zwitterionic betaines have utilized reversed phase high performance liquid chromatography (RP-HPLC).² This is mainly because other methods of separation such as ion exchange chromatography are less feasible due to the strong internal charge balance of amphoteric surfactants, and are better suited for analysis of cationic or anionic surfactants.³ Several examples of RP-HPLC coupled to a variety of detectors such as UV,⁴ chemiluminescent nitrogen,⁵ and mass spectrometry (MS) have been introduced for zwitterionic surfactants.^{1,6-8} The drawbacks to the former two detection methods are that not all zwitterionic surfactants contain a chromophore or nitrogen functionality, whereas the MS methods are more universal because most zwitterionic surfactants can be ionized and detected using either the positive or negative mode. In many cases, there is considerable room for improved separation performance regarding chromatographic efficiency, higher peak capacity and speed of analysis. Therefore, this opens the door for the development of new and innovative methods for these complex and difficult analytes.

Electrodriven separation techniques such as capillary electrochromatography (CEC) coupled to MS offer a powerful alternative to the aforementioned methods of analysis. Currently, CEC-MS has the ability to complement HPLC-MS by utilizing most of the same methodology. However, CEC has the potential to surpass HPLC because the former separation method is based upon a combination of electrophoretic and chromatographic mechanisms. Several advantages of CEC-MS over HPLC-MS include higher plate numbers (N) attainable in CEC-MS, as well as more compatible flow rate

(sub-micro liter) when coupled to ESI-MS, and finally less consumption of toxic organic solvents. Consequently, the number of CEC-MS publications in recent years has seen substantial growth that encompasses a variety of useful applications.⁹⁻¹⁸ There are also several current review articles covering the hyphenation of CEC to MS, which reiterates the growing interest in establishment of the technique.¹⁹⁻²¹ Furthermore, since CEC-MS is still a relatively new technique as compared to LC-MS, there is still a need for fundamental study which will help to deliver this powerful hyphenation methodology to the mainstream. These concepts include study of MS compatible packings, column frit preparation,²²⁻²⁴ interfacing CEC to new ionization sources and mass analyzers,²⁵⁻²⁸ and finally development of tapers and restrictors not only for retention of the packing material, but also to achieve stable electrospray.²⁹⁻³⁰

Although there is numerous literature for LC-MS comparing ESI to APCI,³¹⁻³⁴ our literature search provided only one report each for CE-APCI-MS and CEC-APCI-MS respectively.^{35,25} In addition, there is only one report that shows the application of an internally tapered CEC-MS column for analysis of phenylthiohydantoin amino acids.²⁹ In this report, we demonstrate the use of a hydrophobic, non-encapped C₁₈ stationary phase with an internally tapered CEC-MS column for the separation of a variety of non-chromophoric C₈-C₁₈ Zwittergent® surfactant mixtures. We believe that the use of the internal tapered CEC column is a key to the development of a stable and rugged on-line CEC-MS. To the best of our knowledge, this is the first known report of CEC-MS that entails the analysis of zwitterionic surfactants while comparing the ability of both electrospray (ESI)-MS and atmospheric pressure chemical ionization (APCI)-MS

ionization sources. Therefore, our work presents novel insight for coupling of CEC to APCI-MS, as well as comments on the method development using both ESI and APCI sources. A rugged, stable and sensitive hyphenated method is developed by a careful evaluation of both CEC and MS parameters. The CEC-ESI-MS and CEC-ESI-APCI spectra of the standard Zwittergent® and a commercial sample are compared, which provide a useful source of spectral library for these detergents.

EXPERIMENTAL SECTION

Reagents and Chemicals. The 3- μm CEC Reliasil ODS-1 (100Å pore size) non-endcapped stationary phase was purchased from Column Engineering Inc. (Ontario, CA, USA). Platinum EPS C₁₈ 1.5- μm (100Å pore size) packing was purchased from Alltech Associates, Inc. (Deerfield, IL, USA). Zwitterionic amidosulfobetaines detergents, (Zwittergent®) 3-08, 3-10, 3-12, 3-14, 3-16 were obtained from Calbiochem (La Jolla, CA, USA). It can be seen in Figure 2.1 that annotation 3-# refers to the nitrogen atom at position 3, followed by the number of carbons (C₈-C₁₆) in the aliphatic tail (e.g., C₈H₁₇-C₁₆H₃₃). *Rewoteric AM CAS* (an aqueous solution of fatty acid amido alkyl betaine) was kindly donated from Degussa Goldschmidt Chemical Corporation (Hopewell, VA, USA). Acetonitrile (ACN) and methanol (MeOH) of HPLC grade were purchased from Burdick and Jackson (Muskegon, MI, USA). Tris (hydroxymethyl) aminomethane (Tris) (99.9+%) was purchased from Sigma Chemical Company (St. Louis, MO, USA).

Ammonium hydroxide (NH_4OH), acetic acid (HOAc), hydrochloric acid (HCl) and sodium chloride (NaCl) were supplied by Fisher Scientific (Springfield, NJ, USA). Acetone of HPLC grade was purchased from EM Science (Gibbstown, NJ, USA). Ammonium formate (A.F.) (97%) was obtained from Aldrich (Milwaukee, WI, USA). Finally, water was purified by a Barnstead Nanopure II purification system (Barnstead International, Dubuque, IA, USA).

CEC-MS Column Fabrication. Fused silica capillary (o.d. $363\ \mu\text{m}$, i.d. $75\ \mu\text{m}$) obtained from Polymicro Technologies Inc. (Phoenix, AZ, USA) was marble cut to approximately 80 cm total length (typical final length ~ 65 cm). The first step in fabrication of the internally tapered CEC-MS tip involved preparation of a perfectly square tip, as any imperfection could affect both chromatographic separations and electrospray stability. This was accomplished by first attaching a small micro syringe filled with deionized water to the inlet end of the capillary in order to pass water through the column. Then, using a CE(C) column cutter from Agilent Technologies (Palo Alto, CA, USA), the capillary outlet was diamond cut with the aid of water as lubricant to smooth the cut. This was followed by visual inspection at 100X magnification using a CTI/VTEK digital microscope (Tracy, CA, USA). Finally, any small imperfection at the tip was manually sanded by applying very soft pressure using the underside of a marble capillary cutter. It was most important to flush water through the column not only for lubrication, but to expel any particulates remaining in the column tip during sanding. Any

remaining particles could become entrapped in the narrow taper (fabricated in the next step) and may contaminate the packing material when pumped into the tip (last step).

The internal taper of the CEC column was fabricated using a high temperature flame produced from a Little Torch purchased from Smith Equipment (Watertown, SD, USA). A mixture of methane (laboratory grade supplied in-house) and compressed oxygen of industrial grade was used to fuel this mini torch equipped with tip size #4 (orifice diameter = 0.020"). It was first necessary to introduce the capillary tip into the cooler outer flame (enriched with methane) for removal of the exterior polyamide coating. Rotation of the column by hand was crucial in order to avoid prolonged heat build-up and warping of the tip which could occur if the tip was allowed to remain in the flame for more than approximately 1-2 seconds. This was followed by rotation of the tip in the hotter part of the flame (enriched with oxygen) to facilitate the actual tapering process which occurred when the heat build-up was enough to make the tip glow. Once the tip glowed, it was removed very quickly to avoid warping as previously mentioned. It was found that approximately 15 glow steps would produce a finely tapered tip on the order of 7-9 μm , as shown in Figure 2.2 which presents several slides regarding the quality control of the column. First, in Fig. 2.2a, the microscope was calibrated followed by overall inspection at 100X magnification in Fig. 2.2b-c. Lastly, both the tapered end and untapered section of the column were measured utilizing 400X as can be seen in Fig. 2.2d.

After fabrication of the internal taper, the column was slurry pressure packed according to the procedure set forth in previous work from our laboratory,⁹ with slight

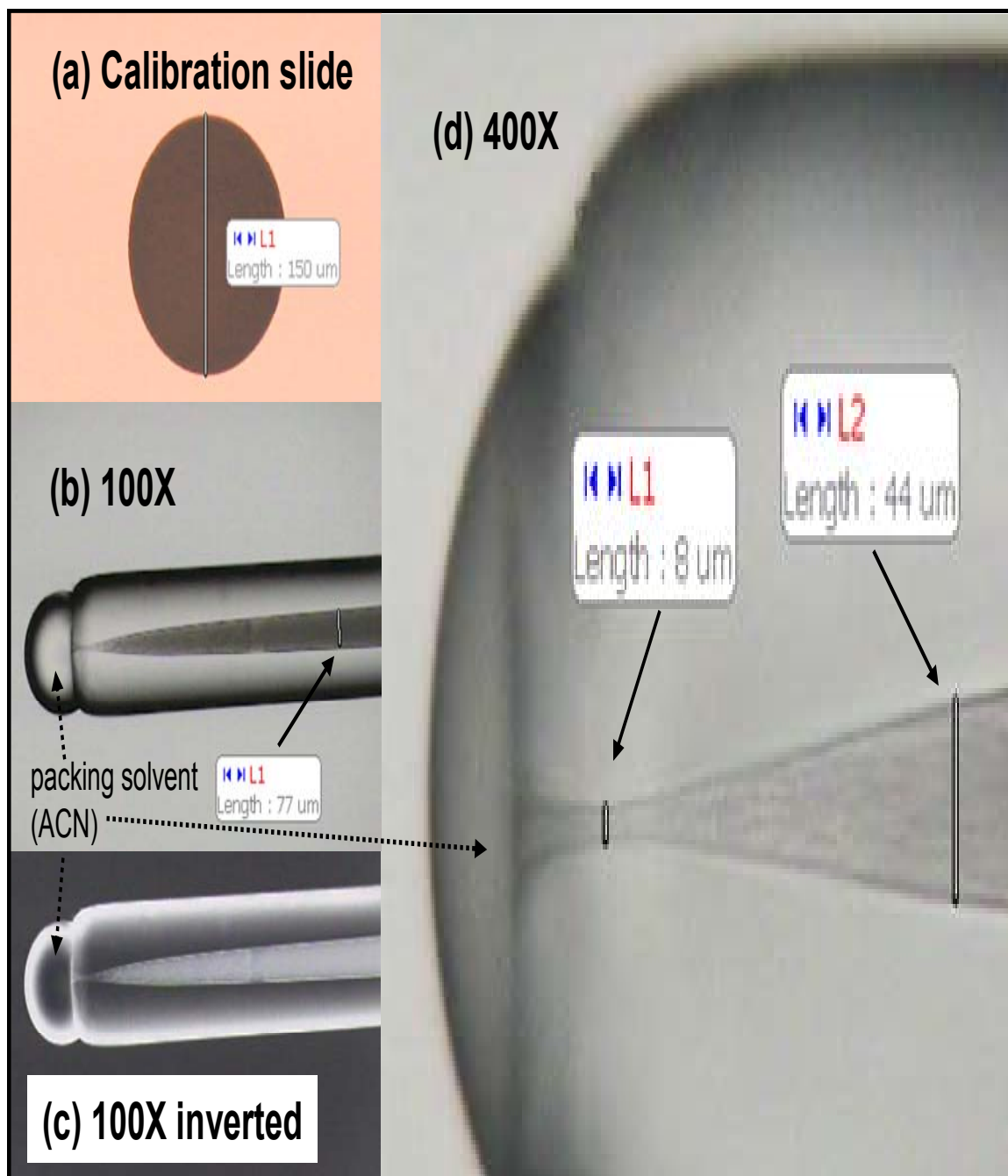


Figure 2.2: Microscopic images (a-d) of internal taper for CEC-MS. Capillary: 360 μm o.d., 78 μm i.d. stationary phase: CEC-C18-3 μm -100 \AA . a) Calibration slide, manufacturer spec = 150 μm . b) Magnification at 100X showing the CEC-MS column packed with stationary phase and flushed with solvent. c) Same as b) except inverted color. d) Same as b) except 400X magnification. Diameters of internal tapered tips shown were measured using Motic Images Software (v.2.0).

modification allowing for internal taper CEC-MS application. Briefly, the slurry, prepared from ca. 25 mg of packing material and 300 μ L ACN, was allowed to sonicate for 20-25 min. The sonicated slurry was then transferred to a stainless steel packing loop, followed by attachment of the non-tapered inlet end of the capillary to the loop, and then application of 200 bar pressure from a Knauer Pneumatic Pump (Wissenschaftliche Gerätebau, Berlin, Germany). Visual inspection of the tapered outlet tip upon application of pump pressure first showed a fine spray of ACN for 1-2 seconds, and then clogging of the outlet taper by the packing material initiating the packing to build up inside the column. Approximately 8-10 cm before the desired packed bed length, the pump pressure is turned off. The column is then removed and the loop cleansed by application of pressure to allow ACN to flush the excess slurry out of the loop into a beaker. This is quickly followed by re-attachment of the column and re-application of 200 bar pressure. At this point, the packing material that remained above the packed bed in the unpacked open segment of the column is then packed to add an approximate length of 8-10 cm. This added length was found to be dependent on the thickness of the slurry. In general, preliminary studies suggested that slurry composition (grams of packing/mL of solvent) and sonication time are important parameters that influence slurry thickness. It was found that a reproducible packed bed length was more easily attainable using a longer sonication time of ~25 min which promoted a thinner more homogenous slurry.

In contrast, a shorter sonication time of ~10 min. produced a much thicker slurry which was more difficult to work with due to problems with clogging of the column inlet, and required a longer time to build up the packed bed. For this study, the length of the packed bed was made to fall between 20-25 cm, leaving an open section of ~40 cm (total length duplex column ~60-65 cm). Once, the column was packed it was immersed in a Branson 2510 sonication bath (Danbury, CT, USA) for 30 min. to ensure homogenous packing, and then left overnight for dense packing. After the pump was turned off the next morning, a 10 mM sodium chloride solution was injected into the loop via an HPLC injector and pumped at 200 bar through the column for 3 hours. This procedure promoted the formation of more robust Na-silicate bonds within the inlet frit which was next fabricated at the top of the packed bed utilizing a homemade burner made of neochrome wire. Immediately following the frit formation, the pump pressure was slowly released and the column removed. The loop was then flushed with ACN to remove the NaCl solution. Finally, the column was reattached and ACN flushed at 50 bar through the column for 2 hours to remove residual NaCl before use. When not in use, the column ends were placed in vials filled with deionized water to prevent any drying of the packed bed. The mobile phase was prepared by first making a stock solution of 625 mM Tris buffer adjusted to pH 8.0 using HCl and Orion 420A pH meter (Beverly, MA, USA). The solution was then transferred to a 100 mL volumetric flask and filled to just below the mark, before sonication for 25 min. After filling the flask to the mark, the solution was filtered using a 0.45 μm PTFE membrane, and degassed for 6 min. An appropriate aliquot of this stock Tris buffer was then added to a known ACN/water mixture to obtain

the desired mobile phase. The final solution was then sonicated, filtered using a 0.45 μm PTFE membrane, and lastly degassed before use. The sheath liquid was prepared using a known volume of MeOH/water, followed by addition of a known concentration (mM) of A.F. solution, followed by filtration using a 0.45 μm PTFE membrane, sonication and degassing. Individual stock solutions of Zwittergent® analyte were prepared in 80/20 (v/v) ACN/H₂O at concentrations of 25 mg/mL. Then a mixture of the five Zwittergent® was prepared by mixing an equal volume from each stock solution to achieve a final concentration of 5 mg/mL. Thiourea was used as the unretained (t_0) marker and was prepared at a concentration of 30 mg/mL in 80/20 (v/v) ACN/H₂O.

CEC-ESI-MS Instrumentation. All CEC-ESI-MS experiments were performed on an Agilent HP^{3D}CE system (Agilent Technologies, Waldbronn, Germany) which was interfaced to an Agilent 1100 series MSD quadrupole mass spectrometer equipped with a CE-MS adaptor kit and a sprayer kit. Sheath liquid was delivered by an Agilent 1100 series HPLC pump equipped with a 1/100 split flow. The Chemstation software was used for data processing.

CEC-ESI-MS Conditions. The new CEC column was first installed into the MS cartridge followed by preparation of the inlet tip which involved diamond cutting and removal of 2 mm polyamide coating using the homemade burner. A manual syringe pump was then attached allowing mobile phase to precondition and equilibrate the column for at least 2 hours. For CEC-ESI-MS conditioning, pressure (12 bar) was

applied to the inlet, and then the voltage sequentially raised in time increments as follows: 2 kV/20 min, 5 kV/20 min, 10 kV/20 min, 15 kV/20 min, and 18 kV/15 min. The maximum separation voltage was 18 kV as higher voltage was found in some cases to create unwanted arcing and shortened lifetime of the column. The total applied voltage to the CEC column was 22 kV (18 kV from the CE instrument, plus 4 kV from the MS detector). Injection was performed electrokinetically at 6 kV for 6 sec. The ESI measurements were conducted in the positive ionization mode. Nitrogen obtained from a nitrogen generator was used for both nebulizing and drying gas. The mass range in full scan mode was set between 50-1500 amu. For single ion monitoring (SIM) mode, the masses were monitored as group SIM with low resolution and a gain setting 4.

Calculations. Chromatographic parameters such as resolution (R_s), efficiency (N), selectivity (α) and signal as well as signal/noise (S/N) ratio were calculated using Chemstation software (V9.0). Before calculating the S/N ratio, all chromatograms were smoothed utilizing a smoothing factor of 0.1 Gaussian.

RESULTS AND DISCUSSION

Selection of the CEC Particle Size. One of the benefits of CEC is the ability to use packing materials with smaller particle size to obtain higher efficiency (N) because the EOF is not dependent on particle diameter.³⁶ This is unlike LC which is limited by the

back pressure commonly associated with the pump. For our initial investigation, it was decided to compare the chromatographic performance of two different particle diameter 100Å non-encapped C₁₈ stationary phases for separation of the Zwittergents®. When comparing stationary phases with particle diameter of 1.5 µm to 3 µm, no significant improvement in plates (*N*) was observed. For example, the average *N* values were 13,000 and 12,000, respectively on the two phases. However, the 3 µm phase offered higher *R_s* values (*R_s*_{avg} = 5.4) of homologous Zwittergent® compared to the 1.5 µm phase (*R_s*_{avg} = 4.1). Average methylene selectivity (*α*_{CH₂, avg}) was also higher for the 3 µm phase (*α*_{CH₂, avg} = 1.26) over the 1.5 µm phase (*α*_{CH₂, avg} = 1.17), although total analysis time was more or less the same for both phases (3 µm = 30 min._{avg}, 1.5 µm = 29 min._{avg}), (electrochromatograms not shown). In addition, it was also found that smaller 1.5 µm particles were more difficult to pack due to problems resulting from too dense aggregation at the internal taper, which in some cases did not allow packing solvent (ACN) to pass through the column during packing. Therefore, it was decided to utilize 3 µm stationary phase throughout our study.

Optimization of the CEC and ESI-MS Parameters. As shown in Fig. 2.1, Zwittergent® possess a strongly basic quaternary ammonium group and an acidic sulfonate group in their structures. Using acidic sheath liquid (e.g., A.F.) the sulfonate group is protonated in the gas phase, which renders the Zwittergent® positive charge. Hence, good ionization efficiency was observed with positive ion ESI. The CEC-ESI-MS performance of protonated Zwittergents® was optimized by varying CEC

parameters, ESI-sheath liquid parameters, and ESI-MS spray chamber parameters as discussed below.

Optimization of the CEC Separation. Several critical CEC mobile phase parameters were investigated in order to achieve optimum separation of the Zwittergents®. These included the effects of varying the % ACN (v/v) fraction, the Tris concentration (mM) and finally the mobile phase pH. Comparison of the R_s , N , and α were considered to choose the best operating CEC conditions.

Optimization of ACN Content. The effect of varying the mobile phase ACN/H₂O content over the ranges of 90% ACN (v/v)/10% H₂O (v/v) to 70% ACN (v/v)/ 30% H₂O at 5 mM Tris, and pH set to 8.0 was investigated. Our previous work with CEC-ultraviolet (UV) detection showed that the same CEC packing had an upper and lower operating range of 95% ACN (v/v) and 70% ACN (v/v), respectively.³⁷⁻³⁸ This is because a faster and more reproducible EOF for this column was found to be generated in this range. Figure 2.3 presents the corresponding electrochromatograms (a-d). Plots of R_s , N , and α were also constructed to evaluate the chromatographic data (Figure 2.3e-g).

The chromatogram obtained at 90% ACN (v/v) (Fig. 2.3a) demonstrates that the Zwittergents® were retained excessively long coupled with broad peak width resulting in the lowest R_s (e.g., $R_{s\text{avg}} C_{10}/C_8 = 2.0 \pm 0.3$), and N (e.g., $N_{\text{avg}} C_8 = 4,100 \pm 700$) values. Although the surfactant is comprised of a long aliphatic hydrophobic chain which is well suited for solubilization, and expected faster separation at a higher ACN fraction, the

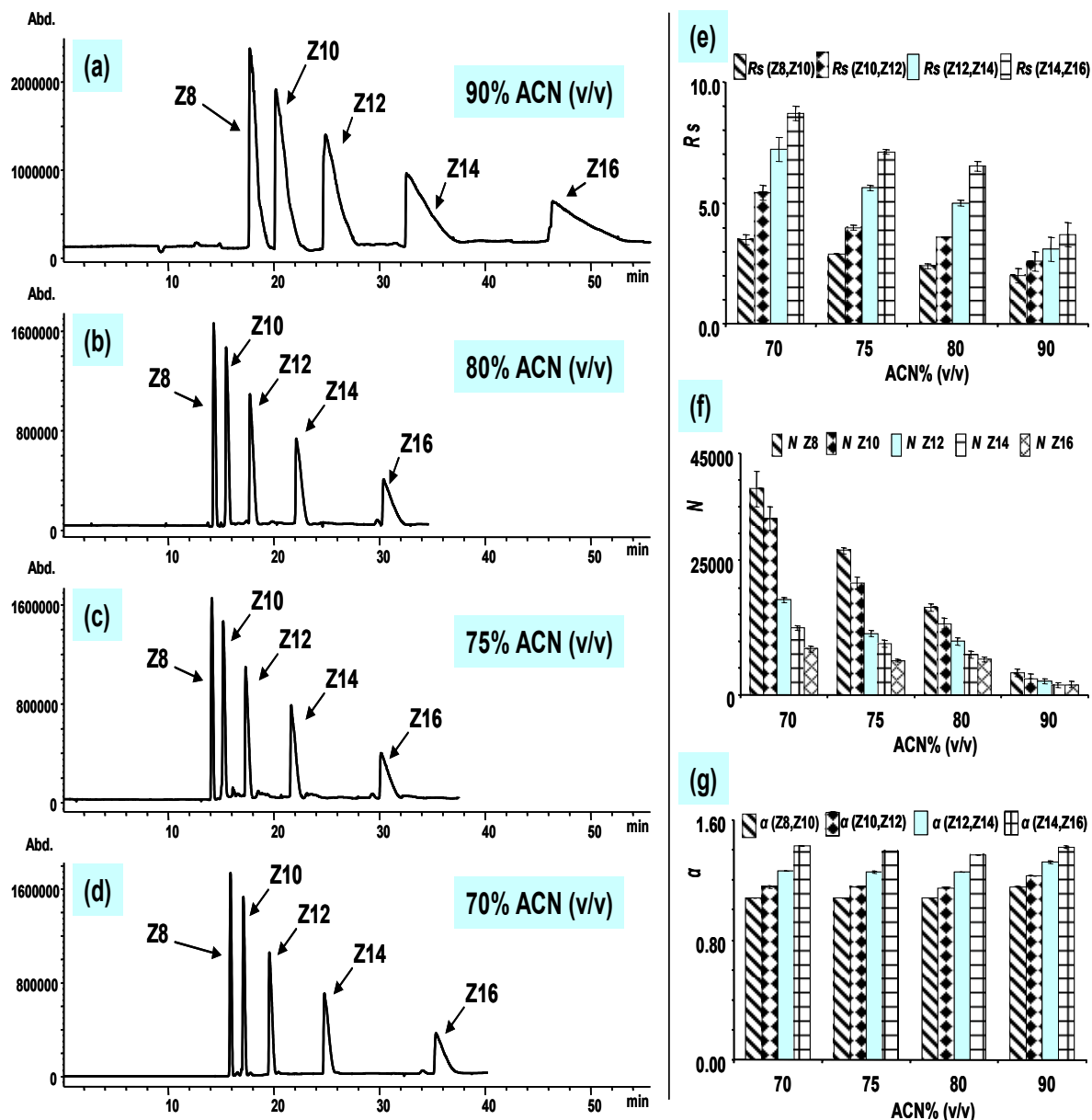


Figure 2.3: Electrophoretograms (a-d) and bar plots (e-g) showing effects of %ACN (v/v) on separation of zwittergents Z8-Z16, (e) R_s , (f) N and (g) α . The error bar in each plot represents one standard deviation (SD) of 3 measurements. Conditions: Column 1: 64 cm long, 22 cm packed bed length, 75 μ m (I.D.) capillary tapered internally (ca. 8-10 μ m) packed with 3 μ m CEC C₁₈ stationary phase; mobile phase, (a) 90% (v/v) ACN, (b) 80% (v/v) ACN, (c) 75% (v/v) ACN, (d) 70% (v/v) ACN, 5 mM Tris, pH 8.0. Sheath liquid, 1 mM HCO₂NH₄ in MeOH-H₂O (80:20, v/v), 7.5 μ L/min. Spray chamber, dry gas flow 4 L/min, nebulizer pressure 5 psi, dry gas temp. 100 °C, V_{cap} 4000 V, fragmentor 125 V. Electrokinetic injection: 6kv, 6 sec., 18 kV run voltage, ESI SIM positive ions (5 ions) monitored at m/z 280, 308, 336, 364, 392.

existence of dual charged (positively charged quaternary amine and negatively charged sulfonate group) counteracts this solubility and gives rise to a longer separation time with poor mass transfer as evidenced by the broader peaks at 90% ACN (v/v). Furthermore, it was also noted that the signal abundance was highest for the smallest chain length (Z8), but then decreased according to increase in chain length (Z8-Z16) due to greater longitudinal diffusion with increasing retention. The peak broadness and retention time of all Zwittergents® lessened upon decreasing the ACN fraction and increasing the H₂O to 80% ACN/20% H₂O (v/v) (Fig. 2.3b). This in turn resulted in a significant improvement in both *Rs* (e.g., $Rs_{avg} C_{10}/C_8 = 2.4 \pm 0.1$) and *N* (e.g., $N_{avg} C_8 = 17,600 \pm 700$) values, along with a decrease in total analysis time to ~30 min. Further decrease of the ACN fraction to 75% (v/v) (Fig. 2.3c) had little to no effect on the analysis time, however *Rs* (e.g., $Rs_{avg} C_{10}/C_8 = 2.88 \pm 0.03$), and *N* (e.g., $N_{avg} C_8 = 26,800 \pm 500$) continue to improve. Finally, at 70% ACN (v/v), a slight increase in retention time (*t_R*) were observed due to the increase in hydrophobic interaction with the stationary phase. The peak shapes were also improved resulting in higher *Rs* (e.g., $Rs_{avg} C_{10}/C_8 = 3.5 \pm 0.2$) and *N* (e.g., $N_{avg} C_8 = 38,400 \pm 3,300$) values but the analysis time increased close to 35 minutes. Interestingly, over the ranges reported above, no significant effects on methylene selectivity (α_{CH2}) were observed. Therefore, it was concluded that the best trade-off between *Rs* and *N* vs. analysis time was offered at 75% ACN (v/v).

Optimization of Tris Concentration. For the coupling of separation technique such as CEC to MS, it is necessary to consider the electrolyte of choice which preferably should

be volatile to avoid contamination of the MS source. However, in this study, Tris buffer was selected since biological buffers are very desirable in CEC-MS because less separation current is produced which decreases the joule heating. In addition, the MS manufacturer allows the use of a nonvolatile buffer in low concentration (<10 mM) coupled with more frequent cleaning of the spray chamber. Accordingly, it was decided to examine the effects of varying Tris concentration over the range of 2.5-10.0 mM [while maintaining 75% ACN (v/v) and pH 8.0]. The results of the study are provided in Figure 2.4. Overall, it was concluded that no deterioration in MS performance was observed. The retention time of all Zwittergents® was shown to slightly increase with added increments of Tris. This could be attributed to a decrease in the thickness of the electrical double layer responsible for generating the EOF with increasing Tris. The R_s between each Zwittergents® surfactant pair of adjacent chain length showed minimal improvement over the range of 2.5-5.0 mM (e.g., 2.5 mM $R_{s_{avg}} C_{10}/C_8 = 2.4 \pm 0.1$; 5.0 mM $R_{s_{avg}} C_{10}/C_8 = 2.88 \pm 0.03$), but then slightly decreased with increasing Tris going from 5.0-10.0 mM (e.g., 7.5 mM $R_{s_{avg}} C_{10}/C_8 = 2.3 \pm 0.3$; 10.0 mM $R_{s_{avg}} C_{10}/C_8 = 2.0 \pm 0.2$). The same trend was observed when considering N (e.g., 2.5 mM $N_{avg} C_8 = 17,500 \pm 1,600$; 5.0 mM $N_{avg} C_8 = 26,800 \pm 500$; 7.5 mM $N_{avg} C_8 = 20,300 \pm 3,600$; 10 mM $N_{avg} C_8 = 12,000 \pm 1,600$). However, no effect on α was demonstrated. Lastly, the signal intensity and S/N were not dramatically affected, although these were expected to be lower at Tris concentrations greater than those utilized in this study. Thus, 5.0 mM Tris was chosen as the optimum concentration.

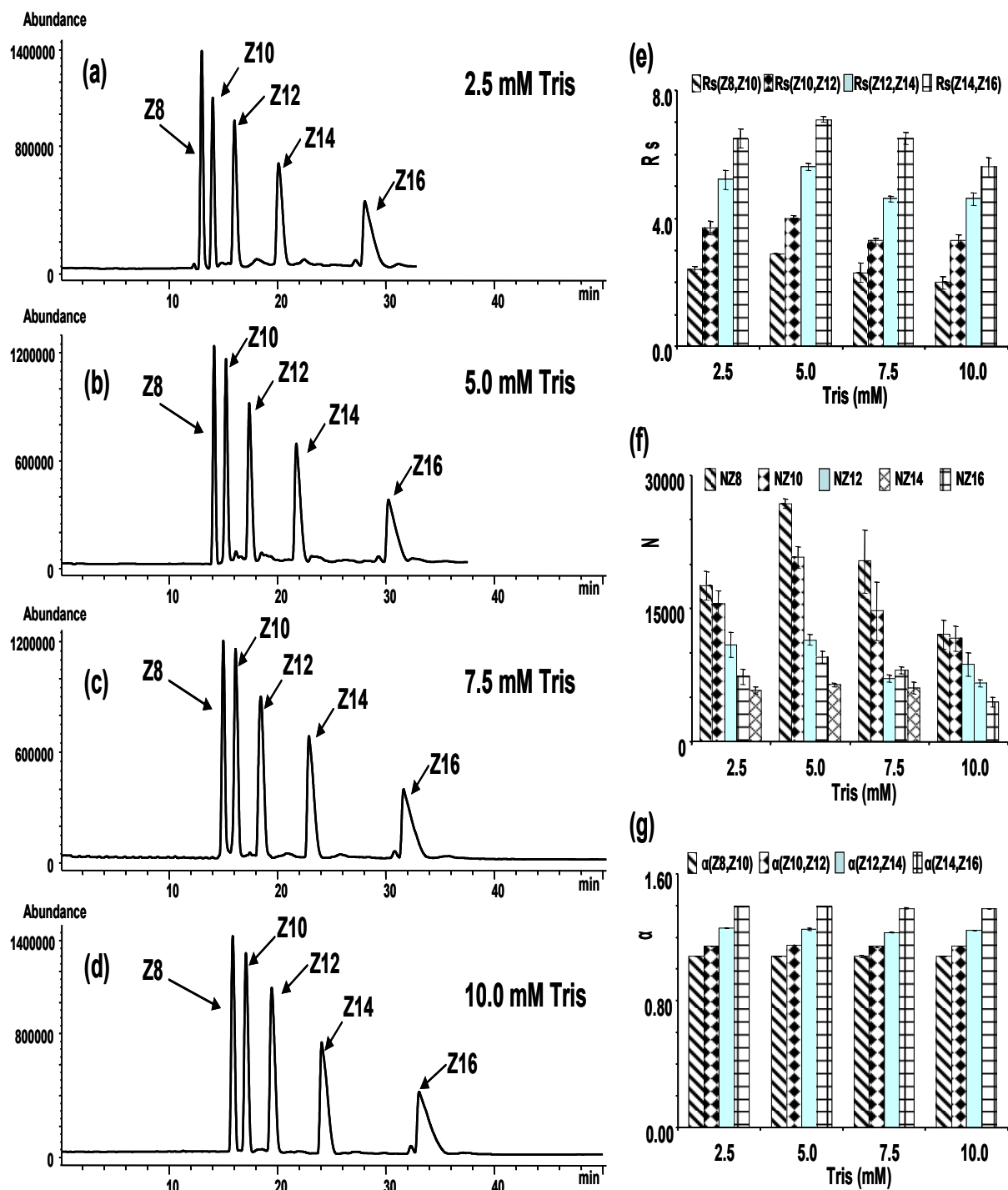


Figure 2.4: Electrophoretograms (a-d) and bar plots (e-g) showing effects of mobile phase BGE content of Tris buffer on the separation of zwittergents Z8-Z16, (e) R_s , (f) N and (g) α . Conditions: mobile phase; 75% (v/v) ACN, pH = 8.0 containing (a) 2.5 mM Tris, (b) 5.0 mM Tris, (c) 7.5 mM Tris, and (d) 10.0 mM Tris. All other conditions same as Figure 2.3.

Effect of Buffer pH. Investigation of the effects of buffer pH over the range of pH 9.0-7.0 were conducted while maintaining previously optimized 75% ACN (v/v) and 5.0 mM Tris. The presence of a strongly basic quaternary ammonium ion and an acidic sulfonate ion of equal strength maintained zwitterionic character of the analyte over a wide range. Therefore, the addition of concentrated HCl in order to lower the pH of the mobile phase was expected to have the greatest effect on the exposed stationary phase silanols rather than influencing ionization of the analyte to any significant degree. Figure 2.5a shows that pH 9.0 provided the longest retention time due to the lowest EOF (see thiourea trend, inset plot Fig. 2.5). Since only a small amount of HCl was added to lower the natural pH (~10) of Tris to 9.0, consequently the presence of fewer protonated Tris at high pH as counterions increases the electrostatic interaction between positively charged nitrogen group of the Zwittergent® and the uncapped anionic silanol of the stationary phase. These effects result in significant peak tailing, hence, lower R_s (e.g., $R_{s_{avg}} C_{10}/C_8 = 0.9 \pm 0.2$; $R_{s_{avg}} C_{12}/C_{10} = 1.9 \pm 0.2$) and N (e.g., $N_{avg} C_8 = 1,700 \pm 400$) values were observed. Furthermore, the aforementioned results observed for EOF, R_s and N are in agreement with our previous work on mobile phase-pH tuning of methylated benzo [a] pyrene (MBAP) isomers using the same stationary phase at pH 9.0.³⁷ In that work, the pH was varied while maintaining similar 75% ACN (v/v) but a higher Tris concentration (12.5 mM). This resulted in lower EOF at pH 9.0, although no peak tailing was observed due to absence of positive charge in the neutral MBAP isomer. Our present studies on the analysis of nonionic surfactants at pH 9.0 using the same packing and mobile phase composition containing higher 90% ACN (v/v) with lower 2.5 mM Tris also provided

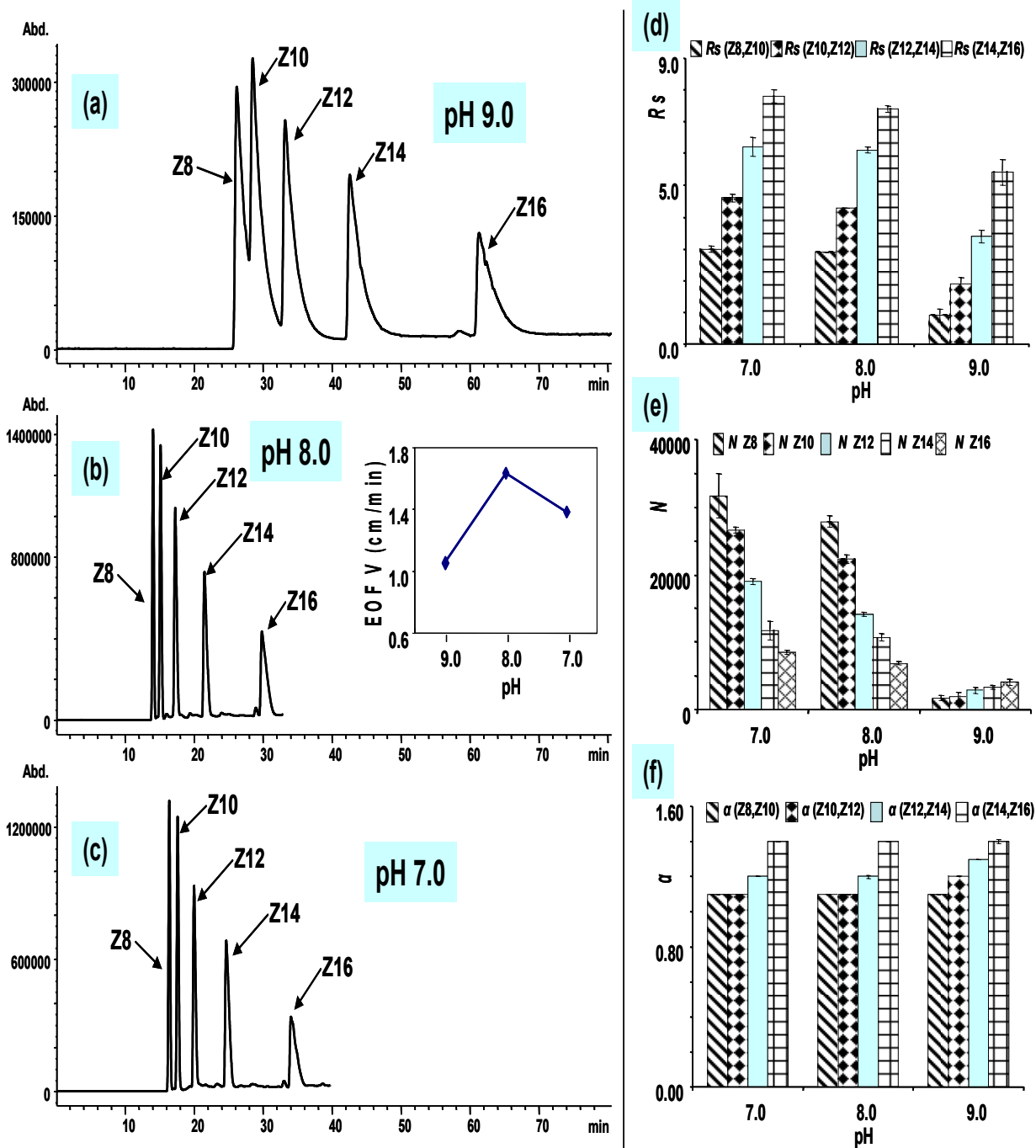


Figure 2.5: Electrochromatograms (a-c) and bar plots (d-f) showing effects of mobile phase pH on separation of zwittergents Z8-Z16, (d) R_s , (e) N and (f) α . Conditions: mobile phase; 75% (v/v) ACN containing 5 mM Tris and pH (a) 9.0, (b) 8.0, (c) 7.0. All other conditions same as Figure 2.4.

longer retention times, which suggests that EOF may be slower (unpublished results). However, when a higher Tris (12.5 mM) at the same pH 9.0 and 90% ACN (v/v) was used in CEC with UV detection, shorter retention times of TX-100 oligomers were observed with only moderate R_s and N .³⁹

Upon decreasing the pH to 8.0, more favorable EOF operating conditions were provided due to approximately 50% protonation of Tris as well as the presence of additional protons from HCl which competes for the ion-exchange sites on anionic silanols. As a result, the total analysis time was reduced to 30 min from 60 min (pH 9.0) along with improved R_s (e.g., $R_{s_{avg}} C_{10}/C_8 = 2.88 \pm 0.03$; $R_{s_{avg}} C_{12}/C_{10} = 4.0 \pm 0.1$) and N (e.g., $N_{avg} C_8 = 27,900 \pm 900$). Further decreasing the pH to 7.0 showed a similar separation as pH 8.0, however, the retention time of all Zwittergents® slightly increased. This was due to an increased ionic strength resulting in decrease of the electrical double layer thickness and extensive neutral silanols, which in turn lowered the zeta potential and ultimately decrease the EOF (Fig. 1.5 inset). The highest R_s (e.g., $R_{s_{avg}} C_{10}/C_8 = 3.0 \pm 0.1$; $R_{s_{avg}} C_{12}/C_{10} = 4.6 \pm 0.1$) and N (e.g., $N_{avg} C_8 = 31,700 \pm 3,300$) values were observed at pH 7.0, and similar to the ACN and Tris studies, no significant change in α was seen. Overall, pH 8.0 offered the best compromise between analysis time versus R_s and N .

Optimization of CEC-ESI-MS Conditions. The use of chemometric tools for the simultaneous analysis of numerous parameters has been shown previously to be a useful approach for optimization of ESI-MS conditions.⁴⁰ A NIST full factorial (2^3) design⁴¹

was therefore chosen to study the effects of sheath liquid parameters including ionic strength (mM), MeOH composition % (v/v), and flow rate ($\mu\text{L}/\text{min}$). For sheath liquid optimization, each experiment was run in duplicate as well as center point runs added at the beginning, middle, and end. A similar but modified table was then used for optimization of the spray chamber settings such as drying gas flow (L/min), nebulizer pressure (psi), and drying gas temperature ($^{\circ}\text{C}$). All experiments were run at optimized CEC separation conditions of 75% ACN (v/v), 5 mM Tris and pH 8.0.

Sheath Liquid Tuning. The effects of sheath liquid composition [i.e., ammonium formate (A.F.) and MeOH concentrations] and sheath liquid flow rate were investigated utilizing coded values as shown in Table 2.1. Sixteen randomized experiments were conducted as well as 5 center point runs added for reference. The experimental design for sheath liquid tuning is shown in Table 2.2. Two back-to-back runs were conducted

Table 2.1: Coded Values of Sheath Liquid Parameters

Level	X_1 ($\mu\text{L}/\text{min}$)	X_2 (MeOH/ H_2O)	X_3 (BGE mM)
-1	3	60/40	1
0	7.5	80/20	5
1	10	95/5	10

Table 2.2: Random Experimental Design for Sheath Liquid Optimization

Exp. No.	MeOH /H ₂ O	A.F. (mM)	S. Flow (μL/min)	Z10 Abundance (% RSD)
5	60/40	1.0	3	1600000 (4)
16	60/40	1.0	3	1060000 (16)
19	60/40	1.0	10	575000 (2)
12	60/40	1.0	10	969000 (6)
13	60/40	10.0	3	901000 (5)
3	60/40	10.0	3	1160000 (2)
17	60/40	10.0	10	431000 (5)
9	60/40	10.0	10	577000 (1)
1	80/20	1.0	7.5	1490000 (1)
21	80/20	1.0	7.5	648000 (8)
2	80/20	5.0	7.5	1060000 (1)
10	80/20	5.0	7.5	900000 (1)
20	80/20	5.0	7.5	483000 (10)
7	95/5	1.0	3	1720000 (3)
18	95/5	1.0	3	949000 (20)
11	95/5	1.0	10	1001000 (18)
8	95/5	1.0	10	1100000 (2)
4	95/5	10.0	3	1290000 (2)
6	95/5	10.0	3	1290000 (9)
14	95/5	10.0	10	505000 (4)
15	95/5	10.0	10	609000 (2)

for each experimental number (exp. no.), and all conditions were randomly repeated (total = 42 runs).

Several trends were observed when considering the effects of sheath liquid parameters on the signal abundance (Table 2.2). First, it was concluded that increasing the sheath liquid flow rate (e.g., 3.0 to 10 $\mu\text{L}/\text{min}$) caused the signal to lower in seven out of eight cases (i.e., compare exp. no. 5 vs. 19, 16 vs. 12, 13 vs. 17, 3 vs. 9, 7 vs. 11, 4 vs. 14, and 6 vs. 15, 18 vs. 8 = exception). This decrease in signal abundance with an increase in sheath liquid flow rate could be attributed to ionization efficiency of the analyte/solvent droplet. A larger sheath flow increases the volume of the solvent droplet surrounding the analyte molecules, which in turn makes it harder to evaporate excess solvent. The subsequent coulombic explosions are therefore affected or hindered, and a decrease in ionization and signal was observed. The effect of raising the A.F. concentration (1-10 mM) resulted in a lower signal for six out of eight cases (i.e., compare exp. no. 5 vs. 13, 16 vs. 3 = exception, 19 vs. 17, 12 vs. 9, 7 vs. 4, 18 vs. 6 = exception, then 11 vs. 14, and 8 vs. 15). This could be attributed to excess A.F. lowering the transmission efficiency of the analytes in a competitive manner. It is worth mentioning that using the randomized experimental design (Table 2.2), it was not possible to compare the effects of 80% MeOH center point runs because the sheath liquid flow rate of 7.5 $\mu\text{L}/\text{min}$ did not match other settings. Therefore, it was decided to repeat the %(v/v) MeOH experiment while maintaining a sheath liquid flow of 3 $\mu\text{L}/\text{min}$ with 1 mM A.F. The results showed that a composition of 80%(v/v) MeOH offered the highest

signal abundance. However, very similar abundance but higher standard deviation was observed for both 60 and 95% (v/v) MeOH (data not shown).

After completion of the sheath liquid tuning using the NIST full factorial table in random format, it was concluded that the sheath liquid parameters of 3 $\mu\text{L}/\text{min.}$, 1 mM A.F., and 80/20% (v/v) MeOH/H₂O should provide optimum conditions for highest MS sensitivity.

ESI Spray Chamber Tuning. The fragmentor voltage was the first spray chamber parameter to be optimized while maintaining the aforementioned optimum sheath liquid composition. The use of a factorial table was not required at this point because only one parameter was involved. It is well known that a higher voltage induces greater fragmentation and enhances the ion transmission of compounds that do not fragment readily. However, fragmentor voltage is analyte dependent. Figure 2.6a presents the representative electrochromatograms when varying the fragmentor voltage over the range of 75-225 V. Initially, the mass abundance (peak area and peak height) for all Zwittergents® increases with an increase in voltage from 75-150 V. This is due to a decrease in abundance of the adduct ion $[\text{M}+\text{Tris}+\text{H}]^+$ (m/z 429 for Z10, m/z 513 for Z16) as well as m/z 122 corresponding to $[\text{Tris}+\text{H}]^+$ as seen in Fig. 2.6b-c, which shows the corresponding mass spectra for two example Zwittergents®. However, over the range of 150-225 V, the abundance of molecular ion for shorter chain (Z8-Z10) Zwittergents® gradually declined resulting from a loss of n-alkyl chain $[\text{M}-(\text{H}_3\text{C}(\text{CH}_2)_n)$

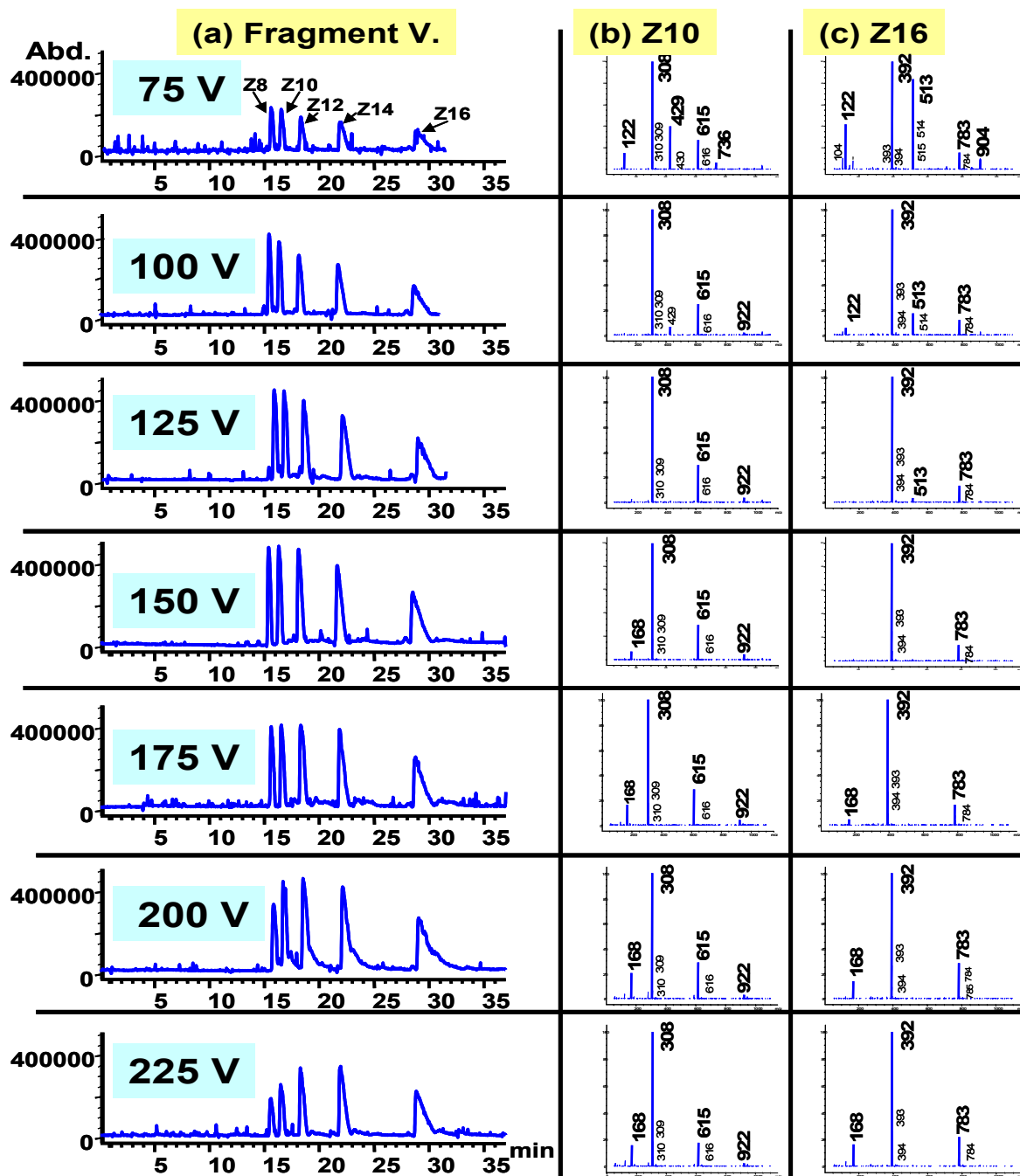


Figure 2.6: Effect of varying ESI fragmentor voltage in the range of 75-225 V. Electrochromatograms (a) and CEC-ESI mass spectral scan (50-1100 amu.) for (b) Z10 and (c) Z16 surfactant. Conditions: same as Figure 2.3 except Column 2 = 63 cm long, 18.5 cm packed bed, and sheath liquid was 3 μ L/min, 1 mM A.F., and 80/20% MeOH/H₂O.

$+2H]^+$ (i.e., the appearance of m/z 168 for Z10 at 150 V and also for Z16 at 175 V). This decrease was more significant for shorter chain (Z8-Z10) compared to longer chain (Z12-Z16) Zwittergents® for which the abundance remained constant, and then finally dropped off at 225 V. Furthermore, it should be noted that at the lowest fragmentor voltage of 75V, a greater number of ions are seen. This includes dimers $[2M+H]^+$ (i.e., m/z 615 for Z10, m/z 783 for Z16) and trimers $[3M+H]^+$ (m/z 922) for Z10 beginning at 100 V, but was not observed for Z16 as this m/z exceeded the scan range (upper limit set to 1100 amu to improve sensitivity of lower m/z). Nevertheless, the highest signal abundance of molecular ion for each Zwittergents® was found at 150 V.

A summary of the major ions observed at the different fragmentor voltages is presented in Table 2.3. The most interesting trend is that for increasing chain length, a larger fragment voltage is required to break the alkyl chain $[M-(H_3C(CH_2)_n)+2H]^+$ from the parent molecule. For example, for Z8-Z10 the minimum fragmentor voltage to break alkyl chain is 125 V, for Z12-Z14 = 150 V, and lastly for Z16 the fragment voltage is 175 V. Otherwise, the remaining ion/fragment pattern was generally the same for all Zwittergents® where the molecular ion $[M+H]^+$ was found to be most abundant (i.e., over the range of 75-225 V), and the dimer $[2M+H]^+$ was overall the second highest in abundance (range 100-225 V).

The spray chamber parameters including drying gas flow rate (L/min), nebulizer pressure (psi) and drying gas temperature (°C) were optimized while maintaining a fragmentor voltage of 150 V. A modified version of the randomized experimental design shown in Table 2.2 was designed in order to minimize time between changing conditions

Table 2.3. CEC-ESI-MS Fragmentation Pattern for Zwittergents at Varying Fragment Voltage^a

Z8:	n=7	m/z 113	
Z10:	n=9	m/z 141	
Z12:	n=11	m/z 169	
Z14:	n=13	m/z 197	
Z16:	n=15	m/z 225	

Zwitter	Frag. Voltage (V)	m/z Observed	Ion/Fragment
Z8	125-225	168	[M-(CH ₃ -(CH ₂) ₇)+2H] ⁺
	75-225	280*	[M+H] ⁺
	75	401	[M+Tris+H] ⁺
	75-225	559	[2M+H] ⁺
	100-225	838	[3M+H] ⁺
Z10	75	122	[Tris+H] ⁺
	150-225	168	[M-(CH ₃ -(CH ₂) ₉)+2H] ⁺
	75-225	308*	[M+H] ⁺
	75-100	429	[M+Tris+H] ⁺
	75-225	615	[2M+H] ⁺
	75	736	[2M+Tris+H] ⁺
Z12	100-225	922	[3M+H] ⁺
	75	122	[Tris+H] ⁺
	150-225	168	[M-(CH ₃ -(CH ₂) ₁₁)+2H] ⁺
	75-225	336*	[M+H] ⁺
	75-100	457	[M+Tris+H] ⁺
	75-225	671	[2M+H] ⁺
Z14	75	792	[2M+Tris+H] ⁺
	100-225	1006	[3M+H] ⁺
	75	122	[Tris+H] ⁺
	150-225	168	[M-(CH ₃ -(CH ₂) ₁₃)+2H] ⁺
	75-225	364*	[M+H] ⁺
	75-100	485	[M+Tris+H] ⁺
Z16	75-225	727	[2M+H] ⁺
	75	848	[2M+Tris+H] ⁺
	75-100	122	[Tris+H] ⁺
	175-225	168	[M-(CH ₃ -(CH ₂) ₁₅)+2H] ⁺
	75-225	392*	[M+H] ⁺
	75-100	513	[M+Tris+H] ⁺
	75-225	783	[2M+H] ⁺
	75	904	[2M+Tris+H] ⁺

* Highest abundance ion

^a Conditions: Same as Figure 2.5.

and avoid excess conditioning of the CEC capillary. The coded values are shown in Table 2.4 The structured experimental design which calls for maintaining a constant

Table 2.4. Coded Values of Spray Chamber Parameters

Level	X₁ (L/min)	X₂ (psi)	X₃ (°C)
-1	2	2	100
0	5	5	200
1	10	10	300

drying gas flow and nebulizer pressure, the drying gas temperature was then changed and the experiments repeated (total = 54 runs).

The significant results of ESI spray chamber tuning are summarized in Table 2.5 (column 5). First, an increase in nebulizer pressure (e.g., 2-10 psi) at fixed drying gas temperature and drying gas flow rate decreased the signal abundance in most cases (24 out of 27 cases, e.g., Table 2.5 exp. no. 1-3, 4-6, 7-9 etc.). Second, increasing the drying gas flow rate (e.g., 2-5 L/min) at drying gas temperatures of 100 °C and 300 °C enhanced the signal only slightly (e.g., Table 2.5 exp. no. 1 vs. 4; 19 vs. 22). However, a further increase in drying gas flow rate up to 10 L/min at fixed drying gas temperature and nebulizer pressure showed relatively pronounced decline in signal abundance (e.g., Table

Table 2.5. Structured Experimental Design for Spray Chamber Optimization

Exp. No.	Drying Gas Flow Rate (L/min)	Neb. Press. (psi)	Drying Gas Temp. (°C)	Z10 Abundance (%RSD)
1	2	2	100	1520000 (1)
2	2	5	100	1420000 (5)
3	2	10	100	1320000 (1)
4	5	2	100	1580000 (3)
5	5	5	100	1500000 (15)
6	5	10	100	1400000 (1)
7	10	2	100	1290000 (8)
8	10	5	100	1290000 (1)
9	10	10	100	1180000 (4)
10	2	2	200	1330000 (1)
11	2	5	200	1200000 (4)
12	2	10	200	1100000 (2)
13	5	2	200	1220000 (6)
14	5	5	200	1220000 (1)
15	5	10	200	1070000 (8)
16	10	2	200	1120000 (13)
17	10	5	200	1150000 (12)
18	10	10	200	1010000 (1)
19	2	2	300	990000 (9)
20	2	5	300	980000 (11)
21	2	10	300	870000 (2)
22	5	2	300	1030000 (3)
23	5	5	300	850000 (1)
24	5	10	300	900000 (1)
25	10	2	300	720000 (3)
26	10	5	300	670000 (14)
27	10	10	300	360000 (28)

2.5 exp. no. 6 vs. 9; 24 vs. 27) as compared to a lower flow rate from 2-5 L/min. This was slightly different with drying gas temperature of 200 °C which showed a decrease in signal abundance upon increasing the drying gas flow from 2-10 L/min in all cases. The result of raising the drying gas temperature from 100 °C to 300 °C (exp. no. 1-27) showed a general decline in signal abundance for all Zwittergents®. Hence, this trend suggests an interesting interdependence between the drying gas flow rate and drying gas temperature. According to the results obtained from spray chamber optimization, a moderate setting for drying gas flow rate (e.g., 5 L/min), lowest settings for the nebulizer pressure (e.g., 2 psi) and a drying gas temperature (e.g., 100 °C) were selected.

The MS capillary voltage (V_{cap}) was next optimized utilizing previously optimized spray chamber settings. The maximum value can be set to 6000 V, and typical value is 4000 V for ESI. The corresponding effects on signal and S/N when varying the V_{cap} from 2000 to 6000 V in 1000 V increments were studied. It was observed that a low V_{cap} of 2000 V was not a high enough voltage for ion transmission, while a higher 6000 V was destructive to the analyte, providing a lower signal and S/N . Increasing the V_{cap} over the range of 3000 to 5000 V showed that 5000 V provided the optimum response. Moreover, in this range, a higher response for both signal and S/N was seen for a smaller chain (Z8) compound as compared to the longer chain (Z16) Zwittergent®.

CEC-Atmospheric Pressure Chemical Ionization (APCI)-MS. Following the optimization of the CEC separation, ESI sheath liquid and spray chamber conditions, the capability of atmospheric pressure chemical ionization (APCI) for ionization and

determination of Zwittergents® surfactants was examined. It was decided to maintain the same CEC mobile phase, sheath liquid composition, and spray chamber settings in order to provide a comparison of ESI to APCI. One significant point of interest is consideration of results from a sheath flow rate study for optimum coupling of CEC to APCI-MS. Data on the limit of detection (LOD) for both sources are also provided. Finally, a comparison of the fragmentation pattern using ESI vs. APCI for both the standard Zwittergents® and the commercial sample is described.

After the installation of the APCI ionization source in place of the ESI interface, the direct transfer of all previously optimized ESI operating conditions over to APCI was investigated. One important technical difference is that the APCI sheath liquid line bypasses the 100:1 splitter used in ESI, and connects directly into the nebulizer in order to provide a higher flow rate. The aim of this part of the investigation was to achieve a reasonable response of Zwittergents® using the APCI source. To date, there are no reports in the literature describing the appropriate settings for coupling of an internally tapered CEC column to APCI-MS. Thus, as a starting point, some minor modifications to several (ESI) parameters were implemented as follows. The sheath liquid flow rate was varied from 3 $\mu\text{L}/\text{min}$ to 200 $\mu\text{L}/\text{min}$. The V_{cap} of 4000 V and fragmentor voltage of 100 V were set to provide typical operating conditions as suggested by the manufacturer.

Optimization of APCI Operating Parameters. Using the aforementioned conditions and spray chamber settings transferred from ESI, the effect of sheath flow rate was studied. As shown in Figure 2.7a, at a sheath liquid flow rate of 200 $\mu\text{L}/\text{min}$ and electrokinetic injection of 6 kV for 6 sec., the detection response was very poor. Interestingly, upon decreasing the sheath flow rate to 50 $\mu\text{L}/\text{min}$ and raising the injection time to 6 kV for 15 sec, (Fig. 2.7b), the sensitivity was dramatically improved. Although increasing the injection time (6-15 sec.) contributed some, the decrease in sheath flow rate (50-200 $\mu\text{L}/\text{min}$) was more significant in improving the detector response (data not shown). The effect of drying gas temperature over the range of 100-300 $^{\circ}\text{C}$ was examined utilizing a sheath liquid flow rate of 50 $\mu\text{L}/\text{min}$ (data not shown). The highest signal abundance and sensitivity were achieved using the lowest temperature of 100 $^{\circ}\text{C}$, analogous to the trend observed for ESI. Therefore, it was decided to maintain the same ESI spray chamber settings for drying gas flow of 5 L/min, and a nebulizer pressure of 2 psi because these conditions provide acceptable sensitivity in APCI.

Briefly, the remaining APCI operating variables were investigated individually. These include studying the corona current in the range of 3-5 μA whereupon 4 μA was found to be optimum. The V_{cap} was varied over the range of 4000-5000 V as a V_{cap} lower than 3000 V was expected to provide lower signal and S/N . The vaporizer temperature was set to 350 $^{\circ}\text{C}$ compared to 400 $^{\circ}\text{C}$ as a higher temperature was found to decrease the lifetime of the column. Using the optimum sheath liquid and spray chamber conditions for APCI, the fragmentor voltage was studied at 0, 20, 75, 100, 150 and 225 V. The

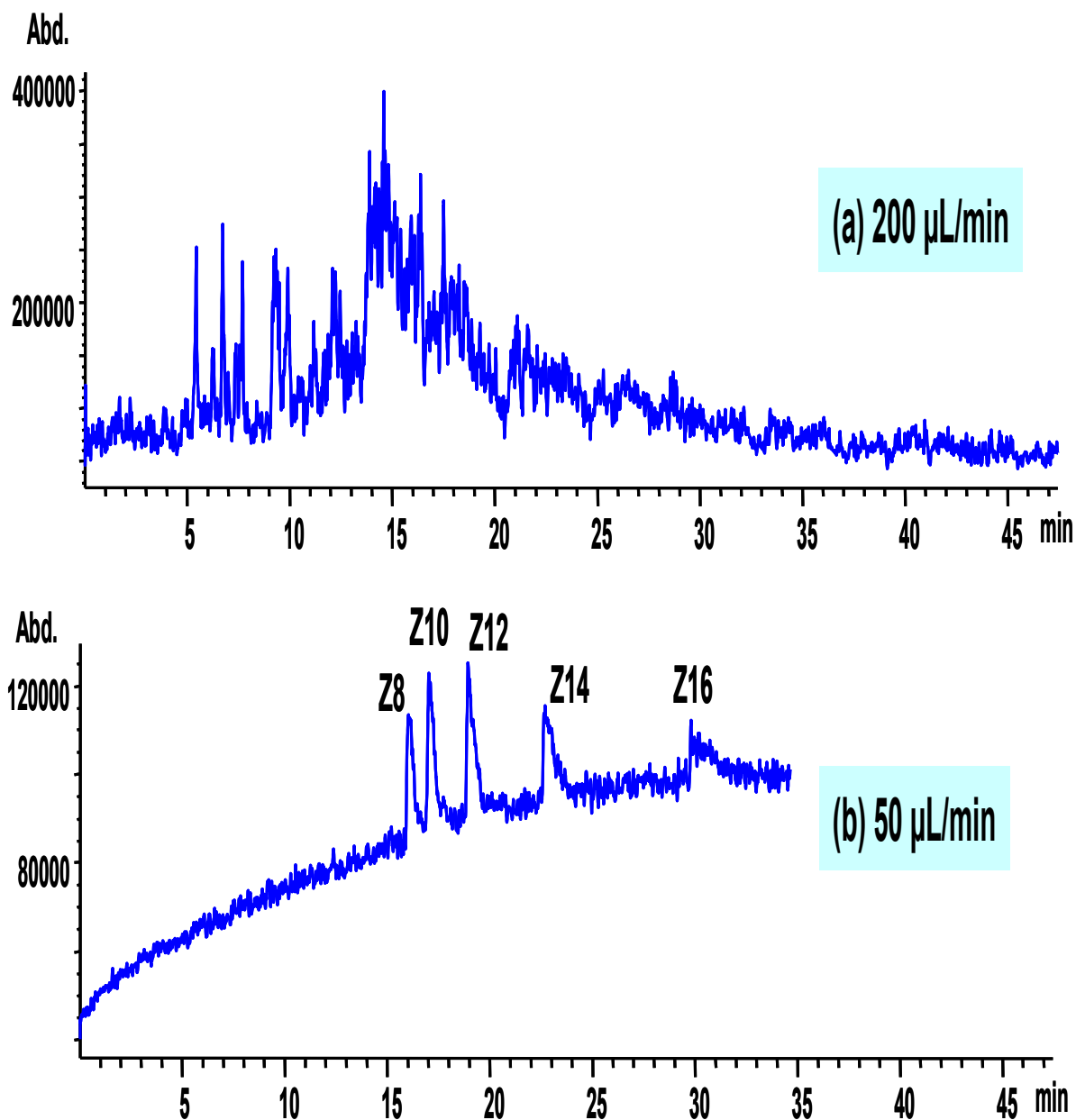


Figure 2.7: Effect of sheath liquid flow rate on the detection of zwittergent in APCI-MS mode. Conditions: Column 2, 75% (v/v) ACN, 5 mM Tris, pH 8.0; sheath liquid: (a) 200 $\mu\text{L}/\text{min}$, 6 kV 6 sec. inj., (b) 50 $\mu\text{L}/\text{min}$, 6 kV 15 sec. inj., 1 mM A.F., and 80/20% MeOH/H₂O. Spray chamber: dry gas flow 5 L/min, nebulizer pressure 2 psi, dry gas temp. 100 °C, V_{cap} 4000 V, vaporizer temperature 400 °C, corona current 4 μA , fragmentor voltage 100 V, 18 kV applied voltage. A mixture of five zwittergent homologues at a concentration of 5 mg/mL were monitored as positive ions in APCI SIM at m/z 158, 186, 214, 242, and 270.

highest MS signal was obtained at 100 V. Thus, the optimized conditions (sheath liquid: 80/20 (v/v) MeOH/H₂O, 1 mM A.F., 50 μ L/min; spray chamber: drying gas flow 5 L/min, nebulizer pressure 2 psi, drying gas temperature 100 °C) were then used to compare the fragmentation pattern in the full scan mode.

Comparison of ESI to APCI. As discussed earlier, the Zwittergents® are overall positively charged in the gas phase. Hence, sensitive detection of protonated molecular ions was possible in ESI. For APCI, it is suggested that the presence of both positive charged quaternary nitrogen and negatively charged sulfonate groups provide a pseudo-neutral character which enables the Zwittergent® molecule to enter the gas phase where proton transfer can then occur. Thus, it is interesting to compare the fragmentation pattern resulting from different ionization approaches between the ESI and APCI sources.

Fragmentation Pattern. Figure 2.8a presents the CEC-APCI chromatogram for the five Z8-Z16 Zwittergents® standard over a full m/z 50-1500 range. All of the corresponding mass spectra of each homologue shows that the most abundant ion results from bond breakage between the sulfonated side chain and the quaternary nitrogen (Fig. 2.8b). This is quite different to ESI ionization shown previously in Fig. 2.6b where the most abundant ion was the molecular ion. The ion spectrum of the selected Z10 homologue as shown with its structure in Fig. 2.8c is presented together with the interpretation of the fragmentation behavior of this homologue. The spectrum of Z10 exhibited $[M-(CH_2)_3SO_3+H]^+$ as the base peak at m/z 186 as well as abundant $[M-(CH_2)_2SO_3+H]^+$ and

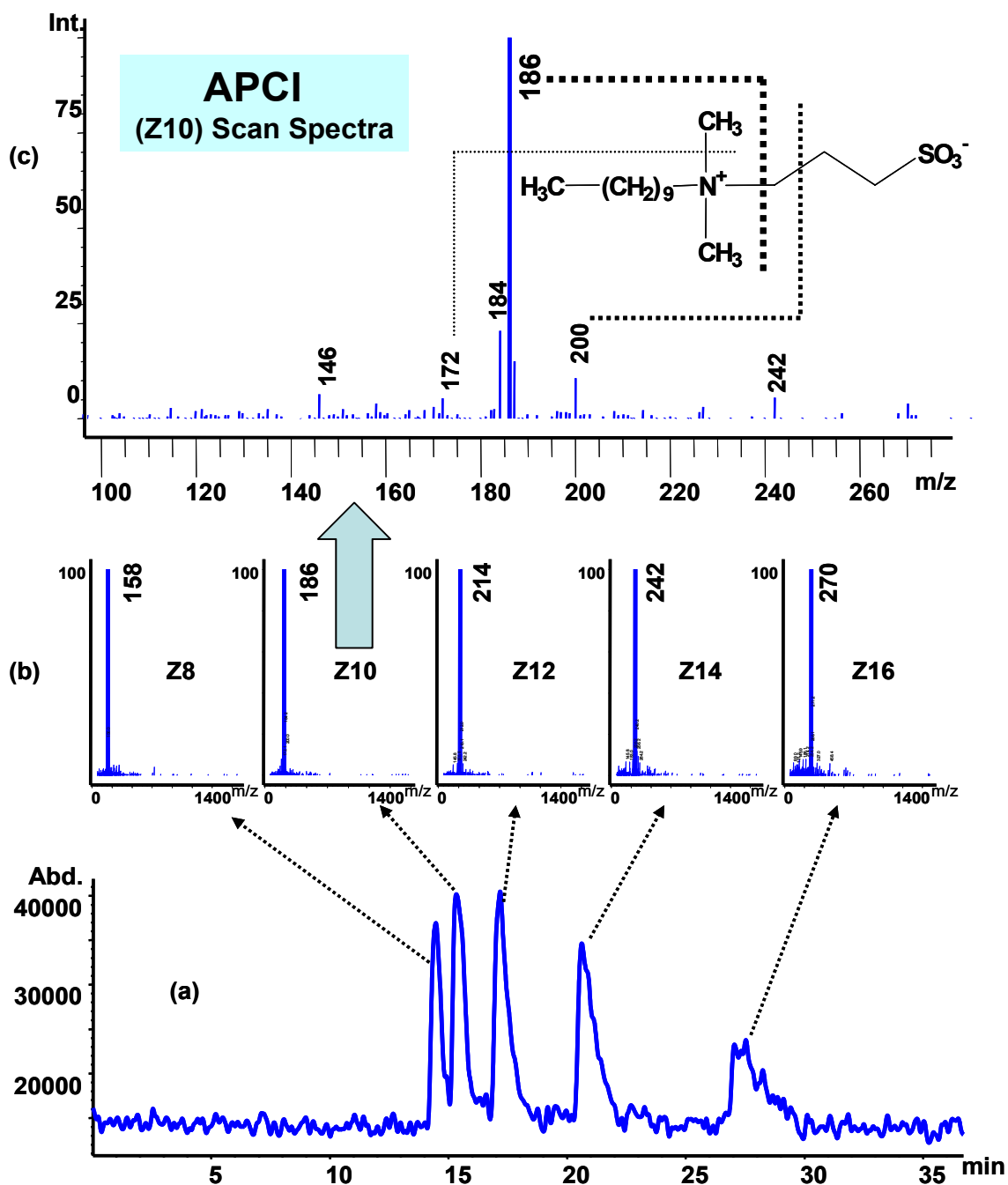


Figure 2.8: (a) CEC-APCI-MS scan (50-1500 amu.) electrochromatogram of a mixture of five zwittergent standards. (b) mass spectra of each zwittergent homologue and (c) expanded view of the mass spectra of Z10 zwittergent. Conditions: column 3, 64 cm total length, 23 packed bed; 10 kV 13 sec. injection. All other conditions are the same as Figure 2.7 except the concentration of each zwittergent homologue in the mixture was 25 mg/mL.

$[M-(CH_2)_3SO_3+H+N_4]^+$ ions at m/z 200 and 242, respectively. The presence of m/z 242 may be attributed to addition of N_4^+ which is generated during the corona discharge. Besides these major fragments, mass traces at m/z 172 probably corresponds to the loss of the methylene group from the base peak, as well as m/z 146 is most likely due to addition of Na^+ and H^+ to propane sulfonate to form $[(CH_2)_3SO_3+H+Na]^+$. As will be shown later, the mass spectrum of a commercial detergent sample also showed m/z 146. Overall, it can be summarized that for Zwittergents® analytes, comparison of ESI APCI mass spectra suggests that the former ionization technique is less destructive or softer than the latter.

Limit of Detection (LOD). The limit of detection (LOD) for the five Zwittergents® standard mixture was determined for both APCI and ESI in full Scan and SIM mode (Figure 2.9 a-d). For ESI, under optimized CEC-MS conditions, duplicate runs were performed at 5 mg/mL, 50 μ g/mL, 5 μ g/mL, 500 ng/mL, 5 ng/mL, and 500 pg/mL for each compound. It was found that for the ESI full Scan mode (Fig. 2.9a), the lowest reproducible injection could be obtained at 500 ng/mL, as compared to 5 ng/mL for ESI SIM mode (Fig. 2.9b), which as expected was significantly lower. Furthermore, when monitoring in SIM mode, it was possible to increase the sensitivity by dividing the ions into two groups as seen in the Fig. 2.9b. A drop in the baseline and substantial decrease in noise were seen when changing from group 1, which contained four analytes (Z8-Z14) eluting close to one another, to group 2, which contained only one analyte (Z16). Hence,

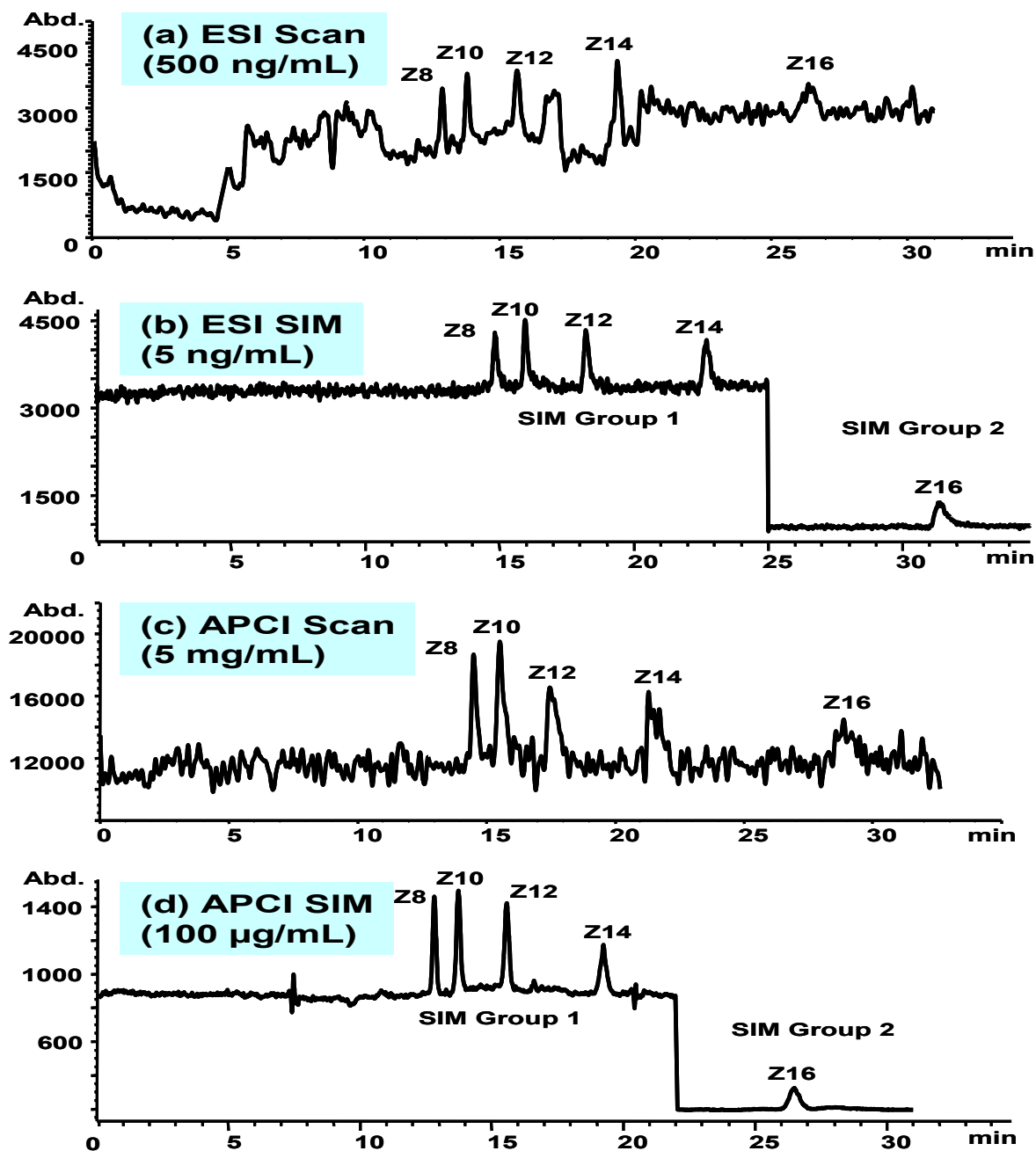


Figure 2.9: Zwittergent limit of detection (LOD) electrochromatograms in (a) ESI positive ion scan mode, range 50-1500 amu. (b) ESI positive ion SIM, group 1 = 4 ions monitored at m/z 280, 308, 336, 364 and group = 1 ion monitored at m/z 392. (c) APCI positive ion scan, range same as ESI. (d) APCI positive ion SIM, group 1 = 4 ions monitored at m/z 158, 186, 214, 242 and group 2 = 1 ion monitored at m/z 270. Conditions for ESI same as Figure 2.3 except fragmentor voltage was 150 V and $V_{cap} = 5000$ V; APCI parameters same as Figure 2.8.

fewer m/z within a SIM group is preferable for increasing the S/N . Finally, for ESI in both full Scan and SIM modes, a linear response was observed for all Zwittergents® ($R^2 > 0.9989 \pm 0.0017$) ranging from highest concentration (i.e., 5 mg/mL) down to the detection limit (i.e., 500 ng/mL for full scan, 5 ng/mL for SIM).

For APCI, in both full Scan and SIM modes, duplicate runs were performed at 50 mg/mL, 25 mg/mL, 10 mg/mL, 5 mg/mL, 1 mg/mL, and 100 μ g/mL. It can be seen in Figure 2.9 c-d that the limits of detection for APCI are at least 5 and 3 orders of magnitude higher than ESI in full Scan and SIM mode, respectively. Furthermore, the linear response was found to be slightly lower in APCI than for ESI in both scan and SIM mode, ($R^2 > 0.9738 \pm 0.0099$), again ranging from highest concentration (i.e., 50 mg/mL) down to the detection limits (i.e., 5 mg/mL for full Scan, 100 μ g/mL for SIM). Thus, our preliminary investigation shows that ESI is a more suitable ionization source for the analysis of Zwittergents® surfactants than APCI.

Application to Commercial Sample. In order to show real application of this CEC-MS method, an industrial commercial mixture of Zwittergents® surfactant (*Rewoteric AM-CAS*) was analyzed at optimum conditions. Preliminary investigation of the *Rewoteric* sample found the ESI LOD in full Scan mode to be close to 1 mg/mL, which was slightly higher (data not shown) than that for the standard C₈-C₁₆ Zwittergents®. Figure 2.10a-b shows that the separation by both CEC-ESI and CEC-APCI can be accomplished in under 35 min using a 23 cm packed bed, whereupon a shorter packed bed could be used for a slightly faster analysis of less than 30 min (data not shown).

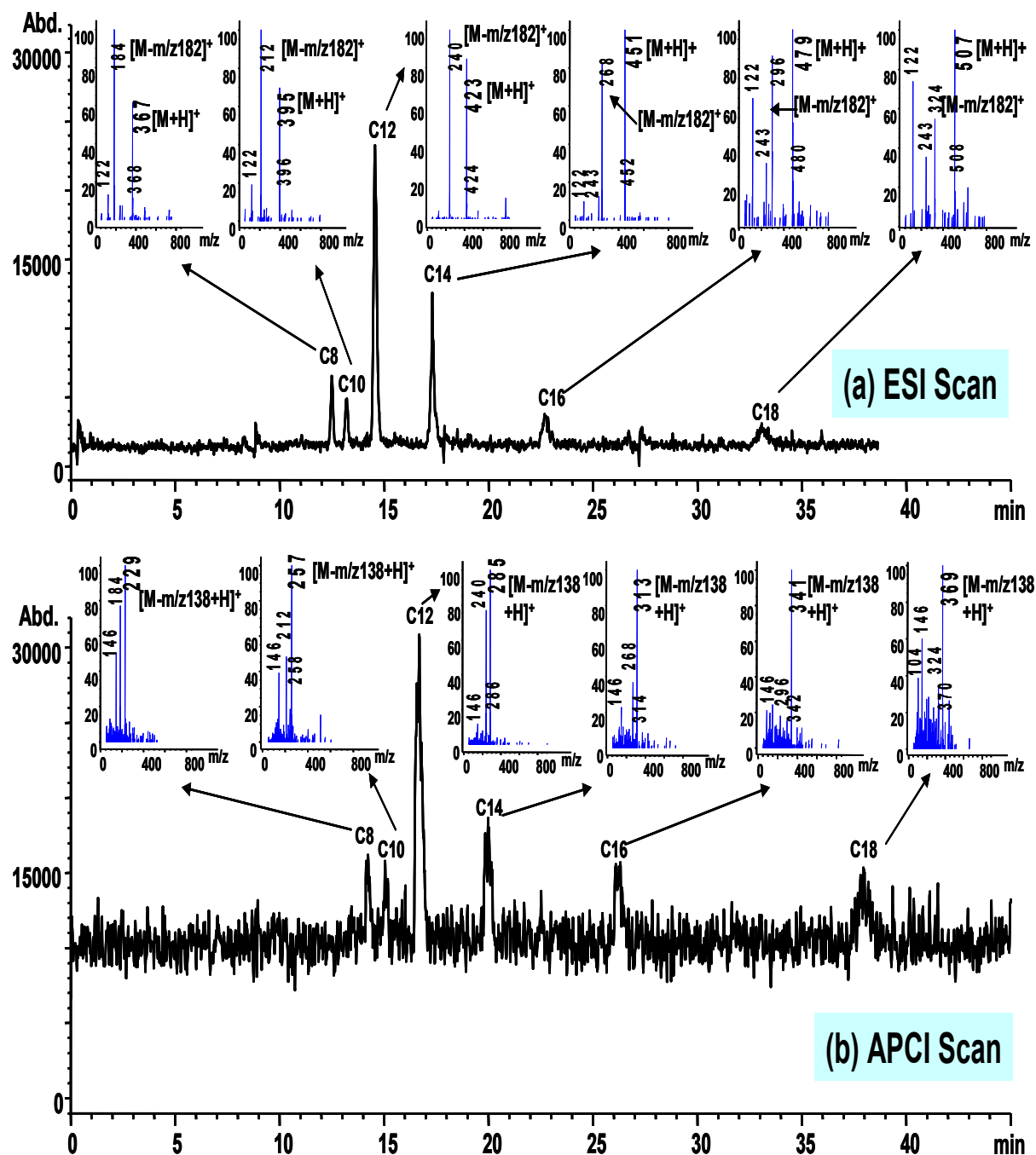


Figure 2.10: Rewoteric AM CAS commercial sample analysis. (a) CEC-ESI-MS scan mode (50-1500 amu.) with corresponding mass spectra. Conditions: same as Figure 2.8 except sample concentration = 1 mg/mL. (b) CEC-APCI-MS scan mode (50-1500 amu.) with corresponding mass spectra. Conditions are same as Figure 2.8 except sample concentration was 40 mg/mL.

Structural identification of the respective mixture was easily accomplished by obtaining the mass spectra which is a benefit of using ESI or APCI as compared to other detection techniques. For the ESI fragmentation pattern (Fig. 2.9a insets), it was interesting to note that the molecular ion peak is not always the highest intensity peak. For example, the highest intensity peak observed for the C₈-C₁₂ *Rewoteric* surfactant corresponded to loss of the sulfonic acid quaternary amine functional group containing side chain $[M-C_2H_6NC_2H_3OHCH_2SO_3]^+$ (m/z 182) which fragments from the quaternary nitrogen position (Figure 2.11a). In contrast, for the longer chain C₁₄-C₁₈ *Rewoteric* surfactant sample the molecular ion $[M+H]^+$ was the most abundant peak in the corresponding mass spectra (Fig. 2.10a insets). Thus, for ESI, both the R-group containing fragment (due to protonated secondary amine group) and the molecular ion (due to protonated sulfonic acid/quaternary amine group) are observed as highest or second highest abundant ions according to variation in chain length of the *Rewoteric* surfactant (Fig. 2.11a-b). In addition, the abundance of protonated Tris at m/z 122, and Tris dimer at m/z 243 were more distinguishable in the mass spectra of longer chain *Rewoteric* surfactants than for the shorter ones (Fig. 2.10a insets).

The CEC-APCI-MS trace and spectra of *Rewoteric* sample is shown in Figure 2.10b. It is clear that the sensitivity of this commercial sample (injected at 40 mg/mL) in APCI is much lower as compared to the same sample (injected at 1 mg/mL) in ESI. The corresponding APCI mass spectra (Fig. 2.10b insets) show that the fragmentation pattern is again different than that for ESI. The highest abundant ion observed in APCI results from loss of the sulfonate side chain (m/z 138) (Figure 2.11c), which is similar to

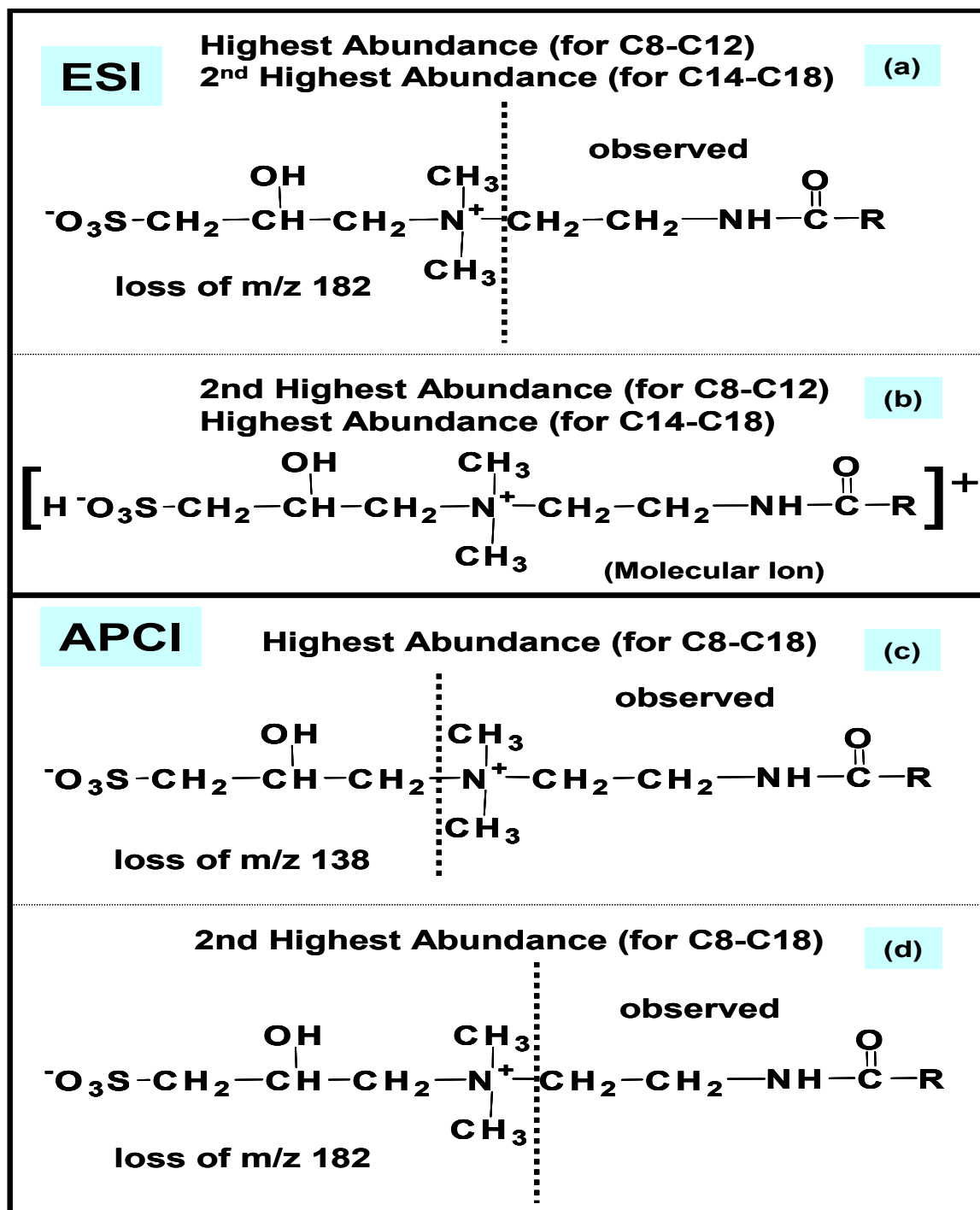


Figure 2.11: Summary of the fragment pattern observed for the commercial sample using (a-b) CEC-ESI-MS and (c-d) CEC-APCI-MS scan mode. Conditions are same as Figure 2.10.

the trend observed for the APCI fragmentation patterns of the standard Zwittergents® (Fig. 2.8c). In contrast to ESI, the APCI highest and second highest abundant fragments were the same for all the homologues of the *Rewoteric* sample (Fig. 2.11c-d). In addition, it is interesting to note that fragmentation occurs on different side of the quaternary nitrogen for the two sources (Fig. 2.11a vs. Fig. 2.11c). However, one important similarity in the fragment pattern is also observed. The major ion observed in ESI (Fig. 2.11a) is the same as the minor ion observed in APCI (Fig. 2.11d). Finally, it is worth mentioning that m/z 146 (corresponding to addition of Na and H to the fragmented sulfonic acid side chain ie., $[(CH_2)_3-SO_3+H+Na]^+$) that appears in the APCI mass spectrum of the commercial sample (Fig. 10b) was also observed previously in the APCI spectrum of the standard Zwittergents® (Fig. 2.8c).

Finally, separations of the *Rewoteric* sample (injected at a concentration of 1 mg/mL for ESI and 40 mg/mL for APCI) are presented in the ESI and APCI SIM mode (Figure 2.12 a,b respectively). Here, it is demonstrated that either ionization source can be utilized for sensitive monitoring of these specific ions in industrial mixtures, thus demonstrating the usefulness of the methods for possible quantitation.

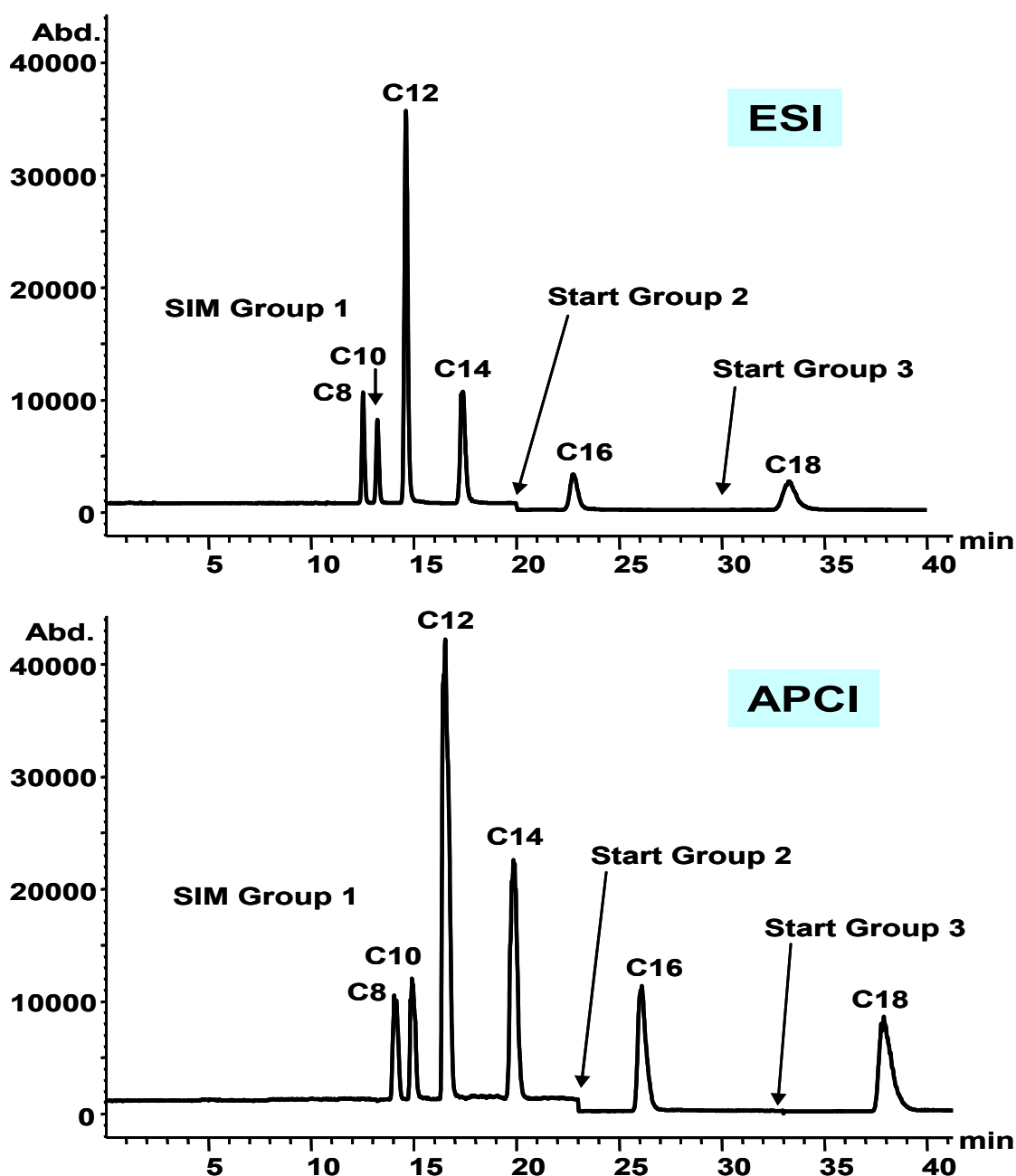


Figure 2.12: CEC-ESI-MS and CEC-APCI-MS SIM mode analysis of the commercial sample. Conditions for ESI are same as Figure 2.9 except 6 kV 12 sec. injection and ESI-SIM positive ions monitored in three groups. Group 1 = 4 ions monitored at m/z 367, 395, 423, 451; group 2 = 1 ion at m/z 479 and group 3 = 1 ion monitored at m/z 507. For APCI conditions, same as Figure 2.10 except ions are grouped as follows: group 1 = 4 ions monitored at m/z 229, 257, 285, 313; group 2 = 1 ion at m/z 341 and group 3 = 1 ion monitored at m/z 369.

CONCLUSIONS

This work is the first of its kind to present a novel CEC-MS method development for the separation and analysis of betaine-type zwitterionic surfactants (Zwittergents®) with application to a real industrial sample (*Rewoteric AM-CSU*). Our results showed that CEC-MS using an internally tapered tip can be successfully utilized for method development using either an ESI or APCI source. Overall, the durability of the CEC-MS column showed a lifetime of approximately 150 consecutive runs (~75 hours). Optimization of the CEC separation using 3 μm C₁₈ packing showed that all mobile phase operating variables (ACN, Tris, and pH) were found to influence the retention of Zwittergents® mainly due to changes in the EOF profiles. An investigation of the ESI-MS sheath liquid parameters using coded values and a randomized factorial experimental design (Table 2.4) suggest that lower flow rate (3 $\mu\text{L}/\text{min}$) and ionic strength (1 mM A.F.) provide higher MS signal abundance, whereas varying the MeOH composition from 65-90% (v/v) had little to no effect. Using a more structured factorial table (Table 5), more moderate or lower ESI spray chamber operating conditions provided higher MS signal (optimum conditions: 2 psi, 5 L/min, 100 °C) and were better suited than randomized factorial table for coupling of ESI-MS to CEC. In addition, a study of the effects of ESI fragmentor voltage demonstrated that both MS signal abundance and fragmentation pattern of the Zwittergents® were dependent upon chain length.

For comparison of on-line ESI-MS to APCI-MS, it was established experimentally that APCI requires a much higher sheath liquid flow rate (50 $\mu\text{L}/\text{min}$) as

compared to ESI (3 $\mu\text{L}/\text{min}$). The sensitivity between the two sources determined an impressive LOD for ESI SIM (5 ng/mL), which is similar to sensitivity achievable in LC-MS. However, this was about 3 orders of magnitude lower than for APCI SIM (100 $\mu\text{g}/\text{mL}$). Interestingly, the ESI vs. APCI spectra showed that ESI was less destructive exhibiting predominantly the molecular ion as compared to APCI which fragmented the Zwittergents® between the sulfonated side chain and the quaternary nitrogen. Finally, the successful application of the optimized method for analysis of the industrial sample *Rewoteric AM-CAS* is presented. A comparison of the fragmentation pattern between the two sources again revealed dependence on chain length for ESI, as well as variation in the point of cleavage for APCI. In conclusion, the hyphenation of CEC to either ESI-MS or APCI-MS is shown to be a powerful and useful hyphenation technique for sensitive monitoring and characterization of zwitterionic surfactants.

ACKNOWLEDGMENTS

This work was supported by a grant from the National Institute of Health (Grant No. 62314-02) and funding from Solvay Pharmaceuticals (Marietta, GA, USA). Special thanks to Jack Zheng and Neil D. Danielson for their input in this work.

References:

- (1) Eichhorn, P.; Knepper, T. P. *J. Mass Spectrom.* **2001**, 36, 677.
- (2) Eichhorn, P.; in: Knepper, T.P.; Barceló, D.; de Voogt, P., (Eds.) *Comprehensive Analytical Chemistry: Analysis and Fate of Surfactants in the Environment*, 1st ed.; Elsevier Science: Amsterdam, 2003.
- (3) Nair, L. M.; Saari-Nordhaus, R. *J. Chromatogr. A* **1998**, 804, 233.
- (4) Haefliger, O. P. *Anal. Chem.* **2003**, 75, 371.
- (5) Harrison, R. C.; Lucy, C. A. *J. Chromatogr. A* **2002**, 956, 237.
- (6) Levine, L. H.; Garland, J. L.; Johnson, J. V. *Anal. Chem.* **2002**, 74, 2064.
- (7) Levine, L. H.; Garland, J. L.; Johnson, J. V. *J. Chromatogr. A* **2005**, 1062, 217.
- (8) Miyamae, Y.; Yoshizawa, K.; Tsuchiya, J. *Bunseki Kagaku* **2001**, 50, 61.
- (9) Zheng, J.; Shamsi, S. A. *Anal. Chem.* **2003**, 75, 6295.
- (10) Santos, B.; Simonet, B. M.; Ríos, A.; Valcárcel, M. *Electrophoresis* **2004**, 25, 3231.
- (11) Zhu X.; Kamande, M. W.; Thiam, S.; Kapnissi, C.P.; Mwongela, S.M.; Warner, I. *Electrophoresis* **2004**, 25, 562.
- (12) Que, A. H.; Mechref, Y.; Huang, Y.; Taraszka, J. A.; Clemmer, D. E.; Novotny, M. V. *Anal. Chem.* **2003**, 75, 1684.
- (13) Lazar, I. M.; Li, L.; Yang, Y.; Karger, B. L. *Electrophoresis* **2003**, 24, 3655.
- (14) Que, A.H.; Novotny, M. V. *Anal. BioChem* **2003**, 375, 599.

- (15) Ivanov, A.R.; Horváth, C.; Karger, B. L. *Electrophoresis* **2003**, *24*, 3663.
- (16) Que, A. H.; Novotny, M. V. *Anal. Chem.* **2002**, *74*, 5184.
- (17) von Brocke, A.; Wistuba, D.; Gfrörer, P.; Stahl, M.; Schurig, V.; Bayer, E. *Electrophoresis* **2002**, *23*, 2963.
- (18) Cahours, X.; Cherkaoui, S.; Rozing, G.; Veuthey, J-L. *Electrophoresis* **2002**, *23*, 2320.
- (19) Barceló-Barrachina, E.; Moyano, E.; Galceran, M. T. *Electrophoresis* **2004**, *25*, 1927.
- (20) Klampfl, C.W. *J. Chromatogr. A* **2004**, *1044*, 131.
- (21) Shamsi, S.A.; Miller, B.E. *Electrophoresis* **2004**, *25*, 3927.
- (22) Piraino, S. M.; Dorsey, J. D. *Anal. Chem.* **2003**, *75*, 4292.
- (23) Mayer, M.; Rapp, E.; Marck, C.; Bruin, G. J. M. *Electrophoresis* **1999**, *20*, 43.
- (24) Frame, L. A.; Robinson, M. L.; Lough, W. J. *J. Chromatogr. A* **1998**, *798*, 243.
- (25) Jarvis, S.A.; Bateman, R.H.; Carruthers, R.; Doorbar, P.; Green, M. *Adv. Mass Spectrom.* **1998** (Abstract).
- (26) Steiner, F.; Scherer, B. *J. Chromatogr. A* **2000**, *887*, 55.
- (27) Pyell, U. *J. Chromatogr. A* **2000**, *892*, 257.
- (28) Tomer, K. B. *Chem. Rev.* **2001**, *101*, 297.
- (29) Choudhary, G.; Horváth, C.; Banks, J. F. *J. Chromatogr. A* **1998**, *828*, 469.

- (30) Lord, G. A.; Gordon, D. B.; Myers, P.; King, B. W. *J. Chromatogr. A* **1997**, 768, 9.
- (31) Keski-Hyynilä, H.; Kurkela, M.; Elovaara, E.; Antonio, L.; Magdalou, J.; Luukkanen, L.; Taskinen, J.; Kostiainen, R. *Anal. Chem.* **2002**, 74, 3449.
- (32) Leinonen, A.; Kuuranne, T.; Kostiainen, R. *J. Mass Spectrom.* **2002**, 37, 693.
- (33) Castillo, M.; Riu, J.; Ventura, F.; Boleda, R.; Scheduling, R.; Schröder, H.Fr.; Nistor, C. ; Émneus, J.; Eichhorn, P.; Knepper, Th.P.; Jonkers, C. C.A.; de Voogt, P.; González-Mazo, E.; León, V.M.; Barceló, D. *J. Chromatogr. A* **2000**, 889, 195.
- (34) Thurman, E.M.; Ferrer, I.; Barceló, D. *Anal. Chem.* **2001**, 73, 5441.
- (35) Tanaka, Y.; Otsuka, K.; Terabe, S. *J. Pharm. Biomed. Anal.* **2003**, 30, 1889.
- (36) Rathore, A.S.; Horváth, C. in Deyl, Z.; Švec, F. (Eds.) *Capillary Electrochromatography; J. Chromatogr. Library-Vol. 62*, 1st ed.; Elsevier Science: Amsterdam, **2001**.
- (37) Norton, D.; Zheng, J.; Shamsi, S. A. *J. Chromatogr. A* **2003**, 1008, 205.
- (38) Norton, D.; Shamsi, S. A. *J. Chromatogr. A* **2003**, 1008, 217.
- (39) Norton, D.; Shamsi, S. A. *Electrophoresis* **2004**, 25, 586.
- (40) Varesio, E.; Cherkaoui, S.; Veuthey, J. L. *J. High Resol. Chromatogr.* **1998**, 21(12) 653.

(41) *NIST/SEMATECH e-Handbook of Statistical Methods*,

<http://www.itl.nist.gov/div898/hadbook/>, 06/16/04, Table 3.9.

Chapter 3:
Capillary Electrochromatography-Mass Spectrometry
of Cationic Surfactants

Abstract

The capillary electrochromatography-mass spectrometry (CEC-MS) of alkyltrimethyl-ammonium ions (ATMA^+) with chain length ranging from C_1 - C_{18} is optimized using an internally tapered CEC-MS column packed with mixed mode C_6 /strong cation exchange stationary phase and coupled to an electrospray ionization (ESI) source. A systematic study of the CEC separation parameters is conducted followed by evaluation of the ESI-MS sheath liquid and spray chamber settings. First, the optimization of CEC separation parameters are performed including the acetonitrile (ACN) concentration, triethylamine (TEA) content, buffer pH and ammonium acetate (NH_4OAc) concentration. Using 90%(v/v) ACN with 0.40% (v/v) TEA as mobile phase the separation of longer chain C_6 - C_{18} - TMA^+ surfactants could be achieved in 15 min. Lowering the ACN concentration to 70%(v/v) provided resolution of shorter chain C_1 , C_2 - TMA^+ from C_6 - TMA^+ although the total analysis time increased to 40 min. Furthermore, variation of both the ACN and TEA content as well as ionic strength has found to significantly influence the retention of longer chain surfactants as compared to short chains. The optimum CEC conditions are 70%(v/v) ACN, 0.40%(v/v) TEA, pH 3.0 and 15 mM NH_4OAc . Next, the optimization of the ESI-MS sheath liquid composition is conducted comparing methanol to isopropanol followed by use of experimental design for the analysis of spray chamber parameters. Overall, the developed CEC-ESI-MS method allows quantitative and sensitive monitoring of ATMA^+ from $\leq 10 \mu\text{g/mL}$ down to 10 ng/mL. Utilizing the optimized CEC-ESI-MS protocol, the challenging analysis of

commercial sample Arquad S-50 ATMA⁺ containing *cis-trans* unsaturated and saturated soyabean fatty acid derivatives is demonstrated.

Introduction

Cationic surfactants are surface active agents utilized as chemical intermediates and as functional ingredients in numerous formulations. Generally, the chemical structure contains both a hydrophobic alkyl chain and a hydrophilic group, which is often a quaternized nitrogen functionality that renders the cationic surfactant overall permanently positively charged in solution. Moreover, there are a diverse group of cationic surfactants that has different substitutions around the nitrogen atom including mono-, di-, and tri-methyl, alkyl and benzylated configurations. Alkyltrimethylammonium (ATMA⁺) compounds with chloride, bromide or iodide counterions are one of the major types of non-chromophoric quaternary ammonium surfactants, which are widely used in industrial applications as well as in cosmetics and pharmaceutical preparations. For example, longer chain ATMA⁺ are utilized in the personal care industry due to unique ability to impart detangling, conditioning, and static control properties in hair care formulas including crème rinse, mousses, sprays, shampoos and conditioners. In addition to being good cleansing agents, they also possess germicidal properties, which make them useful in hospitals as disinfectants.

Atypically, the manufacture of fatty amine nitrogen derived surfactants including ATMA⁺ first utilize natural feedstock raw materials such as animal fats and vegetable based oils (e.g., palm, kernel, and coconut oil based). As a consequence, the products contain a homologous range of alkyl chain lengths typically C₈-C₂₂ whereupon C₁₂-C₁₈ is predominant. Since these surfactants containing different alkyl chain lengths are added as ingredients to end products such as shampoo and conditioners, it is of importance to

develop analytical separation/detection methods in order to monitor the composition that can ultimately affect the performance of these end products. To date, the analysis of ATMA⁺ has been accomplished using different methods such as gas chromatography mass spectrometry (GC-MS) requiring conversion to tertiary amine,¹⁻³ high performance liquid chromatography (HPLC) utilizing various detection such as chemiluminescent nitrogen,⁴ electrospray ionization mass spectrometry (ESI-MS),⁵⁻⁷ and conductometric detection.⁸ In addition, capillary electrophoresis methods using indirect photometric detection⁹⁻¹³ or MS detection¹⁴ have also been employed for the analysis of ATMA⁺.

As a recent alternative to these traditional methods of analysis, capillary electrochromatography (CEC) is gaining recognition as a powerful separation technique that combines both electrophoretic separation based on charge-to-mass (z/m) ratio, along with HPLC retention mechanisms including ion-exchange and hydrophobic/-hydrophilic interactions with a stationary phase. These attributes therefore make CEC well suited for analysis of cationic surfactants due to differences in electrophoretic mobility and chain length inherent to these molecules. In particular, when coupled to MS, the hyphenated CEC-MS technique offers highly efficient separation along with sensitive and low limit of detection (e.g., ng/mL). Recent reviews of the numerous CEC-MS modes and applications demonstrate the growing acceptance of this capable technique in the analytical community.¹⁵⁻¹⁶ Several very recent publications from our group has shown utility of packed column CEC-ESI-MS utilizing a specialized internally tapered tip CEC-MS column for sensitive analysis of achiral and chiral compounds.¹⁷⁻¹⁸

This manuscript describes a novel CEC-ESI-MS optimized method utilizing an internally tapered tip column for analysis of C_1 - C_{18} ATMA⁺ compounds (Figure 3.1).

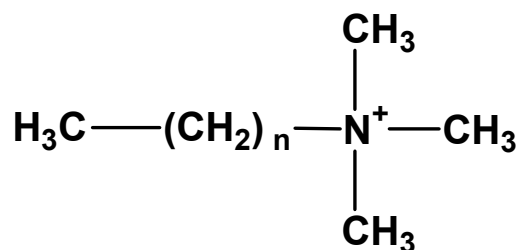


Figure 3.1: Generalized chemical structure of the alkyltrimethylammonium surfactant.

Typically, only the longer chain C_6 - C_{18} are classified as surfactants which aggregate to form micelles at a concentration greater than the critical micellar concentration (CMC), whereas the short chain cationic compounds of chain length C_1 and C_2 are included in this work in order to better characterize the developed CEC-MS method. A commercially available non-encapped mixed mode packing consisting of C_6 alkyl chain and sulfonate (SO_3^-) strong cation exchange (SCX) functionality (i.e., CEC- C_6 /SCX) was used for in-house packing of the CEC-MS column. The influence of several critical mobile phase parameters including acetonitrile (ACN) concentration, addition of triethylamine (TEA), ionic strength effect, and pH are studied. This is followed by a strategy for the ESI-MS optimization including sheath liquid and spray chamber optimization using experimental design for the latter. A study of the system

durability and performance proved that excellent interday and intraday reproducibility of migration time and chromatographic resolution is possible for greater than 165 runs over 111 hours of continuous use. Finally, utilizing the optimized CEC-ESI-MS method protocol, the application to commercial Arquad S-50 ATMA⁺ detergent sample containing soyabean fatty acid derivatives is next presented. The presence of *cis/trans* geometrical isomers for unsaturated ATMA⁺ is found to occur in the S-50 sample. The developed CEC-MS method is not only suitable for the challenging separation of *cis/trans* isomers, but also provides high degree of selectivity for simultaneous separation of saturated and unsaturated ATMA⁺ as compared to the manufacturer method based on acid/base titrations.

EXPERIMENTAL SECTION

Materials and Methods. Chemicals. Tetramethylammonium chloride (C₁-TMA⁺Cl⁻) (98%), ethyltrimethylammonium iodide (C₂-TMA⁺I⁻) (99%), oleyl chloride and trimethylamine hydrochloride (98%) were purchased from TCI America (Portland, OR, USA). The n-hexyltrimethyl ammonium bromide (C₆-TMA⁺Br⁻) (98%), n-octyltrimethyl ammonium bromide (C₈-TMA⁺Br⁻) (97%), n-decyltrimethylammonium bromide (C₁₀-TMA⁺Br⁻) (98%), n-tetradecyltrimethyl ammonium bromide (C₁₄-TMA⁺Br⁻) (98%), and n-hexadecyltrimethyl ammonium bromide (C₁₆-TMA⁺Br⁻) (98%) were obtained from Lancaster Synthesis (Pelham, NH, USA). The n-octadecyltrimethyl ammonium bromide (C₁₈-TMA⁺Br⁻) (99%), n-dodecyltrimethyl ammonium bromide (C₁₂-TMA⁺Br⁻) (99%),

and ammonium acetate (NH_4OAc) (molecular biology grade) were purchased from Sigma (St. Louis, MO, USA). Triethylamine (99.5%) was supplied from Aldrich (Milwaukee, WI, USA). Commercial sample, Arquad S-50 (batch SR576363X) was kindly donated from Akzo Nobel (Illinois, USA). Acetonitrile (ACN) and methanol (MeOH) of HPLC grade were purchased from Burdick and Jackson (Muskegon, MI, USA). Ammonium hydroxide ($\text{NH}_3\text{H}_2\text{O}$), acetic acid (HOAc), and sodium chloride (NaCl) were supplied by Fisher Scientific (Springfield, NJ, USA). Acetone of HPLC grade was purchased from EM Science (Gibbstown, NJ, USA). Finally, water was purified by a Barnstead Nanopure II purification system (Barnstead International, Dubuque, IA, USA).

Buffer, Sheath Liquid and Sample Preparation. The CEC running buffer was prepared by first making stock solution of concentrated 100 mM NH_4OAc in 75 mL triply deionized H_2O , followed by adjustment of pH using HOAc. This solution was then transferred to a 100 mL volumetric flask, filled to just below the mark, sonicated and degassed, and finally filled to the mark. An appropriate aliquot of stock solution was then combined with ACN, triply deionized H_2O and TEA using volumetric pipettes, followed by 25 min sonication, filtering using 0.45 PTFE membrane syringe filter and finally degassing for 10 min. The MS sheath liquid was prepared by mixing appropriate volume fractions of MeOH and H_2O using a 100 mL graduated cylinder followed by sonication and degassing. Stock solutions of $\text{C}_1\text{-C}_2\text{-TMA}^+$ and $\text{C}_6\text{-C}_{18}\text{-TMA}^+$ analytes were dissolved at a concentration of 20 mg/mL and 10 mg/mL, respectively in 65/35

(v/v) ACN/H₂O. A test mixture containing equal aliquot of each TMA⁺ was then combined to constitute the final injection solution.

CEC-MS Column Preparation. The mixed mode CEC-C₆/strong cation exchange (CEC-C₆/SCX) stationary phase (ReliaSil 100Å, 3 μm) was purchased from Column Engineering Inc. (Ontario, CA, USA). In the literature, this type of mixed-mode packing has been utilized for CEC-MS of basic anti-depressants,^{19,20,21} pyrimidine derivatives,²² and also for fundamental study of the electroosmotic flow (EOF).²³ Fused silica capillary (75 μm ID, 362 μm OD) was obtained from Polymicro Technologies Inc. (Phoenix, AZ, USA). The fabrication of the CEC-MS column including slurry pressure packing and internally tapered outlet tip is the same as documented in our previous work^{17,18} with several important technical differences which are discussed as follows. First, it was found that the composition of the packing solvent plays an important role in maintaining a constant packed bed during the procedure for inlet frit fabrication. Second, the ionic strength of the NaCl flushed through the column during the frit construction is also equally important. As shown previously for reversed phase CEC-C₁₈ stationary phase¹⁷, the general packing protocol calls for four basic steps: 1) overnight packing at 200 bar using ACN; 2) manual syringe injection of 10 mM aqueous NaCl solution followed by flushing at 200 bar for 3 hrs; 3) frit construction using neochrome wire burner while flushing with aqueous NaCl under 200 bar pressure; 4) removing the excess NaCl by flushing with ACN at 50 bar for ~1 hr. When this protocol was followed using CEC-C₆/SCX stationary phase, the packed bed was observed to shrink approximately 0.5 cm

away from the inlet frit during final step 4 mentioned above. In order to address the packed bed shrinkage, the composition of the packing solution as well as the ionic strength of aqueous NaCl was investigated. The final modified protocol is summarized as follows: 1) overnight packing at 200 bar using 70% ACN/30% H₂O; 2) manual syringe injection of 10 mM NaCl in 70% ACN/30% H₂O, followed by flushing at 200 bar for 3 hrs; 3) frit construction using neochrome wire burner while the column was still under 200 bar pressure; 4) removal of the NaCl solution using running buffer (containing 70% ACN/30% H₂O, pH 3.0, 15 mM NH₄OAc, 0.4% TEA). Thus, the aforementioned modified procedure showed no shrinkage in CEC-C₆/SCX packed bed length.

CEC-ESI-MS Instrumentation. All CEC-ESI-MS experiments were performed on an Agilent HP^{3D}CE system (Agilent Technologies, Waldbronn, Germany), which was interfaced to an Agilent 1100 series MSD quadrupole mass spectrometer, equipped with a CE-MS adaptor kit and a sprayer kit. Sheath liquid was delivered by an Agilent 1100 series HPLC pump equipped with a 1/100 split flow. The Chemstation software (v. 10.02) was used for data processing. The CEC-MS column was installed into the nebulizer according to manufacturer specification with one important difference. It was found experimentally that the optimum positioning of the column tip should be almost flush (protrude ~0.01 mm) with the nebulizer tip instead of protruding ~0.1 mm typically used in open-tubular CE-MS. For CEC-ESI-MS, this correlates to turning the nebulizer adjustment screw counter clockwise by only ¼ mark instead of conventional 2 marks as

described in the manufacturer setup manual for the installation of Agilent CE ESI-MS Sprayer Kit (G1607A).

CEC-ESI-MS Conditions and Capillary Conditioning. The new CEC column was first installed into the MS cartridge followed by preparation of the inlet tip, which involve diamond cutting, and removal of 2 mm polyamide coating using the homemade burner. A manual syringe pump was then attached allowing mobile phase to precondition and equilibrate the column for at least 2 hours. For CEC-ESI-MS conditioning, 12 bar pressure was applied to the inlet end, and then the voltage was sequentially raised in increment as follows: 2 kV/20 min, 5 kV/20 min, 10 kV/20 min, 15 kV/20 min, and finally 18 kV/15 min. The maximum separation voltage was 18 kV as higher voltage was found in some cases to create unwanted arcing and shortened the column lifetime. Injection was performed electrokinetically at 6 kV for 6 sec. The ESI measurements were conducted in positive ion mode. Nitrogen obtained from a nitrogen generator was used for both nebulizing and drying gas. The mass range in full scan mode was set between 50-1500 m/z . For single ion monitoring (SIM) mode, the masses were monitored as group SIM with low resolution and a gain setting 4. The direct infusion of $C_8\text{-TMA}^+$ was conducted using the following settings: Sheath liquid: 70/30 MeOH/H₂O, 10 mM NH₄OAc, pH 6.7, pump flow = 0.5 mL/min. Spray chamber: drying gas flow 6 L/min, nebulizer pressure 10 psi, drying gas temp. 300 °C, V_{cap} 4000 V, fragmentor 125 V.

RESULTS AND DISCUSSION

Initially, the direct infusion of one representative cationic standard ($C_8\text{-TMA}^+$) was conducted in order to obtain SIM ions for on-line CEC-ESI-MS method development. The full scan (50-1500 m/z) MS spectra generated from direct infusion of $C_8\text{-TMA}^+$ showed that only the protonated molecular ion $[M+H]^+$ (m/z 172) was formed in highest abundance (e.g., signal. abundance = 965,000). Therefore, $[M+H]^+$ was used for sensitive SIM monitoring for all standard cationic surfactants.

Optimization of the CEC Separation. Effect of Acetonitrile. As a starting condition, the separation of the nine standards (e.g., $C_1\text{-}, C_2\text{-}, C_6\text{-}, C_8\text{-}, C_{10}\text{-}, C_{12}\text{-}, C_{14}\text{-}, C_{16}\text{-},$ and $C_{18}\text{-TMA}^+$) was first investigated using a mobile phase of 60%(v/v) ACN, 30 mM KH_2PO_4 , pH 3.0. The selection of this mobile phase conditions was based on previous studies by Ye *et al.* for the analysis of protein and peptides.²⁴ Slight modifications to these conditions were made considering the mixed mode C_6/SCX stationary phase and MS detector used in this work. Hence, a greater percentage of 90% ACN (v/v) was used as a starting condition in order to counteract increased hydrophobic interaction due to presence of alkyl chains on both analyte and stationary phase. Furthermore, for better MS compatibility, KH_2PO_4 was replaced with volatile NH_4OAc (10 mM).

The corresponding electrochromatograms in Figure 3.2 show that 90% ACN (v/v) provides separation of all long chain $C_6\text{-}C_{18}\text{-TMA}^+$ cationic surfactants in less than 30 minutes. However, the inset extract ion chromatogram (EIC) at 90% (v/v) for shorter

chains $C_1\text{-TMA}^+$ (m/z 74) and $C_2\text{-TMA}^+$ (m/z 88) suggests that these shorter chain quats are co-eluting with $C_6\text{-TMA}^+$. Therefore, the % (v/v) ACN was lowered sequentially in order to better resolve the short chain $C_1\text{-}$ and $C_2\text{-TMA}^+$. Decreasing the ACN fraction from 90-80% (v/v) ACN was observed to have the greatest influence on the longer chain surfactants, which were retained much longer due to hydrophobic interaction with the stationary phase. Interestingly, the shorter chain $C_1\text{-}$ and $C_2\text{-TMAs}^+$ still co-eluted with $C_6\text{-TMA}^+$. Further decreasing the ACN from 80 to 70% (v/v) provided significantly longer retention for longer chains as well as peak tailing. However, the EIC showed no separation between $C_1\text{-}$ and $C_2\text{-TMA}^+$ at 70% (v/v) ACN but improved resolution from neighboring $C_6\text{-TMA}^+$. Overall, 70% ACN (v/v) was chosen based upon resolution of short chain $C_1\text{-}$ and $C_2\text{-TMA}^+$ from $C_6\text{-TMA}^+$, whereupon the problems of increased retention and peak tailing of longer chain cationic surfactants were next addressed.

Effect of Triethylamine. It is well known in ion-exchange chromatography that addition of a weak base such as triethylamine (TEA) counteracts the peak tailing caused by positively charged analytes with SCX packing materials. This is because the protonated form of TEA competes with the cationic analytes for the sulfonic acid cation exchange sites on the stationary phase, ultimately reducing the retention of cationic analytes. Thus, it was decided to add small increments of TEA to the running buffer with the hopes of decreasing the retention of longer chain surfactants while still achieving resolution of $C_1\text{-}$ and $C_2\text{-TMA}^+$ from $C_6\text{-TMA}^+$. First, as an experiment of interest, TEA was added to 90% ACN (v/v) to investigate whether separation of $C_1\text{-}$ and $C_2\text{-TMA}^+$

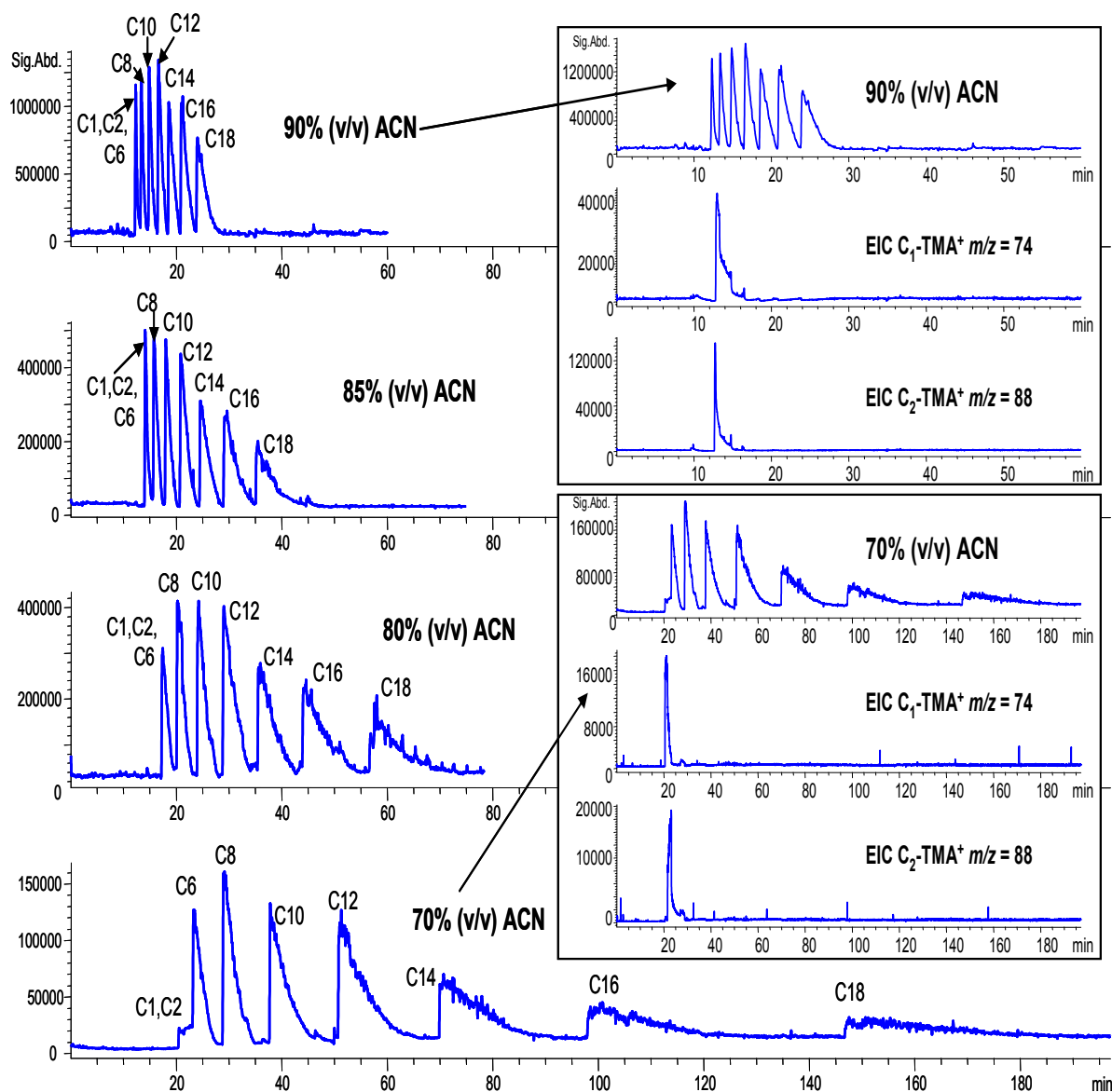


Figure 3.2: Electrophoretograms showing the effect of ACN volume fraction on the separation of nine alkyltrimethylammonium cationic compounds. Inset shows the extract ion chromatogram (EIC) for short chain C₁- and C₂-TMA⁺ at (top) 90% ACN (v/v) and (bottom) 70% ACN (v/v). Conditions: Column 1: 64 cm long, 22 cm packed bed length, 75 μ m (I.D.) capillary tapered internally (ca. 8 μ m) packed with 3 μ m CEC C₆/SCX stationary phase; mobile phase: ACN% (v/v) varied, 10 mM NH₄OAc, pH 3.0. Sheath liquid; 70/30 MeOH/H₂O, 10 mM NH₄OAc, natural pH (6.7), pump flow = 5 μ L/min. Spray chamber: drying gas flow 6 L/min, nebulizer pressure 10 psi, drying gas temp. 300 °C, V_{cap} 4000 V, fragmentor 125 V. Electrokinetic injection: 10 kv, 10 sec., 16 kV run voltage, ESI SIM positive ions (9 ions) monitored as group SIM at m/z 74, 88, 144, 172, 200, 228, 256, 284, 312.

could be enhanced further. The corresponding electrochromatograms in Figure 3.3a show that although the peak tailing and overall analysis time is reduced with added TEA at 90% ACN (v/v), this condition still provided no separation of C_1 - and C_2 -TMA⁺ from each other or from C_6 -TMA⁺.

Furthermore, at greater 0.80% (v/v) TEA, a higher CEC operating current (e.g., 24 μ A) was generated and only one run was able to be conducted after which the operating current became unstable. This is most likely attributed to excess joule heating of the CEC column. Upon repeating the TEA experiment at 70% ACN (v/v) shown in Figure 3.3b, even a small added volume fraction of TEA going from 0% to 0.1% TEA provided significant reduction in retention for all surfactants. In particular, the retention effects were more pronounced for longer chains. Overall, increasing the TEA content over the range of 0.10% to 0.40% at 70% ACN (v/v) still provided no resolution between C_1 - and C_2 -TMA⁺, but their separation selectivity with C_6 -TMA⁺ was maintained. In addition, the total analysis time decreased nearly five-fold and peak tailing of longer chains (e.g., C_{16} - and C_{18} -TMA⁺.) were dramatically improved. Similar to the trend observed at 90%(v/v) ACN (Fig. 3.3a), a higher concentration of TEA resulted in higher current which makes the CEC column unstable. Therefore, a maximum of 0.40% (v/v) TEA at 70% ACN (v/v) was chosen for further study.

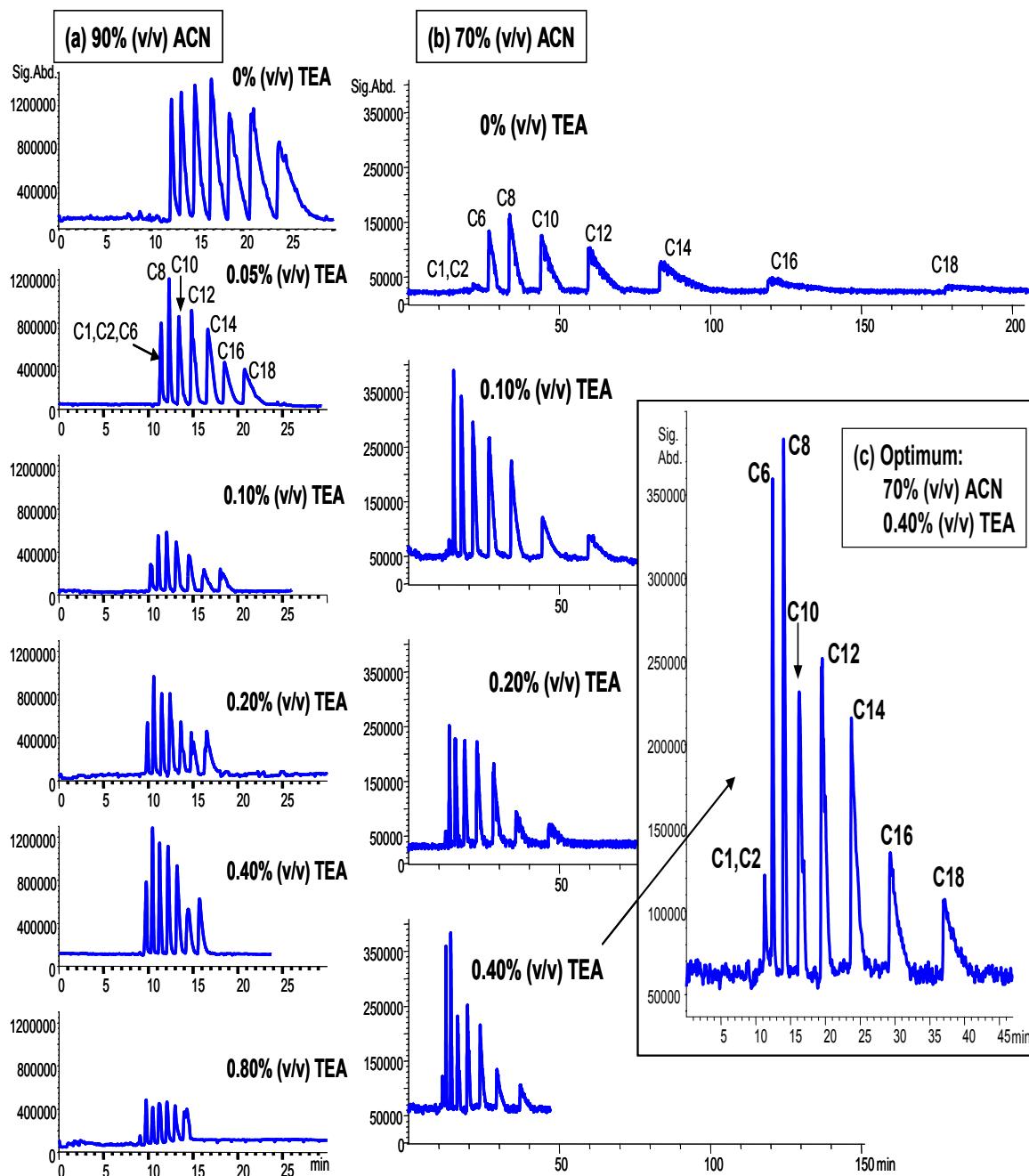


Figure 3.3: Electrochromatograms showing the effect of TEA volume fraction on the separation. Conditions are the same as Fig. 3.2 except (a) % TEA varied at 90%ACN (v/v), (b) % TEA varied at 70% ACN (v/v) on Column 2 packed bed = 27 cm, total length 70 cm with 18 kV runs. Inset (c) shows the optimum separation achieved using 0.4% TEA. Spray chamber and sheath liquid conditions are same as Fig.3.2.

Effect of Buffer pH. Next, the effect of varying the buffer pH over the range pH 2.5-5.0 was investigated maintaining previously optimized 70% (v/v) ACN and 0.40% (v/v) TEA. Adjustment of the pH using HOAc was expected to influence mainly the EOF and ion exchange process rather than analyte or stationary phase ionization. This is because the alkyl-TMA⁺ ions maintain a non-reversible constant positive charge due to quaternization of nitrogen by surrounding alkyl groups (Fig. 3.1), whereas the sulfonic acid group of the stationary phase is negatively charged at pH > 1. The electrochromatograms in Figure 3.4 show that modification of the buffer pH over the range 2.5-4.0 provides almost identical separation and detection. However, increasing the pH to 5.0 lengthens the analysis time along with loss in signal for short chain C₁- and C₂-TMA⁺ and longer C₁₆- and C₁₈-TMA⁺ ions. In order to better understand the elution trends shown in Figure 3.4, thiourea was used as a t₀ marker to monitor the EOF (Fig.3.4 inset). Triplicate runs were performed with %RSD less than 1.1%. As the pK_a of thiourea is 1.44±0.5 (Science Finder Scholar, v.2002), this was expected to be neutral over pH 2.5-5, and therefore deemed acceptable to be used as a t₀ marker.

Since the natural pH of NH₄OAc is ~6.8, increasing volume increments of HOAc were added in order to lower the pH. At pH 5.0, a small added amount of HOAc is not enough to provide adequate ion exchange causing excessive peak tailing and longer retention. This also may be due to presence of fewer dissociated hydronium cations (H₃O⁺) from weak HOAc (pK_a = 4.74) at pH 5.0. As a consequent lower ionic strength provides higher EOF demonstrated by faster elution of thiourea (t₀ = 21 min) due to decreased thickness of the electrical double layer as well as lower viscosity. Adding

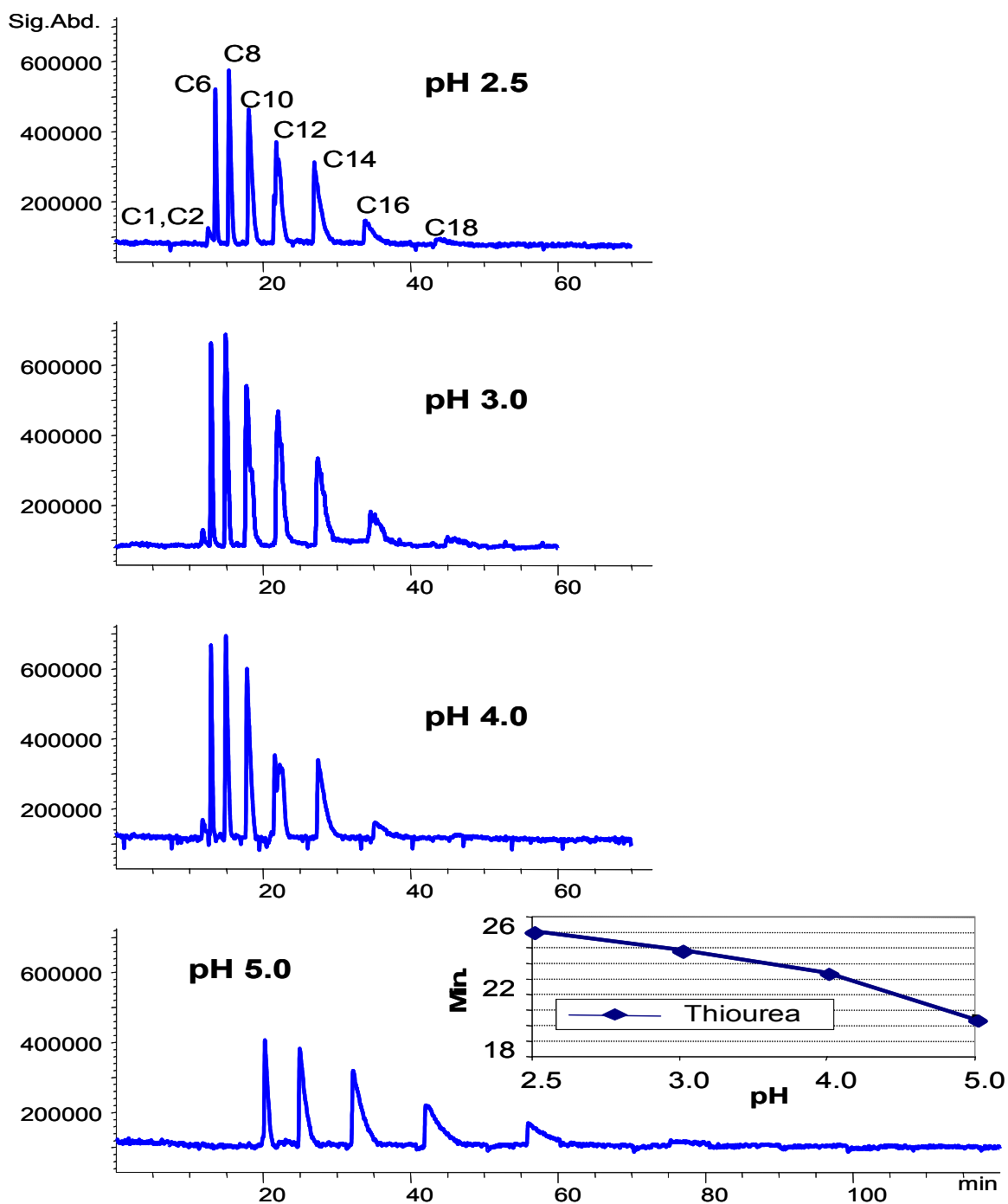


Figure 3.4: Electrochromatograms showing the effect of buffer pH. Inset of pH 5.0 shows effect of thiourea retention as a function of pH, injected at 10 mg/mL in 65/35 ACN/H₂O with 12 kv, 13 sec injection. Conditions are the same as Fig. 3.3 (b) except TEA = 0.40% and Column 3 = 30 cm packed, 70 cm total length. Spray chamber drying and sheath liquid conditions are same as Fig.3.2.

more HOAc decreases the pH from 5.0 to 4.0, which in turn reduces the ion exchange retention of analyte ion due to increase concentration of mobile phase counter ions (e.g., H_3O^+). This results in shorter analysis time and re-appearance of shorter chain (e.g., C_1 - and C_2 -TMA⁺) and less peak tailing of longer chain (e.g., C_{16} -TMA⁺) analytes. Moreover, with increasing ionic strength by decreasing the pH in the same range, the EOF was observed to slow down as shown in Fig.3.4 inset ($t_0 = 24$ min, pH 4.0) due to increase in double layer thickness. A further decrease in pH from 4.0-2.5 showed enhanced detectability of longer chain C_{18} -TMA⁺, however, no mentionable difference was observed in this pH range. Therefore, plots of signal, signal/noise (S/N), resolution (R_s), and efficiency (N) were constructed in Figure 3.5 order to better characterize small variations in the separation performance.

In general, the results of Figure 3.5 indicate that an identical response was shown for signal, R_s and N , however, S/N was slightly higher at pH 3.0. Although the retention of cationic surfactants was expected to continually decrease over the pH 4.0-2.5 in a similar fashion as shown for pH 5.0-4.0 due to greater ion exchange competition between the analyte and mobile phase counterions, the t_R in fact was found to remain constant. It can be concluded that a gradual decrease in EOF counteracts and override any decreasing retention arising from the ion exchange effect. Overall, a pH = 3.0 was selected for further study.

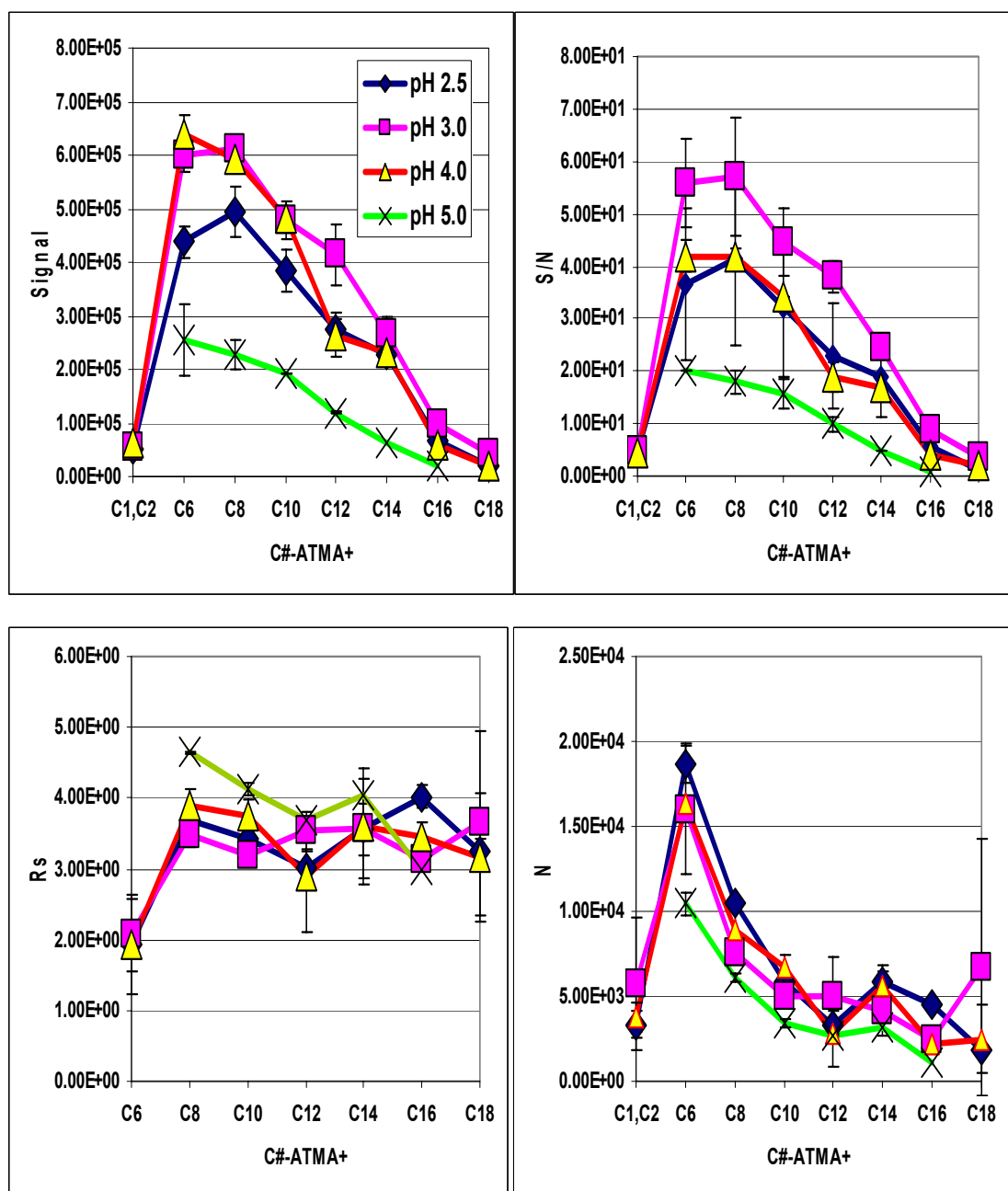


Figure 3.5: Plots of signal, signal/noise (S/N), resolution (R_s), and efficiency (N). Conditions are the same as Fig. 3.4 (b) except TEA = 0.40% and Column 3 = 30 cm packed, 70 cm total length. Spray chamber drying and sheath liquid conditions are same as Fig. 3.2.

Effect of Ammonium Acetate Concentration. Continuing the CEC optimization utilizing conditions of 70% (v/v) ACN, 0.4% (v/v) TEA and pH 3.0, the effects of varying the NH_4OAc concentration over the range 2.5-20 mM were next examined. The corresponding electrochromatograms are presented in Figure 3.6a. Several trends are worth mentioning. First, at a lower NH_4OAc concentration of 2.5 mM there are not enough NH_4^+ ions present in the mobile phase for adequate ion exchange, hence a longer separation and loss of signal for several longer chain cationic surfactants is observed similar to previous trend at pH 5.0 (Fig. 3.4). Second, upon increasing the NH_4OAc concentration to 5.0 mM, the ion exchange is improved and overall better separation and sensitivity is provided. Third, increase in NH_4OAc concentration to 10 mM was shown to enhance S/N observed from stable baseline, as well as significantly decrease the analysis time for longer chain (e.g., $\text{C}_{12}\text{-C}_{18}\text{-TMA}^+$) surfactants. Interestingly, very slight change in migration times were observed for short chains (e.g., $\text{C}_1\text{-C}_{10}\text{-TMA}^+$) as compared to longer chains aforementioned. The same trend was seen when increasing NH_4OAc ionic strength over the range 10-20 mM, whereupon shorter chains exhibited very minor decrease in retention times compared to longer chains, which continued to significantly reduce the retention times of the latter.

In order to better understand the elution trends, thiourea was again monitored as t_0 marker as shown in Figure 3.6b. Only duplicate runs were performed because the %RSD was found to be less than 0.5%, hence error bars are too small to be visible on plot. The general trend in t_0 shows that EOF is slowing down with increasing ionic strength. This

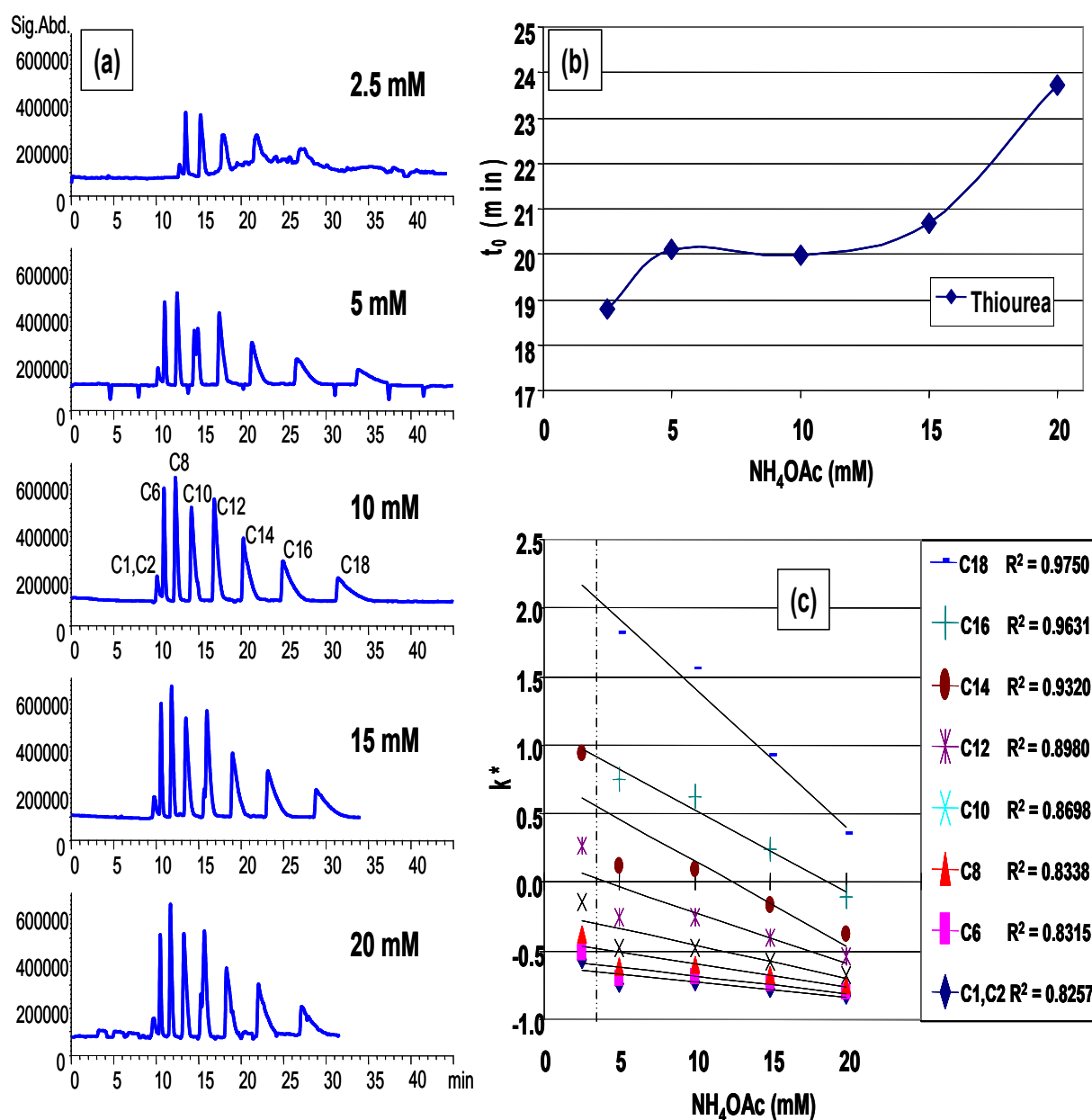


Figure 3.6: Electrochromatograms (a) and plots (b-c) showing the effect of buffer NH_4OAc concentration (mM) on the separation, (b) thiourea retention trend (t_0) and (c) CEC capacity factor (k^*) vs. NH_4OAc concentration (mM) with correlation value (dashed line indicates 2.5 mM is omitted from R^2). CEC conditions are the same as Fig. 3.4. except the mobile phase pH = 3.0 and column 4= 25 cm packed, 67 cm total length. Spray chamber and sheath liquid conditions are same as Fig.3.2.

is in accordance with previous pH discussion that states for increased BGE ionic strength increases the double layer thickness as well as higher viscosity, therefore reducing the EOF. However, as shown earlier when pH was decrease from 4.0-2.5, it caused increase in ionic strength. Consequently, the ion exchange vs. EOF effects ultimately counteracts each other causing no change in net retention time for surfactants (Figure 3.4, pH 4-2.5). In contrast, the effect of increasing NH₄OAc concentration shown in Figure 3.6a clearly shows that ion exchange is predominating over EOF for longer chains (e.g., C₁₂-C₁₈-TMA⁺) seen by decrease in retention times. On the other hand, short chains (e.g., C₁-C₁₀-TMA⁺) exhibit no change suggesting counteracting effects. Therefore, a plot of electrochromatographic capacity factor (k^*) was constructed in Figure 3.6c to better understand these trends, considering both the contributions from electrophoresis vs. chromatographic retention using the equation set forth by Ye *et al* as follows:²⁴

$$k^* = (k' - \mu_{ep}/\mu_{eo}) / (1 + \mu_{ep}/\mu_{eo}) \quad \text{Equation 1}$$

where k' is the chromatographic capacity factor $(t_R - t_0)/t_0$, μ_{ep} is the electrophoretic mobility and μ_{eo} is the electroosmotic mobility. It was decided to omit 2.5 mM from the best-fit line and corresponding equation as outlying data, which considerably lowered the correlation factors (R^2) for short chains (data not shown). This is because this lower ionic strength does not provide adequate operating conditions, hence the dashed vertical line on k^* plot is to omit 2.5 mM. Overall, for longer chain C₁₈- and C₁₆-TMA⁺, the k^* generally decreased with increasing ionic strength over the entire range 5-20 mM. In addition,

reasonably high correlation factors are observed which suggests that retention due to ion-exchange is predominant. For shorter chain length, (e.g., C_1 - C_{10} -TMA⁺), the k^* was essentially the same at lower ionic strength of 5-10 mM. However, over the range 15-20 mM the k^* showed gradual decline which was more pronounced for mid-chain length (e.g., C_{14} , C_{12} -TMA⁺) surfactants. Note, that the correlation (R^2) factors were higher for longer chain (e.g. C_{18} - and C_{16} -TMA⁺) but then falls off gradually with decrease in chainlength of cationic surfactants. In general, it can be concluded that for shorter chain cationic surfactants, the separation is controlled by electrophoresis rather than chromatographic retention. This is supported by negative k^* corresponding to elution before thiourea, as well as minor influence of ionic strength with respect to retention times. In contrast, for longer chain surfactants, the separation is controlled by chromatographic as well as ion-exchange retention as shown by a significant decrease in retention time with increasing ionic strength as well as positive k^* values due to their elution following the EOF marker. Although 20 mM NH_4OAc offered the shortest analysis time, this was coupled with increased current (24 μA), which could in turn shorten the column lifetime and promote joule heating. Therefore, 15 mM was selected as final NH_4OAc concentration.

Optimization of the ESI-MS Detection. ESI-MS Sheath Liquid Tuning. Utilizing optimized CEC separation conditions of 70% (v/v) ACN, 0.4% (v/v) TEA, pH 3.0 and 15 mM NH_4OAc , the sheath liquid composition and flow rate were next investigated for effects on MS signal abundance and S/N utilizing two representative surfactants (e.g., C_6 -

and $C_8\text{-TMA}^+$). A comparison of isopropanol (IPA) volume fraction over the range of 20-70% versus using 30-90% MeOH all containing 10 mM NH_4OAc is presented in Figure 3.7a-d. The results showed that for IPA, a smaller volume fraction of 30% provided highest abundance for both C_6^- and $C_8\text{-TMA}^+$, although consideration of the error bars suggests only minor effects of IPA on signal abundance over the range studied. A similar effect of %IPA on the S/N was observed that followed the same trend as the aforementioned signal abundance. The use of %MeOH in the sheath liquid showed that both signal and S/N to be higher in the range of 50-70% (v/v) for both C_6^- and $C_8\text{-TMA}^+$ ions. Since S/N with %MeOH at its optimum composition (Figure 3.7b) is more than two fold higher compared to the optimum for %IPA (Figure 3.7d), it was decided to select 50% (v/v) MeOH for increased sensitivity.

Next, the effect of addition of NH_4OAc to the sheath liquid over the range of 2-50 mM was examined for further improvement of MS signal and S/N. The corresponding plots shown in Figure 3.7e-f demonstrate that similar response for both surfactants was achieved over entire concentration range, however, 10 mM NH_4OAc provided highest signal (Fig. 3.7e) abundances as well as improved S/N (Fig. 3.7f). Finally, the variation of sheath liquid pump flow on both signal intensity and S/N in the range of 3-9 $\mu\text{L}/\text{min}$ is illustrated in Figure 3.7g-h. Opposite trends for signal vs. S/N were observed. The signal continually decreased with increasing pump flow probably due to the dilution effect with the sheath liquid. On the other hand, the S/N continually increased over the same flow rate settings due to increased electrospray stability and reduction in background noise. Overall, 7 $\mu\text{L}/\text{min}$ was selected as a compromise for stable and

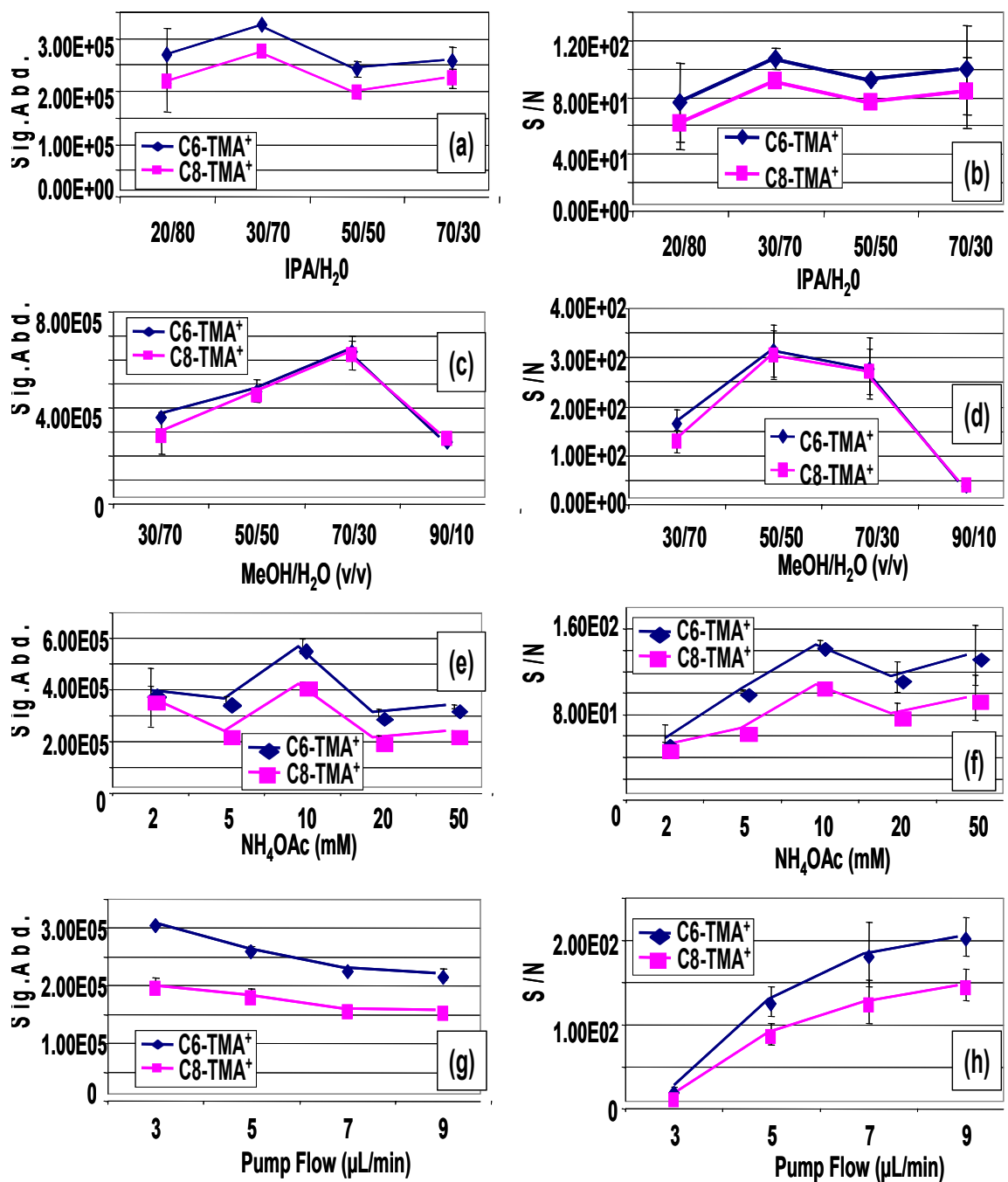


Figure 3.7: Sheath liquid tuning plots. Effects of (a) IPA volume fraction on (a) MS signal, (b) S/N, (c) MeOH volume fraction on (c) MS signal, (d) S/N. (e) NH₄OAc concentration effects on (e) MS signal (f) S/N using 50/50 MeOH/H₂O (g) pump flow effect on (g) MS Signal (h) S/N using 10 mM NH₄OAc. Conditions: same as Fig. 3.6. except CEC mobile phase contains 15 mM NH₄OAc and 15 kV runs using 3000 V_{cap}.

sensitive ESI-MS detection.

ESI-MS Spray Chamber Tuning. First, the effects of fragmentation voltage (V) and MS capillary voltage (V_{cap}) on MS signal and S/N was evaluated utilizing previously optimized CEC conditions and sheath liquid containing 50/50(v/v)MeOH/H₂O, 10 mM NH₄OAc delivered at 7 $\mu\text{L}/\text{min}$. The MS fragmentor voltage is applied at the exit end of the capillary which affects ion transmission and fragmentation. This voltage also gives the ions a push that enables them to traverse the relatively high pressure region between the exit of the capillary and the skimmer. The results of varying the fragmentor V in the range of 50-150 are shown in Figure 3.8a-b using two representative surfactants C₆- and C₈-TMA⁺ similar to sheath liquid tuning. As shown in Figure 3.8a, increasing the fragmentor V from 50-100 improved the MS signal intensity of both C₆- and C₈-TMA⁺, but then continually decreased above 100V. The effects on S/N shown in Figure 3.8b proved that increasing the fragmentor V systematically decreased the S/N for both analytes. This is because increased arcing was found to occur at moderate to higher fragmentor voltage (e.g., $\geq 100\text{V}$). Therefore, a fragmentor of 50 V was chosen as this provided the highest S/N value.

Next, the electrospray V_{cap} was studied in the range of 1500-4000 V. In contrast to the fragmentor V that is applied at the exit of the MS capillary, the V_{cap} parameter controls the voltage applied to the entrance of the capillary. Generally, the effects of raising the V_{cap} were shown to continuously enhance the MS signal in Figure 3.8c over the range of 2000-3000 V. A similar trend was observed regarding the S/N over the same

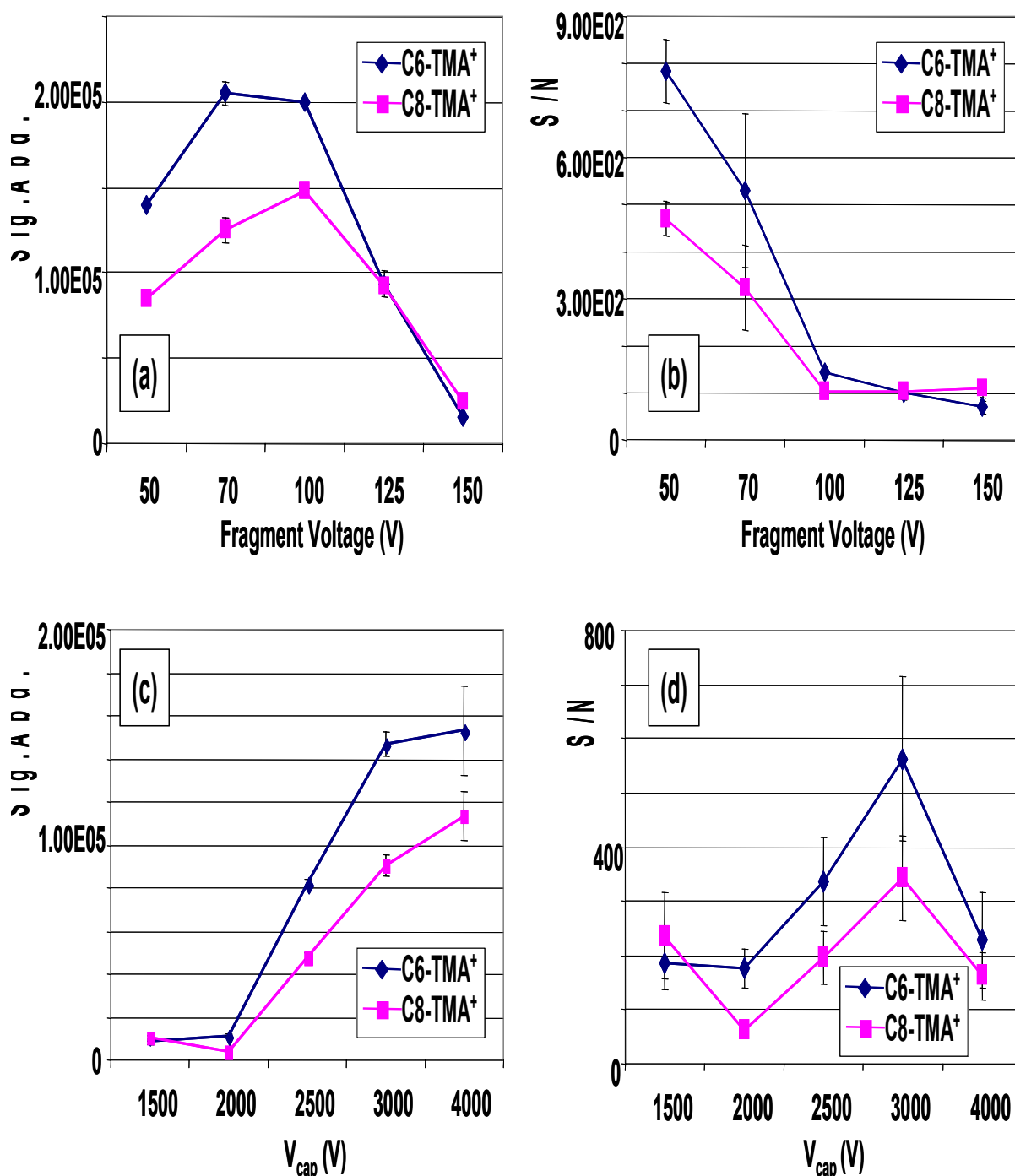


Figure 3.8: ESI fragment voltage and capillary voltage (V_{cap}) optimization using two representative cationic surfactants C₆-TMA⁺ and C₈-TMA⁺. Effect of fragment voltage on (a) MS signal and (b) S/N. Effect of V_{cap} on (c) MS signal, (d) S/N. Conditions: (a-d) 50/50 MeOH/H₂O, 10 mM NH₄OAc, 7 μ L/min, (c-d) same as (a-b) except fragment voltage = 50 V.

range (Fig. 3.8d). Although signal intensity either leveled off or increased slowly, S/N was decreased (due to increase in noise) in the range of 3000-4000 V. Furthermore, V_{cap} at 4000 V was found to be too high of a setting regarding the lifetime of the CEC column, which caused decrease in S/N due to significant arcing of the capillary. Therefore, a V_{cap} equal to 3000 V was selected as a compromise between MS signal, S/N and stability of the CEC column.

For spray chamber parameters including nebulizer pressure, drying gas flow rate and drying gas temperature, our previous work has shown that the use of structured or tailored experimental design are an efficient and effective means of optimizing these settings.¹⁷ The corresponding plots showing effects of aforementioned spray chamber parameters on the MS signal and S/N for representative C_6^- and $\text{C}_8\text{-TMA}^+$ can be seen in Figure 3.9a-d. First, the design calls for maintaining a drying gas temperature (e.g., 150 °C, 200 °C, and 250 °C) while varying the drying gas flow and nebulizer pressure in a systematic fashion. Essentially, the two variables are held constant while one is varied in order to monitor the effects of individual parameters. For example, in Figure 3.9a for $\text{C}_6\text{-TMA}^+$ at each drying gas temperature the design calls for maintaining the drying gas flow (e.g., 3, 6 or 9 L/min) then varying the nebulizer pressure in the range of 7-13 psi. This format allows optimization while minimizing time between changing spray chamber settings.

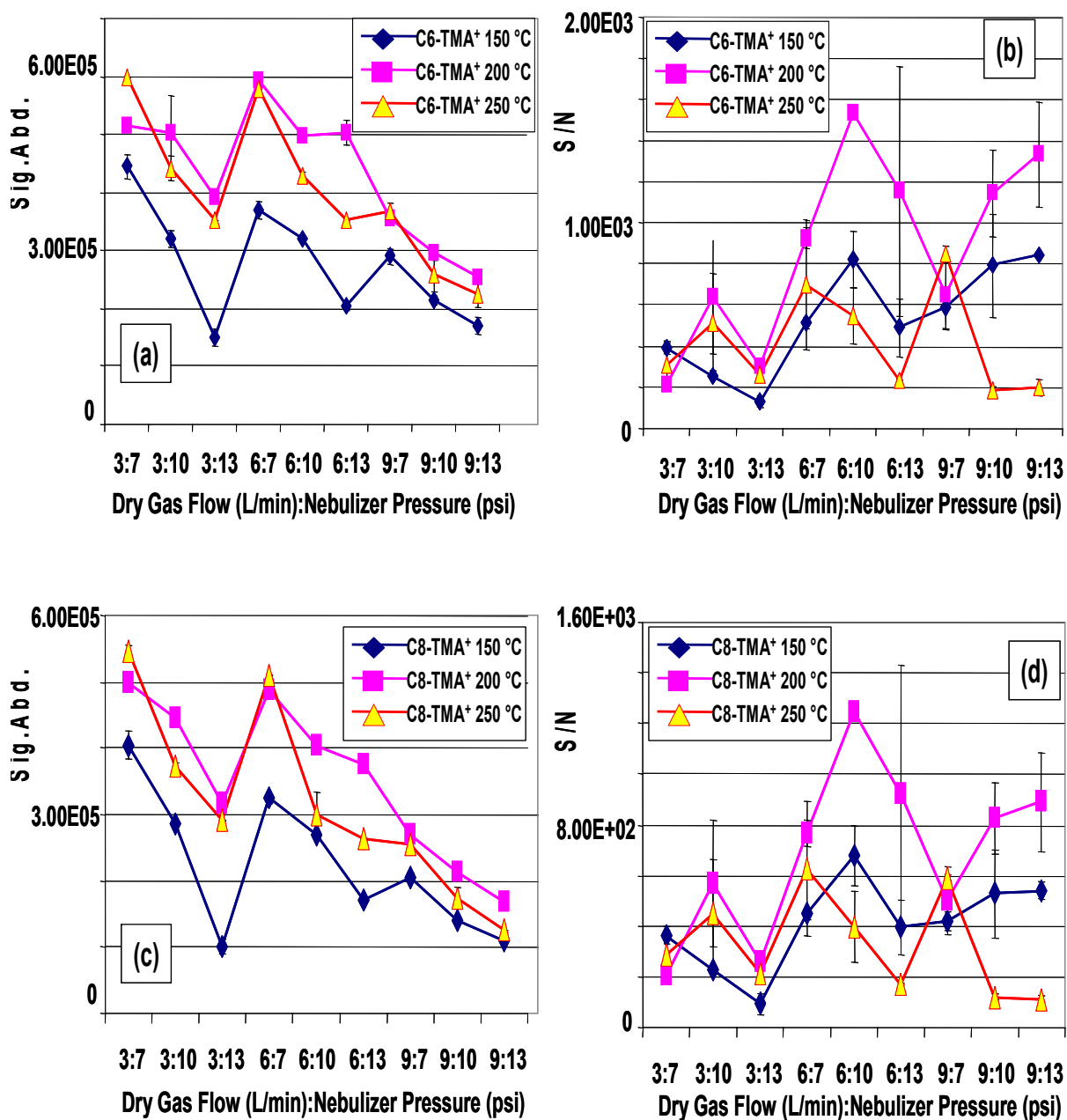


Figure 3.9: ESI spray chamber optimization. Structured experimental design calls for maintaining two of three spray chamber parameters constant for analysis of trends when varying the drying gas temperature, drying gas flow rate, and nebulizer pressure. For two representative surfactant $C_6\text{-TMA}^+$ and $C_8\text{-TMA}^+$, plots show effects on $C_6\text{-TMA}^+$ (a) MS signal, (b) S/N and $C_8\text{-TMA}^+$, (c) MS signal, (d) S/N. Conditions: same as Fig. 3.8 (c-d) except $V_{\text{cap}} = 3000$ V.

Overall, the trends were observed to be more or less the same for both C_6^- and $C_8^-TMA^+$ and can be summarized as follows. Variation in the drying gas temperature showed that lower drying gas temperature of 150 °C always provided lower MS signal (Fig. 3.9a,c) as compared to higher temperatures of 200 °C and 250 °C, which were very similar in intensity (Fig. 3.9a,c). A moderate drying gas temperature of 200 °C provided slightly higher MS signal in some cases (e.g., Fig. 3.9a, 3:10, 6:10, 6:13; Fig. 3.9c, 6:10, 6:13). Comparison of the three drying gas temperature effect on S/N shown in Figure 3.9b,d demonstrate that 200 °C overall provided the highest S/N as compared to low 150 °C and high 250 °C temperature. Next, analysis of the nebulizer pressure maintaining constant drying gas temperature and drying gas flow revealed that in all cases the MS signal decreases with increase in nebulizer pressure. For example, in Figure 3.9a increasing the nebulizer pressure from 7-13 psi at each drying gas flow rate (3,6 or 9 L/min) and each drying gas temperature (150 °C, 200 °C and 250 °C) decreases the signal abundance. The effect of nebulizer pressure on S/N for both C_6^- and $C_8^-TMA^+$ suggested that in several cases moderate setting at 10 psi was slightly higher than lower 7 psi or higher 13 psi (e.g., Fig. 3.9b at 200 °C drying gas temperature, increasing nebulizer pressure from 3:7 to 3:10 to 3:13, as well as 150 °C increasing from 6:7 to 6:10 to 6:13). Finally, for effect of varying the drying gas flow rate from 3-6-9 L/min showed general systematic decline in MS signal with increase in flow for both C_6^- and $C_8^-TMA^+$ (e.g., compare 3:7, 6:7, 9:7) although 10 psi was similar in some cases (e.g., 3:10, 6:10). The effect of drying gas flow on S/N suggested that moderate drying gas flow rate at 6 L/min provided the highest S/N (e.g., 6:10). This way, it can be concluded that the optimum

spray chamber settings for ESI-MS detection of cationic surfactant are 6 L/min, 10 psi, and 200 °C.

Linearity, Limit of Detection (LOD) and Limit of Quantitation (LOQ). The linearity, LOD and LOQ of the CEC-ESI-MS system were evaluated utilizing the optimized CEC separation and MS detection conditions. As the longer chain cationic surfactants including C_{12} - C_{18} -TMA⁺ are most frequently used in commercial formulations, these analytes were quantitated while choosing C_8 -TMA⁺ as an internal standard. For n=5 runs, the concentration of C_{12} - C_{18} -TMA⁺ was varied over the range 5 ng/mL-10 µg/mL at 8 concentration levels while C_8 -TMA⁺ concentration was held constant at 300 ng/mL. Overall, 10 ng/mL-3 µg/mL was found to be the widest concentration range that provided acceptable R^2 (data not shown). For the LOD and LOQ, Table 3.1 provides a summary of the calibration parameters over the linear range of 10 ng/mL-3 µg/mL. The satisfactory linear regression coefficients indicate that the cationic surfactant responses were linear over the concentration range studied and that these lines pass through the origin. Using 3X S/N value, the LOD was determined for longer chain C_{18} -TMA⁺ to be 5 ng/mL, although higher S/N was observed for shorter chain C_{12} - C_{14} -TMA⁺. For example, at 5 ng/mL the EIC for C_{12} -, C_{14} -, C_{16} - and C_{18} -TMA⁺ provided S/N of 30, 20, 6 and 4, respectively. The LOD estimated for cationic surfactants based on the aforementioned S/N is tabulated in Table 3.1. This data suggests that the LOD for shorter chain TMA⁺ should be much lower than the longer ones. For example, at 5 ng/mL C_{12} -TMA⁺ and C_{18} -TMA⁺ provided a S/N = 30 and 4, respectively. Thus, LODs for C_{12} -TMA⁺ and

Table 3.1: Linearity, LOD and LOQ of C₁₂-C₁₈-TMA⁺ surfactants.^a

Analyte (TMA ⁺)	Linearity Range	Calibration Parameters			LOD ^b	LOQ ^b (ng/mL)
		Slope	Intercept	R ²		
C ₁₂	10 ng/mL-3 µg/mL	0.0023	0.0236	0.9994	500 pg/mL ^c	10
C ₁₄	10 ng/mL-3 µg/mL	0.0013	0.0185	0.9966	500 pg/mL ^c	10
C ₁₆	10 ng/mL-3 µg/mL	0.0005	0.0038	0.9905	2.5 ng/mL ^c	10
C ₁₈	10 ng/mL-3 µg/mL	0.0002	0.0023	0.9872	5 ng/mL	10

(a) **Conditions:** optimum CEC separation conditions 70% ACN, 0.04% TEA, pH 3.0 and 15 mM NH₄OAc. sheath liquid optimized to 70/30 MeOH, 10 mM NH₄OAc delivered at 7 µL/min, ESI-MS operating and spray chamber parameters : fragmentor voltage = 50 V, V_{cap} = 3000 V, drying gas flow rate 6 L/min, nebulizer pressure 10 psi, drying gas temperature 200 °C.

(b) Determined experimentally for n=5 runs.

(c) Estimated from S/N at 5 ng/mL.

C₁₈-TMA⁺ was estimated to be 500 pg/mL and 5ng/mL, respectively whereas the LOQ was determined experimentally at 10X S/N. A concentration of 10 ng/mL was established as the LOQ for all C₁₂-C₁₈-TMA⁺.

Precision. The precision of the optimized CEC-MS method was evaluated regarding the repeatability. For this, the separation of a mixture of nine cationic standards was run continuously over a one week period in order to simulate running the system in a rigorous industrial laboratory setting. In all, the system was run for 7 consecutive days approximately 16 hours per day, 40 min each run. The result of the experiment proved that the system is durable for greater than 167 runs, over 111 hours which was deemed as

an acceptable stopping point. System durability and repeatability for one representative cationic surfactant $C_8\text{-TMA}^+$ is demonstrated in Table 3.2 which shows the intraday and interday precision of the migration time, peak area, normalized peak area (NPA), efficiency (N) and resolution (R_s).

First, for consideration of the migration time reproducibility shown in column 3, all individual day %RSD was acceptably less than 2.0%. Similarly, both the t_R intraday ($n=22$) and interday ($n=167$) %RSD was impressively less than 1.5 and 5% respectively. Next, an evaluation of the peak area response shown in column 4 exhibited slightly higher error with %RSD as high as 10.0% (Day 1). Moreover, intraday and interday %RSD was as large as 21.0%. This larger deviation is expected due to the absence of internal standard and variation in MS response. Therefore, the following column 5 shows the NPA using $C_6\text{-TMA}^+$ as an internal standard. The NPA provides significantly improved in-day %RSD lower than 4.0%, with much improved intraday %RSD of 2.9% and interday %RSD of 4.3%. The peak efficiency (N) data provided in column 6 showed % RSD in the range of 4.6-9.5% with intraday and interday %RSD of 7.1 and 10.3, respectively. Lastly, the reproducibility for R_s shown in column 7 demonstrates very low deviation for all seven days, intraday %RSD of 2.9, and impressive 4.2% RSD for interday ($n= 167$ injections). Overall, the experimental data demonstrates a precise yet rugged and durable CEC-MS system suitable for applications in an industrial setting.

Table 3.2: Intraday and interday precision of the migration time, peak area, normalized peak area (NPA), efficiency (N) and resolution (R_s).^(a)

		t_R (min)	Peak area	NPA ^(b)	N	R_s
Day 1 n=22	avg.	13.0	3,100,000	1.3	31,000	5.5
	%RSD	1.9	10.0	2.9	5.9	2.8
Day 2 n=23	avg.	12.9	2,500,000	1.3	30,000	5.4
	%RSD	1.5	4.3	2.6	4.6	1.9
Day 3 n=30	avg.	13.1	1,900,000	1.3	29,000	5.4
	%RSD	0.7	8.9	2.2	6.7	2.9
Day 4 n=25	avg.	13.1	2,000,000	1.4	27,000	5.2
	%RSD	0.8	7.9	3.9	9.5	3.4
Day 5 n=22	avg.	11.9	1,900,000	1.3	27,000	5.3
	%RSD	0.9	7.1	3.7	7.7	3.0
Day 6 n=30	avg.	12.0	1,800,000	1.4	25,000	5.1
	%RSD	1.4	7.5	2.5	8.0	3.4
Day 7 n=15	avg.	11.8	2,200,000	1.4	26,000	5.1
	%RSD	0.5	8.5	2.6	7.5	3.0
Intraday ^(c) n _{avg.} =~22	avg.	12.5	2,200,000	1.4	28,000	5.3
	%RSD	1.1	7.7	2.9	7.1	2.9
Interday ^(d) n _{avg.} =167	avg.	12.6	2,200,000	1.4	28,000	5.3
	%RSD	4.6	20.6	4.3	10.3	4.2

(a) Conditions: Same as Table 3.1.

(b) NPA: normalized peak area=peak area C₈-TMA⁺/peak area C₆-TMA⁺.

(c) Calculated using the average values of day 1-7.

(d) Calculated using all 167 injections.

Application to Commercial Sample. Next, the developed CEC-ESI-MS method was applied for analysis of a commercial cationic detergent Arquad S-50. This soyabean fatty acid derivative or alkyl trimethylquaternary ammonium compound has the general formula $[R-N(CH_3)_3]^+Cl^-$ where R represents a straight alkyl chain mainly consisting of a mixture C_{16} - C_{18} . The uses of the product include microbiocides as well as oil field industrial applications. According to the manufacturer product guide,²⁵ the alkyl chains present in S-50 include both saturated $R=C_{12}$, C_{14} , C_{16} , and C_{18} as well as unsaturated $R=C_{16}$, C_{18}' (one double bond), and C_{18}'' (two double bonds). Similar to previous analysis of the standards, ESI direct infusion of the S-50 was first conducted in order to obtain the ion spectra. The results showed high abundance of m/z 310 (C_{18}), m/z 312 (C_{18}') and m/z 312 (C_{18}'') followed by less intense m/z 284 (C_{16}). Therefore, it was decided to monitor the SIM molecular ions $[M+H]^+$ corresponding to the respective chain lengths (e.g., C_{12} - C_{18}) surfactants reported in the manufacturer product guide.

Figure 3.10a presents the corresponding electrochromatogram of S-50 along with the EIC for all respective alkyl chain included in the SIM method. Most interestingly, the EIC shows that for unsaturated compounds more than one peak was observed. For example, the EIC of C_{16}' -TMA⁺ and C_{18}' -TMA⁺ showed 2 peaks as compared to only one for both C_{16} -TMA⁺ and C_{18} -TMA, respectively. Similarly, C_{18}'' -TMA⁺ shows the presence of four peaks. Therefore, it was hypothesized that these multiple peaks observed for unsaturated cationic surfactants were representative of the *cis/trans* composition arising from the double bond configuration. This is illustrated in Figure 3.10b which shows the separation of four C_{18}'' -TMA⁺ isomers and two C_{18}' -TMA⁺

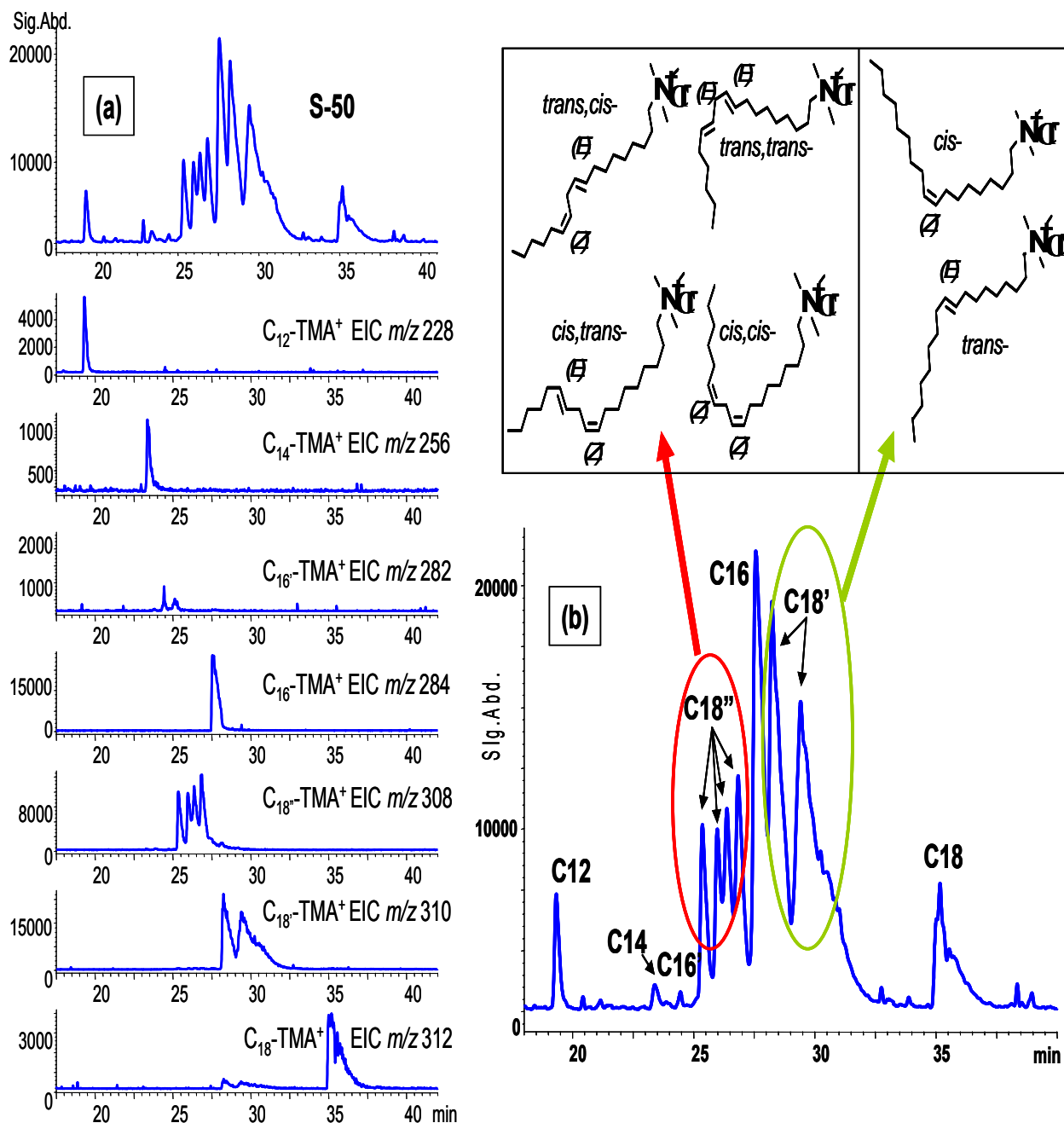


Figure 3.10: CEC-ESI-MS analysis of Arquad S-50 industrial sample. Conditions same as Fig. 3.9 except sample concentration was 15 $\mu\text{g/mL}$ and injection was 6 kV for 8 sec. (a) top shows SIM group method monitoring m/z for C_{12} - C_{18} -TMA⁺, while the bottom shows EIC of each ion, (b) same as (a) four peaks in the region of 25-27 min (left circle) corresponding to separation of four cis-trans isomer for C_{18}'' -TMA⁺ with two degrees of unsaturation; two peaks in the region of 28-30 min (right circle) corresponding to separation of two cis-trans isomer for C_{18}' -TMA⁺ with one degree of unsaturation.

isomers in S-50. As expected $C_{18''}$ -TMA⁺ isomers with two double bonds are more hydrophilic, and they eluted faster than $C_{18'}$ -TMA⁺ isomers with one double bond. In addition, a comparison of the experimental (EXP) % alkyl distribution for most of the chain length using Chemstation v.10.02 was found to correlate closely to the manufacture product guide (MPG) (Table 3.3).

Table 3.3: Composition of S-50 Sample Experimental Vs. Manufacturer Value.^a

TMA ⁺	C ₁₂	C ₁₄	C _{16'}	C ₁₆	C ₁₈	C _{18'}	C _{18''}
Soya alkyl percent ¹ (manufacturer)	0.5	1.0	1	16.0	15.0	49.5	13.0
CEC-ESI-MS (% peak area):	2.5±1.5	0.9±3.1	0.3± 7.8	19.6±1.1	6.6±1.5	47.2±1.4	22.9±2.2

a. manufacturer method uses back titration of base acids from which amines were derived

Synthesis of *cis*-C_{18'}-TMA⁺. In order to validate the separation of *cis/trans* isomers shown in Figure 3.10b, it was decided to obtain a pure (1) *cis*- or (2) *trans*- isomer of C₁₆-C₁₈-TMA⁺ surfactant then spike the S-50 sample followed by comparison of the peak area. However, a search for these compounds from all chemical manufacturers showed that only the carboxylic acid form was available in *cis* form (e.g., *cis*-oleic acid), not the trimethylated ammonium surfactant. Therefore, an alternate route was approached which involved in-house synthesis of representative *cis*-C_{18'}-TMA⁺ with hopes of identifying the C_{18'} (*cis*) component presented in Figure 3.10b.

Typically, the conversion of commercially available *cis*-oleic acid to *cis*-C₁₈-TMA⁺ can be accomplished by first reduction of the carboxylic acid to alcohol, followed by halogenation of the alcohol and finally quaternization by trimethylated amine.²⁶ However, this synthetic scheme calls for several chemoselectivity problems which generate by-products that can render isolation of the product cumbersome. Alternately, a straight forward and more efficient pathway calls for conversion of commercially available *cis*-oleyl chloride into trimethylammonium surfactant, thereby eliminating two tedious steps mentioned above for converting carboxylic acid into alcohol, then alkyl chloride, and ultimately to the desired product.²⁶

In house conversion of *cis*-oleyl chloride into the corresponding quaternary surfactant involved first generation of trimethylamine in reflux solvent. Trimethylamine was formed by reaction of trimethyl amine hydrochloride salt with Na₂CO₃ in IPA, and then filtered to obtain trimethylamine in IPA solution. Next, *cis*-oleyl chloride was added to trimethyl amine IPA solution then boiled at 80 °C for 48 hours, followed by rotoevaporation of IPA. Overall, the reaction temperature was kept at 80 °C to prevent conversion of the oleyl chloride chain from *cis*- to *trans*-, which could occur at higher temperature (~600 °C). The resulting product was dissolved in water and extracted with ethyl acetate to remove organic impurities. The clear solution was next freeze dried to obtain yellowish solid final product. Finally, the purity and identity of the synthetic product was verified by ¹H-NMR analysis of alkene protons and also ESI-MS direct infusion, which showed intense *m/z* spectra at 310.

Spiking of Synthetic *cis*-C₁₈'-N⁺(CH₃)₃ into S-50. Following the synthesis of *cis*-C₁₈-TMA⁺, a spiking study of S-50 was next undertaken with hope of identifying the *cis*-component C₁₈'. Initially, two different spiking methods comparing one vs. two vials injection were conducted. The results showed that two vial injections involving first S-50 injection followed by injection of *cis*-C₁₈-TMA⁺ worked slightly better than one injection vial containing both S-50 and *cis*-C₁₈-TMA⁺ (data not shown). The corresponding electropherograms for the spiking study are presented in Figure 3.11a-c. Duplicate runs are shown for qualitative reproducibility including the EIC for comparison of *cis*-*trans* peak ratios. In Figure 3.11a, both EIC for C₁₈' component in S-50 shows that the *cis*-*trans* peak ratio is very similar in height. However, for the synthesized *cis*-C₁₈-TMA⁺ shown in Figure 3.11b, the *cis*-*trans* ratio is much higher as evident from the increase height of the left peak which indicates that *cis* C₁₈'-TMA⁺ elutes before the *trans* C₁₈'-TMA⁺. Similarly, when the *cis*-C₁₈-TMA⁺ is spiked into the S-50 commercial sample shown in Figure 3.11c, an increase in *cis* height was observed. Although the qualitative differences in peak height are clearly established in the Figure 3.11a-c, for proper quantification and identification it was decided to repeat the experiment running each sample six times (n=6) replicated on two more columns and monitor the differences in peak area rather than peak height. Table 3.4 presents the data when monitoring the *cis*-*trans* isomeric peak area for two trials both n=6. The data was obtained using EIC for C₁₈'-TMA⁺ *m/z* 310 and % peak area in the Chemstation software. In Trial 1, the concentration of S-50 was maintained at 15 µg/mL while synthesized *cis*-C₁₈'-TMA⁺ was injected at 10 µg/mL. Overall, the average of six runs on S-50 sample shows that the

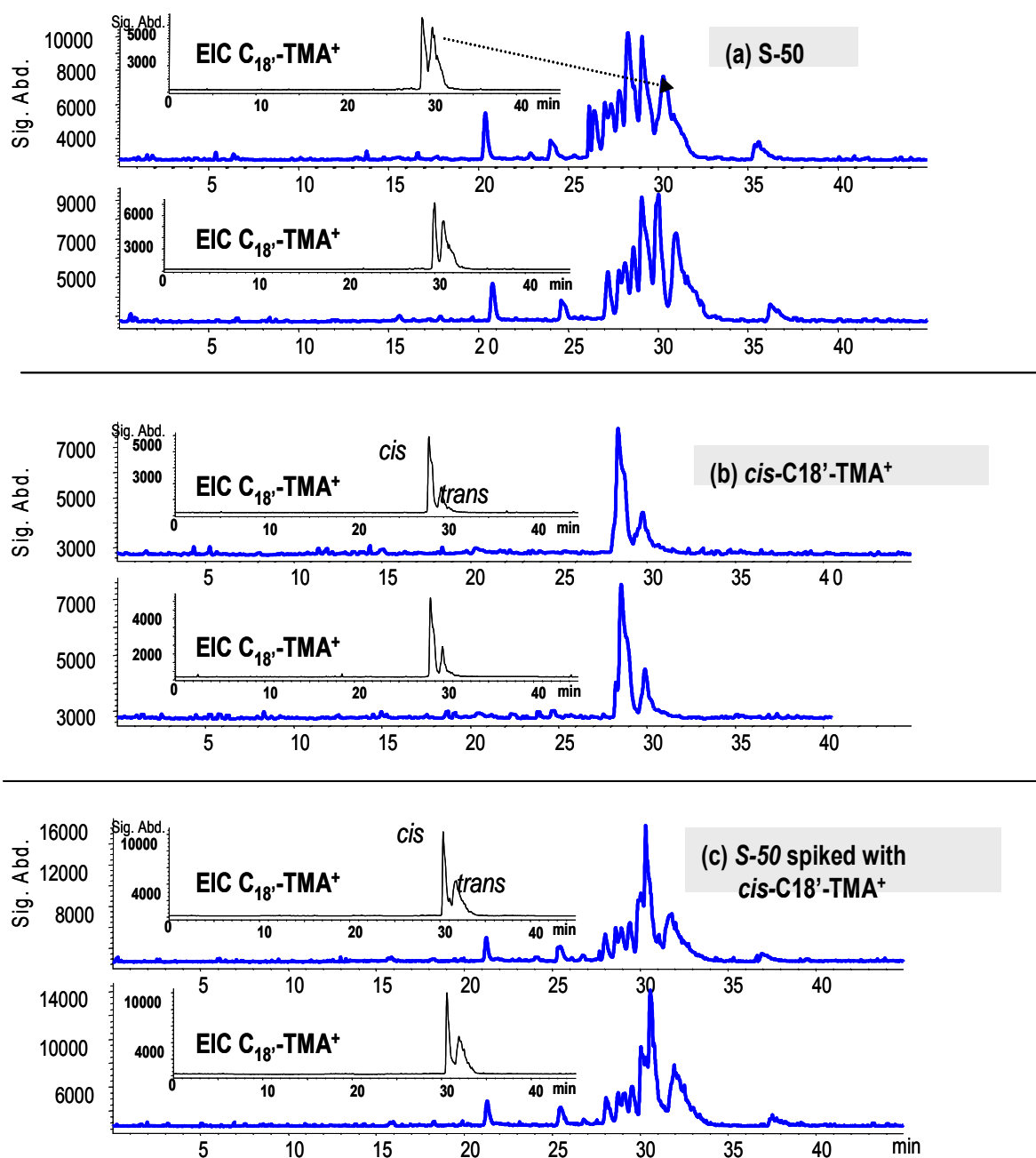


Figure 3.11: Spiking study of the cis-trans C18' component present in Arquad S-50 sample. Duplicate injections for each study are shown for reproducibility. Conditions are same as Fig. 3.10. (a) SIM analysis of S-50 sample. The inset EIC shows extracted m/z corresponding to C_{18'}, (b) Analysis of synthetic cis-C_{18'}-TMA⁺ injected at 10 $\mu\text{g/mL}$ with corresponding EIC (shown as inset) for C_{18'}-TMA⁺, (c) spiking of synthetic cis-C_{18'}-TMA⁺ into Arquad S-50 using two vial injections both 6 kV 8 sec. SIM ions and analyte concentrations are same as (a-b) above.

Table 3.4: Comparison of the peak area percent for C₁₈ *cis/trans* isomers in Arquad S-50 versus S-50 spiked with *cis*-C₁₈-TMA⁺ (a)

Trial 1	S-50 (15 µg/mL)		<i>cis</i> -C ₁₈ -TMA ⁺ (10 µg/mL)		S-50 spiked+ <i>cis</i> -C ₁₈ -TMA ⁺	
	<i>cis</i>	<i>trans</i>	<i>cis</i>	<i>trans</i>	<i>cis</i>	<i>trans</i>
	26.6	73.4	60.5	39.5	33.7	66.3
	34.6	65.4	60.6	39.4	32.9	67.1
	29.9	70.1	61.5	38.5	35.9	64.1
	27.7	72.3	59.7	40.3	33.9	66.1
	31.0	69.0	63.3	36.7	33.8	66.2
	28.3	71.7	62.3	37.7	37.1	62.9
avg.	29.7	70.3	61.3	38.7	34.6	65.5
stdev.	2.9	2.9	1.3	1.3	1.6	1.6
%RSD	9.7	4.1	2.2	3.4	4.6	2.4
<hr/>						
Trial 2	S-50 (15 µg/mL)		<i>cis</i> -C ₁₈ -TMA ⁺ (15 µg/mL)		S-50 spiked+ <i>cis</i> -C ₁₈ -TMA ⁺	
	<i>cis</i>	<i>trans</i>	<i>cis</i>	<i>trans</i>	<i>cis</i>	<i>trans</i>
	31.9	68.1	61.4	38.6	39.8	60.2
	27.3	72.7	61.9	35.2	35.0	65.0
	28.3	71.7	59.1	40.9	40.9	59.1
	30.6	69.4	60.6	39.4	40.1	59.9
	32.0	68.0	58.5	41.5	41.7	58.3
	29.8	70.2	59.0	41.0	43.6	56.4
avg.	30.0	70.0	60.1	39.4	40.2	59.8
stdev.	1.9	1.9	1.4	2.3	2.9	2.9
%RSD	6.4	2.7	2.3	5.9	7.2	4.8

(a) Conditions: Same as Figure 3.11.

cis-trans %peak area ratio is ~30/70, for *cis*-C₁₈'-TMA⁺ ~60/40, and for spiked sample ~35/65. Therefore, the increase in *cis* ratio is ~5% in the spiked sample. A similar result was achieved for S-50 and the synthesized *cis*-C₁₈'-TMA⁺ in Trial 2 where injection of each was performed at slightly higher concentration (15 µg/mL). However, the spiked sample shows increase in *cis-trans* % area. For example, the spiked sample (Trial 2, column 3) shows increase in *cis*-C₁₈'-TMA⁺ to ~40% from 30% and decrease in *trans* from 70% to 60%. These results suggest that indeed the challenging separation of *cis-trans* geometrical isomers is occurring in the CEC-MS system. Furthermore, the *cis* isomer is shown to elute faster than the *trans* isomer most likely due to steric interactions. Overall, the elution order is consistent with previous work on CZE separation of *cis/trans* adamantane isomers where *cis*- eluted before *trans*- isomer.¹²

CONCLUSIONS

We have developed a simple, robust and reproducible CEC-MS method for the analysis of C_1 - C_{18} -TMA⁺ compounds utilizing an internally tapered CEC-MS column packed with a mixed mode CEC-C6/SCX stationary phase. The CEC separation was first optimized by varying the volume fraction of ACN, TEA, volatile buffer (NH₄OAc) pH and concentration. When higher volume fraction of 90% ACN was utilized as mobile phase, the short chain cationic compounds C_1 -TMA⁺ and C_2 -TMA⁺ co-eluted with C_6 -TMA⁺. Upon lowering ACN to 70% (v/v) improved the separation of short chain C_1 , C_2 -TMA⁺ compounds from neighboring C_6 -TMA⁺, but at the expense of significantly increased retention and peak tailing of longer chain cationic surfactants such as C_{18} -TMA⁺. This was next counteracted by addition of 0.40% (v/v) TEA to the mobile phase which in turn did not compromise the separation selectivity of short chain C_1 - C_2 -TMA⁺ from C_6 -TMA⁺, but in fact significantly reduced peak tailing and provided shorter retention. Overall, the results of TEA study at both 90% and 70% (v/v) ACN showed that separation of longer chain cationic surfactants (C_6 - C_{18} -TMA⁺) can be performed with 90% ACN in 15 min, but simultaneous separation of short chain cationic compounds (C_1 - C_2 -TMA⁺) with longer chain (C_6 - C_{18} -TMA⁺) requires a much weaker solvent (e.g., 70% ACN) that in turn increases the total analysis time to 40 min. Despite a decrease in EOF when the pH of NH₄OAc was decreased from 5.0-2.5, the retention time first decrease up to pH 4.0 due to ion exchange mechanisms. Further decrease in pH from 4.0-2.5 results in no significant drop in retention times of cationic surfactants, which suggest that ion-exchange and EOF effects compete with each other over this pH range. Optimization of

the buffer ionic strength was found to mainly influence the longer chain C_{10} - C_{18} -TMA⁺ surfactants. A comparison of the k^* values suggested that these C_{10} - C_{18} -TMA⁺ were retained under chromatographic mechanism, while the shorter chain C_1 - C_8 -TMA⁺ compound migrated mainly due to difference in electrophoretic mobility. The optimum CEC separation conditions were 70% ACN, 0.40% TEA, pH 3.0 and 15 mM NH₄OAc.

An optimization of the ESI-MS sheath liquid composition comparing the use of MeOH vs. IPA showed that similar ionization is achieved using higher volume fraction of MeOH (e.g., 70%) as compared to lower volume of IPA (e.g., 30%). The sheath liquid was optimized to 70/30 MeOH, 10 mM NH₄OAc delivered at 7 μ L/min. The ESI-MS operating voltages and spray chamber parameters were next investigated utilizing experimental design for the latter. The settings that provided highest sensitivity were as follows: fragmentor voltage = 50 V, V_{cap} = 3000 V, drying gas flow rate 6 L/min, nebulizer pressure 10 psi, drying gas temperature 200 °C. These conditions were then utilized to determine the linearity and LOQ. The LOD was estimated to be as low as 500 pg/mL for the shortest chain C_6 -TMA⁺. The durability and performance of the system is assessed which proved reproducible for greater than 165 runs over 111 hours, thus validating the approach to be suitable for rigorous industrial setting. Finally, the developed CEC-ESI-MS method was applied for analysis of real sample S-50 whereupon the simultaneous separation of saturated and unsaturated cationic surfactants (containing *cis/trans* geometrical isomers) was achieved. The identity and elution order of the *cis/trans* isomer of C_{18} -TMA⁺ in S-50 sample was confirmed via synthesis of *cis* isomer and spiking this isomer in S-50 sample.

ACKNOWLEDGMENTS

This project was supported by National Institute of Health (Grant No. GM 62314-02) and Solvay Pharmaceuticals (Marietta, GA). Additionally, we thank Akzo Nobel (Illinois, USA) for providing Arquad S-50 (batch SR576363X) sample. Also, a special thanks to Syed Asad Ali Rizvi for his participation in this work.

References:

- (1) Tsai, P.-C., Ding, W.-H. *J. Chromatogr. A* **2004**, 1027, 103.
- (2) Ding, W.-H., Tsai, P.-C. *Anal. Chem.* 2003, 75, 1792.
- (3) Hind, A.R., Bhargava, S.K., Grocott, S.C. *J. Chromatogr. A* 1997, 765, 287.
- (4) Harrison, C.R., Lucy, C.A. *J. Chromatogr. A* **2002**, 956, 237.
- (5) Radke, M., Behrends, T., Förster, J., Herrmann, R. *Anal. Chem.* **1999**, 71, 5362.
- (6) Di Corcia, A. *J. Chromatogr. A* **1998**, 794, 165.
- (7) Fernández, P., Alder, A.C., Suter, M.J.-F., Giger, W. *Anal. Chem.* **1996**, 68, 921.
- (8) Shibukawa, M., Eto, Kira, R., A., Miura, F., Oguma, K., Tasumoto, H., Ogura, H., Uchiumi, A. *J. Chromatogr. A* **1999**, 830, 321.
- (9) Liu, H.-Y., Ding, W.-H. *J. Chromatogr. A* **2004**, 1025, 303.
- (10) Wycherley, D., Rose, M.E., Giles, K., Hutton, T.M., Rimmer, D.A. *J. Chromatogr. A* **1996**, 734, 339.
- (11) Heinig, K., Vogt, C., Werner, G. *J. Chromatogr. A* **1997**, 781, 17.
- (12) Shamsi, S.A., Danielson, N.D. *J. Chromatogr. A* **1996**, 739, 405.
- (13) Heinig, K., Vogt, C. *Electrophoresis* **1999**, 20, 3311.
- (14) Buchberger, W., Schöftner, R. *Electrophoresis* **2003**, 24, 2111.
- (15) Klampfl, C.W. *J. Chromatogr. A* **2004**, 1044, 131.
- (16) Barceló-Barrachina, E., Moyano, E., Galceran, M.T. *Electrophoresis* **2004**, 25, 1927.
- (17) Norton, D., Zheng, J., Danielson, N., Shamsi, S.A. *Anal. Chem.* **2005**, 77, 6874.
- (18) Zheng, J., Norton, D., Shamsi, S.A. *Anal. Chem.* **2006**, 78, 1323.

- (19) Steiner, F., Lobert, T. *Chromatographia* **2003**, 58, 207.
- (20) Spikmans, V., Lane, S.J., Tjaden, U.R., Greef, J.v.d. *Rapid Commun. Mass Spectrom* **1999**, 13, 141.
- (21) Jiskra, J., Claessens, H.A., Cramers, C.A., *J. Sep. Sci.* **2003**, 26, 1305.
- (22) Klampfl, C.W., Buchberger, W., Haddad, P.R., *J. Chromatogr. A* **2001**, 911, 277.
- (23) Smith, N., Evans, M.B., *J. Chromatogr. A* **1999**, 832, 41.
- (24) Ye, M., Zou, H., Liu, Z., Ni, J., *J. Chromatogr. A* **2000**, 869, 385.
- (25) Product Care Guide, 2002 Akzo Nobel Surface Chemistry, *Publication SC02-01*.
- (26) Holmberg, K., Jönsson, B., Kronberg, B., Lindman, B., *Surfactants and Polymers in Aqueous Solutions 2nd ed.*, John Wiley and Sons, West Sussex, **2003**.

Chapter 4:
Capillary Electrochromatography of Triton X-100

Abstract

Non-ionic surfactants such as Triton X 100 are comprised of a mixture of oligomers with a varying degree of length in the polyethoxy chain. Consequently, the distribution of these oligomers can affect the chemical composition and end-use of these types of surfactants. The development of chromatographic methods for resolution of the various oligomers is of environmental importance, and can be useful for quality control and characterization in industrial manufacture. Capillary electrochromatography (CEC) is fast becoming a capable separation technique that combines the benefits of both high performance liquid chromatography (HPLC) and capillary electrophoresis (CE). This report presents a novel CEC method for separation of the various Triton X 100 oligomers. A systematic mobile phase tuning and comparison of monomeric vs. polymeric stationary phases for separation of Triton X 100 was conducted. Various mobile phase parameters such as ACN content, Tris concentration, pH, voltage and temperature were manipulated in order to achieve the optimum separation. The CEC experiments were conducted utilizing a CEC-octadecylsilica (ODS) stationary phase and fused-silica capillary [(75 μm I.D., 363 μm O.D.) 37.5 cm total length, 25.0 cm effective length] which was slurry pressure packed in our laboratory. Optimum CEC separation conditions were achieved using 90% (v/v) ACN/10% (v/v) 12.5 mM Tris, pH 7.0, and 20 kV at 20°C. The results of this work demonstrate that a separation of greater resolution is achievable with CEC as compared to existing chromatographic methods for the analysis of non-ionic surfactants such as Triton X 100.

Introduction

Non-ionic surfactants find a broad range of application due to their unique chemical composition. They are used as defoamers, emulsifiers, and to improve the solubility of pesticide formulations in water.¹ In addition, non-ionic surfactants can also enhance the properties of other surfactant systems.² Owing to their relative ionic insensitivity and sorptive properties,³ non-ionic surfactants of the alkylphenol polyethoxylate (APE) type are commonly used in both domestic and industrial detergent formulations,⁴ wetting agents as well as industrial cleaners.⁵ Triton X-100 (TX-100) is one of the most important APE that is extensively used in biological systems.⁶⁻⁸ Due to the varying degree of ethoxylation in TX-100, there is a large distribution of oligomers with different lengths that comprise the polyethoxy chain (Figure 4.1).⁵ Consequently, the number of EO units that comprise each oligomer can differ considerably making TX-100 a surprisingly complex mixture. Therefore, the ability to separate and resolve APEs and other similar non-ionic surfactants into their respective oligomers is of biological, environmental and industrial importance.

Several analytical techniques have been developed for the chromatographic separation and identification of the numerous oligomers of TX-100 including gas chromatography (GC),⁹ supercritical fluid chromatography (SFC),¹⁰ and high performance liquid chromatography (HPLC),^{4,5,11} In the case of HPLC, our literature search provided us with no separations of TX-100 or similar surfactants that were able to achieve high resolution between the oligomers in a short analysis time. Thus, the development of new chromatographic techniques for improved separation of TX-100 and

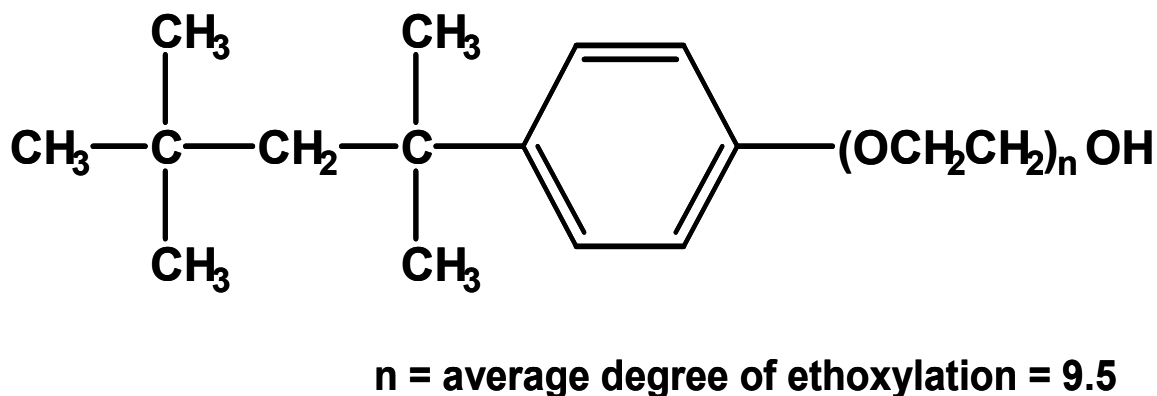


Figure 4.1: The chemical structure of Triton X-100 (TX-100).

other non-ionic surfactants is warranted.

Capillary electrochromatography (CEC) is rapidly gaining recognition as a technique capable of resolving a wide range of analytes.¹² This can be attributed to the fact that CEC enables simultaneous separation of both neutral and charged compounds. Similar to HPLC, neutral compounds in CEC can be separated based on interactions with the stationary phase, while for charged compounds, resolution is achieved based upon differences in electrophoretic mobility that result from varying charge to mass ratio, which is similar to capillary electrophoresis (CE). Recently, we have demonstrated the utility of several commercially available monomeric and polymeric CEC packings for separation of highly hydrophobic and geometrically similar methylated polycyclic aromatic hydrocarbons.^{13,14} It was therefore a logical choice to extend the applicability of

these CEC stationary phases for separation of other “*difficult-to-separate*” non-ionic compounds.

In this study, we used Triton X-100 (TX-100) as a model non-ionic heterogeneous octylphenol ethoxylate surfactant to conduct a systematic CEC optimization to achieve the best separation of this oligomer. To our knowledge, this is the first application of CEC for analysis of non-ionic surfactants.

EXPERIMENTAL SECTION

Materials and Methods. Chemicals. Acetonitrile (ACN) of HPLC grade was purchased from Burdick and Jackson (Muskegon, MI, USA). TX-100 (octylphenolethoxylate), Tris (hydroxymethyl) aminomethane (Tris) (99.9+%), thiourea (99%), biphenyl (99.5%), o-terphenyl (99%), thalic acid diethyl ester (99%), and dimethyl ester (99+%) were purchased from Sigma Chemical Company (St. Louis, MO, USA). Hydrochloric acid was purchased from Fisher Scientific (Springfield, NJ, USA). Acetone of HPLC grade was purchased from EM Science (Gibbstown, NJ, USA).

Buffer and Analyte Preparation. All mobile phases were obtained by first preparing the stock background electrolyte (BGE) which was prepared by weighing and dissolving 7.57 g Tris in triply deionized water (ca. 60 mL) in a 100 mL beaker. Next, the desired

pH of Tris in the range of 6.0–9.0 was achieved by adjusting with HCl. The pH adjusted solution was then transferred to a 100 mL volumetric flask and filled to just below the mark. This solution was sonicated for 15 min and finally filled to the mark with triply deionized water. The BGE was filtered through a 0.45 μm syringe filter, and thoroughly degassed for 6 min. A small aliquot of the stock (625 mM) Tris BGE was then added to the appropriate amount of filtered organic solvent, followed by addition of triply deionized water in appropriate ratio in order to prepare a mobile phase of constant ionic strength for all CEC experiments. The final mobile phase was lastly sonicated for 7 min and thoroughly degassed for 6 min prior to use. Sample was prepared at a concentration of 10 mg/mL in running buffer.

CEC Instrumentation. The CEC experiments were conducted on an Agilent model 3D-CE (Palo Alto, CA, USA). Ultraviolet (UV) detection was utilized due to the presence of the benzene aromatic ring in TX-100. Data at 214, 220, 254, and 280 nm were monitored on a PC using Chemstation software. Since a higher response and better signal-to-noise ratio was obtained by detecting the TX-100 at 214 nm, this wavelength was used for the entire study. Electrokinetic injection of analyte was performed at 5 kV for 5sec, followed by a 5 kV 3 sec buffer injection. Reliasil monomeric C_{18} (100 \AA , 3 μm) stationary phase was purchased from Column Engineering (Ontario, CA, USA). The stationary phase was packed into fused-silica capillary (75 μm I.D. x 363 μm O.D.) which was purchased from Polymicro Technologies (Phoenix, AZ, USA). The total length of the capillary was 37.5 cm, including a 25 cm packed bed, a 4 cm and 8.5 cm

open segments at the inlet and outlet end, respectively. The capillary packing was performed as described previously.¹³

The newly packed capillary column was installed into the Agilent cassette and then preconditioned with 80/20% (v/v) (ACN/ 5 mmol Tris, pH 8). The column was conditioned by applying successively increasing voltages in 5 kV increments for 10 min each up to 30 kV using 12 bar on the inlet vial. Finally, the capillary was conditioned for 30 min using 12 bar pressure at 30 kV on both inlet and outlet vials. The temperature was maintained at 20°C and all CEC separations were performed with 12 bar pressure applied to both vials to prevent bubble formation.

Following the manufacture of each column, a neutral test mixture containing thiourea, biphenyl, o-terphenyl, thalic acid dimethyl and diethyl ester was initially run in order to establish correct operation of the column, whereupon high N and Rs was achieved (data not shown). Table 4.1 summarizes the specifications of the three stationary phases that were utilized in this study.

RESULTS AND DISCUSSION

First, the capability of two polymeric C₁₈ packing materials and one monomeric CEC-C₁₈ material were evaluated for separation of TX-100 oligomers. The specifications of each

phase are shown in Table 4.1. Figure 4.2 compares the representative electrochromatograms of TX-100 separation under the same mobile phase conditions. As can be seen from Figure 4.2a-b, both polymeric phase materials with high carbon content and surface coverage offer inferior separations due to a narrow elution window as compared to the monomeric CEC-C₁₈ material. Interestingly, monomeric CEC-C₁₈ provides a much wider separation window with considerably higher Rs, selectivity, and N as evident from the electrochromatogram (Figure 4.2c). The results of our previous CEC work comparing different packing materials showed that polymeric PAH material was more suitable for analysis of geometrical isomers of methylated PAH.¹⁴ However, for the ethoxylated oligomers of TX-100, interestingly, a monomeric CEC-C₁₈ material provides a superior separation.

Table 4.1: Commercial stationary phases utilized in this study.

Stationary phase	Particle size (μm)	Pore size (Å)	% Carbon loading ^a	Surface coverage (μmoles/m ²) ^a	Endcapping
Reliasil Monomeric-CEC-C ₁₈	3	100	14.0	2.5	No
Reliasil Polymeric-C ₁₈	3	100	15.9	2.8	Yes
Reliasil Polymeric-C ₁₈ -PAH	5	100	16.1	2.8	Yes

a) % carbon loading and surface coverage data provided by Column Engineering.

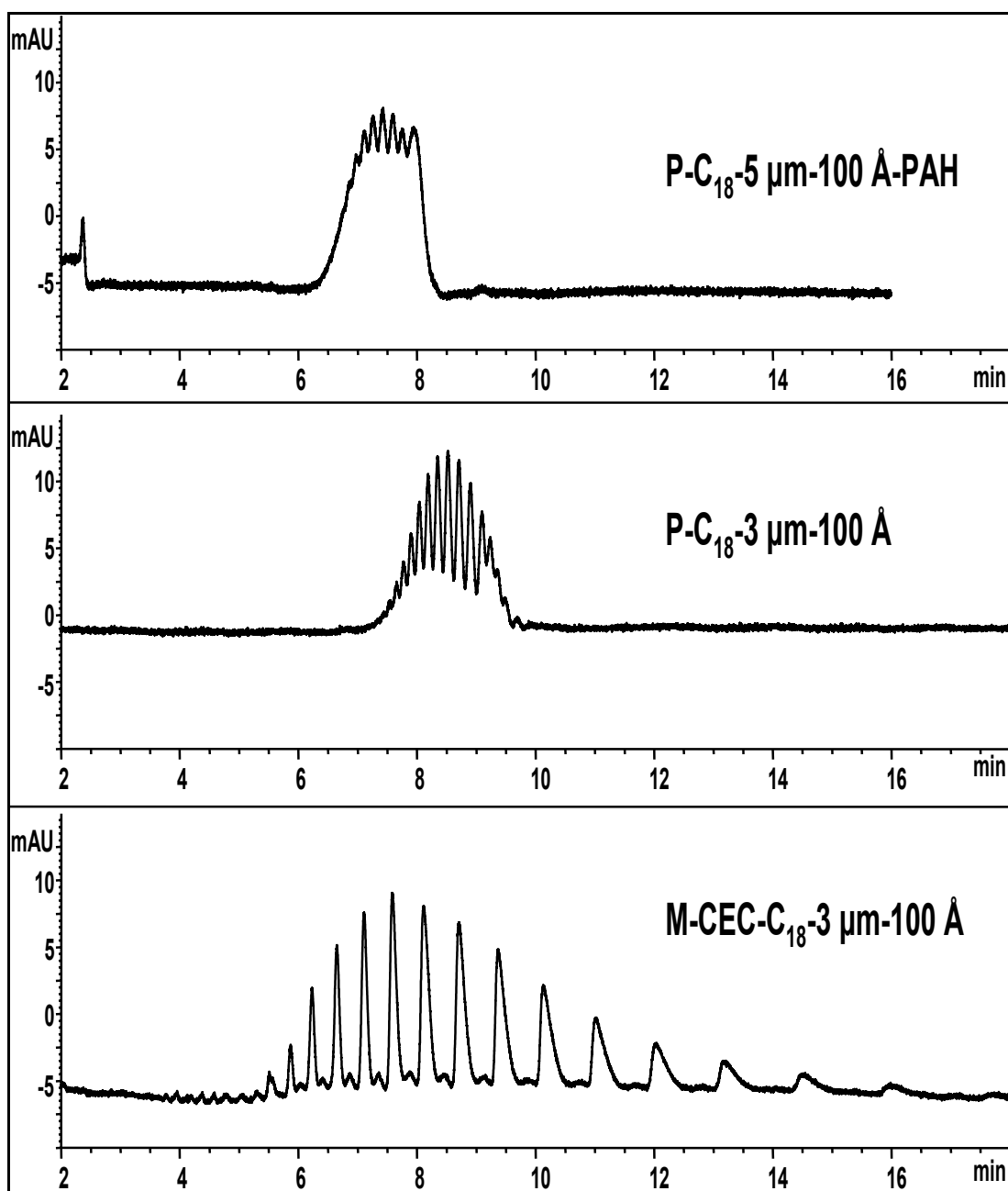


Figure 4.2: Electrochromatograms showing the comparison between monomeric and polymeric stationary phase for separation of TX-100 oligomers. Conditions: 80% (v/v) ACN / 12.5 mM Tris buffer; pH 8.0; 20°C; separation voltage, 30 kV; electrokinetic sample injection 5 sec, 5 kV, followed by a 3 sec, 5 kV run buffer injection; UV detection at 214 nm.

These characteristic differences in separation suggest that superiority of one phase over the other is solute dependent. For the separation of TX-100, it is apparent that the presence of uncapped silanol groups on the stationary phase contributed to the selectivity of separation in a useful manner possibly through H-bonding (proton acceptor/-proton donor) interactions. Therefore, utilizing a monomeric CEC-C₁₈ stationary phase, various critical mobile phase parameters were varied in order to optimize the separation of TX-100. These included the effect of acetonitrile (ACN) content, Tris concentration, pH, voltage, and temperature. All CEC separations were conducted on the same column to avoid variation due to difference in column fabrication.

Influence of Acetonitrile Content. For hydrophobic solute such as non-ionic long chain TX-100, acetonitrile (ACN) is a logical choice due to its low viscosity, superior solubilizing capability, and low UV absorbance. In HPLC, both ACN and methanol (MeOH) have been equally used as the buffer additive for separation of non-ionic surfactants.^{2,4,15,16} However, because of its favorable dielectric constant-viscosity ratio (ϵ/η), ACN is a solvent of choice in CEC for the separation of a wide range of compounds including PAHs,¹⁷ antidepressants,¹⁸ steroids,¹⁹ and diuretics.¹⁸ Utilizing a monomeric CEC-C₁₈ packing designed specifically for CEC with no endcapping (Table 4.1), the effect of ACN on the separation of TX-100 oligomers was investigated with various fractions of ACN added to the running buffer in the range of 65% to 95% (v/v), while maintaining a BGE of 12.5 mM Tris, pH 8, and operating conditions of 20°C and 30 kV.

Several trends are apparent when comparing the electrochromatograms in Figure 4.3. When increasing the volume fraction of ACN over the range of 65% to 80% (v/v), the retention time of all oligomers of TX-100 decreases due to a lowering of the bulk solution polarity, which is in accordance with reversed phase HPLC mechanism. This in turn results in greater efficiency (N) (bar plot (A)), but only a slight increase in resolution (Rs) (bar plot (B)) between oligomers (peak nos. 1-15). However, when increasing the volume fraction of ACN from 80 % (v/v) to 90% (v/v), an interesting phenomena of longer retention with a significant increase in both N and Rs were observed. For example, when arbitrarily considering peak number 6, an increase in N from 22 803 at 80% (v/v) to 30 134 at 90% (v/v) was noted (bar plot (B)). In addition, a significant gain in Rs between peak 6 and 7 from 2.57 (80% ACN (v/v)) to 3.84 (90% ACN (v/v)) was observed. This can be attributed to a unique feature of CEC for which at large volume fraction of ACN ($\sim >90\%$ (v/v)), the electroosmotic mobility begins to decrease due to changes in viscosity and dielectric constant ratio,¹⁴ which produces longer retention. This in turn counteracts or overrides the strong elutropic effect of the solvent. As a result, the combination of electrophoretic and elutropic separation mechanisms at this volume fraction provides an environment that is well suited for the resolution of TX-100 oligomers. Since such a significant improvement in Rs was observed at 90% ACN (v/v), this condition was chosen for further study.

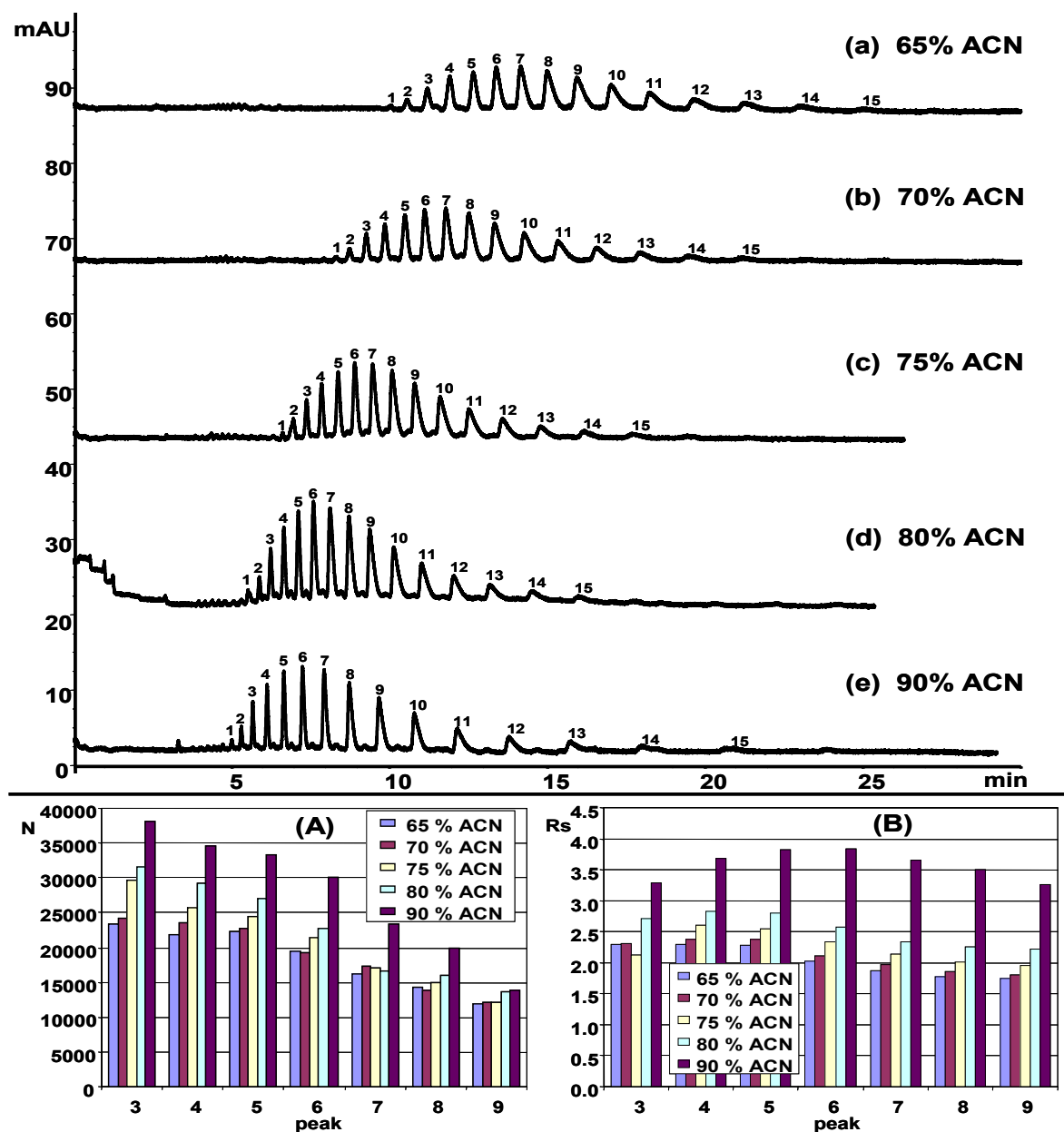


Figure 4.3: Electrochromatograms showing the effect of ACN volume fraction on the separation of TX-100. The numbered peaks represent the oligomers. The inset bar plots (A) and (B) shows N and R_s respectively over the same volume fraction of ACN. Mobile phase, 12.5 mM Tris buffer; pH 8.0, [% (v/v)] of ACN varied: (a) 65% ACN, (b) 70% ACN, (c) 75% ACN, (d) 80% ACN, (e) 90% ACN. Other conditions: capillary temperature 20°C; separation voltage, 30 kV; electrokinetic sample injection 5 sec, 5 kV, followed by a 3 sec, 5 kV run buffer injection; UV detection at 214 nm.

Influence of the Ionic Strength. The effect of Tris concentration on the CEC separation of TX-100 ethoxymers was next studied using 3.12, 6.25, 12.5, 18.7, and 25.0 mM of Tris buffered at pH 8.0 and previously optimized 90% (v/v) ACN with operating conditions of 20°C and 30 kV. Figure 4.4 shows that when increasing the Tris concentration over the range of 3.12-25.0 mM, the retention time increases due to a decrease in EOF. This decrease in EOF can be attributed to interactions of Tris with the silica surface that affects the thickness of the double layer and the zeta potential [20], which is a similar trend observed in our previous work.¹³ When comparing the *N* over the same range, a general overall increase in plate number was observed (bar plot (A)). Similarly, the *R_s* for most of the oligomers increases from 3.12 to 18.7 mM Tris, but then slightly decreases going from 18.7 to 25.0 mM (bar plot (B)). Although the *R_s* is overall largest at 18.7 mM Tris, an increase in current from 7 μ A at 12.5 mM Tris to greater than 10 μ A at 18.7 mM was observed (data not shown). Since a larger current of the running buffer in CEC can create unwanted Joule heating, it was concluded to limit the current under 10 μ A. Therefore, a reasonable compromise was best offered by 12.5 mM Tris.

Influence of Buffer pH. The effect of pH on the separation of TX-100 was investigated by varying the mobile phase pH from 6.0 to 9.0 with previously optimized 90% (v/v) ACN in 12.5 mM Tris buffer at operating conditions of 20°C and 30 kV. Since Tris solution has a natural pH = 10, concentrated HCl was added in order to lower the pH. The resulting increase in ionic strength of the buffer decreased the EOF due to increased viscosity and protonation of exposed silanol groups responsible for promoting the EOF

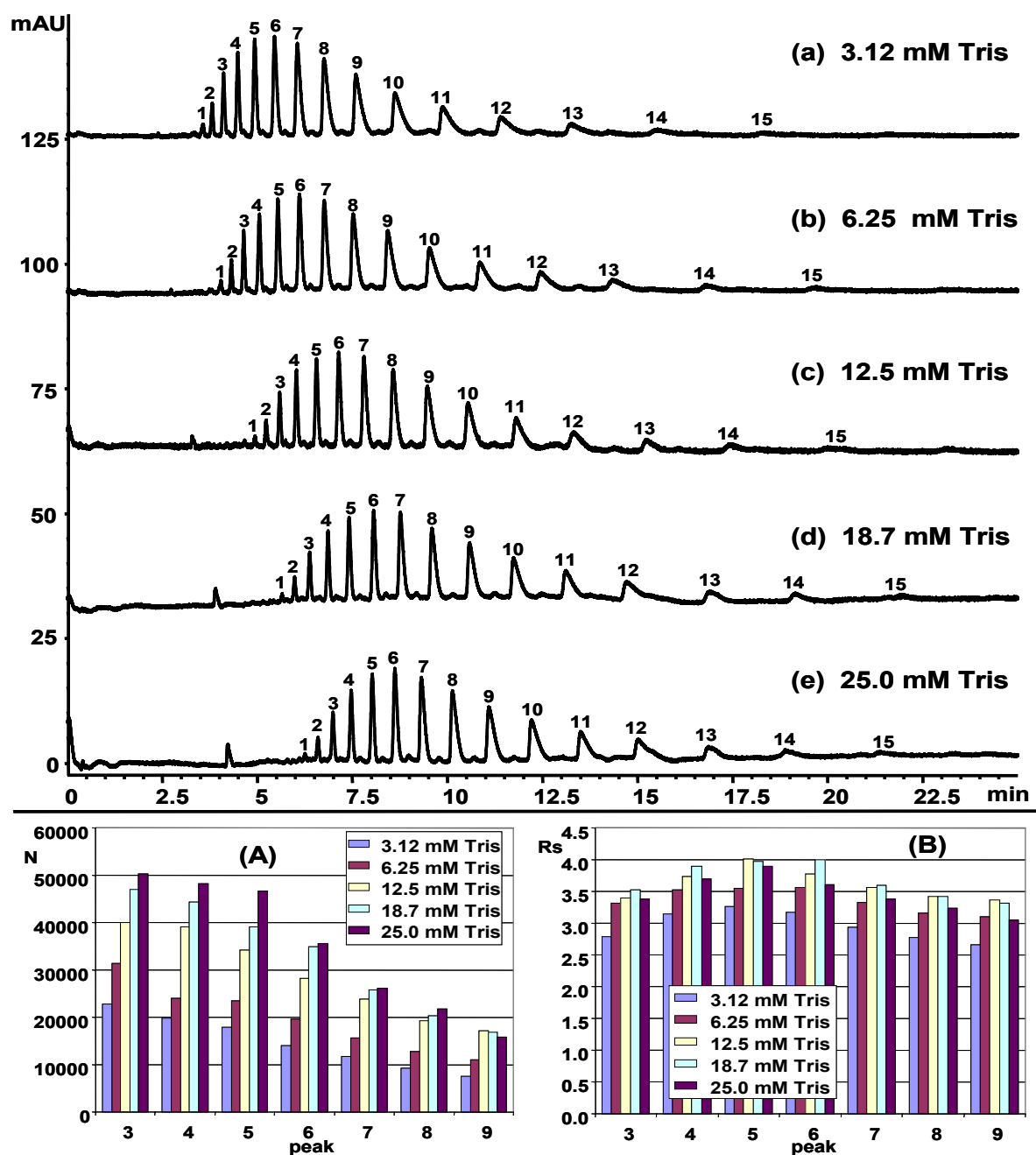


Figure 4.4: Electrochromatograms showing the effect of Tris concentration on the separation of TX-100. The inset bar plots provide N (A) and Rs (B) for TX-100 oligomers. Conditions are the same as Fig. 4.3 except 90% (v/v) ACN in various Tris buffers, pH 8.0: (a) 3.12 mM, (b) 6.25 mM, (c) 12.5 mM, (d) 18.7 mM, (e) 25.0 mM.

¹² These effects are demonstrated in the electrochromatograms of Figure 4.5, which show a general increase in retention time with a decrease in pH. This is due to lower EOF and is consistent with the results of others.²¹ The N of TX-100 oligomers shows a general overall increase in the range of pH 9-7, but then significantly lowers from pH 7-6 (bar plot (A)) due to significant peak tailing at pH 6.0. Furthermore, at pH 6.0, fewer oligomers were observed due to a loss in detectability as a result of increased ionic strength and lower EOF conditions. Bar plot (B) shows the effect of pH on the Rs which is observed to increase with a decrease in pH. Overall, it was concluded that a pH of 7.0 offered the best compromise between Rs and analysis time.

Influence of Voltage and Temperature. Next, the effect of voltage on TX-100 separation was investigated over the range of 10-30 kV while maintaining previously optimized conditions of 90% (v/v) ACN in 12.5 mM Tris, pH 7.0 buffer at operating conditions of 20°C. The flow of mobile phase ions in CEC and the resulting EOF is directly proportional to the amount of field strength or voltage applied over the length of the capillary. In normal mode CEC, at lower voltage, there is less attraction of cations toward the cathode, hence lower EOF and longer retention should be observed. Conversely, at higher voltage, there is a faster flow of ions which will increase the EOF and reduce the retention time. This is supported in the electrochromatograms of Figure 4.6 which show decreasing retention over the range of 10-30 kV. The effect of voltage on the N is shown in bar plot (A). An increase in N was observed going from 10-15 kV, followed by a gradual decrease from 15-30 kV. Exactly the same trend was observed for

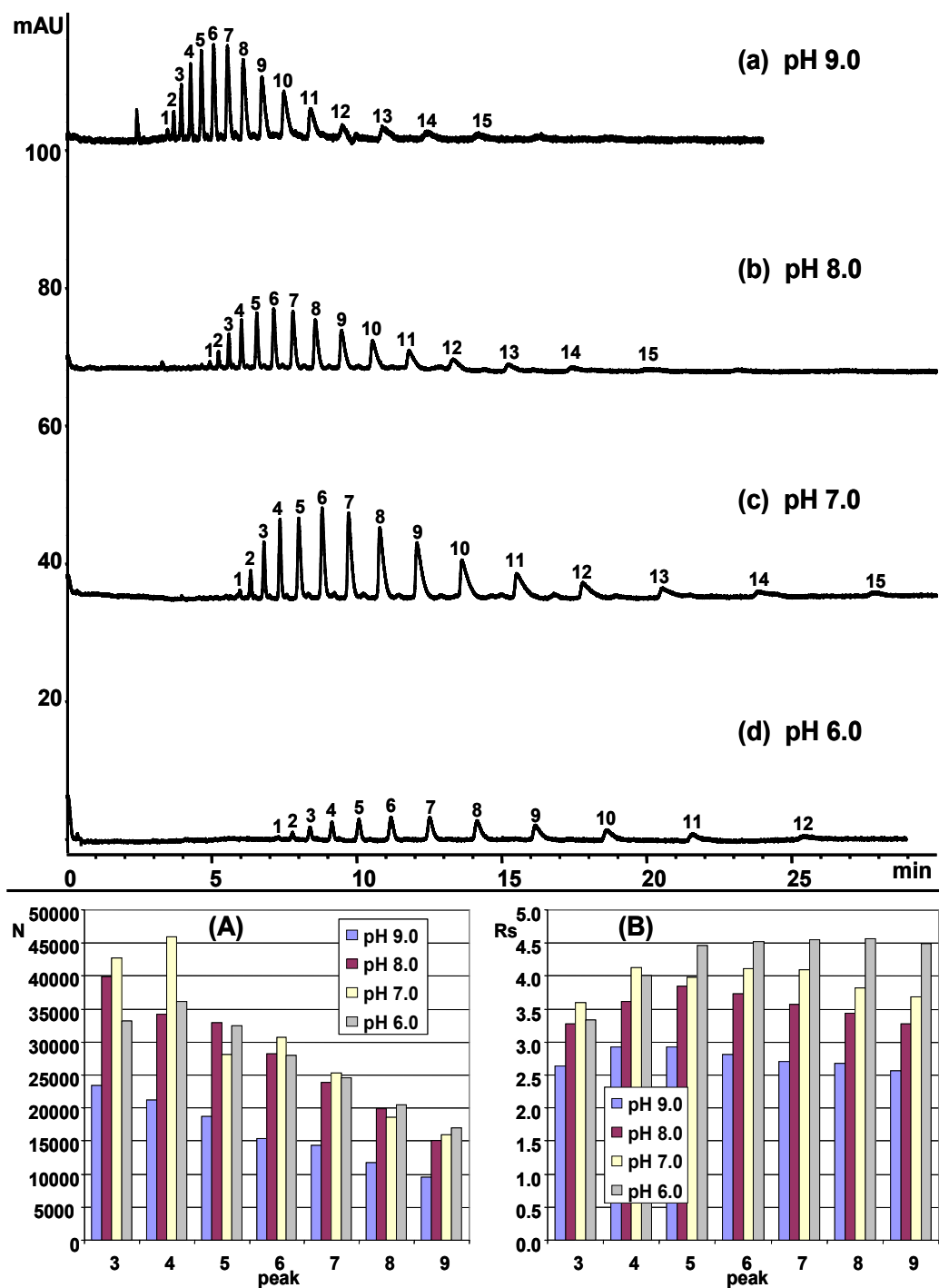


Figure 4.5: Electrochromatograms showing the effect of pH on the separation of TX-100. The inset bar plots provide N (A) and Rs (B) for critical TX-100 oligomers. Conditions are the same as Fig. 4.4 except 12.5 mM Tris / 90% (v/v) ACN and pH was varied: (a) pH 9.0, (b) pH 8.0, (c) pH 7.0, (d) pH 6.0.

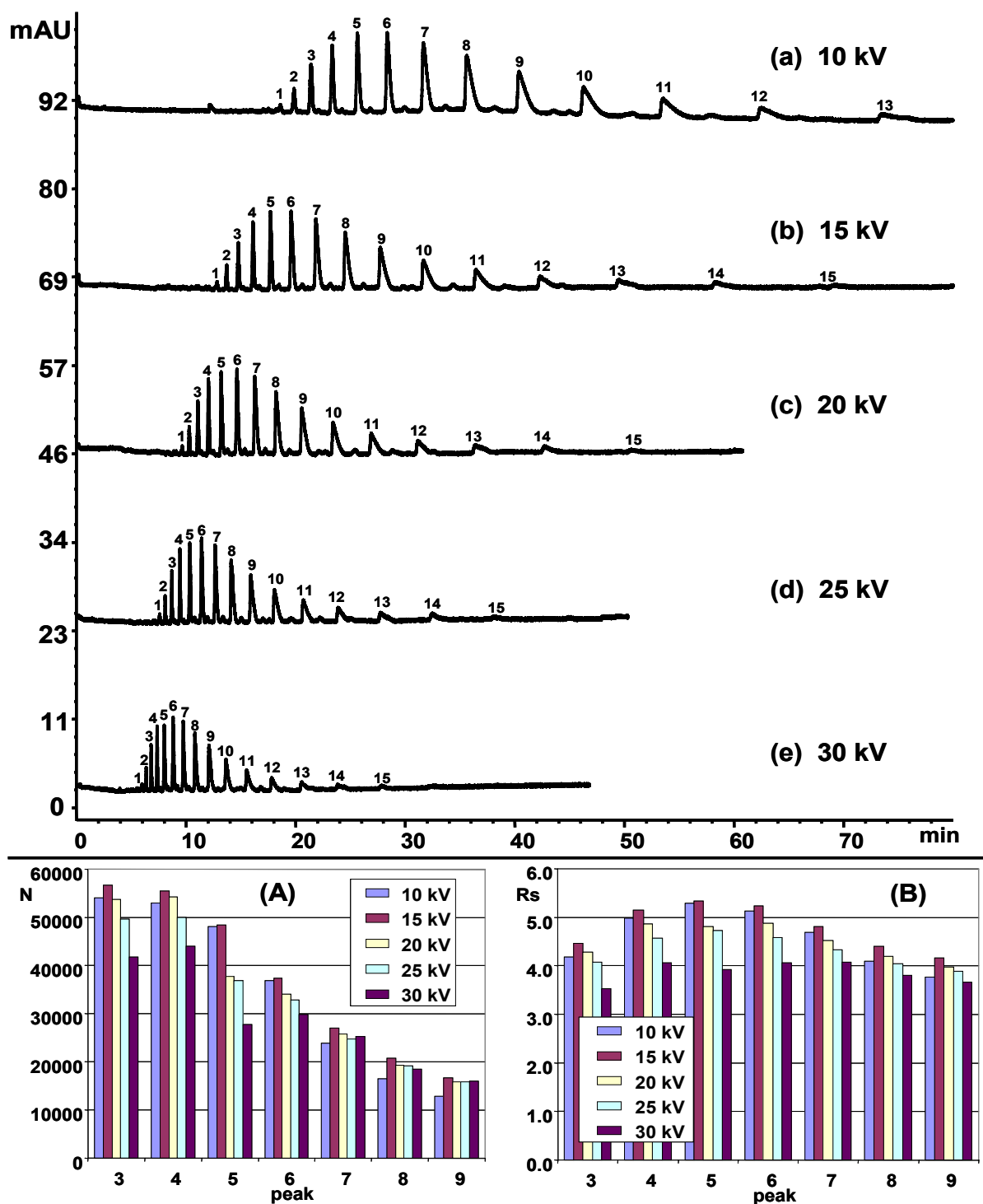


Figure 4.6: Electrochromatograms showing the effect of voltage on the separation of TX-100. The inset bar plots provide N (A) and Rs (B) for critical TX-100 oligomers. Conditions are the same as Fig. 4.5 except 12.5 mM Tris / 90% (v/v) ACN, pH 7.0.

the effect of voltage on the R_s , as demonstrated in bar plot (B). Although the highest N and R_s is obtained at 15 kV, significantly longer analysis time of nearly 60 min was observed. In addition, the last few oligomers showed either poor or no detectability. Therefore, the best compromise is offered at 30 kV, which provides similar N and R_s values to 15 kV, and the benefit of a faster analysis time.

The effect of temperature was also investigated over the range of 15-40°C, while maintaining previously optimized conditions of 90% (v/v) ACN in 12.5 mM Tris, pH 7.0 buffer (data not shown). Although a faster analysis time was achievable at higher temperature (e.g., 40°C), the interactions of the solute with the stationary phase were suppressed due to the faster EOF, which decreased the R_s between TX-100 oligomers. On the other hand, a temperature of 15°C was compromised by a longer analysis time and slight peak tailing of the later eluting peaks. A temperature of 20°C seems to provide the best trade off between R_s and overall retention of TX-100 oligomers.

CONCLUSIONS

A comparison of monomeric stationary phase vs. two polymeric stationary phases showed that a monomeric CEC-C₁₈ phase was capable of a much wider elution window with higher Rs and N. A systematic CEC mobile phase optimization using monomeric CEC-C₁₈-3 µm-100 Å stationary phase for separation of non-ionic TX-100 surfactant has been demonstrated. Optimum CEC conditions of 90% ACN (v/v) / 10% 12.5 mM Tris, pH 7.0, and 30 kV at 20°C provided the best separation of TX-100 oligomers in less than 30 min. Finally, the results of this study prove that CEC is a powerful separation technique capable for the separation of oligomers of TX-100. The satisfactory results for the resolution of TX-100 indicate that the monomeric CEC-C₁₈-3 µm-100 Å phase could be employed for analysis of oligomers of non-ionic surfactants in complex samples (e.g., sewage sludge). As a future development, coupling with mass spectrometry would further increase the sensitivity and applicability of CEC for a broad range of aliphatic and aromatic non-ionic surfactants.

ACKNOWLEDGMENTS

This project was supported by National Institute of Health (Grant No. GM 62314-02) and Solvay Pharmaceuticals (Marietta, GA).

References:

- (1) Aranda, R., Burk, R.C. *J. Chromatogr. A* **1998**, 829, 401.
- (2) Benomar, S.H., Clench, M.R. *Anal. Chim. Acta* **2001**, 445, 255.
- (3) Falbe, J., *Surfactants in Consumer Products*, Springer-Verlag, Berlin, **1987**.
- (4) Kamiyusuki, T., Monde, T., Nemoto, F., Konakahara, T., Takahashi, Y. *J. Chromatogr. A* **1999**, 852, 475.
- (5) Wang, Z., Fingas, M. *J. Chromatogr.* **1993**, 673, 145.
- (6) Wyrwas, B., Szymanski, A., Lukaszewski, Z. *Talanta* **1998**, 47, 325.
- (7) Ushakova, A.V., Grivennikova, V.G., Ohnishi, T., Vinogradov, A.D. *Biochimica et Biophysica Acta* **1999**, 1409, 143.
- (8) Preté, P.S.C., Malheiros, S.V.P., Meirelles, N.C., de Paula, E., *Biophysical Chemistry* 2002, 97, 1.
- (9) Lipsky, S.R., Duffy, M.L. *LC·GC* **1986**, 4, 898.
- (10) Smith, R.D., Udseth, H.R. *Anal. Chem.* **1987**, 59, 13.
- (11] Freeman Allen, C., Rice, L.I. *J. Chromatogr.* 1975, 110, 151.
- (12) Colón, L.A., Maloney, T.D., Fermier, A.M., in: Deyl, Z., Švec, F., (Eds.), *Capillary Electrochromatography*, J. of Chromatography Library-Vol. 62, Elsevier, Amsterdam, **2001**, pp. 111-159.
- (13) Norton, D., Zheng, J., Shamsi, S.A. *J. Chromatog. A* **2003**, 1008, 205.
- (14) Norton, D., Shamsi, S.A. *J. Chromatogr. A* **2003**, 1008, 217.
- (15) Wang, Z., Fingas, M. *J. Chromatogr. Sci.* **1993**, 31, 509.
- (16) Cserhádi, T., Forgács, E. *J. Chromatogr. A* **1997**, 774, 265.

- (17) Dittman, M.M., Rozing, G.P. *J. Microcol. Sep.* **1997**, 9, 399.
- (18) Smith, N.W., Evans, M.B. *Chromatographia* **1995**, 41, 197.
- (19) Mayer, M., Rapp, E., Marck, C., Bruin, G.J.M. *Electrophoresis* **1999**, 20, 43.
- (20) Thiam, S., Shamsi, S.A., Henry III, C.W., Robinson, J., Warner, I.M. *Anal. Chem.* **2000**, 72, 2541.
- (21) Walhagen, K., Unger, K.K., Hearn, M.T.W. *J. Chromatogr. A* **2000**, 887, 165.

Chapter 5:
Capillary Electrochromatography-Mass Spectrometry
of Nonionic Surfactants

Abstract

The Triton X (TX-) series are alkylphenol polyethoxylate (APEOs) type nonionic surfactants of varying number of ethylene oxide units. Applications include industrial and household detergent formulations as well as emulsifying agents. For analysis of these surfactants, capillary electrochromatography-electrospray ionization-mass spectrometry (CEC-ESI-MS) offers several unique advantages over the traditional hyphenation methods based on HPLC-MS. These include higher plate numbers (N) attainable in CEC-MS, as well as more compatible flow rate (sub-micro liter) when coupled to ESI-MS, and perhaps most importantly less consumption of toxic and costly organic solvents. In this work, different CEC-ESI-MS parameters such as mobile phase composition, sheath liquid and spray chamber parameters were optimized to provide suitable and sensitive analysis of short to medium chain length (e.g., $X=1-16$) TX-series nonionic surfactants. The optimized CEC-ESI-MS conditions were mobile phase containing 90/10 ACN/2.5 mM Tris, pH 8; sheath liquid containing 50/50 MeOH/10 mM HCO_2NH_4 delivered at 5 $\mu\text{L}/\text{min}$; spray chamber set to drying gas flow of 6 mL/min, nebulizer pressure = 5 psi, and drying gas temperature set to 200 °C. This is followed by the more challenging analysis of very long chain TX-series with a large number ($n=30-70$) of ethoxy units which were initially found to exhibit extreme retention using the developed method. It was observed that through addition of small volume fraction of polar-aprotic tetrahydrofuran solvent to the running buffer, the retention time could be significantly reduced thus enhancing the feasibility for CEC-ESI-MS analysis of these very long chain nonionic surfactants for the first time. The detection limit was $\sim 37 \mu\text{g}/\text{mL}$ of total OPE

for TX-45, and acceptable precision of migration time $<1\%$ RSD and peak area ($n=3$) $\sim 4\%$ were achieved.

Introduction

Nonionic surfactants are industrially important chemicals which are often added to a wide range of formulations and processes. These chemicals provide excellent capability for solubility enhancement due in part to their ability to lower the surface tension of aqueous solutions. This is because the nonionic surfactant is comprised of polar functional groups that have a high affinity for water. The most common nonionic surfactants are alkyl alcohol ethoxylates (AEOs) which combine variable number of hydrophilic ethoxy units and a hydrophobic alkyl chain tails for superior detergent properties. Similarly, other types of nonionic surfactants are manufactured from carbohydrates (e.g., glucoside and glucamide derivatives), fatty alcohols, amides and organosilicones. One class of AEOs, the alkylphenolethoxylates (APEOs) can be derived from either nonylphenol (NP) (e.g., nonylphenol ethoxylates, NPEOs) which comprise about 80% of the total market volume, or from octylphenol (OP) (e.g., octylphenol ethoxylate, OPEOs) with market shares of 15-20%.¹ The environmental monitoring of APEOs is becoming increasingly important owing to their persistence as toxic degradation products following the discharge of effluents from wastewater treatment. As such, the occurrence of APEs including APEOs degradation products (NP, OP, NPEO) are reported in surface waters, lakes and coastal waters globally.² Therefore, the development of new analytical methods for the determination and characterization of these specialized nonionic surfactants is of both industrial and environmental importance.

Analytical methodologies utilizing various techniques have been applied previously for investigation of nonionic surfactants including AEs and APEOs. Gas

chromatography-mass spectrometry (GC-MS) provides highly efficient separations, although the need for derivatization of polar phenol and ethoxylate groups which are less volatile can add excessive sample preparation time to the analysis.³ In addition, some difficulty in analysis of APEOs also arises from the limited volatility of high molecular weight surfactant homologues. Direct spectrophotometric determination⁴ and ion titration⁵ of Triton X-100 (TX-100) have been reported, although the individual oligomers were not characterized. Flow injection analysis coupled to electrospray ionization mass spectrometry (FIA-ESI-MS),^{6,7} atmospheric pressure chemical ionization (FIA-APCI-MS),^{7,8} and matrix assisted desorption ionization (FIA-MALDI-MS) can provide spectral selectivity and specificity.⁹ However, the lack of chromatographic separation can be problematic in terms of interference. Thus, an additional solid phase extraction (SPE) cleanup procedure prior to FIA-MS is alternatively employed.

Most commonly, high performance liquid chromatography (HPLC) combined with either ESI-MS and APCI-MS are traditionally used for nonionic surfactants.¹⁰⁻²⁶ The HPLC coupled to evaporative light scattering detection (ELSD) is reported,²⁷ although the method has slightly lower sensitivity as compared to MS. One of the important advantages of HPLC coupled to MS is the possibility for separation of both aliphatic or polar homologues constituting AEs and APEOs using either normal or reversed phase chromatography. However, for high throughput analysis (e.g., worldwide industrial and institutional use) one of the most important disadvantages of HPLC-MS is the consumption of large volumes of toxic and costly organic solvent that must be disposed of. With flow rates typically in mL/min, the excess waste is not only expensive

to dispose but also contributes to environmental pollution. Therefore, the development of complimentary techniques can offer possible alternatives to these traditional means of analysis.

Separation techniques based on electrophoresis are recently growing in popularity. Under the influence of electric field, charged solutes can be separated in capillary zone electrophoresis (CZE) based upon varying electrophoretic mobility arising from different mass to charge (m/z) ratio. In contrast, the neutral analytes (e.g., ethoxylate surfactants) do not separate from one another in CZE as all of the ethoxylate oligomers migrate with the electroosmotic flow (EOF) and elute at the same time. To overcome this challenge, the derivatization of nonionic surfactants using phthalic anhydride to provide charge as well as chromophoric components for use in CZE with UV detection has been approached.²⁸ Alternatively, nonionic surfactants (TX-100 and TX-405) can be separated by the addition of anionic surfactants (e.g., bile salts) forming micelles in micellar electrokinetic chromatography (MEKC) with UV detection.^{29,30} One beneficial aspect of CE including CZE and MEKC is significantly lower flow rates in the sub $\mu\text{L}/\text{min}$ range, which consumes considerably less solvent, buffers, and surfactants for separation. Overall, this can be cost effective and is more environmentally friendly.

Another mode of separating neutral analytes in CE is capillary electrochromatography (CEC), which employs the use of a fixed stationary bed inside the fused silica capillary. This configuration combines HPLC chromatographic retention along with CE electrophoretic mechanisms that are ultimately capable of separating a wide range of neutral and charged compounds. In particular, highly efficient separations

in CEC with plate numbers exceeding $10^6/m$ have been achieved due in part to the flat profile of the EOF.³¹ The advantage of CEC-MS over LC-MS is that the amount of stationary phase and sample required for CEC-MS is much less than that for an HPLC column. For example, only a few milligrams of stationary phase are needed to pack the CEC column compared to approximately 100 times larger amount of packing material used in HPLC. Although ultraviolet (UV) detection is often combined with CEC, the coupling of CEC to MS not only can provide higher sensitivity but also added selectivity and specificity such as molecular mass and structural information through analysis of the MS spectra. As such, the application of CEC-MS for the analysis of pharmaceuticals, biomolecules, natural products and chiral compounds have been undertaken.³² However, to the best of our knowledge, there are no reports for the CEC-MS analysis of nonionic surfactants.

In this work, we present the first application of CEC coupled to MS for analysis of Triton X (TX-) series surfactants utilizing the internally tapered CEC-MS column that was fabricated in our laboratory. Characterization from the viewpoint of the ion and adduct formation for TX-series nonionic surfactants with a variable number of ethoxy units ($n=1.5-16$) in the scan mode are first discussed. Next, utilizing the TX-series as model APEOs, a detailed investigation of the chromatographic separation and MS detection are performed. In addition, very long chain TX series with $n=30-70$ are profiled under the optimum CEC-ESI-MS conditions.

EXPERIMENTAL SECTION

Reagents and Chemicals. Acetonitrile (ACN), methanol (MeOH), and tetrahydrofuran (THF) of HPLC grade were purchased from Burdick and Jackson (Muskegon, MI, USA). Tris (hydroxymethyl) aminomethane (Tris) (99.9+%) and ammonium acetate (NH₄OAc) (molecular biology grade) were purchased from Sigma Chemical Company (St. Louis, MO, USA). Hydrochloric acid was obtained from Fisher Scientific (Springfield, NJ, USA). All TX-Series nonionic detergents (99%) as shown in Table 5.1 were obtained from Sigma.

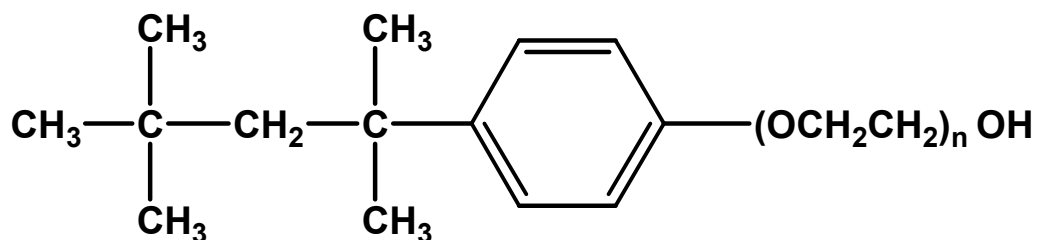


Table 5.1. Triton X Surfactants Used in this Work^{a,b}

Triton X-15	n=1
Triton X-45	n=4.5
Triton X-100	n=9-10
Triton X-165	n=16
Triton X-305	n=30
Triton X-405	n=40
Triton X-705	n=70

a) Triton X is a trademark of Dow Chemicals.

b) n=average degree of ethoxylation

CEC-MS Instrumentation and Settings. All CEC-MS experiments were performed on an Agilent HP^{3D}CE system (Agilent Technologies, Waldbronn, Germany) which was interfaced to an Agilent 1100 series single quadrupole mass spectrometer equipped with a CE/MS adaptor kit and a sprayer kit. Sheath liquid was delivered by an Agilent 1100 series HPLC pump equipped with a 1/100 split flow. The Chemstation (v.10.0) software was used for data processing. All electrochromatograms were Gaussian smoothed with a factor of 0.1 min. The noise level was determined using 6* standard deviation of the linear regression of the baseline drift for a selected time range between 0 and 10 min. The signal-to-noise ratio (*S/N*) was calculated as the ratio of peak height over noise level.

The 3- μ m CEC Reliasil ODS-1 (100Å pore size) non-encapped stationary phase was purchased from Column Engineering Inc. (Ontario, CA, USA). The fabrication and packing procedures of the internally tapered CEC-MS column were the same as our previously published method.³³ Following the installation of the newly packed CEC-MS column into the MS cartridge, the inlet was squarely cut using the Agilent diamond cutter. The homemade capillary window burner was then placed over the inlet tip for 10 seconds in order to remove the polyamide coating, and lastly wiped clean using MeOH to remove particulate. A manual syringe pump was next attached to the inlet to condition and equilibrate the column with mobile phase for 2 hours. Finally, the CE-MS cartridge was placed into the CE instrument, and the outlet of the capillary column was inserted into the nebulizer for electrospray.

For CEC-MS conditioning, 12 bar pressure was applied to the inlet, and then the voltage sequentially raised in time increments as follows: 2 kV/20 min, 5 kV/20 min, 10

kV/20 min, 15 kV/20 min, and 18 kV/15 min. The maximum separation voltage was 18 kV as higher voltage was found in some cases to create unwanted arcing and shortened lifetime of the column. Injection was performed electrokinetically at 6 kV for 6 sec. The ESI measurements were conducted in the positive ionization mode. Nitrogen obtained from a nitrogen generator was used for both nebulizing and drying gas. For optimization of the chromatographic separation, MS sheath liquid and spray chamber settings, the single ion monitoring (SIM) mode was used for monitoring as group SIM with low resolution and a gain setting 4. The SIM ions used for chromatographic and ESI-MS method development are shown in Table 5.2.

Buffer, Sheath Liquid and Sample Preparation. The CEC running buffers with various compositions were prepared by first making stock solution of 625 mM Tris adjusted to pH 8 using concentrated HCl. This solution was then transferred to a 100 mL volumetric flask, filled to just below the mark, sonicated and degassed, and finally filled to the mark. An appropriate aliquot of stock solution was then combined with various volume fractions of ACN or THF, triply deionized H₂O using volumetric pipettes, followed by 25 min sonication, filtering using 0.45 PTFE membrane syringe filter and finally degassing for 10 min. The MS sheath liquid was prepared by mixing appropriate volume fractions of MeOH and H₂O using a 100 mL graduated cylinder followed by addition of ammonium formate then sonication and finally degassing. Individual stock solutions of TX-15, -45, -100 and -165 were dissolved at a concentration of 10 mg/mL in 65/35 (v/v) ACN/H₂O. The stock solutions of longer chain TX-305, -405, and -705 were

Table 5.2: TX-15-165 SIM Mode Ions Used for Optimization of the CEC and MS Detection

TX-15			TX-45			TX-100			TX-165		
m/z	n	Ion	m/z	n	Ion	m/z	n	Ion	m/z	n	Ion
227	3	$[\text{M}-\text{C}_8\text{H}_{17}]^+$	312	2	$[\text{M}+\text{NH}_4]^+$	405	4	$[\text{M}+\text{Na}]^+$	532	7	$[\text{M}+\text{NH}_4]^+$
271	4	$[\text{M}-\text{C}_8\text{H}_{17}]^+$	356	3	$[\text{M}+\text{NH}_4]^+$	427	5	$[\text{M}+\text{H}]^+$	576	8	$[\text{M}+\text{NH}_4]^+$
273	1	$[\text{M}+\text{Na}]^+$	400	4	$[\text{M}+\text{NH}_4]^+$	471	6	$[\text{M}+\text{H}]^+$	620	9	$[\text{M}+\text{NH}_4]^+$
317	2	$[\text{M}+\text{Na}]^+$	444	5	$[\text{M}+\text{NH}_4]^+$	532	7	$[\text{M}+\text{NH}_4]^+$	664	10	$[\text{M}+\text{NH}_4]^+$
361	3	$[\text{M}+\text{Na}]^+$	488	6	$[\text{M}+\text{NH}_4]^+$	576	8	$[\text{M}+\text{NH}_4]^+$	708	11	$[\text{M}+\text{NH}_4]^+$
405	4	$[\text{M}+\text{Na}]^+$	532	7	$[\text{M}+\text{NH}_4]^+$	620	9	$[\text{M}+\text{NH}_4]^+$	752	12	$[\text{M}+\text{NH}_4]^+$
			576	8	$[\text{M}+\text{NH}_4]^+$	664	10	$[\text{M}+\text{NH}_4]^+$	796	13	$[\text{M}+\text{NH}_4]^+$
			620	9	$[\text{M}+\text{NH}_4]^+$	708	11	$[\text{M}+\text{NH}_4]^+$	840	14	$[\text{M}+\text{NH}_4]^+$
			664	10	$[\text{M}+\text{NH}_4]^+$	752	12	$[\text{M}+\text{NH}_4]^+$	884	15	$[\text{M}+\text{NH}_4]^+$
			708	11	$[\text{M}+\text{NH}_4]^+$	796	13	$[\text{M}+\text{NH}_4]^+$	928	16	$[\text{M}+\text{NH}_4]^+$
						840	14	$[\text{M}+\text{NH}_4]^+$	972	17	$[\text{M}+\text{NH}_4]^+$
						884	15	$[\text{M}+\text{NH}_4]^+$	1016	18	$[\text{M}+\text{NH}_4]^+$
						928	16	$[\text{M}+\text{NH}_4]^+$	1060	19	$[\text{M}+\text{NH}_4]^+$
						972	17	$[\text{M}+\text{NH}_4]^+$	1104	20	$[\text{M}+\text{NH}_4]^+$
						1016	18	$[\text{M}+\text{NH}_4]^+$	1148	21	$[\text{M}+\text{NH}_4]^+$
									1192	22	$[\text{M}+\text{NH}_4]^+$
									1236	23	$[\text{M}+\text{NH}_4]^+$
									1280	24	$[\text{M}+\text{NH}_4]^+$

dissolved at a concentration of 22, 30 and 30 mg/mL in 65/35 (v/v) ACN/H₂O, respectively.

CEC-ESI-MS Conditions. For evaluation of the CEC separation conditions, Triton series surfactants with ethoxy units (n=1.5-16) utilizes SIM ions listed in Table 5.2. The effect of mobile phase ACN % (v/v) was first investigated in the range of 70-90%. Next, the concentration of Tris background electrolyte (BGE) was optimized in the range of 2.5-7.5 mM. Finally the pH of the Tris buffer was evaluated in the range of 7-9 using HCl for adjustment. For ESI-MS method optimization also using Table 5.2 SIM ions, the investigation of the sheath liquid composition and delivery was conducted. For this, first the MeOH/H₂O volume composition was evaluated in the range of 50-90%. Next, the HCO₂NH₄ concentration was varied in the range of 1-50 mM. Finally, the sheath pump flow rate was studied from 3-9 μ L/min. A variation of MS capillary voltage (V_{cap}) and fragmentor voltage in Full Scan mode (range 50-1500 AMU) for effects on *S/N* was investigated. Lastly, Full Scan analysis of longer chain surfactants TX-305-705 using the optimized conditions as well as modified binary solvent through addition of THF was conducted.

Linearity, Precision and Sensitivity of the CEC-MS System. The linearity, precision and sensitivity of the CEC-MS system were determined. The linear calibration curve for one representative surfactant (TX-45) was comprised of 5 calibration levels in the range of 20-500 μ g/mL, and a blank. The linearity was obtained by linear regression ($y = mx +$

b), including the intercept. The calibration curve was constructed using the average of the sums of all the homologue peak areas for three replicate injections at each concentration.²⁹ The limit of detection was calculated for a 50 µg/mL solution of TX-45 using a peak area equal to three times the standard deviation of the average peak area of summed homologues for three replicate injections.²⁹

RESULTS AND DISCUSSION

Characterization of TX-Series Surfactants. The initial CEC-ESI-MS investigation of the TX-15, -45, -100 and -165 series surfactants was conducted utilizing Full Scan mode range over the range 50-1500 AMU. From the corresponding electrochromatograms shown in Figures 5.1-5.4, an analysis of the individual mass spectral ion pattern for each degree of ethoxylation showed that in general the most abundant ions included the protonated molecular ion $[M+H]^+$, ammonium adducts $[M+NH_4]^+$, sodium adducts $[M+Na]^+$, fragment ions corresponding to the loss of the alkyl chain from the phenyl ring $[M-C_8H_{17}+2H]^+$, and loss of ethoxylate groups resulting in one degree of ethoxylation $[C_8H_{17}(C_6H_4)E+H]^+$ as well as two degrees of ethoxylation $[C_8H_{17}(C_6H_4)E_2+H]^+$. The formation of ions and adducts was found to be dependent upon the magnitude of the fragmentor voltage as well as the degree of ethoxylation for each oligomer. For the initial investigation, the fragmentor voltage was set to 125 V.

For TX-15 (Figure 5.1), the oligomeric mass spectral pattern was found to be comprised of sodium adducts $[M+Na]^+$ and fragments $[M-C_8H_{17}+2H]^+$ corresponding to a

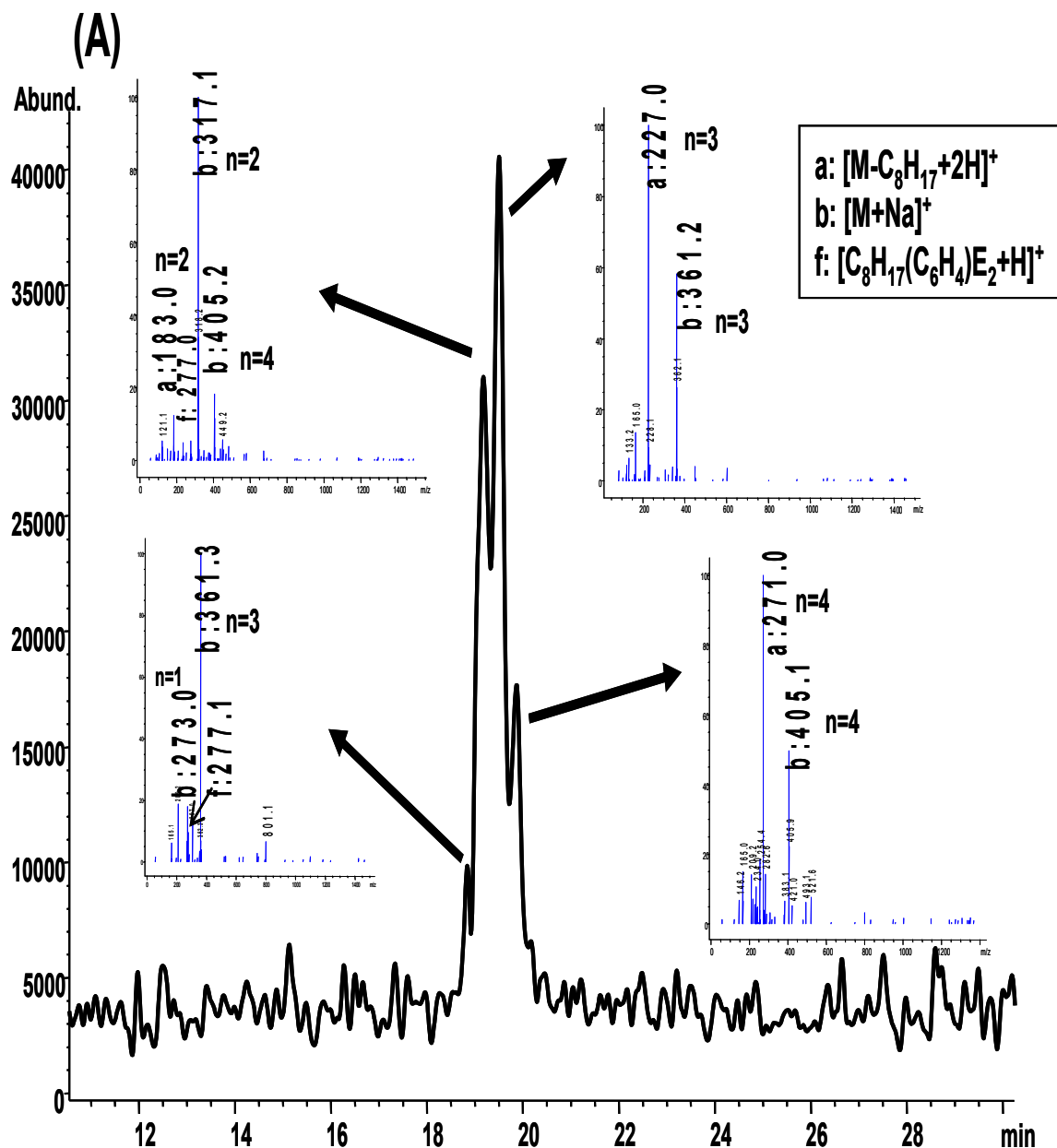


Figure 5.1: Full Scan CEC-MS of TX-15. In the legend, E=ethoxylate group. Conditions: Buffer 80/20 ACN/H₂O 5 mM Tris, pH 8. Sheath liquid: flow rate 5 μ L/min, 80/20 MeOH/H₂O, 1 mM HCO₂NH₄. MS spray chamber: Drying gas flow rate 10 L/min, Nebulizer pressure 10 psi, drying gas temperature 300 $^{\circ}$ C, Fragment voltage 125 V, Capillary voltage 4000 V, Gain 4. Full Scan 50-1500 amu. CEC 16 kV runs, column 20 cm packed bed, 60 cm total length and 75 μ m I.D. x 363 μ m O.D., 6 kV 6 sec injection. TX -15 injected at 10 mg/mL dissolved in 65/35 ACN/H₂O.

mixture of ethoxylation in the range of $n=1$ to $n=4$. Most interestingly, the spectra suggests that the longer $n=4$ chains co-elute with the short $n=1$ chain. For example, the first peak of TX-15 shows highest abundance of m/z 361 corresponding to Na^+ adduct with $n=3$ degree of ethoxylation, along with Na^+ adduct at $m/z=273$ for $n=1$. In addition, fragmentation of the ethoxylated chain to leave 2 ethoxylate groups was observed (e.g., $[\text{C}_8\text{H}_{17}(\text{C}_6\text{H}_4)\text{E}_2+\text{H}]^+$ at m/z 277. For the second eluting peak (Figure 5.1), the most abundant ion at $m/z=317$ was the Na^+ adduct corresponding to $n=2$, although the smaller chain $n=1$ Na^+ adduct ($m/z=273$) was also observed along with longer $n=4$ ($m/z=405$) fragment ion and $[\text{C}_8\text{H}_{17}(\text{C}_6\text{H}_4)\text{E}_2+\text{H}]^+$ ($m/z=277$) in lower abundance. The mass spectra of third and fourth eluting peak (Figure 5.1) were comprised of fragment ion $[\text{M}-\text{C}_8\text{H}_{17}+2\text{H}]^+$ at $m/z=227$ and 271 respectively, in highest abundance, and of Na^+ adducts of each oligomer as second highest abundance. However, these spectra suggests that the last two peaks are relatively pure and mainly comprised of their individual degree of ethoxylation (e.g., $n=3$ and $n=4$ only), respectively.

For TX-45 (Figure 5.2), the mass spectra for each oligomer was not comprised of mixed degree of ethoxylation like that of TX-15. Instead, a distribution following the elution order of short to long degree of ethoxylation was observed. The following pattern for ion and adduct formation of TX-45 is described. The b-series Na^+ adducts were only formed at lower n value. For example $n=2$ to $n=4$, but not at higher n value. The fragment a-series ion $[\text{M}-\text{C}_8\text{H}_{17}+2\text{H}]^+$ was formed in lower abundance at $n=2$, then increases to a maximum going from $n=2$ to $n=5$, but then decreases in abundance from $n=5$ to $n=6$, finally disappearing after $n=6$. The d-series NH_4^+ adducts begun to form at $n=4$ then

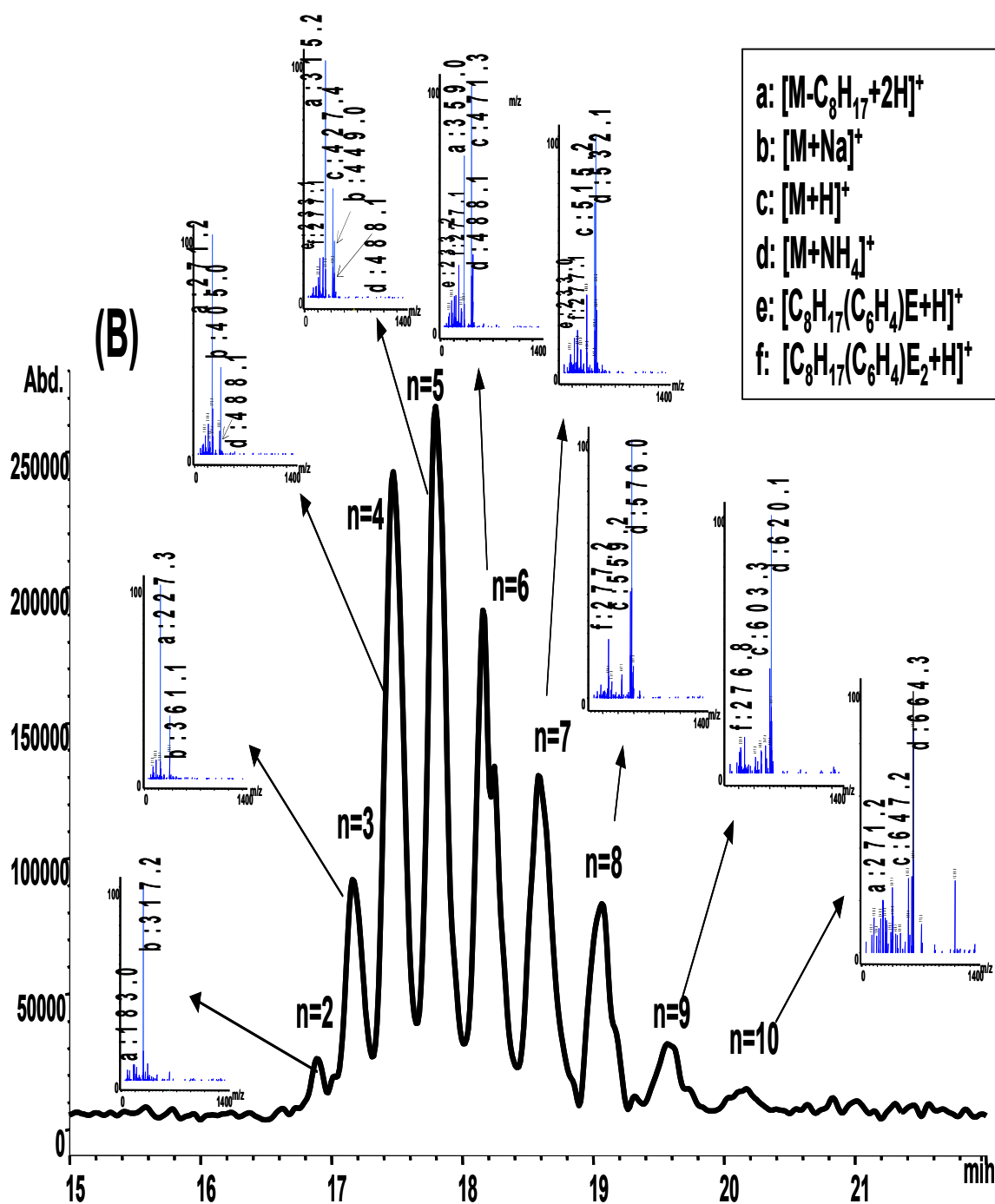


Figure 5.2: Initial Full Scan CEC-MS of TX-45. Conditions are the same as Figure 5.1.

systematically increase to maximum intensity from $n=4$ to $n=7$, and were of much higher intensity for $n=7$ to $n=10$. Interestingly, as the NH_4^+ adduct ions began to form, the fragment ion $[\text{M}-\text{C}_8\text{H}_{17}+2\text{H}]^+$ started to fall off in abundance going from $n=5$ to $n=6$, while at the same time the protonated molecular ion (c-series) starts to form at $n=5$. Furthermore, the protonated molecular ion increased in abundance from $n=5$ to $n=6$ to a maximum, then decreased at $n=7$, during which time the NH_4^+ adduct ion continue to increase in intensity. Finally, the e-series $[\text{C}_8\text{H}_{17}(\text{C}_6\text{H}_4)\text{E}+\text{H}]^+$ and f-series $[\text{C}_8\text{H}_{17}(\text{C}_6\text{H}_4)\text{E}_2+\text{H}]^+$ fragment ions were observed in lower abundance ranging for $n=5$ to $n=9$ ethoxylate units.

For TX-100 (Figure 5.3), the a-series fragment ion $[\text{M}-\text{C}_8\text{H}_{17}+2\text{H}]^+$ is formed in high abundance (e.g., 100% relative intensity) at shorter degree of ethoxylation $n=4-6$, but then decreased to 50% relative intensity at $n=7$, and finally disappears at $n>7$. The b-series sodium adduct $[\text{M}+\text{Na}]^+$ formation was observed at 50% relative intensity in the range of $n=4-6$, but not at longer degree of ethoxylation. The c-series protonated molecular ion $[\text{M}+\text{H}]^+$ began to form at shorter degree of ethoxylation $n=5$ then increased to maximum intensity at $n=6$. This was followed by gradual decline in formation going from $n=7$ (40% relative intensity) to $n=10$ (20% relative intensity). The d-series ammonium adduct $[\text{M}+\text{NH}_4]^+$ started forming in low abundance at $n=5$. This adduct then increased in formation to maximum intensity going from $n=5$ to $n=7$, and was the most abundant ion with 100% relative intensity for longer degree of ethoxylation in the range of $n=8$ to $n=13$. Finally, the e- and f-series mono- and di-ethoxylated fragment ions (e.g., $[\text{C}_8\text{H}_{17}(\text{C}_6\text{H}_4)\text{E}+\text{H}]^+$ and $[\text{C}_8\text{H}_{17}(\text{C}_6\text{H}_4)\text{E}_2+\text{H}]^+$) were in general formed in lower

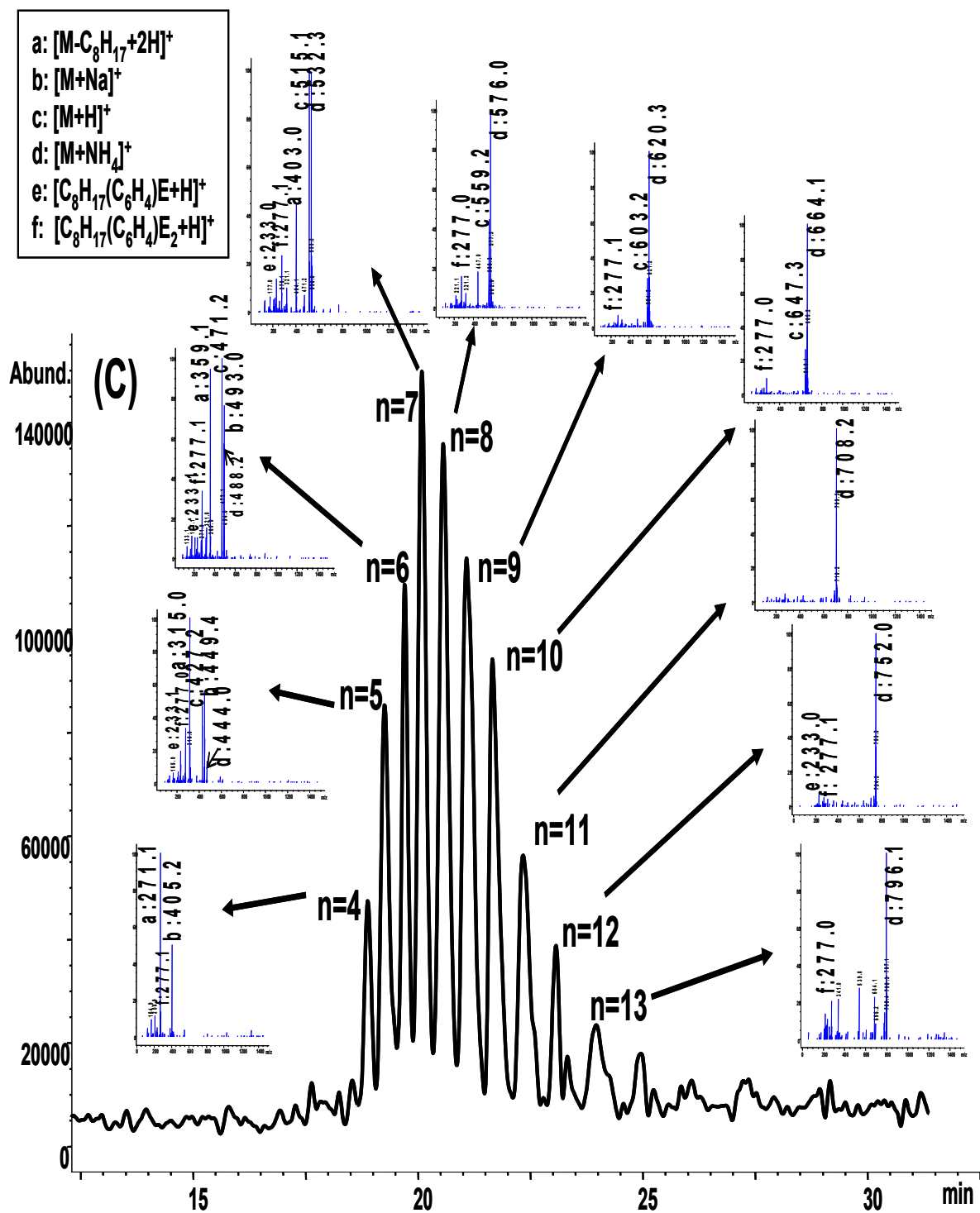


Figure 5.3: Initial Full Scan CEC-MS of TX-100. Conditions are the same as Figure 5.1.

abundance ~30% relative intensity. The $[\text{C}_8\text{H}_{17}(\text{C}_6\text{H}_4)\text{E}+\text{H}]^+$ ion was observed in the range of $n=4$ to $n=7$, disappears at $n>7$ and reappears at $n=12$. In contrast, the $[\text{C}_8\text{H}_{17}(\text{C}_6\text{H}_4)\text{E}_2+\text{H}]^+$ was formed at all degree of ethoxylation.

Finally, for TX 165 (Figure 5.4), the mass spectral distribution of ions was very similar to TX-100 except that the sodium adduct was not formed. The a-series fragment ion $[\text{M}-\text{C}_8\text{H}_{17}+2\text{H}]^+$ corresponding to $n=4$ ($m/z=271$) was observed in low abundance in the mass spectra of longer ethoxylate chain of $n=9$ and $n=13$ only. This suggests that degradation of the longer ethoxylated chain within the ESI to form shorter ethoxylate units is then able to form adducts. The c-series protonated molecular ion $[\text{M}+\text{H}]^+$ formed at shortest chain $n=7$ in high abundance (e.g., 100% relative intensity), but then decreased going from $n=8$ (60% relative intensity) to $n=9$ (20% relative intensity) and finally disappears for longer ethoxylated units (i.e., $n\geq 10$). The d-series ammonium adducts $[\text{M}+\text{NH}_4]^+$ were in general formed in high abundance for all degree of ethoxylation (except $n=17$), which was the most prevalent oligomer observed for TX-165. Lastly, the e-series mono- and f-series di-ethoxylated ions (e.g., $[\text{C}_8\text{H}_{17}(\text{C}_6\text{H}_4)\text{E}+\text{H}]^+$ and $[\text{C}_8\text{H}_{17}(\text{C}_6\text{H}_4)\text{E}_2+\text{H}]^+$) were formed randomly at longer n values, but were of greater intensity as compared to TX-100. A summary of the ion and fragment formation for a typical TX-series ethoxylate ($n=4$) is summarized in Figure 5.5. Overall, the surfactant ionized in the ESI either by loss of ethoxylate chain to leave two ethoxylate groups (m/z 277) or one ethoxylate group (m/z 233), by loss of the octyl alkyl chain (m/z 271), or by formation of the molecular ion (m/z 383), ammonium (m/z 400) and sodium adducts (m/z 405). These ions are similar to those described by Plomley et. al.⁷ for ESI fragmentation

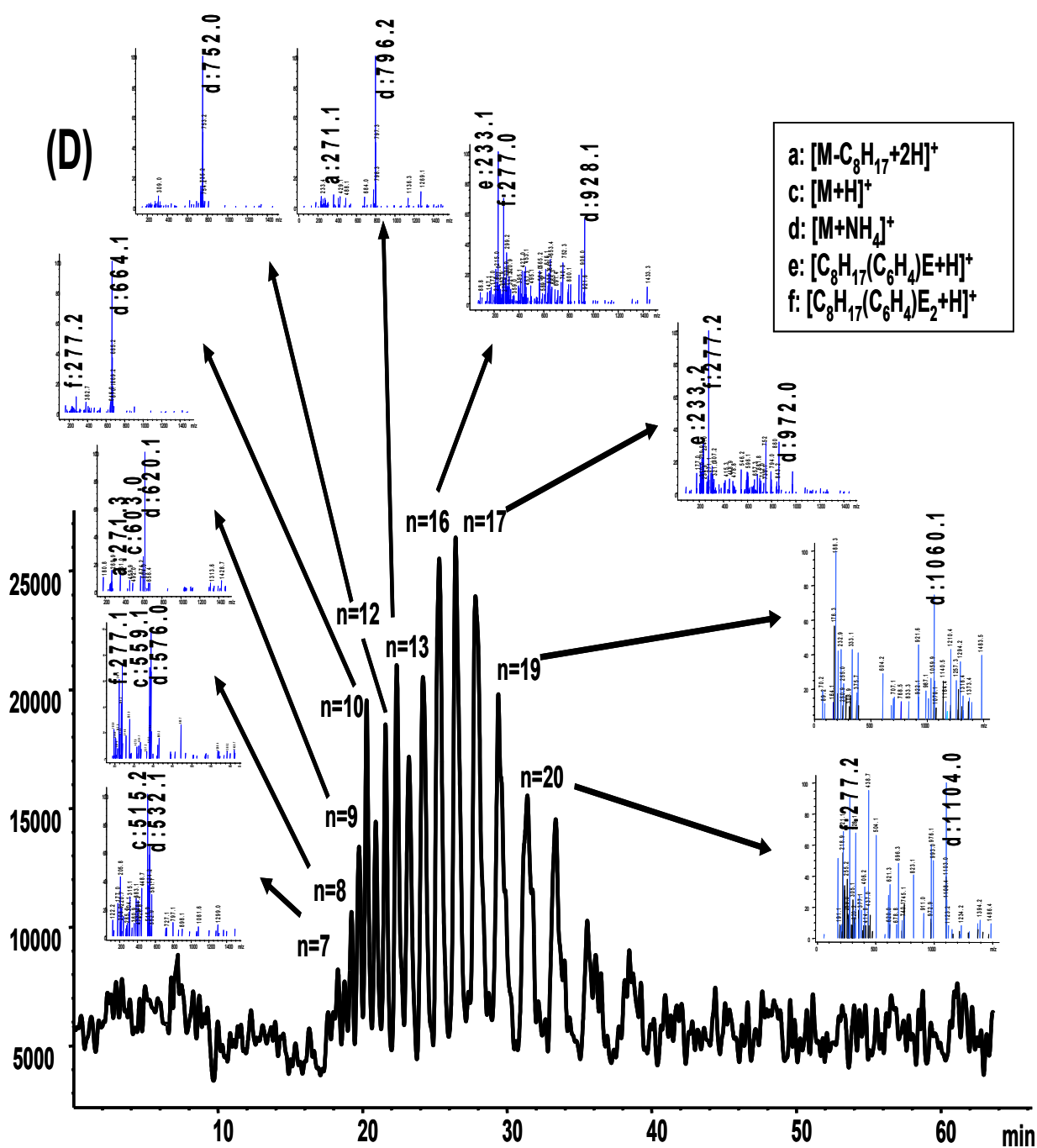


Figure 5.4: Initial Full Scan CEC-MS of TX-165. Conditions are the same as Figure 5.1.

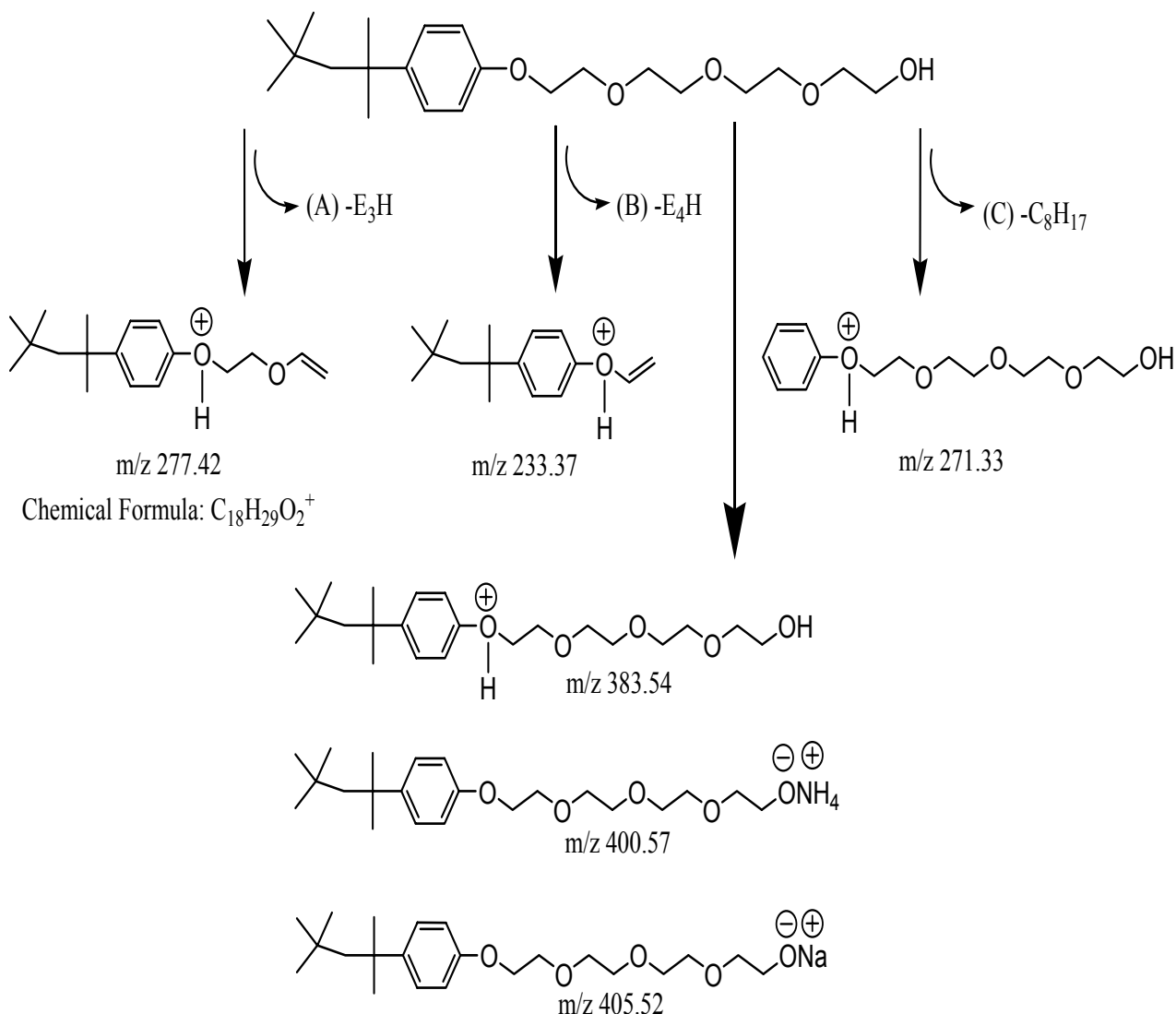


Figure 5.5: Summary of the fragmentation, ion and adduct formation of the TX series surfactants (TX-45 used as example). Fragments, the protonated molecular ion, ammonium and sodium adducts were observed. (A) a loss of 3 ethoxylate groups to leave 2 degrees of ethoxylation, $m/z=277$ observed; (B) a loss of 4 ethoxylate groups to leave 1 degree of ethoxylation, $m/z=233$ observed; (C) loss of octyl chain $m/z=271$ observed.

of nonylphenol ethoxylates, except that unlike pathway A+B (Figure 5.5), in their work the nonyl alkyl side chain fragmented from the aromatic ring. In addition to the loss of C_8H_{17} shown in pathway C in Figure 5.5, they also describe loss of the aromatic ring.

From the analysis of these full scan spectra, the ions shown in Table 5.2 were utilized for the CEC-ESI-MS method development. For sensitive SIM mode monitoring these ions generally consisted of b-series Na^+ adducts for TX-15, and d-series $[M+NH_4]^+$ adducts for TX-45, TX-100 and TX-165 as these ions were formed in much higher abundances. First, the chromatographic separation was optimized by systematic tuning of the mobile phase parameters including ACN content, effect of background electrolyte (BGE) Tris concentration, and the effect of the buffer pH. This was followed by the optimization of the MS detection which included the sheath liquid composition, flow rate, and consideration of the MS spray chamber parameters including drying gas flow rate, nebulizer pressure, and drying gas temperature. In addition, the effects of varying the MS capillary voltage and fragment voltage on S/N were investigated. Finally, the analysis of longer chain Triton series surfactants utilizing a binary organic solvent mobile phase containing ACN and THF is described.

CEC/ESI/MS Separation Optimization. Effect of Mobile Phase Acetonitrile Content.

The effect of ACN content in the mobile phase was optimized in the range of 70-90% (v/v). It was found that the electroosmotic flow (EOF) was unstable outside of this ACN range due to unfavorable dielectric constant/viscosity ratio which results in change in the double layer thickness and zeta potential. The corresponding electrochromatograms of all

four Triton series surfactants can be seen in Figure 5.6. A composition of 70% ACN provided longer analysis time for all TX-15 through TX-165. Upon increasing the ACN content from 70 to 80% ACN, the retention of all TX oligomers slightly decreased in accordance with reverse phase mechanism. Further increasing the ACN content from 80 to 90% ACN continued to slightly decrease the retention of TX-15 only. However, most interestingly for TX-45, TX-100 and TX-165 series the retention was observed to increase. In addition, a marked improvement in the oligomeric resolution for TX-45, -100 and -165 was demonstrated at 90% ACN. This same trend was observed in our previous work for CEC-UV analysis of TX-100.³⁴ At large volume fraction of ACN ($\sim >90\%$ (v/v)), the electroosmotic mobility begins to decrease from variation in dielectric constant ratio and viscosity ratio,³⁵ which results in longer retention. This counteracts or overrides the strong elutropic effect of the solvent, whereupon the combination of electrophoretic and elutropic separation mechanisms at this volume fraction greatly improves the chromatographic resolution of TX-45, -100, and -165 oligomers. The exception is TX-15 which does not follow this trend and maybe due to the fact that more hydrophilic, short ethoxylated chain provides less stationary/mobile phase interaction and consequently lower resolution. A consideration of varying ACN content on the S/N , chromatographic efficiency (N_{overall}) was also considered in order to establish the optimum ACN volume fraction. In all cases (except for TX-45) the S/N was lowest for 70% ACN (data not shown). For TX-100, a similar S/N was observed in the range of 80-90% ACN. For TX-45 and TX-165, a composition of 90% ACN provided the highest S/N . These trends in S/N are most likely attributed to improved solubility of the nonionic surfactants at higher

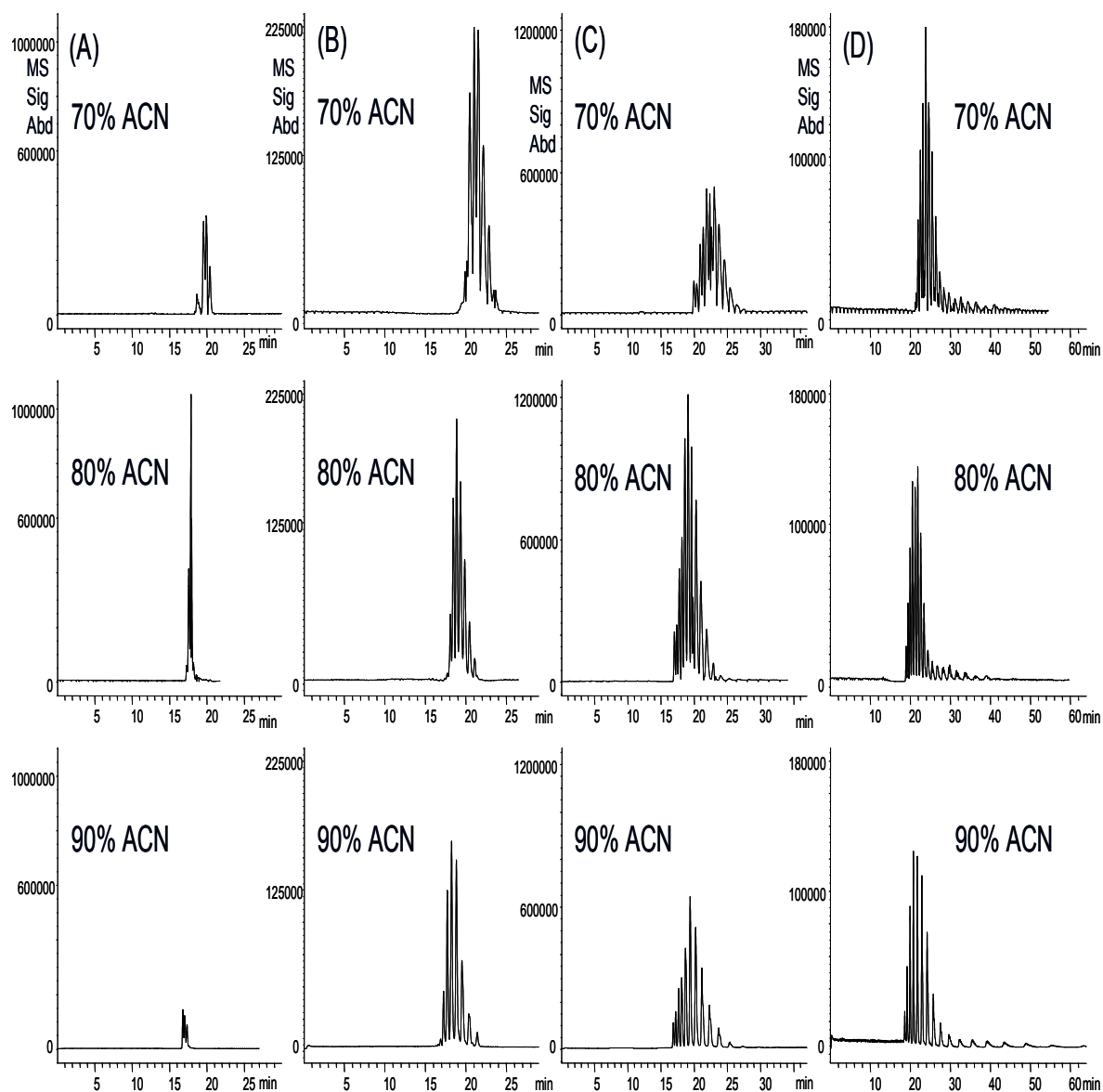


Figure 5.6: Effect of mobile phase ACN content (v/v) on the CEC-MS separation of Triton series (A) TX-15, (B) TX-45, (C) TX-100, (D) TX-165. Column dimensions are the same as Figure 5.1, packed with 3 μm / 100 \AA Reliasil ODS. Conditions: buffer ACN varied/5 mM Tris, pH 8.0. Sheath liquid: flow rate 5 $\mu\text{L}/\text{min}$, 80/20 MeOH/ H_2O , 1 mM HCO_2NH_4 . MS spray chamber: drying gas flow 10 L/min, nebulizer pressure 10 psi, drying gas temperature 300 $^\circ\text{C}$, fragmentor voltage 125 V, capillary voltage 4000 V, gain 4. SIM ions as described in Table 5.2, applied voltage 16 kV runs, 6 kV 6 sec injection. Analytes: 10 mg/mL 65/35 ACN/ H_2O .

ACN volume fraction. An evaluation of N_{overall} showed that all composition in the range 70-90% (v/v) ACN provided similar value, although 70% ACN was lower in several cases. Overall, a mobile phase composition containing 90% ACN (v/v) was selected for further study due to significant improvements in the resolution of oligomers.

Effect of Mobile Phase Tris Concentration. The effect of varying Tris concentration on the CEC-MS separation and detection was next studied comparing 2.5, 5.0 and 7.5 mM Tris buffered at pH 8.0 and previously optimized 90% (v/v) ACN. Although Tris is non-volatile, the use of this buffer in low concentration (i.e., <10 mM) was deemed acceptable for use in the electrospray. The results of the study can be seen in Figure 5.7. The retention time of all TX series was observed to increase upon increasing Tris concentration from 2.5 to 5.0 mM. This can be attributed to interactions of Tris with the silica surface that affects the thickness of the double layer and the zeta potential³⁶ resulting in decreased EOF which is a similar trend observed in our previous work.³⁷ Upon increasing Tris going from 5.0 to 7.5 mM Tris, no mentionable effects on retention were observed, although the MS signal significantly decreased. This signal suppression may be explained by competition between BGE (e.g., Tris) ions and target analytes (e.g., TX series) for desolvation and gas phase ionization. Further consideration of the online S/N , chromatographic N and R_s were evaluated. In general, the S/N was found to be highest for Tris 2.5 mM, then systematically decreased upon raising the Tris content in the range of 2.5 to 7.5 mM. Although the baseline noise remained fairly constant, the decrease in MS signal was mainly responsible for the observed trend in S/N . For

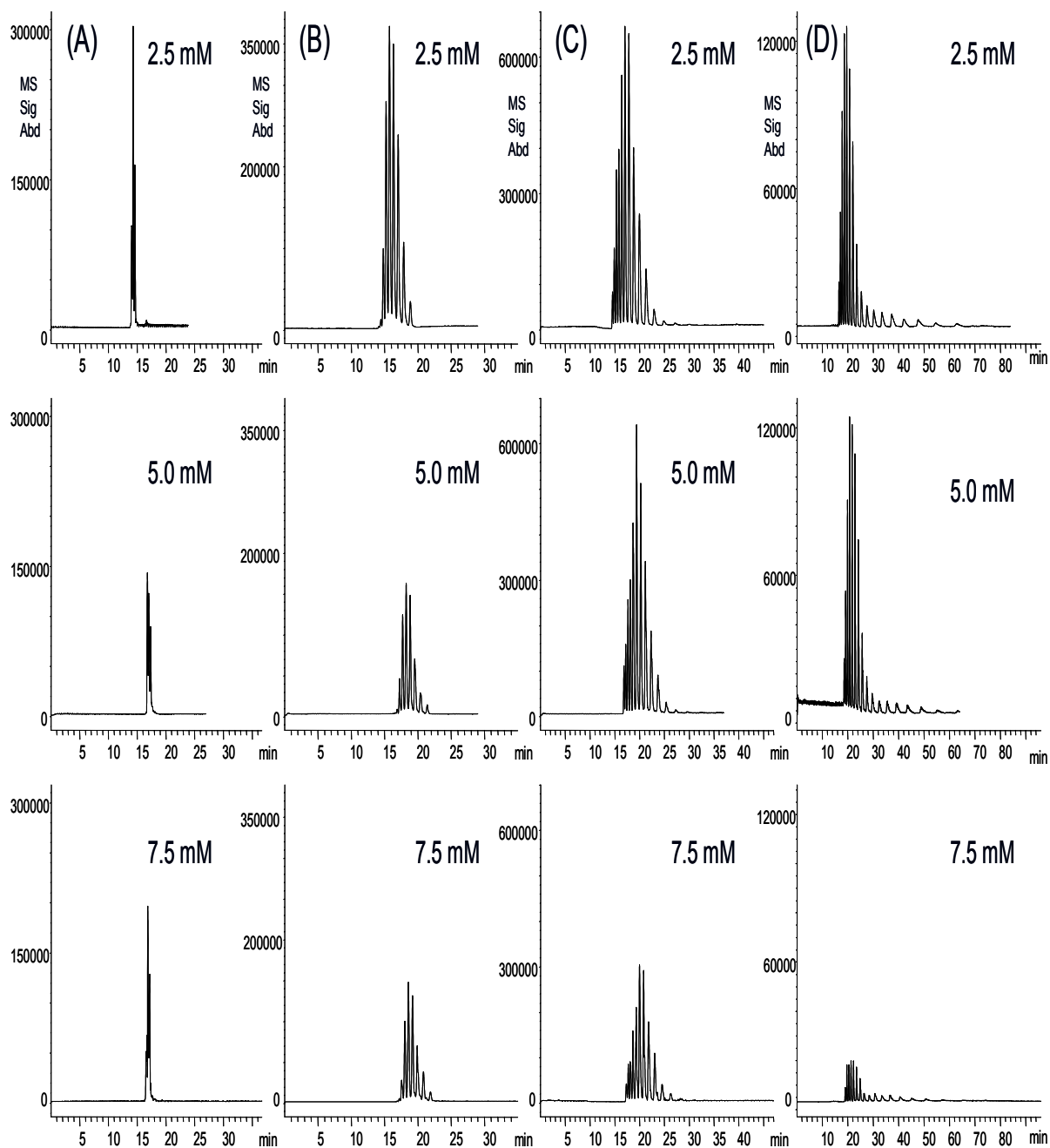


Figure 5.7: Effect of BGE Tris concentration (mM) on the CEC-MS separation of Triton series (A) TX-15, (B) TX-45, (C) TX-100, (D) TX-165. Conditions are the same as Figure 5.6 except 90% (v/v) of ACN.

chromatographic efficiency, a similar trend to that of ACN optimization was observed in that the N_{overall} was very similar in all cases. This was also the case for consideration of R_s which provided no mentionable difference over the range of concentration studied. For further study, Tris 2.5 mM was selected due to highest S/N and overall fastest analysis time.

Effect of Mobile Phase pH. The effect of varying the mobile phase pH in the range of pH 7-9 was investigated utilizing previously optimized 90% (v/v) ACN in 2.5 mM Tris buffer. The results of the study can be seen in Figure 5.8. As the natural pH of Tris is ~ 10 , concentrated HCl was utilized to lower the pH. This provides the addition of protons that aid in generation of EOF, as well as counter ions that together increase the ionic strength in solution. In addition, the ionization of Tris (pK_a of Tris = ~ 8) relative to pH also plays an important role in the separation. As shown in the Figure 5.8, at pH = 9 the separation of all TX oligomers is very poor most likely due to low EOF resulting from too few protons as well as few ionized Tris cations. Adding more HCl to lower the pH to 8 was found to significantly improve the separation of all TX series. This can be attributed to more favorable EOF due to the presence of excess protons and $\sim 50\%$ ionization of Tris. Consequently the analysis time was decreased for all analytes going from pH 9 to pH 8. Further addition of HCl going from pH 8 to pH 7 was found to slightly increase the analysis time, although no detrimental effect on the separation was observed. This effect could be attributed to protonation of stationary phase and silica wall silanol groups responsible for generation of the EOF. In addition, the increased ionic

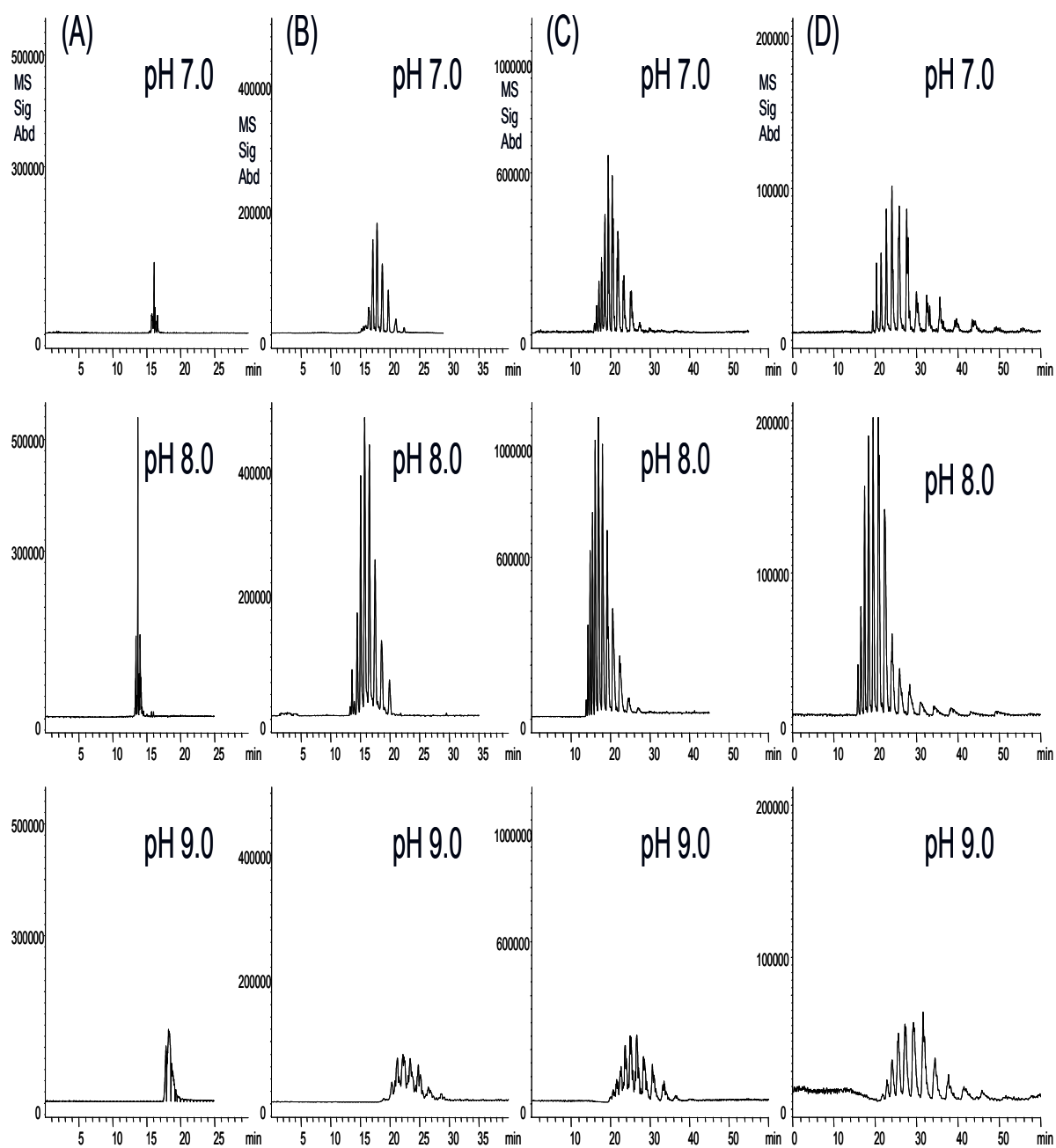


Figure 5.8: Effect of mobile phase pH on the CEC-MS separation of Triton series (A) TX-15, (B) TX-45, (C) TX-100, (D) TX-165. Conditions are the same as Figure 5.7 except ACN = 90% (v/v), and Tris = 2.5 mM.

strength decreases the thickness of the electrical double layer and increases viscosity, and hence a longer separation is observed. A consideration of the online S/N , chromatographic N and R_s were again evaluated for varying mobile phase pH. In all cases, the S/N was improved at pH 8, while pH 7 and 9 showed significantly lower S/N for all TX series. The chromatographic N was slightly higher at pH 7 than pH 8, although pH 9 demonstrated very poor peak N as compared to lower pH 7-8. Finally, the R_s showed a similar trend to N . The R_s was slightly improved over pH 8, but pH 9 exhibited much lower R_s compared to pH 7-8. Although, pH 7 was found to provide slightly improved N and R_s , due to higher S/N and faster analysis time, a pH = 8 was chosen (due to shorter retention) for sheath liquid and spray chamber optimization.

CEC-ESI-MS Sheath Liquid Optimization. The sheath liquid composition and flow rate were systematically evaluated. First, the MeOH/H₂O content in the range of 50%-90% MeOH was investigated. The corresponding plots showing effects of MeOH content on S/N are shown in Figure 5.9. For the shorter chain surfactants TX-15 (Figure 5.9A), TX-45 (Figure 5.9B) and TX-100 (Figure 5.9C), a larger volume fraction of MeOH in the sheath liquid in general provides lower S/N values. However, no clear trend was seen for TX-15 at 90% ACN where some oligomers showed higher S/N than the others. This may be explained by higher MeOH percentage in the sheath liquid which promotes unstable spray at high volume fraction.³⁸ A similar trend was observed for longer chain TX-165 (Figure 5.9D) although 80% MeOH showed comparable abundance to 65% MeOH. Nevertheless, the MeOH sheath liquid content to 50% volume fraction was found to

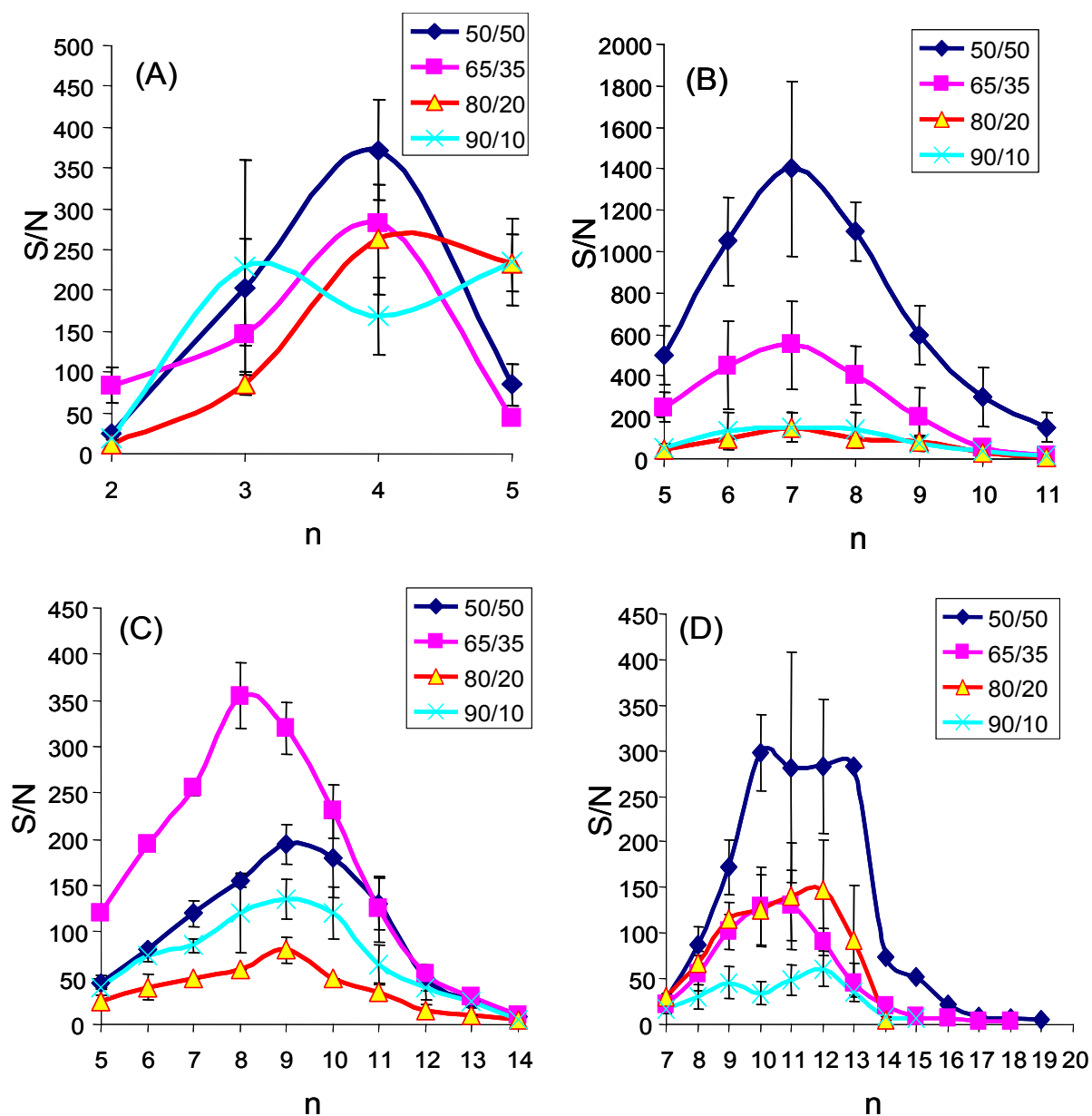


Figure 5.9: Variation in sheath liquid MeOH composition in the range 50-90% (v/v) for effects on S/N (A) TX-15, (B) TX-45, (C) TX-100, (D) TX-165. Conditions are the same as Figure 5.8 except pH = 8.

provide higher *S/N* most likely due to the most suitable surface tension of the electrospray droplet containing nonionic surfactant, MeOH and H₂O. Overall, 50/50 MeOH/H₂O was found to provide improved *S/N* in several cases and was therefore selected for further study.

The ionic strength of the sheath liquid affects conductivity and formation of stable electrospray. Therefore, the addition of HCO₂NH₄ to the sheath liquid in concentration range of 1-50 mM was evaluated. The corresponding plots for *S/N* are shown in Figure 5.10. Recent studies in our laboratory suggested that lower ionic strength of the sheath liquid (e.g., 1 mM) provides higher signal abundance, however, the instability of the electrospray results in the generation of excessive baseline noise.³⁸ In this work, a lower *S/N* was observed for all surfactants at 1 mM HCO₂NH₄ due to the high baseline noise level. In contrast, a higher ionic strength of the sheath liquid (e.g., 50 mM) generates a more stable electrospray. However, the addition of excess interfering ions can compete for ionizable sites in the ESI droplet formation, which often result in lower signal abundance of the analyte. This can be seen in Figure 5.10 which shows that in many cases the *S/N* values for 25 and 50 mM HCO₂NH₄ are only slightly higher than for lower 1 mM and 5 mM HCO₂NH₄. The exception can be seen for TX-165 (Figure 5.10C) where increased degree of ethoxylation requires greater ionic strength to ionize these surfactants. In general, a moderate 10 mM HCO₂NH₄ provided a suitable balance between stable electrospray and generation of MS signal. Since a larger *S/N* was observed in several cases and this concentration was therefore utilized for further study.

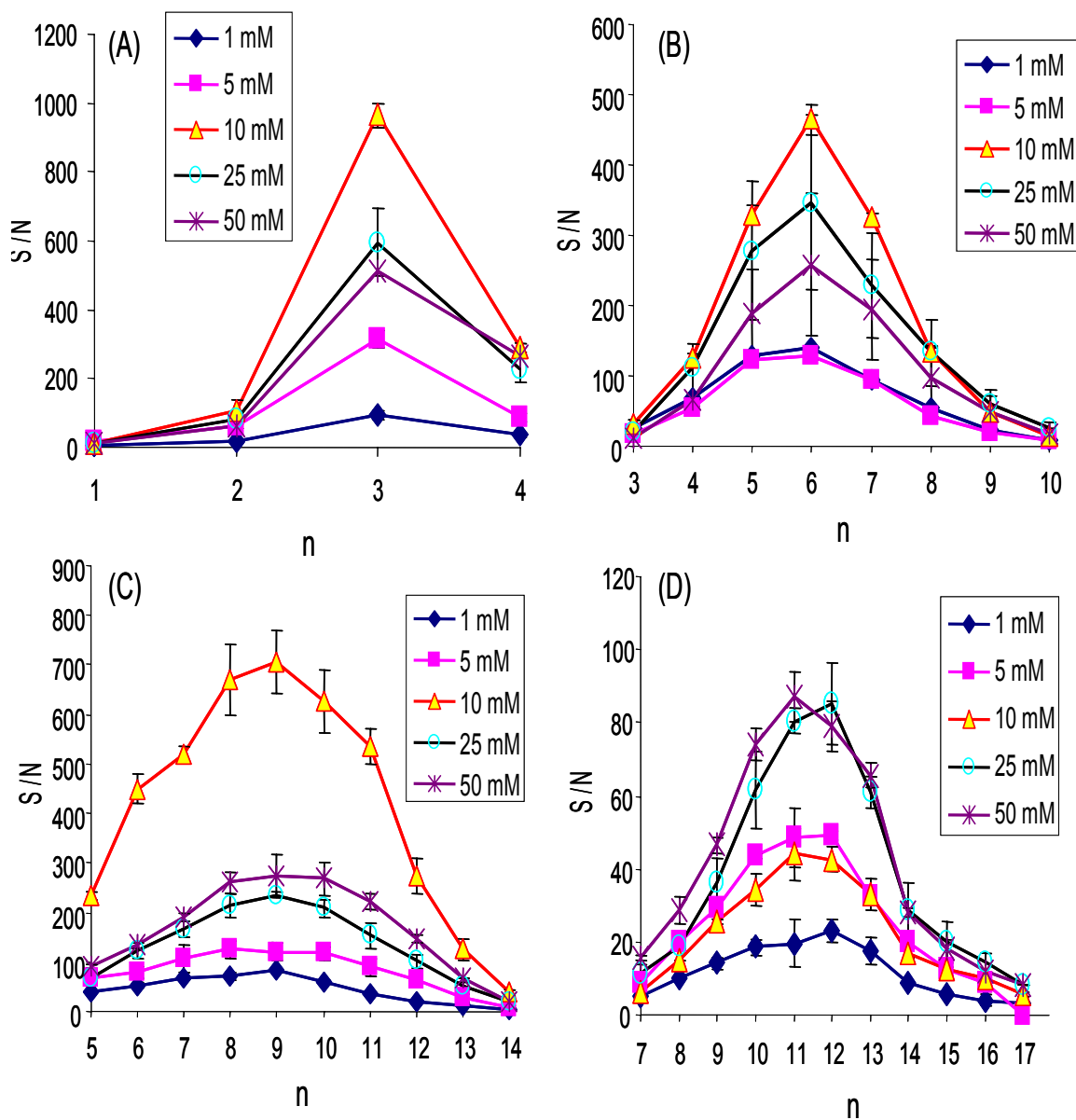


Figure 5.10: Variation in sheath liquid HCO_2NH_4 concentration in the range 1-50 mM for effects on S/N : (A) TX-15, (B) TX-45, (C) TX-100, (D) TX-165. Conditions are the same as Figure 5.9 except MeOH/ H_2O 50/50.

Finally, the effects of varying the sheath liquid pump flow rate from 3-9 $\mu\text{L}/\text{min}$ were compared (data not shown). A consideration of the S/N showed that the S/N was of similar value for all flow rate except for 3 $\mu\text{L}/\text{min}$ which was lower for TX-15 and TX-100 (data not shown). This suggests that lower sheath flow 3 $\mu\text{L}/\text{min}$ in CEC-MS does not provide adequate conductivity. Higher flow rates in the range of 5-9 $\mu\text{L}/\text{min}$ provided higher S/N , and no mentionable dilution resulting in decreased S/N was observed as shown by the similarity in S/N for all surfactant. Overall, a sheath flow rate of 5 $\mu\text{L}/\text{min}$ as this flow rate provided higher S/N in several cases. The final optimized sheath liquid composition was 50/50 MeOH/10 mM HCO_2NH_4 delivered at a flow rate of 5 $\mu\text{L}/\text{min}$.

CEC-ESI-MS Spray Chamber Optimization. For the optimization of the CEC-ESI-MS spray chamber parameters, the drying gas flow rate, nebulizer pressure, and drying gas temperature were evaluated. For drying gas flow rate, our previous study of cationic surfactants³⁹ demonstrated that 6 mL/min optimized in that study was in close agreement to the direct infusion of TX-100 (data not shown), which also showed that the highest signal achieved with either 4 or 6 mL/min. Therefore, 6 mL/min was considered a suitable drying gas flow rate for further study. Next, the online optimization of the spray chamber nebulizer pressure was evaluated in the range of 2-10 psi (data not shown). A lower setting of 2 psi was found to provide the lowest S/N for all surfactants as this lower flow rate does not provide adequate electrospray. Raising the flow rate to 5 psi significantly improved the S/N in all cases, whereas too high flow rate of 10 psi lowered

the S/N . Therefore, too high or too low nebulizer pressure adversely affects the formation of the Taylor cone as well as the online S/N . A moderate nebulizer pressure of 5 psi was found to provide higher S/N for all TX surfactants.

Finally, for the spray chamber drying gas temperature, our previous studies on cationic surfactants³⁹ indicated that 200 °C was a well suited temperature to provide higher signal and S/N while allowing for maximum lifetime of the CEC-MS column tip (data not shown). In particular we have experienced that the column tip gets fragile at very high temperature (e.g., ≥ 300 °C). Overall, the final optimized spray chamber parameters were: drying gas flow = 6 mL/min, nebulizer pressure = 5 psi, and drying gas temperature = 200 °C.

Optimization of the MS Capillary Voltage and the MS Fragmentor Voltage. For one representative surfactant TX-100, the effect of varying the online MS capillary voltage (V_{cap}) and the fragmentor voltage were examined. The V_{cap} controls the voltage applied to the entrance of the capillary, and the optimum voltage can vary for different compounds. An evaluation of the V_{cap} in the range of 2000-5000 V for effects on S/N is shown in Figure 5.11. It is clear that a lower V_{cap} (e.g., 2000-2500 V) provides lower S/N . In contrast, too high V_{cap} setting of 5000 V also results in lower S/N . The highest S/N was in the range of 4000-4500 V, however, this was found experimentally to decrease the lifetime of the internally tapered column over time. Overall, the optimum setting of this parameter was chosen at 3000 V as this V_{cap} value also prolongs column lifetime during

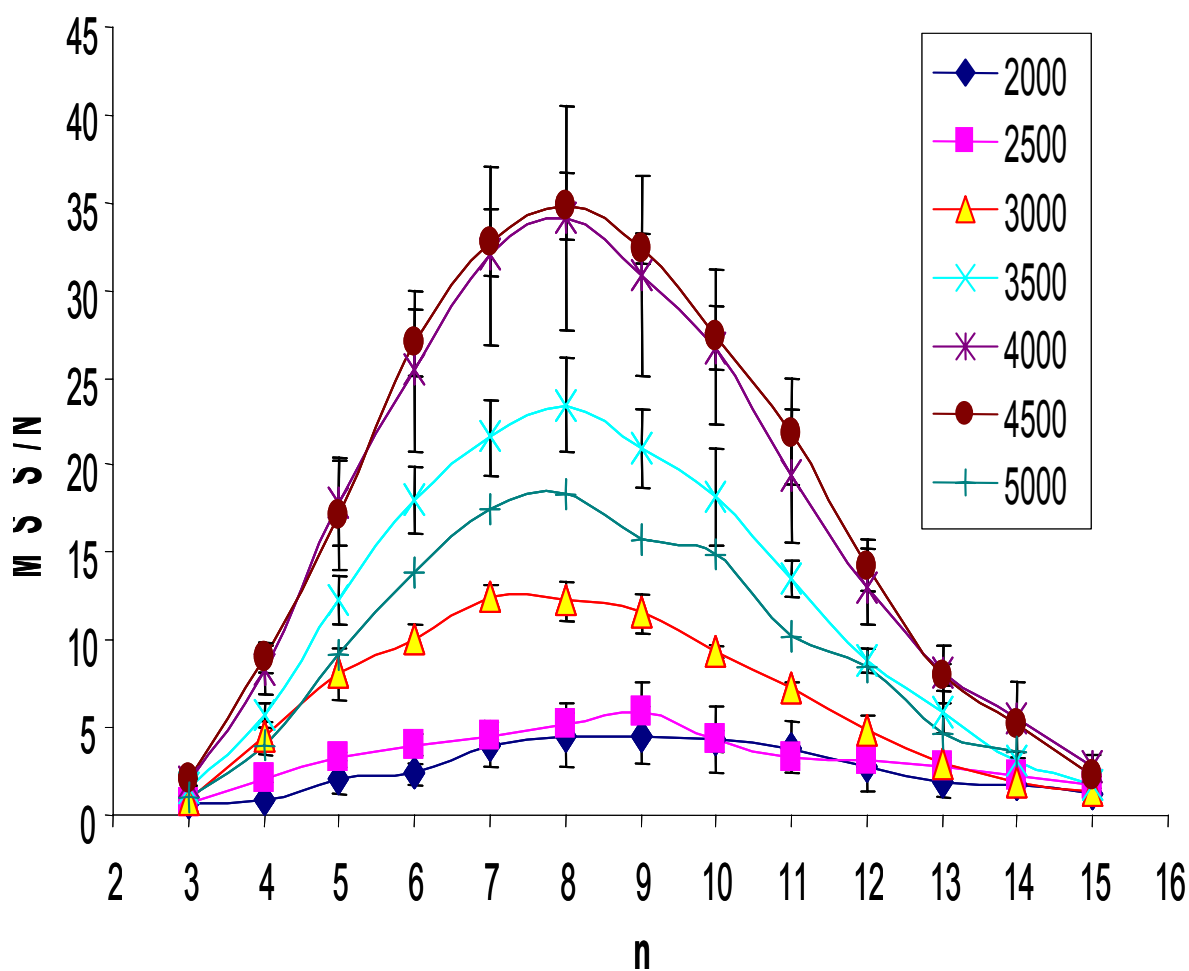


Figure 5.11: Investigation of MS capillary voltage in the range of 2000-5000 V for effects on S/N. TX-100 was used as the model analyte. Conditions are the same as Figure 5.10 except $\text{HCO}_2\text{NH}_4 = 10 \text{ mM}$, and spray chamber drying gas flow set to 6 mL/min, nebulizer pressure = 5 psi, and drying gas temperature set to 200 °C.

method development. However, for more sensitive monitoring, higher V_{cap} of 4000 V can be used.

Next, the effect of varying the online fragmentor voltage on the MS signal for TX-100 was investigated. This parameter controls the voltage applied at the exit end of the MS capillary which influences both ion transmission and fragmentation. Variation in the fragmentor voltage over the range of 25-200 V was investigated for effects on the S/N as shown in Figure 5.12. The results showed that too low (e.g., 25-75 V) or too high (e.g., 175-200 V) fragmentor voltage lowers the S/N . A more moderate voltage setting of 150 V provided higher S/N than 175 V or 200 V. The highest S/N was observed at 125 V and it was considered as the best setting.

Analysis of Longer Chain Triton X-305, 405, 705 Surfactants. The optimized method was applied to the analysis of very long chain Triton X surfactants including TX-305 ($n=30$), TX-405 ($n=40$), and TX-705 ($n=70$). From the initial CEC-ESI-MS investigation operating in full scan mode, the chromatographic results indicated extensive retention (e.g., >3hrs) using binary solvent of 90/10 ACN/H₂O along with substantial peak band broadening that ultimately provided poor sensitivity of these long chain ethoxylated surfactants (data not shown). In order to reduce the significant interaction of these analytes with the stationary phase as well as improve the efficiency and sensitivity, a minor modification to the previously optimized mobile phase composition was approached. Previous work by Thiam *et al.*³⁶ has demonstrated that the addition of THF

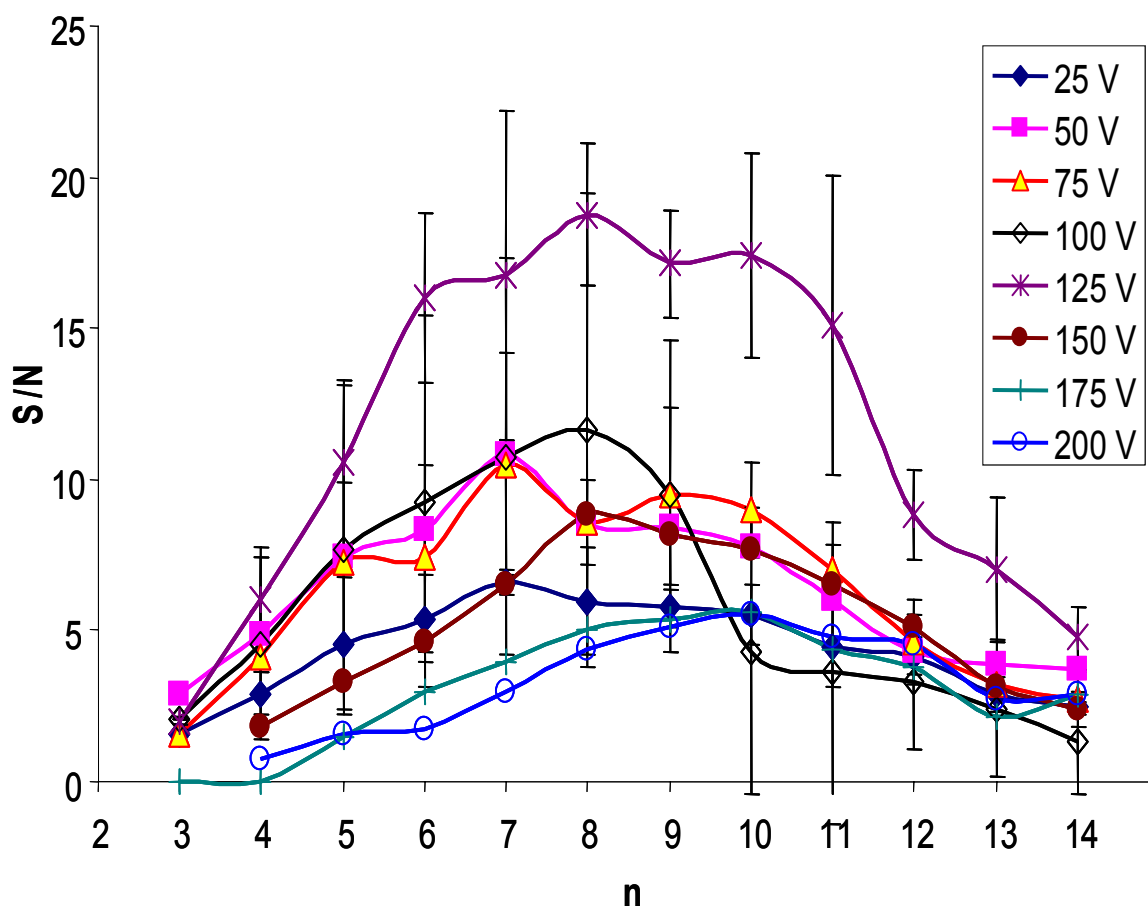


Figure 5.12: Variation in MS fragmentor voltage range 25-200 V. TX-100 was used as a representative surfactant. Conditions are the same as Figure 5.11 except $V_{\text{cap}} = 3000$ V.

to the running buffer can provide up to five fold reduction in the analysis time of highly hydrophobic cholesterol and ester derivatives in CEC-UV. Therefore, a similar methodology was investigated for analysis of the three very long chain non-ionic surfactants (TX-305,-405,-705) with the hopes of improving the resolution and decreasing the analysis time.

Starting with the optimized mobile phase conditions, the small replacement of ACN with THF in the range of 1-5% was evaluated for the separation of TX-305, TX-405 and TX-705. For TX-305, the results of the addition of THF can be seen in Figure 5.13 (A). At 1% THF, the chromatograms show that the total analysis time is greater than 150 min. Upon increasing the volume fraction of THF in the range of 3-5 % THF, a significant reduction in the retention was observed. In fact, a composition made up of 5% THF reduced the retention to such a large extent that the resolution of the oligomers with lower number of ethoxylate units started to decrease. Therefore, it can be concluded that for TX-305, the addition of 4% THF provided a reasonable analysis time of ~90 min for elution of oligomers which is drastically improved as compared to the use of ACN by itself that requires >200 min for separation of TX-305 (data not shown) with very poor detectability. For longer chain TX-405, a similar result was achieved. As shown in Figure 5.13(B), the retention time decreased with addition of THF in the range of 1-5%. Overall, the chromatograms suggest that modification of the mobile phase by adding 3% THF provides a reasonable trade-off between resolution and analysis time for TX-405 oligomers. The longest chain TX-705 was found to exhibit poor sensitivity due to the large degree of ethoxylation ($n=70$). The results of the analysis of TX-705 are shown in

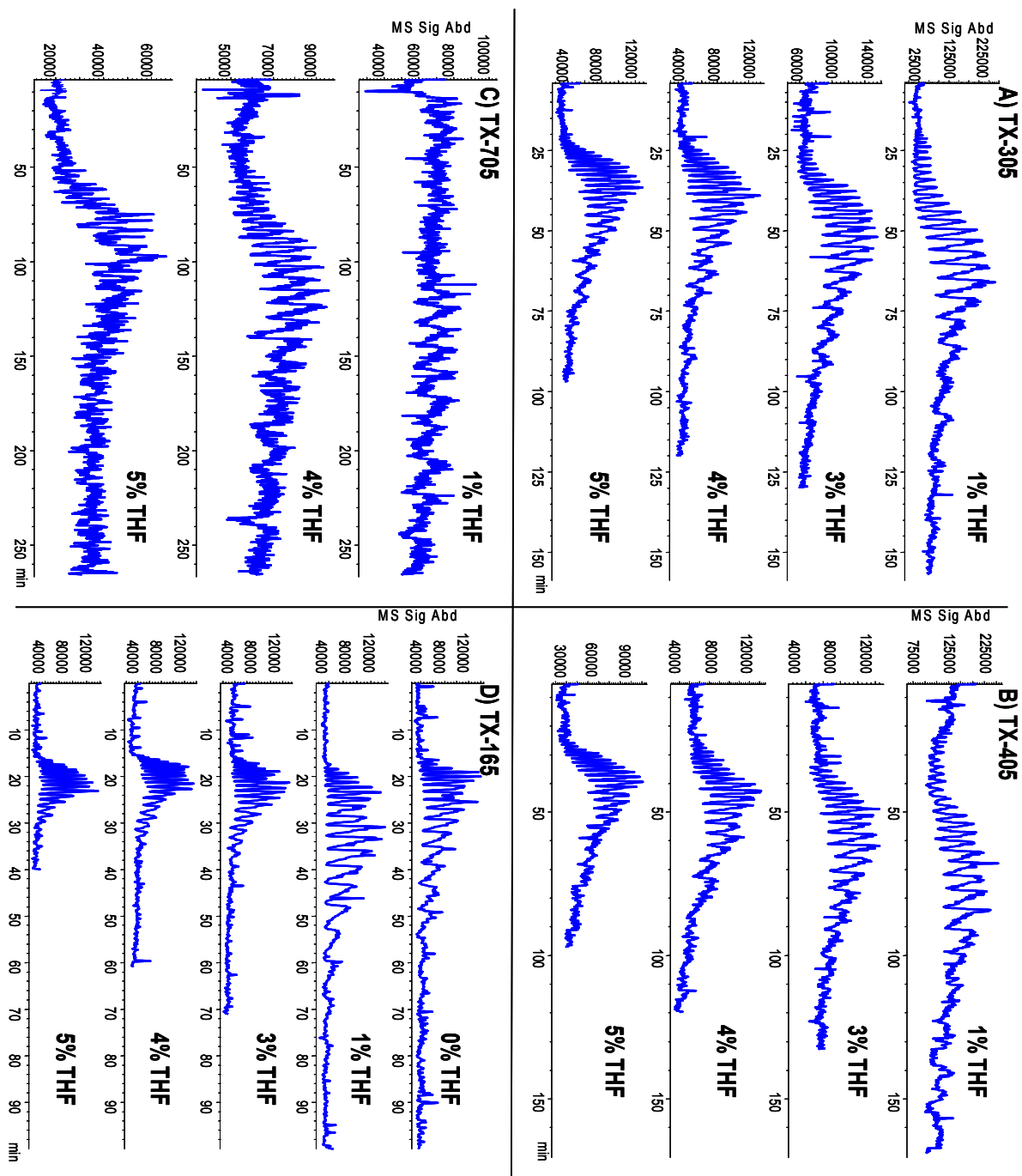


Figure 5.13: CEC-MS of long chain nonionic surfactants (A) TX-305, (B) TX-405, (C) TX-705 and midlength (D) TX-165 combining small volume fractions of polar aprotic solvent THF with previously optimized mobile phase. Conditions are the same as Figure 5.12 except for substitution of 90% ACN with THF as follows: 1% THF/89% ACN/10% H₂O; 2% THF/88% ACN/10% H₂O; 3% THF/87% ACN/10% H₂O; 4% THF/86% ACN/10% H₂O; 5% THF/85% ACN/10% H₂O.

Figure 5.13(C). Overall, the addition of 4% THF was found to provide reasonable analysis, although the sensitivity was poor. Lastly, as the results of adding THF were found to be beneficial for analysis of very long chain Triton series, the modified tertiary mobile phase was applied for separation of TX-165 surfactant with lower degree of ethoxylation ($n=16$). Impressively, the results shown in Figure 5.13(d) demonstrate that addition of 5% THF decreases the analysis from 70 min down to just 30 min. Overall, a tertiary mobile phase consisting of small volume fraction (3-5% (v/v)) THF with large volume ACN (85-87% (v/v)) and small aqueous buffer (10% (v/v), 2.5 mM Tris) was found to significantly improve the throughput for analysis of this very long chain Triton X series surfactants.

Precision, Linearity and Sensitivity. The reproducibility of migration time and peak area, as well as the linearity of calibration and sensitivity were determined for one representative surfactant TX-45. The results of the study are listed in Table 5.3. Satisfactory reproducibility for retention time for three replicate injections was observed with less than 1% RSD for all degree of ethoxylation ranging from $n=2-9$. The peak area showed acceptable but slightly higher deviation in the range of 1.6-4.5 % RSD. The only exception was the shortest chain oligomer ($n=2$) that provided %RSD of 10.5. The calibration curve obtained using the sum of average peak areas was linear with a correlation coefficient = 0.9986. A detection limit of 36.8 $\mu\text{g/mL}$ was obtained which is similar to that reported in the literature.²⁹

Table 5.3. Reproducibility, Linearity and Sensitivity of TX-45

n	migration time^a (%RSD)	peak area (%RSD)	linearity^b (20-500 µg/mL)	LOD^c
2	16.1 (0.8)	1.14E5 (10.5)	y=16890x + 53269 r ² = 0.9986	36.8 µg/mL
3	16.5 (0.9)	6.40E5 (1.6)		
4	16.9 (0.8)	1.92E6 (2.9)		
5	17.4 (0.9)	1.90E6 (2.9)		
6	17.9 (0.8)	1.57E6 (2.0)		
7	18.7 (0.9)	1.16E6 (3.3)		
8	19.5 (0.7)	6.98E5 (4.2)		
9	20.5 (0.8)	4.09E5 (4.5)		

a) triplicate injection at 500 µg/mL

b) average sum of the areas of all homologue peaks for triplicate injection at each concentration

c) three times the standard deviation of the average sum of homologue peak area for triplicate injection at 50 µg/mL

CONCLUSIONS

A characterization of the CEC-ESI-MS full scan mass spectra four TX-series nonionic surfactants produced the molecular ion $[M+H]^+$, ammonium adducts $[M+NH_4]^+$, sodium adducts $[M+Na]^+$, fragment ions corresponding to the loss of the alkyl chain from the phenyl ring $[M-C_8H_{17}+2H]^+$, and loss of ethoxylate groups resulting in one degree of ethoxylation $[C_8H_{17}(C_6H_4)E+H]^+$ and two degrees of ethoxylation $[C_8H_{17}(C_6H_4)E_2+H]^+$ as the most abundant ions. The short chain TX-15 was mainly comprised of sodium adducts. In contrast, the mid-chain TX-45 and TX-100 series were found in general to form the sodium adducts, fragment ions, and molecular ions at shorter degree of ethoxylation. At longer degree of ethoxylation, the ammonium adducts were mostly observed with minor fragment ions. This was supported in the analysis of longer chain TX-165, for which mostly the ammonium adducts were predominant.

An optimization of the CEC separation showed that a higher percentage of organic solvent using ACN in the range of 70-90% was required for stable CEC-ESI-MS operation. A composition containing 90% ACN was found to provide the best separation of oligomers for TX-15, -45, -100 and -165 with improved resolution of the later eluting ethoxylates. The investigation of mobile phase Tris showed that lower buffer concentration of 2.5 mM Tris provided the fastest separation, while a pH 8.0 was found to be optimum in terms of peak shape and S/N . For the study of sheath liquid parameters, a larger volume fraction of MeOH (e.g., 90%) in general provided lower S/N values. Hence, a moderate 50/50% composition of MeOH/H₂O produced the highest S/N in several cases. Next, a variation in buffer concentration of the sheath liquid showed that a

moderate 10 mM HCO_2NH_4 provided a suitable balance between stable electrospray and generation of MS signal, hence a larger S/N was observed in several cases at 5 $\mu\text{L}/\text{min}$ sheath flow rate. For spray chamber settings, the drying gas flow rate of 6 L/min and drying gas temperature 200 $^\circ\text{C}$ were found to be suitable and consistent with the previous studies of cationic surfactants.³⁹ Upon variation in nebulizer pressure, a moderate setting of 5 psi was selected for generation of optimum S/N . The online MS capillary voltage (V_{cap}) was set to 3000 V for maximum durability of the CEC column. In addition, the fragmentor voltage provided highest S/N at 125 V.

With slight modification in organic solvent composition using a binary solvent of ACN/ H_2O replacing ACN with up to 5% THF, the successful fingerprinting of very long chain TX-305, -405 and -705 surfactants was achieved. Most interestingly, a 2-4 fold decrease in the retention of these highly ethoxylated surfactants resulted in improved throughput of these APEOs. Finally, the repeatability and LOD were assessed.

ACKNOWLEDGMENTS

This work was supported by a grant from the National Institute of Health (Grant No. 62314-02) and funding from Solvay Pharmaceuticals (Marietta, GA, USA). Dean Norton is grateful to Dr. Brian Crow and Michael Bishop at Metamatrix Clinical Laboratory, Duluth, GA, for helpful discussion of the MS spectra.

References:

- (1) Knepper, T.P., Barceló, B., de Voogt, P. (Eds.), Knepper, T.P. and Berna, J.L. in
Analysis and Fate of Surfactants in the Aquatic Environment, Elsevier, Amsterdam
2003, Ch. 1, p.17.
- (2) Ying, G.G., Williams, B., Kookana, R. *Env. Int.* **2002**, 28, 215.
- (3) Ding, W.H., Wu, C.Y. *Rapid Commun. Mass Spectrom.* **2001**, 15, 2193.
- (4) Zhu, Z., Li, Z., Hao, Z., Chen, J. *Water Research* **2003**, 37, 4506.
- (5) Sakai, T., Teshima, N., Takatori, Y. *Anal. Sciences* **2003**, 19, 1323.
- (6) Barco, M., Planas, C., Palacios, O., Ventura, F., Rivera, J., Caixach, J. *Anal. Chem.*
2003, 75, 5129.
- (7) Plomley, J. B., Crozier, P.W., Taguchi V.Y. *J. Chromatogr. A* **1999**, 854, 245.
- (8) Jewett, B.N., Ramaley, L., Kwak, J.C.T. *J. Am. Soc. Mass Spectrom.* **1999**, 10, 529.
- (9) Willetts, M., Clench, M.R., Greenwood, R., Mills, G., Carolan, V. *Rapid Commun.*
Mass Spectrom. **1999**, 13, 251.
- (10) Vanhoenacker, G., Sandra, P. *J. Chromatogr. A* **2005**, 1082, 193.
- (11) Sparham, C.J., Bromilow, I.D., Dean, J.R. *J. Chromatogr. A* **2005**, 1062, 39.
- (12) Jonkers, N., Govers, H., de Voogt, P. *Anal. Chim. Acta* **2005**, 531, 217.
- (13) Cantero, M., Rubio, S., Pérez-Bendito, D. *J. Chromatogr. A* **2005**, 1067, 161.
- (14) Cantero, M., Rubio, S., Pérez-Bendito, D. *J. Chromatogr. A* **2004**, 1046, 147.
- (15) Jahnke, A., Gandrass, J., Ruck, W. *J. Chromatogr. A* **2004**, 1035, 115.
- (16) Shao, B., Hu, J., Yang, M. *J. Chromatogr. A* **2002**, 950, 167.
- (17) Levine, L.H., Garland, J.L., Johnson, J.V. *Anal. Chem.* **2002**, 74, 2064.

- (18) Espejo, R., Valter, K., Simona, M., Janin, Y., Arrizabalaga, P. *J. Chromatogr. A* **2002**, 976, 335.
- (19) Krogh, K.A., Verjup, K.V., Mogensen, B.B., Halling-Sørensen, B. *J. Chromatogr. A* **2002**, 957, 45.
- (20) Petrovic, M., Diez, A., Ventura, F., Barceló, D. *Anal. Chem.* **2001**, 73, 5886.
- (21) Petrovic, M., Barceló, D. *J. Mass Spectrom.* **2001**, 36, 1173.
- (22) Ferguson, P.L., Iden, C.R., Brownawell, B.J. *J. Chromatogr. A* **2001**, 938, 79.
- (23) Castillo, M., Riu, J., Ventura, F., Boleda, R., Scheduling, R., Schröder, H.Fr, Nistor, C., Émneus, J., Eichorn, P., Knepper, Th.P., Jonkers, C.C.A., de Voogt, P., González-Mazo, E., León, V.M., Barceló, D. *J. Chromatogr. A* **2000**, 889, 195.
- (24) Shang, D.Y., Ikonomou, M.G., Macdonald, R.W. *J. Chromatogr. A* **1999**, 849, 467.
- (25) Kamiyusuki, T., Monde, T., Nemoto, F., Konakahara, T., Takahashi, Y. *J. Chromatogr. A* **1999**, 852, 475.
- (26) Scullion, S.D., Clench, M.R., Cooke, M., Ashcroft, A.E. *J. Chromatogr. A* **1996**, 733, 207.
- (27) Park, H.S., Rhee, C.K. *J. Chromatogr. A* **2004**, 1046, 289.
- (28) Heinig, K., Vogt, C., Werner, G. *Anal. Chem.* **1998**, 70, 1885.
- (29) Herrero-Martinez, J. M., Fernández-Martí, M., Simó-Alfonso, E., Ramis-Ramos, G. *Electrophoresis* **2001**, 22, 526.
- (30) Heinig, K., Vogt, C. *Electrophoresis* **1999**, 20, 3311.
- (31) Klampfl, C.W. *J. Chromatogr. A* **2004**, 1044, 131.

- (32) Barceló-Barrachina, E., Moyano, E., Galceran, M.T. *Electrophoresis* **2004**, 25, 1927.
- (33) Norton, D., Zheng, J., Danielson, N.D., Shamsi, S.A. *Anal. Chem.* **2005**, 77, 6874.
- (34) Norton, D., Shamsi, S.A. *Electrophoresis* **2004**, 25, 586.
- (35) Norton, D., Shamsi, S.A. *J. Chromatogr. A* **2003**, 1008, 217.
- (36) Thiam, S., Shamsi, S.A., Henry III, C.W., Robinson, J.W., Warner, I.M. *Anal. Chem.* **2000**, 72, 2541.
- (37) Norton, D., Zheng, J., Shamsi, S.A. *J. Chromatogr. A* **2003**, 1008, 205.
- (38) Akbay, C., Rizvi, S.A.A., Shamsi, S.A. *Anal Chem* **2005**, 77, 1672.
- (39) Norton, D., Rizvi, S.A.A., Shamsi, S.A. *Electrophoresis* **2006**, 27, 4273.

Chapter 6:
Capillary electrochromatography-Mass Spectrometry Characterization
of Nonionic Surfactants Using In-Source Collision Induced Dissociation
(IS-CID)

Abstract

Capillary electrochromatography-mass spectrometry (CEC-MS) utilizing full scan positive ion mode of electrospray ionization (ESI) was employed to study the effect of fragmentor voltage on the in-source collision induced dissociation (IS-CID) of several alkylphenolpolyethoxylated (APEO) nonionic surfactants. A characterization of the IS-CID mass spectral pattern for the oligomers Triton X (TX) -series surfactants (e.g., TX-45) at varying fragmentor voltage is described. The results showed that distinct and unique mass spectral fingerprints were comprised mainly of varying abundance of ammonium adducts $[M+NH_4]^+$, protonated molecular ions $[M+H]^+$, sodium adducts $[M+Na]^+$ and fragment ions $[M-C_8H_{17}+2H]^+$. In addition, to a lesser extent the spectra contained fragments corresponding to the loss of both the octyl chain and varying length ethoxylate chain which were observed mostly at higher fragmentor voltage. Next, the breakdown curves (plots of relative ion abundance vs. fragmentor voltage) for each ion as a function of varying fragmentor voltage is presented for the oligomers of all four TX-series (TX-15, TX-45, TX-100, and TX-165). This is followed by breakdown plots overlaying the adducts, protonated molecular ions as well as fragment ions for each TX-series oligomer at varying fragmentor voltage. For increasing APEO chainlength, an interesting crossover pattern for the $[M+NH_4]^+$ and $[M-C_8H_{17}+2H]^+$ ions demonstrated a shift to increasing n-values upon raising the fragmentor voltage. In addition, the maximum abundance of the $[M+H]^+$ ion behaved in a similar fashion exhibiting a shift to higher n-values upon raising the fragmentor voltages. In this manner, the IS-CID for several TX-series surfactants has been assessed and characterized. Overall, the

breakdown curves allow the selective and sensitive monitoring of the appropriate ion or adducts formed at each fragmentor voltage which has the potential to be applied for industrial and environmental applications.

Introduction

Alkylphenol ethoxylates (APEOs) are an important class of nonionic surfactants that find numerous applications in domestic and industrial products. This is due in part to their excellent capability of defoaming, emulsification, solubilization and detergent properties. Hence, the worldwide production of these surfactants is in the 500 kton range.¹ In the past, the analysis of APEOs was often accomplished by direct injection into the mass spectrometer (MS) utilizing a technique known as flow injection analysis (FIA-MS). Although this method has the advantage of fast analysis time, the trade off was lower selectivity due to the large number of homologues or oligomers inherent to APEO and surfactant blends. In addition, the interfering components present in the sample matrix were found to compromise the ability to identify real samples using the FIA-MS analysis. However, when combined with more modern MS instrumentation such as tandem-MS (e.g., FIA-MS-MS), the ability to provide unique fragmentation significantly improved the selectivity. Hence, there are a large number of publications on FIA-MS in combination with FIA-MS-MS techniques.²⁻⁵ Although FIA-MS(-MS) methods often can provide valuable qualitative information such as molecular weight and fragmentation behaviour, the quantification of APEOs has remained challenging using FIA-MS due to the interfering components in the sample matrix that cause ion suppression. Therefore, the alternative has been the advent of hyphenated separation techniques coupled to MS which can separate out interference and considerably improve the ionization of APEOs.

Gas chromatography-mass spectrometry (GC-MS) has been used for analysis of APEOs and other nonionic surfactants.⁶ However, some of the inherent disadvantages of

GC-MS include the need for derivatization, problems of low volatility inherent to high molecular weight oligomers of non-ionic surfactant, and the lack of specificity due to interfering ions. Alternatively, high performance liquid chromatography (HPLC) combined with either ESI-MS and atmospheric pressure chemical ionization (APCI-MS) has been widely used for nonionic surfactants.⁷⁻²³ In this work, a new approach utilizing capillary electrochromatography-mass spectrometry (CEC-MS) for the characterization of APEOs has been undertaken. Some of the advantages of CEC-MS over HPLC-MS include higher plate numbers, less solvent consumption, and the ability to selectively pack columns in-house utilizing only a few milligrams of packing material which saves cost over expensive HPLC columns.

The coupling of CEC to MS for analysis of APEOs provides the capability for sensitive and selective detection due in part to the unique mass spectra generated by each oligomer in the ESI source. As such, during the CEC-MS method development it is important to optimize the ESI parameters controlling ion and adduct formation as well as fragmentation in order to maximize both the selectivity and the sensitivity. Hence, the ability to control the mass spectral pattern can be a useful tool for the identification of unknown compounds. In the case of single quadrupole mass spectrometers, the extent of fragmentation or in-source collision induced dissociation (IS-CID) is accomplished by control of the fragmentor voltage which is located at the exit end of the MS capillary. In addition, the degree of fragmentation or ion and adduct formation depends upon the voltage difference between the capillary and the skimmer.

The fragmentor voltage affects the fragmentation and transmission of sample ions. In general, as the fragmentor voltage is increased, more fragmentation will occur which can provide improved ion transmission of compounds that do not fragment readily. Moreover, the fragmentor voltage gives the ions a "push" that aids them in crossing the relatively high pressure region between the exit of the capillary and the skimmer. This is in contrast to triple quadrupole mass spectrometers which utilize a collision cell in order to control fragmentation. Ultimately, the control of the fragment voltage allows the selective formation of ions and adducts that can be monitored to improve the sensitivity. Consequently, some of the applications of CID include characterization of quaternary ammonium salts,²⁴ microcystins,²⁵ peptides,²⁶ glucuronides,²⁷ lutein esters,²⁸ and pharmaceutical compounds of interest such as triphenylethylenes.²⁹

In this work utilizing CEC-MS, the in-source CID fragmentation study of APEOs using Triton X series as model analytes was investigated. Utilizing previously optimized CEC separation conditions with the single quadrupole MS detector set to full scan mode in the range of 50-1500 amu, the fragmentor voltage was systematically varied for different chainlength TX-series surfactants TX-15, TX-45, TX-100 and TX-165 (Table 6.1). The results showed distinct and unique mass spectral fingerprints when utilizing the IS-CID. First, the example CEC-MS chromatograms of one representative surfactant (TX-45) showing the effect of varying fragmentor voltage are presented. This is followed by an interpretation of the individual mass spectra of TX-45 obtained from each peak in

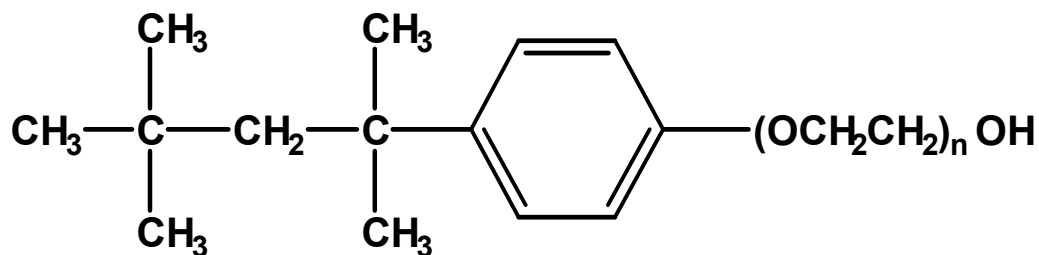


Table 6.1: Triton X surfactants used in this work.^{a,b}

Triton X-15	n=1
Triton X-45	n=4.5
Triton X-100	n=9-10
Triton X-165	n=16

a) Triton X is a trademark of Dow Chemicals.

b) n=average degree of ethoxylation

the chromatograms at varying fragmentor voltage using a fragmentation pathway to describe some of the fragments observed. Next, the spectra of all four TX-series surfactants were used to generate breakdown plots for each surfactant showing the relative percent abundance of individual adduct and fragment ions with varying fragmentor voltage. Finally, the breakdown plots overlaying all four ions for each surfactant at varying fragmentor voltage are provided. In this manner, the in-source CID for TX-series surfactants has been assessed and characterized.

EXPERIMENTAL SECTION

Chemicals and Reagents The organic solvents methanol (MeOH) and acetonitrile (ACN) of HPLC grade were purchased from Burdick and Jackson (Muskegon, MI,

USA). Ammonium acetate (NH_4OAc) (molecular biology grade) and Tris (hydroxymethyl) aminomethane (Tris) (99.9+%) were obtained from Sigma Chemical Company (St. Louis, MO, USA). Hydrochloric acid was obtained from Fisher Scientific (Springfield, NJ, USA). The Triton X Series nonionic detergents (99%) as shown in Table 6.1 were received from Sigma.

CEC-MS Instrumentation and Settings. The CEC/ESI/MS experiments were conducted on an Agilent HP^{3D}CE system (Agilent Technologies, Waldbronn, Germany) which was interfaced to an Agilent 1100 series MSD quadrupole mass spectrometer equipped with a CE/MS adaptor kit and a sprayer kit. The sheath liquid was provided by an Agilent 1100 series HPLC pump equipped with a 1/100 split flow. The Chemstation (v.10.0) software was used for data processing. All electrochromatograms were Gaussian smoothed with a factor of 0.1 min.

The internally tapered CEC-MS column (75 μm ID x 363 μm OD, 25 cm packed bed, 60 cm total length) was fabricated in our laboratory and packed with 3- μm CEC Reliasil ODS-1 (100Å pore size) non-encapped stationary phase (Column Engineering Inc., Ontario, CA, USA). The procedures of the column manufacture are described previously.³⁰ For CEC/ESI/MS conditioning, 12 bar pressure was applied to the inlet vial, and then the voltage sequentially raised in time increments as follows: 2 kV/20 min, 5 kV/20 min, 10 kV/20 min, 15 kV/20 min, and 18 kV/15 min. The maximum separation voltage was 18 kV as higher voltage was found in some cases to create unwanted arcing and shortened lifetime of the column. Injection was performed electrokinetically at 6 kV

for 6 sec. Individual stock solutions of TX-15, -45, -100 and -165 were dissolved at a concentration of 10 mg/mL in 65/35 (v/v) ACN/H₂O.

The previously optimized chromatographic, MS sheath liquid and spray chamber parameters were utilized as follows.³¹ The mobile phase contained 90/10 ACN/2.5 mM Tris, pH 8; sheath liquid containing 50/50 MeOH/10 mM HCO₂NH₄ delivered at 5 μ L/min; spray chamber set to drying gas flow of 6 mL/min, nebulizer pressure = 5 psi, and drying gas temperature set to 200 °C. The MS capillary voltage (V_{cap}) was set to 3000 V. The fragment voltage was varied in the range of 25-250 V in steps of 25 V utilizing the full scan mode in the range 50-1500 amu, peakwidth of 0.07 min, cycle time of 0.42 sec/cycle and gain set to 4. The ESI measurements were conducted in the positive ionization mode. Nitrogen obtained from a nitrogen generator was used for both nebulizing and drying gas.

The breakdown plots showing the fractional abundance of the protonated molecular ion, adduct ions, and fragment ions for each nonionic surfactant were constructed from full scan analysis of each peak in duplicate measurements obtained directly from two CEC-ESI-MS electrochromatograms. The CEC/ESI/MS full scan mass spectra of all four TX-series APEOs showed that the molecular ion $[M+H]^+$, ammonium adducts $[M+NH_4]^+$, sodium adducts $[M+Na]^+$, and fragment ions corresponding to the loss of the alkyl chain from the phenyl ring $[M-C_8H_{17}+2H]^+$ were always formed in high enough abundance relative to other ions. The mass/charge (m/z) values for the individual ethoxylate oligomers monitored in this study are shown in Table 6.2. Therefore, the average value of fractional abundance of these ions is presented in breakdown plots as a

function of varying the fragmentor voltage and degree of ethoxylation (n value) for each TX series surfactant.

RESULTS AND DISCUSSION

The effect of varying the MS fragmentor voltage on the mass spectral pattern of the TX-15, TX-45, TX-100 and TX-165 nonionic surfactants was studied using online CEC-ESI-MS. At varying fragmentor voltage ranging from 25-250 V, each oligomer of the individual surfactant was characterized using full scan MS mode. It is noted that the upper range of voltage studied for TX-15 and TX-45 (e.g., 25-175 V for TX-15, 25-200 V for TX-45) is slightly narrower compared to TX-100 and TX-165. This is because the ions used to construct the breakdown plots were not formed in high enough abundance at higher voltage. The example CEC-MS electrochromatograms showing the effect of varying fragmentor voltage for one representative surfactant (TX-45) are shown in Figure 6.1. Although there is no significant difference in the elution profile, poor signal noise was observed at low (e.g., 25 V) and high voltage (e.g., 200 V) respectively. However, when the mass spectra of TX-45 is compared at varying fragmentor voltage as shown in Figure 6.2, it can be seen that a distinct and unique fingerprint for each peak is obtained. Upon closer inspection of these mass spectra, the most interesting behaviour was

Table 6.2: Reference Table for Full Scan mass/charge (m/z) values of the protonated molecular ions, adducts and fragment ions used in the breakdown graphs of TX-15, TX-45, TX-100 and TX-165 nonionic surfactants.

m/z	n	Ion	m/z	n	Ion	m/z	n	Ion	m/z	n	Ion
251	1	$[M+H]^+$	268	1	$[M+NH_4]^+$	273	1	$[M+Na]^+$	139	1	$[M-C_8H_{17}+2H]^+$
295	2	$[M+H]^+$	312	2	$[M+NH_4]^+$	317	2	$[M+Na]^+$	183	2	$[M-C_8H_{17}+2H]^+$
339	3	$[M+H]^+$	356	3	$[M+NH_4]^+$	361	3	$[M+Na]^+$	227	3	$[M-C_8H_{17}+2H]^+$
383	4	$[M+H]^+$	400	4	$[M+NH_4]^+$	405	4	$[M+Na]^+$	271	4	$[M-C_8H_{17}+2H]^+$
427	5	$[M+H]^+$	444	5	$[M+NH_4]^+$	449	5	$[M+Na]^+$	315	5	$[M-C_8H_{17}+2H]^+$
471	6	$[M+H]^+$	488	6	$[M+NH_4]^+$	493	6	$[M+Na]^+$	359	6	$[M-C_8H_{17}+2H]^+$
515	7	$[M+H]^+$	532	7	$[M+NH_4]^+$	537	7	$[M+Na]^+$	403	7	$[M-C_8H_{17}+2H]^+$
559	8	$[M+H]^+$	576	8	$[M+NH_4]^+$	581	8	$[M+Na]^+$	447	8	$[M-C_8H_{17}+2H]^+$
603	9	$[M+H]^+$	620	9	$[M+NH_4]^+$	625	9	$[M+Na]^+$	491	9	$[M-C_8H_{17}+2H]^+$
647	10	$[M+H]^+$	664	10	$[M+NH_4]^+$	669	10	$[M+Na]^+$	535	10	$[M-C_8H_{17}+2H]^+$
691	11	$[M+H]^+$	708	11	$[M+NH_4]^+$	713	11	$[M+Na]^+$	579	11	$[M-C_8H_{17}+2H]^+$
735	12	$[M+H]^+$	752	12	$[M+NH_4]^+$	757	12	$[M+Na]^+$	623	12	$[M-C_8H_{17}+2H]^+$
779	13	$[M+H]^+$	796	13	$[M+NH_4]^+$	801	13	$[M+Na]^+$	667	13	$[M-C_8H_{17}+2H]^+$
823	14	$[M+H]^+$	840	14	$[M+NH_4]^+$	845	14	$[M+Na]^+$	711	14	$[M-C_8H_{17}+2H]^+$
867	15	$[M+H]^+$	884	15	$[M+NH_4]^+$	889	15	$[M+Na]^+$	755	15	$[M-C_8H_{17}+2H]^+$
911	16	$[M+H]^+$	928	16	$[M+NH_4]^+$	933	16	$[M+Na]^+$	799	16	$[M-C_8H_{17}+2H]^+$
955	17	$[M+H]^+$	972	17	$[M+NH_4]^+$	977	17	$[M+Na]^+$	843	17	$[M-C_8H_{17}+2H]^+$
999	18	$[M+H]^+$	1016	18	$[M+NH_4]^+$	1021	18	$[M+Na]^+$	887	18	$[M-C_8H_{17}+2H]^+$
1043	19	$[M+H]^+$	1060	19	$[M+NH_4]^+$	1065	19	$[M+Na]^+$	931	19	$[M-C_8H_{17}+2H]^+$
1087	20	$[M+H]^+$	1104	20	$[M+NH_4]^+$	1109	20	$[M+Na]^+$	975	20	$[M-C_8H_{17}+2H]^+$
1131	21	$[M+H]^+$	1148	21	$[M+NH_4]^+$	1153	21	$[M+Na]^+$	1019	21	$[M-C_8H_{17}+2H]^+$
1175	22	$[M+H]^+$	1192	22	$[M+NH_4]^+$	1197	22	$[M+Na]^+$	1063	22	$[M-C_8H_{17}+2H]^+$
1219	23	$[M+H]^+$	1236	23	$[M+NH_4]^+$	1241	23	$[M+Na]^+$	1107	23	$[M-C_8H_{17}+2H]^+$
1263	24	$[M+H]^+$	1280	24	$[M+NH_4]^+$	1285	24	$[M+Na]^+$	1151	24	$[M-C_8H_{17}+2H]^+$

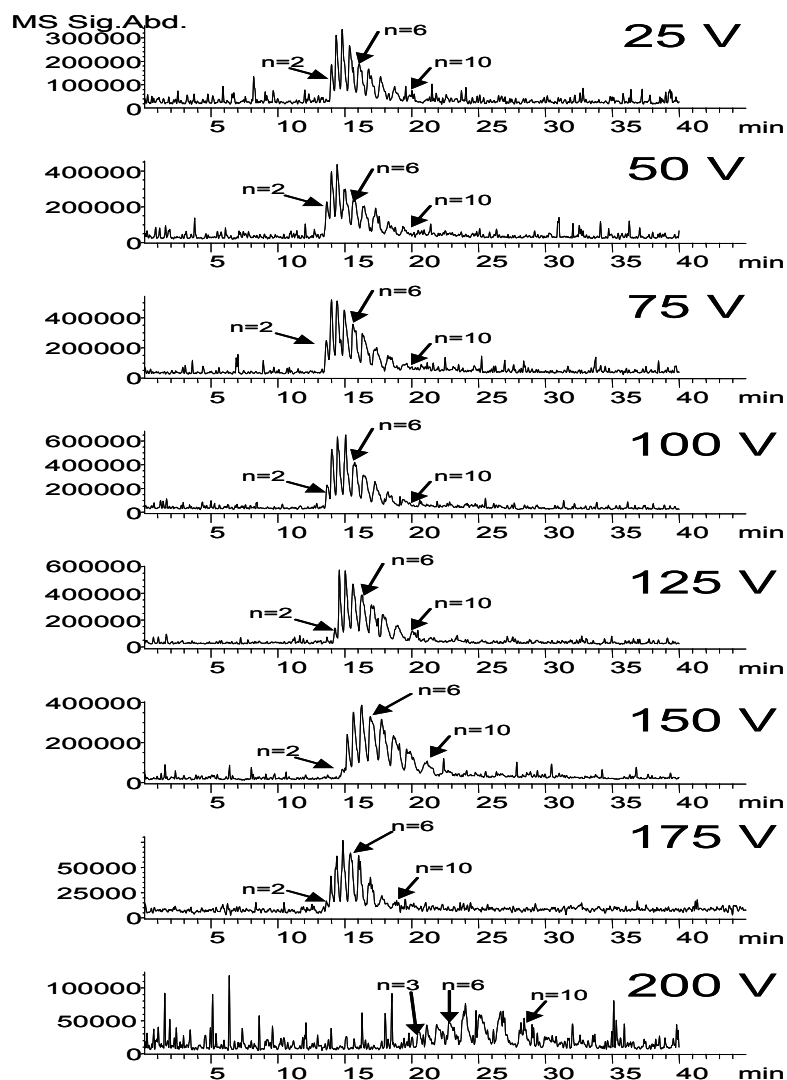


Figure 6.1: Full Scan CEC-MS chromatograms of TX-45 showing the effect of varying fragmentor voltage. Column dimensions 20 cm packed bed, 60 cm total length and 75 μm I.D. x 363 μm O.D., packed with 3 μm / 100 \AA Reliasil ODS. Conditions: 90/10 ACN/2.5mM Tris, pH 8.0. Sheath liquid: flow rate 5 $\mu\text{L}/\text{min}$, 50/50 MeOH/ H_2O , 10 mM HCO_2NH_4 . MS spray chamber: drying gas flow 6 L/min, nebulizer pressure 10 psi, drying gas temperature 200 $^\circ\text{C}$, fragmentor voltage varied, capillary voltage 3000 V, gain 4, applied voltage 16 kV runs, 6 kV 6 sec injection. Analyte: 10 mg/mL 65/35 ACN/ H_2O .

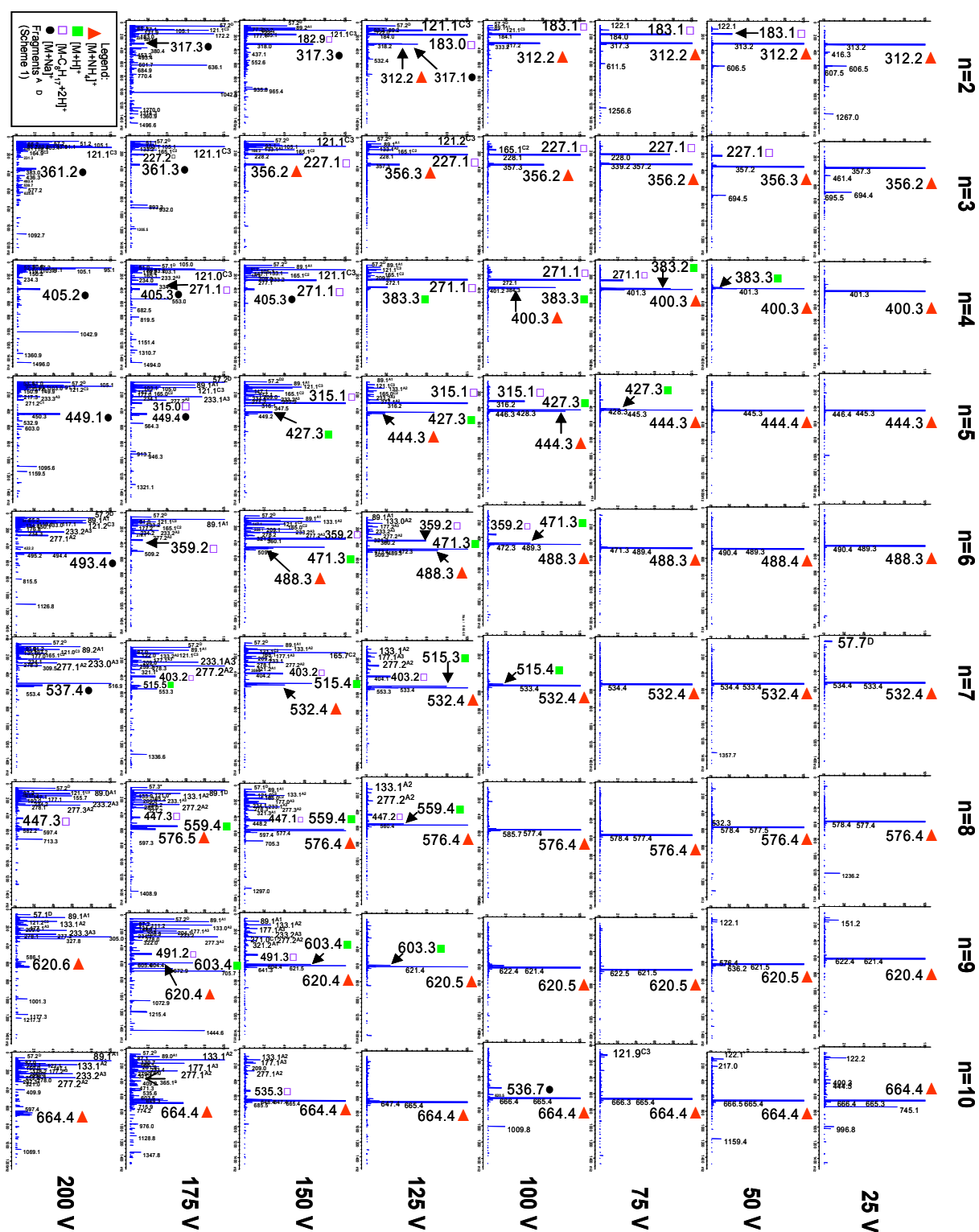
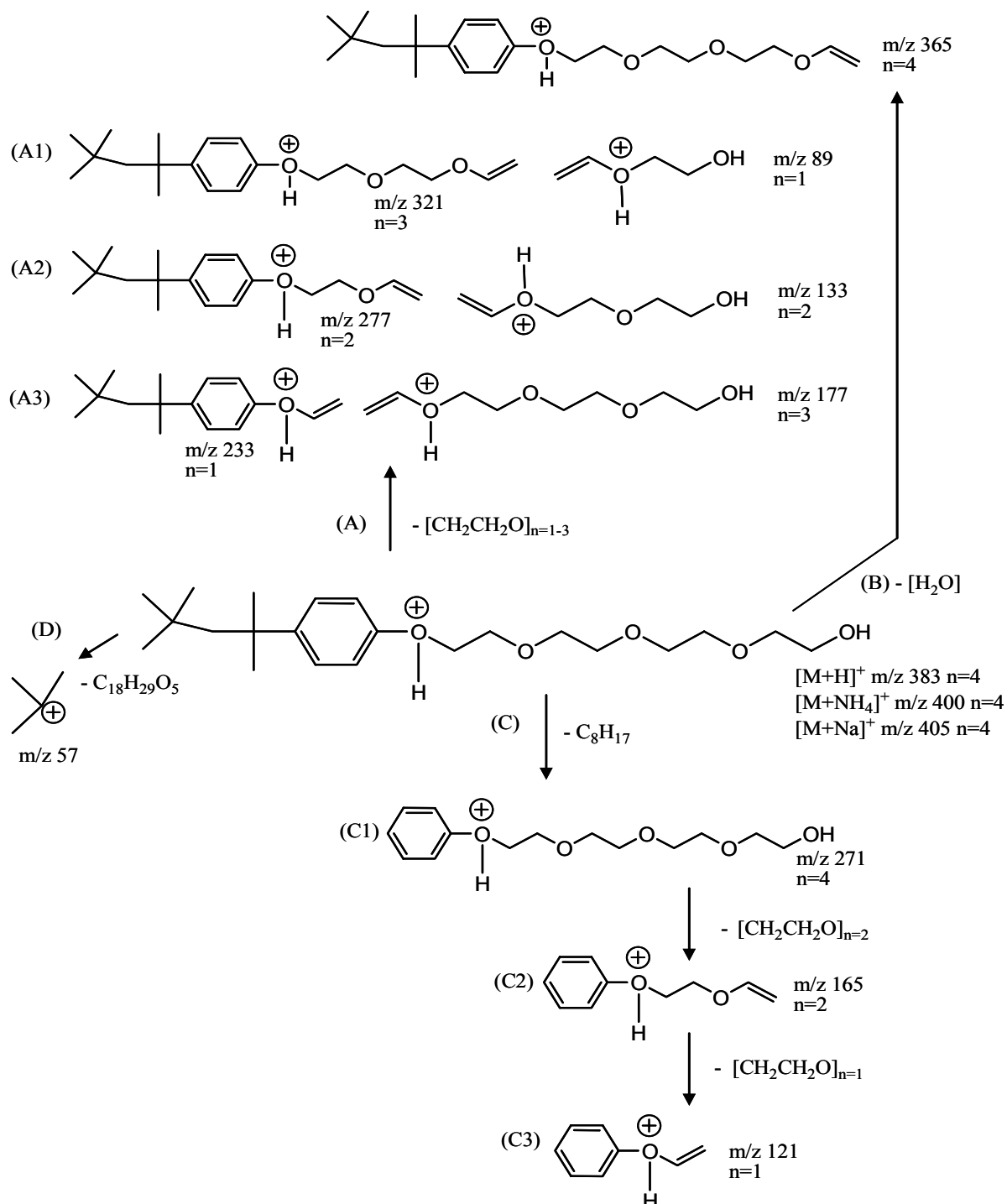


Figure 6.2: Mass spectra of TX-45 at varying fragmentor voltage. Conditions are the same as Figure 6.1.

exhibited by four ions (Table 6.2) including the protonated molecular ion, ammonium and sodium adducts, and a fragment ion which were observed to change intensity when varying the fragmentor voltage. Hence, these ions are provided in the legend of Figure 6.2 and labeled throughout the mass spectra using symbols. Furthermore, there are additional fragments of TX-45 that are summarized in Scheme 1 which exhibit a more random ionization pattern than the four ions of Table 6.2. These fragments are also labeled in Figure 6.2 of TX-45 mass spectra. In addition, it was found that all fragments of Scheme 6.1 correspond mostly to protonated molecular ion species.

In Figure 6.2, at a lower fragmentor voltage of 25 V, the mass spectra for all oligomers ($n=2-10$) was mainly comprised of the ammonium adducts $[M+NH_4]^+$. The exception was the $n=7$ oligomer which showed a fragment ion of $m/z=57$ corresponding to the loss of $C_{18}H_{29}O_5$ as shown in Scheme 1, pathway D. Increasing the fragmentor voltage from 25-50 V showed no effect on the intensity of the $[M+NH_4]^+$ adducts, however, the shorter chainlength oligomers $n=2-3$ began fragmentation by loss of the octyl chain (e.g., $[M-C_8H_{17}+2H]^+$) as $m/z=183$ and $m/z=227$, respectively. In addition, the protonated molecular ion $[M+H]^+$ was observed in small abundance for the $n=4$ oligomer.

Further increasing the fragmentor voltage from 50-75 V again had no effect on the abundance of $[M+NH_4]^+$ adducts (i.e., 100%) for all oligomers. An increase in abundance of the fragment ions $[M-C_8H_{17}+2H]^+$ for $n=2-3$ oligomers was observed, while the longer chainlength oligomer $n=4$ started to fragment in low abundance. Meanwhile the $[M+H]^+$ ion for $n=4$ oligomer increased and $n=5$ oligomer $[M+H]^+$ ion began to form.



Scheme 1: Fragmentation pathway of TX-45 under CID conditions showing (A) loss of ethoxylate group $[\text{CH}_2\text{CH}_2\text{O}]_n$, (B) loss of H_2O , (C) loss of alkyl chain C_8H_{17} and ethoxylate group $[\text{CH}_2\text{CH}_2\text{O}]_n$, and (D) loss of $\text{C}_{18}\text{H}_{29}\text{O}_5$.

At 100 V, the $[M-C_8H_{17}+2H]^+$ ions for the shorter chainlength oligomers $n=2-4$ were formed in 100% abundance, then progressively lower abundance was observed for $n=5-6$ oligomers and no such ion was observed for oligomers higher than $n=6$. The $[M+NH_4]^+$ adducts for $n=2-5$ oligomers began to decline in abundance although the longer chainlength adducts were still formed in 100% abundance. The intensity of the molecular ion for the $n=4$ oligomer showed little change, although the abundance increased to 100% for the longer chain $n=5$ oligomer and $n=6-7$ chainlength oligomers also began to exhibit this ion. Additional fragments were observed especially for short $n=2$ oligomer at 100 V corresponding to $m/z=57$ loss of $C_{18}H_{29}O_5$ (Scheme 1, D), $m/z=89$ corresponding to the loss of one ethoxylate group (e.g., $-[CH_2CH_2O]_{n=1}$, Scheme 1 A1), and also $m/z=121$ due either to loss of the octyl chain and three ethoxylates from the intact TX-45 parent ion (e.g., Scheme 1, C3), or from successive loss of ethoxylate groups (e.g., Scheme 1, C1-C3). The $n=3$ oligomer showed a loss of two ethoxylate groups for $m/z=165$ as shown in Scheme 1, C2. Finally at 100 V, the longest oligomer $n=10$ exhibited a sodium adduct $[M+Na]^+$ for $m/z=537$ (Table 6.2).

Upon further increase in fragmentor voltage going from 100 V to 125 V, the fragment ions $[M-C_8H_{17}+2H]^+$ increased to 100% abundance for the $n=2-5$ oligomers, but this occurred at the expense of a decrease in abundance for the ammonium adducts $[M+NH_4]^+$. However, the $n=6$ oligomer still showed $\sim 75\%$ abundance of $[M+NH_4]^+$ while the $[M+NH_4]^+$ adducts of $n=7-10$ continue to be stable with 100% abundance. In addition at 125 V, the $[M+H]^+$ did not form for the shortest oligomers $n=2-3$, but increased from low abundance at $n=4$ to maximum abundance going from $n=4-6$ and

decreases again at higher n values of 6-10. Several other fragments were observed at 125 V, corresponding to the fragmentation pathways shown in Scheme 1. For example, for the shorter chainlength $n=2-4$ oligomers, the m/z 57, 89, 121, and m/z 165 ions were formed similar to those formed at 100 V for the same oligomers, however, some additional new fragments were seen for the longer chainlength $n=5-8$ oligomers. These were m/z 233 for the $n=5$ oligomer corresponding to the loss of three ethoxylate groups (e.g., $-\text{[CH}_2\text{CH}_2\text{O]}_{n=3}$) as shown in Scheme 1 A3, $m/z=277$ for $n=5-6$ oligomers corresponding to the loss of two ethoxylate groups (e.g., $-\text{[CH}_2\text{CH}_2\text{O]}_{n=2}$ as shown in Scheme 1 A2, and for the $n=6-8$ oligomers the fragments equal to $m/z=133$ and $m/z=177$ were observed corresponding to ionization of the ethoxylate fragment with two ethoxylate groups (e.g., Scheme 1 A2 $m/z=133$) and three ethoxylate groups (e.g., Scheme 1 A3 $m/z=177$), respectively. No additional fragments were observed at 125 V for the $n=9-10$ oligomers.

When increasing the fragmentor voltage from 125 B to 150 V, the shortest $n=2$ oligomer showed a fast drop in abundance of the fragment ion $[\text{M}-\text{C}_8\text{H}_{17}+2\text{H}]^+$ (e.g., $m/z=183$), while an intense $[\text{M}+\text{Na}]^+$ and the ion C3 (Scheme 1) were formed $m/z=317$, and $m/z=121$, respectively. Several additional fragments of Scheme 1 were observed including m/z 57 and 89 as described previously. An increase in n -value from $n=2-6$ gradually increased the abundance of fragment $[\text{M}-\text{C}_8\text{H}_{17}+2\text{H}]^+$, then decreased significantly from $n=7-10$ oligomers. The molecular ion $[\text{M}+\text{H}]^+$ was not formed for shorter chainlength oligomers $n=2-4$, but started to form in low abundance ($\sim 35\%$) for the $n=5$ oligomer gradually increasing to 100% abundance going from $n=5-8$, then

decreasing from $n=8-9$ and finally disappearing at $n=10$ oligomer. The ammonium adducts also did not form for the shorter chainlength oligomers $n=2-6$, with the exception of $n=3$ which showed very low abundance. However, the $[M+NH_4]^+$ adducts increased abundance going from $n=6-8$ oligomers then were of maximum 100% abundance from $n=8-10$ oligomers. Additional fragments of Scheme 1 were observed as before (i.e., m/z 57, 89, 121, 133, 165, 177, 233 and 277) for the short to midlength chainlength oligomers $n=2-6$. However, for the longer oligomers $n=7-9$ a new fragment $m/z=321$ was observed corresponding to loss of one ethoxylate group (e.g., $-[CH_2CH_2O]_{n=1}$ as shown in Scheme 1 A1).

At even higher fragmentor voltage of 175-200 V, for the oligomers $n=2-6$, only fragments were observed including $[M-C_8H_{17}+2H]^+$ in low abundance and those of Scheme 1 mentioned above (i.e., m/z 57, 89, 121, 133, 165, 177, 233 and 277). However, an increased abundance of sodium adducts $[M+Na]^+$ was observed at this higher voltage for $n=2-5$ oligomers. A similar trend was shown for $n=7$ oligomer, although the molecular ion $[M+H]^+$ ($m/z=515$) was formed in low abundance which continued to increase to only ~65% abundance going from $n=7-9$. The ammonium adducts $[M+NH_4]^+$ were not formed until the $n=8$ oligomer chainlength which showed low abundance (e.g., ~30%), then slightly increased for $n=9$ oligomer and finally for $n=10$ oligomer the abundance was only 60%. One new fragment was observed for the $n=10$ oligomer which showed a loss of H_2O ($m/z=365$) as shown in Scheme 1, pathway B. Finally, at the highest fragmentor voltage studied of 200 V, some fragments of Scheme 1 were observed including $m/z=57, 89, 121, 165, 233, 277$, and $[M-C_8H_{17}+2H]^+$ for $n=8$ oligomer with

$m/z=447$. Two ammonium adducts ($m/z=620$ and 664) for longer chainlength $n=9-10$ oligomers were observed in very low abundance. However, the sodium adducts $[M+Na]^+$ showed the highest abundance for several oligomers $n=3-7$. No spectra was obtained for the shortest $n=2$ oligomer, as this oligomer was not able to withstand such high fragmentor voltage.

Next, the relative fractional abundance corresponding to the protonated molecular ion, formation of ammonium and sodiated adducts, and fragmentation ions due to loss of octyl chain as well as ethoxylate group was plotted as a function of fragment voltage for each surfactant. This is followed by an examination of the trend for all four ion formation $[M+H]^+$, $[M+NH_4]^+$, $[M+Na]^+$ and $[M-C_8H_{17}+2H]^+$ plotted together or overlaid as a function of maintaining individual fragmentor voltage for each surfactant. In this manner, the CEC-MS spectral characterization of TX-Series surfactants was assessed.

Fractional Abundance of Ion, Adduct and Fragment Formation at Varying Fragmentor Voltage

Formation of the Protonated Molecular Ion $[M+H]^+$. The formation of the protonated molecular ion $[M+H]^+$ at varying fragment voltage for each surfactant TX-15, TX-45, TX-100 and TX-165 is characterized in Figure 6.3 (A-D) respectively. For TX-15 (Figure 6.3A), the $[M+H]^+$ was observed for $n=1$ to $n=4$ degree of ethoxylation. The $n=1$ and $n=3$

oligomers were formed in the range of 25 to 100 V with maximum abundance at 75 V, and the shorter chain $n=1$ oligomer $[M+H]^+$ was significantly higher in abundance as compared to $n=3$. The $[M+H]^+$ for longer chain $n=4$ oligomer was formed in the range of 50-150 V, with a maximum abundance at 100 V and twice the intensity as compared to $n=2$ oligomer. Interestingly, for $n=2$ oligomer, the molecular ion was not formed in high enough abundance at any fragmentor voltage.

For TX-45 (Figure 6.3B), the $[M+H]^+$ ions were characterized from $n=2$ to $n=10$ degree of ethoxylation. The shorter chainlength $n=2-3$ oligomers did not form $[M+H]^+$ ions greater than 20% abundance. For increasing degree of ethoxylation $n=4-10$, an increasing fragment voltage was required to form the $[M+H]^+$ ion in high abundance. For example, at lower fragmentor voltage of 75 V, the maximum abundance of $n=4$ oligomer was observed. Increasing the fragmentor to 100 V showed a maximum abundance of $n=5$, while 125 V provided maximum $[M+H]^+$ formation for $n=6-7$ oligomers. Finally, further increasing the fragmentor to 150 V was optimum for $n=8$, and $n=9-10$ which formed highest $[M+H]^+$ ions at 175 V. Overall, the $n=5$ and $n=6$ oligomers were formed in highest abundance as compared to the other oligomers.

The $[M+H]^+$ ion formation for TX-100 in the range of $n=3$ to $n=16$ degree of ethoxylation is shown in Figure 6.3C. Interestingly, the shortest chain $n=3$ oligomer formed the $[M+H]^+$ ion with less than 20% abundance. For the short to mid chainlength oligomers of TX-100, a slightly greater fragment voltage was required to form optimum $[M+H]^+$ abundance as compared to TX-45. For example, $n=4$ and 5 oligomers of TX-100

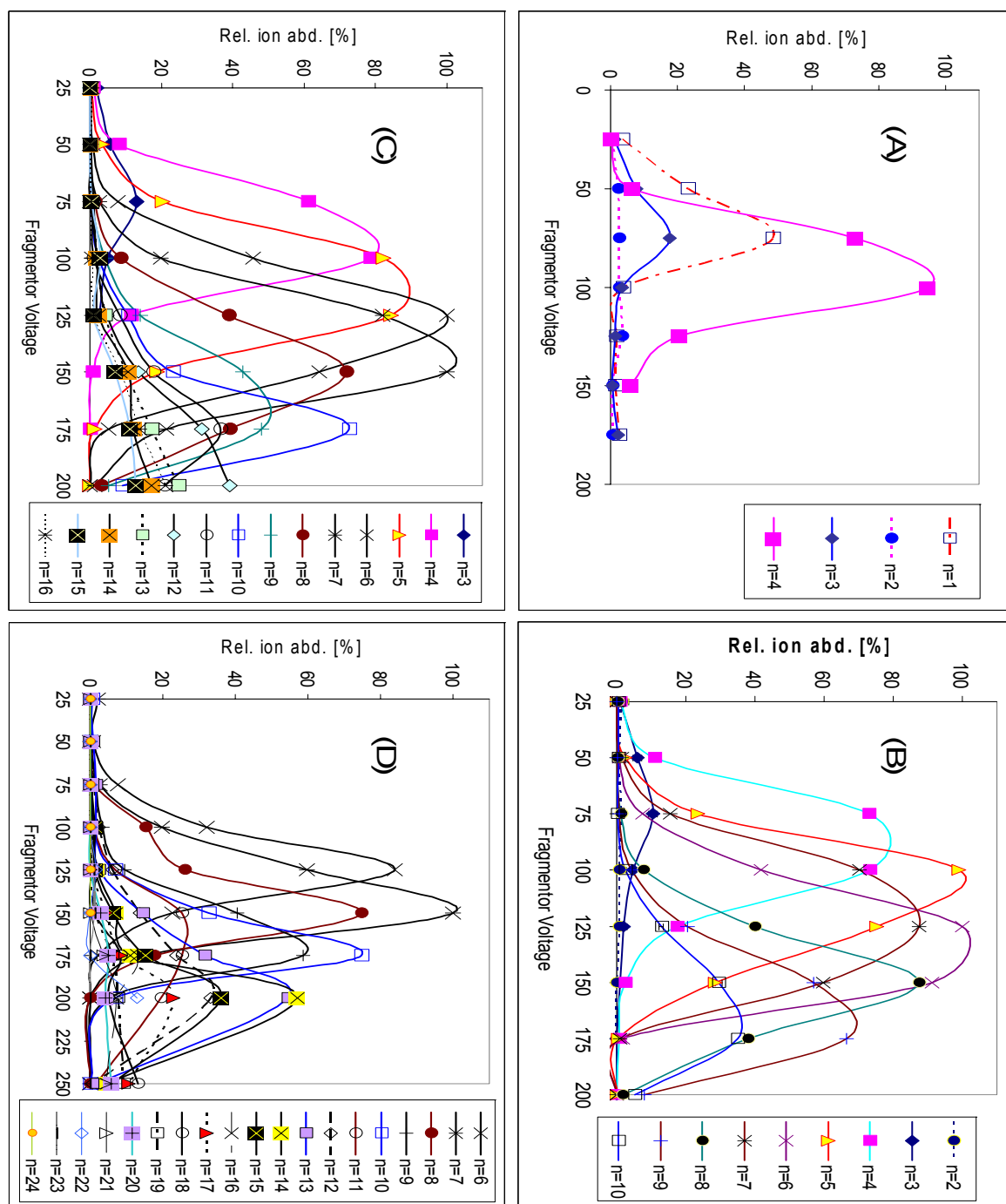


Figure 6.3: Breakdown curves showing the effects of varying fragmentation voltage on the mass spectral fractional abundance of molecular ion $[M+H]^+$ formation for individual degree of ethoxylation (n-value) for A) TX-15, B) TX-45, C) TX-100, and D) TX-165. The conditions and m/z are as listed in the experimental section.

required 100 and 125 V, respectively for maximum abundance as compared to 75 and 100 V required for the same two oligomers of TX-45. Similarly, the $n=7$ oligomer of TX-100 showed maximum abundance at 150 V as compared to 125 V for the same oligomers of TX-45. However, for the longer chain $n=8-11$ oligomers of TX-100, the $[M+H]^+$ ions were formed at the same fragmentor voltage (e.g., 150-175 V) as shown for TX-45. For the longest chain oligomers of TX-100 $n=12-16$, the $[M+H]^+$ ions were unable to form in high enough abundance even at 200 V. For TX-100, the $n=6$ and $n=7$ $[M+H]^+$ ions were formed in highest abundances (e.g., 100%).

The formation of $[M+H]^+$ ions in the range of $n=6-24$ for the longest chain TX-165 surfactant is shown in Figure 6.3D. For TX-165, the optimum fragment voltages for oligomers range $n=6-11$ were the same as those shown for TX-100. The maximum abundances of $[M+H]^+$ ions for longer chain oligomers (i.e., $n=12-17$) observed at a fragmentor voltage of 200 V were only approximately 50% or lower compared with its abundances observed for shorter chain oligomers ($n=6-10$). The highest abundance of $[M+H]^+$ was observed for $n=7$ oligomers of TX-165.

Formation of the Ammonium Adduct $[M+NH_4]^+$. Next, the formation of the ammonium adducts $[M+NH_4]^+$ as a function of varying fragment voltage for TX-series were characterized. The results of the study can be seen in Figure 6.4A-D. Initially, a significantly different pattern of $[M+NH_4]^+$ formation as compared to $[M+H]^+$ ion formation can be seen. For TX-15 (Figure 6.4A), the $[M+NH_4]^+$

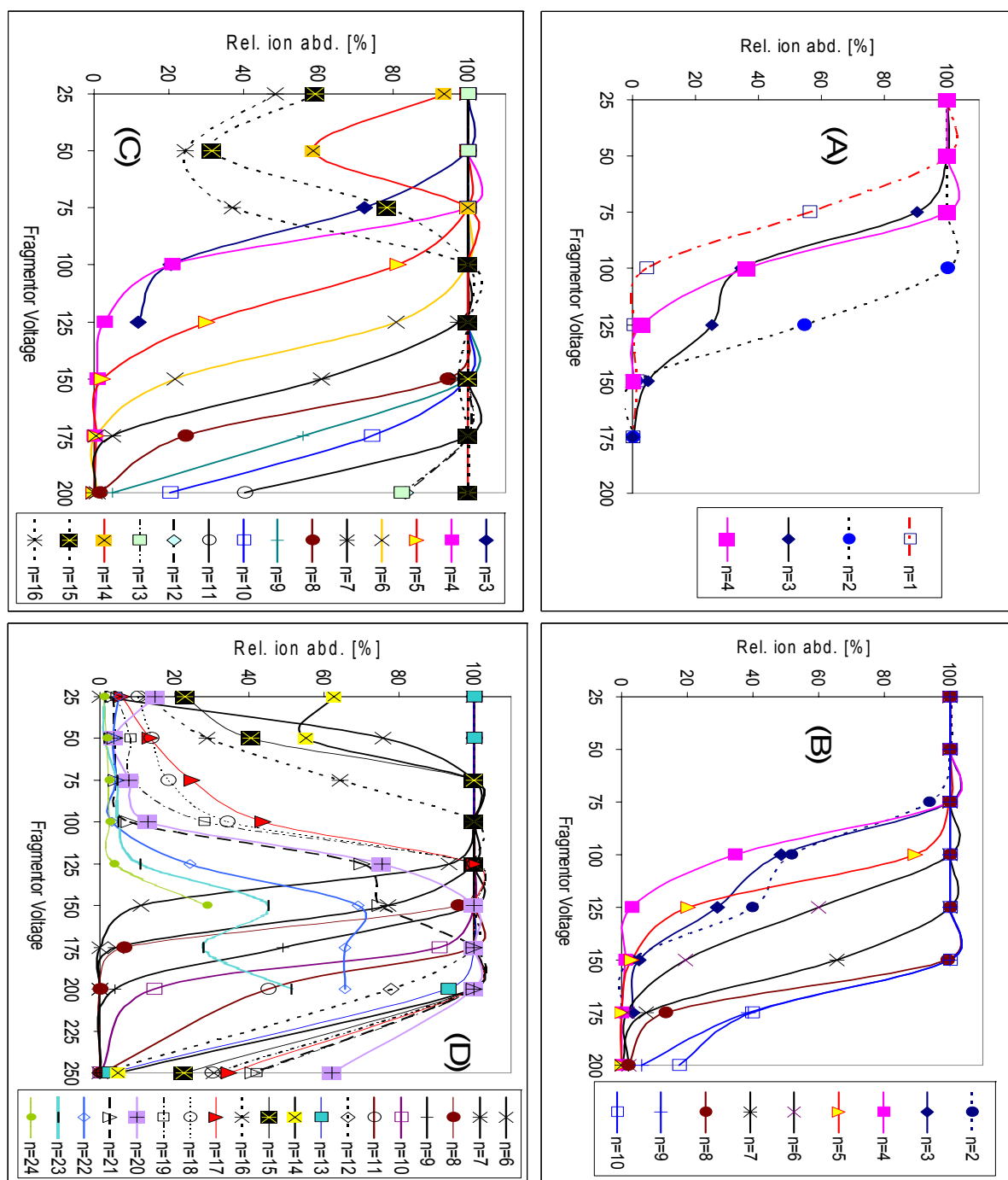


Figure 6.4: Breakdown curves showing the effects of varying fragmentation voltage on the mass spectral fractional abundance of ammonium adduct $[M+NH_4]^+$ formation for individual degree of ethoxylation (n-value) for A) TX-15, B) TX-45, C) TX-100, and D) TX-165.

adducts for $n=1$, $n=3$ and $n=4$ are formed in high abundance at lower fragment voltage in the range of 25-75 V. At higher voltage greater than 75 V, the abundance of these adducts shows a significant drop and essentially falls to zero at 100 V, 125 V and 150 V for the respective $n=1,4$ and 3 oligomers of TX-15. Interestingly, the $n=2$ oligomer of TX-15 was stable up to 100 V, then decreased with higher voltage, and showed trends similar to those oligomers of TX-15.

The profile of the $[M+NH_4]^+$ adduct formation for TX-45 is shown in Figure 6.4B. For the shorter chainlength $n=2-4$ oligomers, maximum (i.e., 100%) abundance of the ammonium adduct was formed in the range of 25 to 75 V, while $n=5$ $[M+NH_4]^+$ was formed at 100% up to approximately 100 V. Increasing the fragment voltage greater than 100 V showed a pronounced drop in abundance of the shorter chains. On the other hand, oligomers with degree of ethoxylation of $n=6-7$ were formed in maximum abundance up to 100 and 125 V respectively, while longer chain $n=8-10$ showed $[M+NH_4]^+$ formation all the way up to 150 V. No $[M+NH_4]^+$ ions of TX-45 were observed to any large extent (i.e., >20% abundance) at greater than 200 V. Nevertheless, the breakdown clearly suggests that up to the fragmentor voltage of 75V, all oligomers form $[M+NH_4]^+$ in high abundance.

A characterization of $[M+NH_4]^+$ adduct formation for TX-100 is provided in Figure 6.4C. At lower fragment voltage of 25-50 V, an interesting pattern was observed as compared to the TX-45 and TX-15 surfactants. The initial observation shows that most $[M+NH_4]^+$ adducts of $n=1-13$ oligomers are formed in high abundance at lower fragment voltage range 25-75 V, as shown before for TX-45. However, the longest chainlength

$n=14-16$ oligomers exhibit a different profile. Initially, at lower 25 V, the $n=14-16$ form $[M+NH_4]^+$ ions in the range of 50-90% abundance, but then decrease approximately by 50% upon raising the fragment voltage to 50 V. Further increasing the fragment voltage to 75 V and higher resulted in 100% transmission and formation of $[M+NH_4]^+$ ions of the longer chain oligomers which remains stable up to 200 V. This is probably due to the higher affinity for the ammonium ions by the longer chain oligomers.

Finally, the $[M+NH_4]^+$ adduct formation for TX-165 at varying fragmentor voltage is shown in Figure 6.4D. The shorter chain oligomers (i.e., $n=6$ to $n=13$) exhibited a trend very similar to that of TX-100. At lower voltage, a trend similar to TX-100 was observed for the longer degree of ethoxylation. For example, at 25 V, the oligomer $n=14$ of TX-45 is formed at slightly lower abundance than TX-100 (e.g., 60% for TX-165 vs. 90% for TX-100). However, at 50 V the abundance of $n=14$ $[M+NH_4]^+$ adduct drops as shown before for TX-100, then increases again at higher fragmentor voltage. However, unlike the trend of TX-100, the longer chain oligomers of TX-165 $n=15-16$ showed a gradual increase in abundance upon raising the voltage from 25-125 V. Finally, at 250 V, all oligomers including longer chain adducts of TX-165 showed a significant drop in abundance. Furthermore, the ammonium adducts of $n=17-21$ oligomers are formed in high abundance in the voltage range of 125-225 V. However, some of the longest chain oligomers (e.g., $n=22-24$) formed adducts of low abundance over the same voltage.

Formation of the Sodium Adduct $[M+Na]^+$. The formation of sodium adducts $[M+Na]^+$ for TX-15-165 as a function of varying ESI fragmentor voltage is shown in Figure 6.5A-D. In general, the $[M+Na]^+$ adducts were formed in much lower abundance as compared to the protonated molecular ions and the ammonium adducts. For example, for TX-15, no sodium adduct formation was observed greater than 40% abundance. The trend for TX-15 (Figure 6.5A) showed that increasing fragmentor voltage resulted in increased $[M+Na]^+$ formation. The highest abundance adducts for $n=1-4$ oligomers was in the range of 125 to 150 V, and the most abundant sodium adduct was observed for $n=3$ oligomer.

For TX-45 (Figure 6.5B), a lower voltage of 25-100 V showed very little $[M+Na]^+$ formation, e.g., less than 20%. From 100 to 150 V an increase of approximately 10% abundance was observed for most oligomers, except for $n=2$ which showed significant increase to ~70% abundance at 150 V. Interestingly, upon increasing fragmentor from 150 V to 175, a decrease in abundance for most oligomers was observed, followed by significant rise in $[M+Na]^+$ formation at 200 V. For TX-45, the $n=6$ oligomer showed the highest $[M+Na]^+$ formation at 200 V.

For TX-100 (Figure 6.5C), no significant $[M+Na]^+$ adduct formation was observed at lower fragment voltage of 25-150 V. Similar to TX-45, several oligomers showed pronounced $[M+Na]^+$ formation at 200 V. Overall, the $n=5$ followed by $n=6$ oligomers exhibited the highest abundance at 200 V.

Finally, the profile for $[M+Na]^+$ formation corresponding to TX-165 at varying fragment voltage is shown in Figure 6.5D. Although the plot is more complex, several

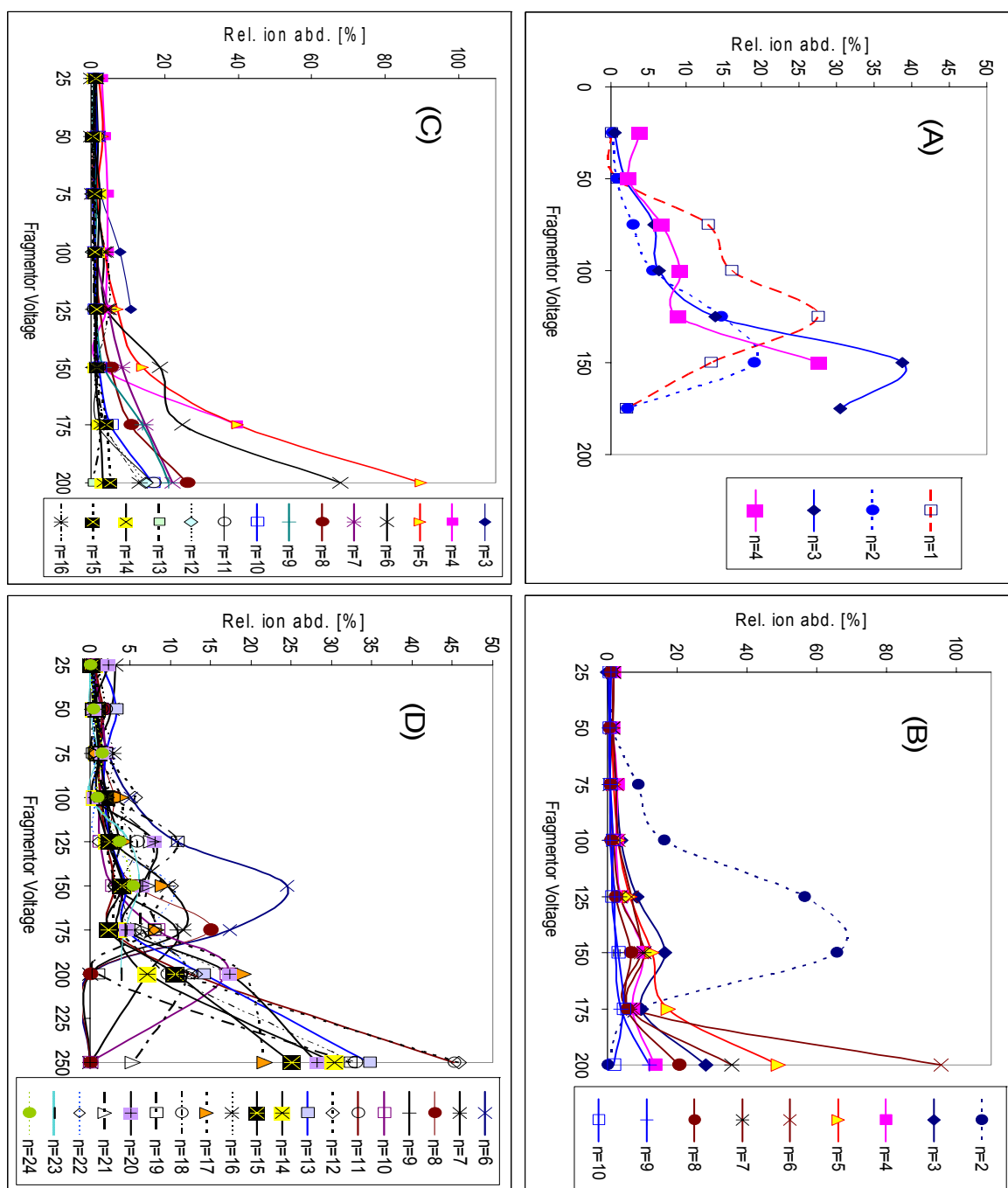


Figure 6.5: Breakdown curves showing the effects of varying fragmentation voltage on the mass spectral fractional abundance of sodium adduct $[M+Na]^+$ formation for individual degree of ethoxylation (n-value) for A) TX-15, B) TX-45, C) TX-100, and D) TX-165.

oligomers showed a significant increase (e.g., 45% abundance) in $[M+Na]^+$ adduct formation at 250 V, which is slightly higher voltage required to form sodium adducts as compared to the other Triton series surfactants. For TX-165, the $n=11$ and $n=12$ oligomers were formed in highest abundance at 250 V.

Formation of the Fragment Ion $[M-C_8H_{17}+2H]^+$

For all surfactants TX-15-165, the fragment ion $[M-C_8H_{17}+2H]^+$ corresponding to the loss of the octyl chain from the aromatic ring was observed at varying fragmentor voltage as shown in Figure 6.6A-D. For TX-15 (Figure 6.6A), fragmentation of octyl chain for $n=1-4$ oligomers occurs at 50 V in low abundance and generally increases to maximum 100% abundance going from 50 V to 125 V. The exception is $n=1$ which only fragments to 20% abundance at 75 V. For TX-15, no significant $[M-C_8H_{17}+2H]^+$ formation was observed at voltage greater than 175 V.

Most of the oligomers of TX-45 shows a typical bell shaped curve for the formation of $[M-C_8H_{17}+2H]^+$ ions. The most striking observation in Figure 6.6B is that the onset for fragmentation depends on the n value of the oligomers. For example, $n=4$ requires ca. 50-75V, $n=5$ requires ca. 75 V, $n=6$ requires ca. 75-100 V, and so on.

A somewhat similar breakdown curve was observed for TX-100 $[M-C_8H_{17}+2H]^+$ ion formation with varying fragmentor voltage which is described in Figure 6.6C. As shown previously for TX-45, the $n=5$ oligomer of TX-100 provided highest abundance at 125 V. In addition, $n=4$ oligomer also provided similar value at the same voltage.

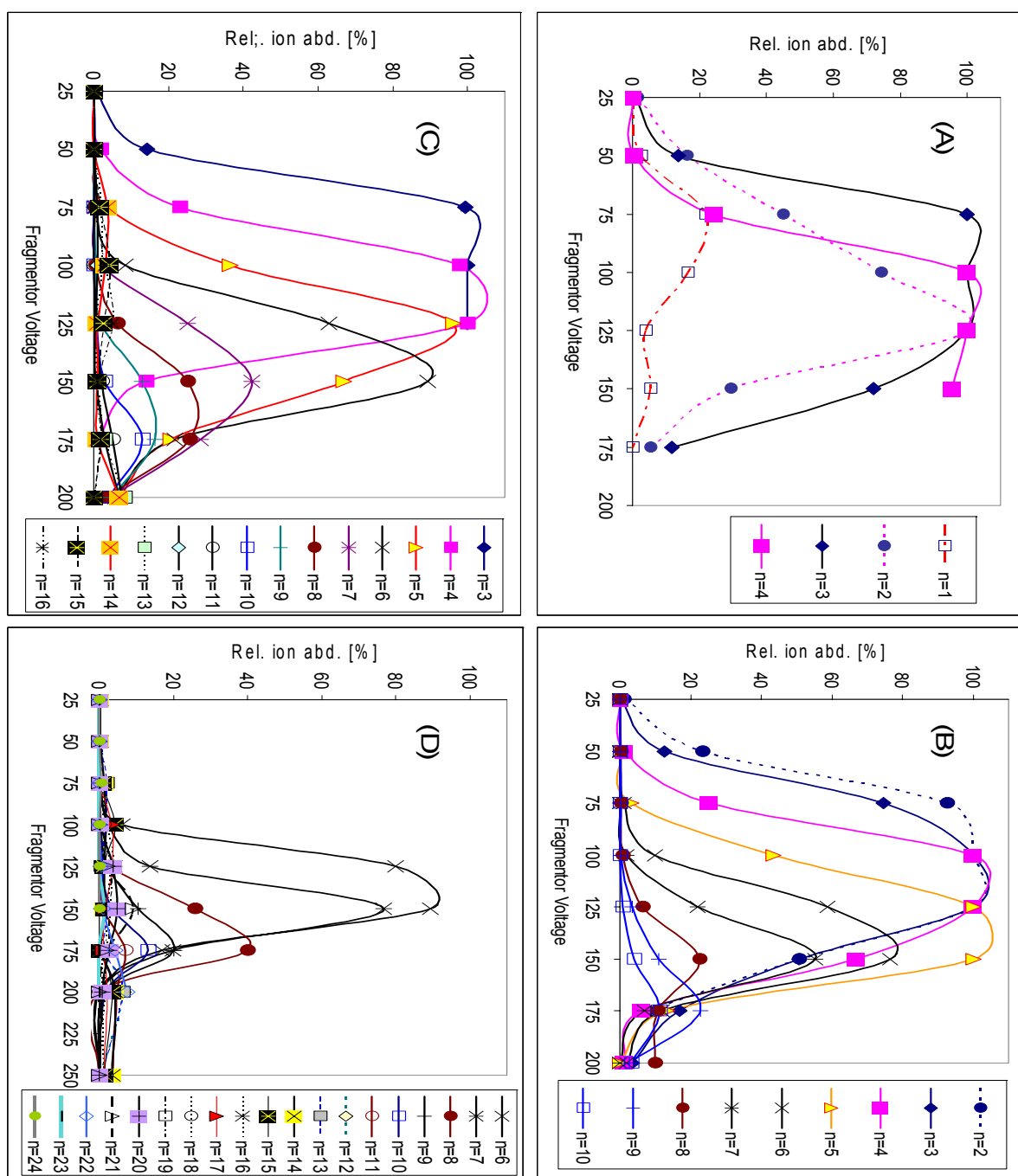


Figure 6.6: Breakdown curves showing the effects of varying fragmentation voltage on the mass spectral fractional abundance of fragment ion $[M-C_8H_{17}+2H]^+$ formation for individual degree of ethoxylation (n-value) for A) TX-15, B) TX-45, C) TX-100, and D) TX-165.

Furthermore, the maximum abundance of the fragment ions $[M-C_8H_{17}+2H]^+$ first increases with the increase in length of the oligomers from 1-5, then an opposite trend of decreasing abundance of the fragment ions were observed for $n=7-10$. Again, the longer chains require incrementally greater voltage to begin fragmenting the octyl chain (e.g., ca. 100 V for $n=7$, ca. 125 V for $n=8-9$, ca. 150 V for $n=10$). The $[M-C_8H_{17}+2H]^+$ ion is only formed in lower abundance $<20\%$ for $n>9$.

Finally, the fragment ion $[M-C_8H_{17}+2H]^+$ for TX-165 at varying fragmentor voltage is shown in Figure 6.6D. Interestingly, only the earlier eluting oligomers ($n=6-8$) were observed to form fragments to any large extent. Otherwise, most of the oligomers for TX-165 only formed $[M-C_8H_{17}+2H]^+$ ions with lower than 20% abundance. Again, similar to other TX-series, no abundant $[M-C_8H_{17}+2H]^+$ ions were observed at greater than 200 V.

Overlaid Fractional Abundance of Ion, Adduct and Fragment Formation at Varying Fragmentor Voltage

Breakdown Curves of $[M+H]^+$, $[M+NH_4]^+$, $[M+Na]^+$ and $[M-C_8H_{17}+2H]^+$ at Varying Fragment Voltage for TX-15

The characterization of the ion and fragment formation at varying fragmentor voltage in the range of 25 V to 175 V for TX-15 is shown in Figure 6.7. At very low fragmentor voltage of 25 V, the only ion formed was the ammonium adduct $[M+NH_4]^+$

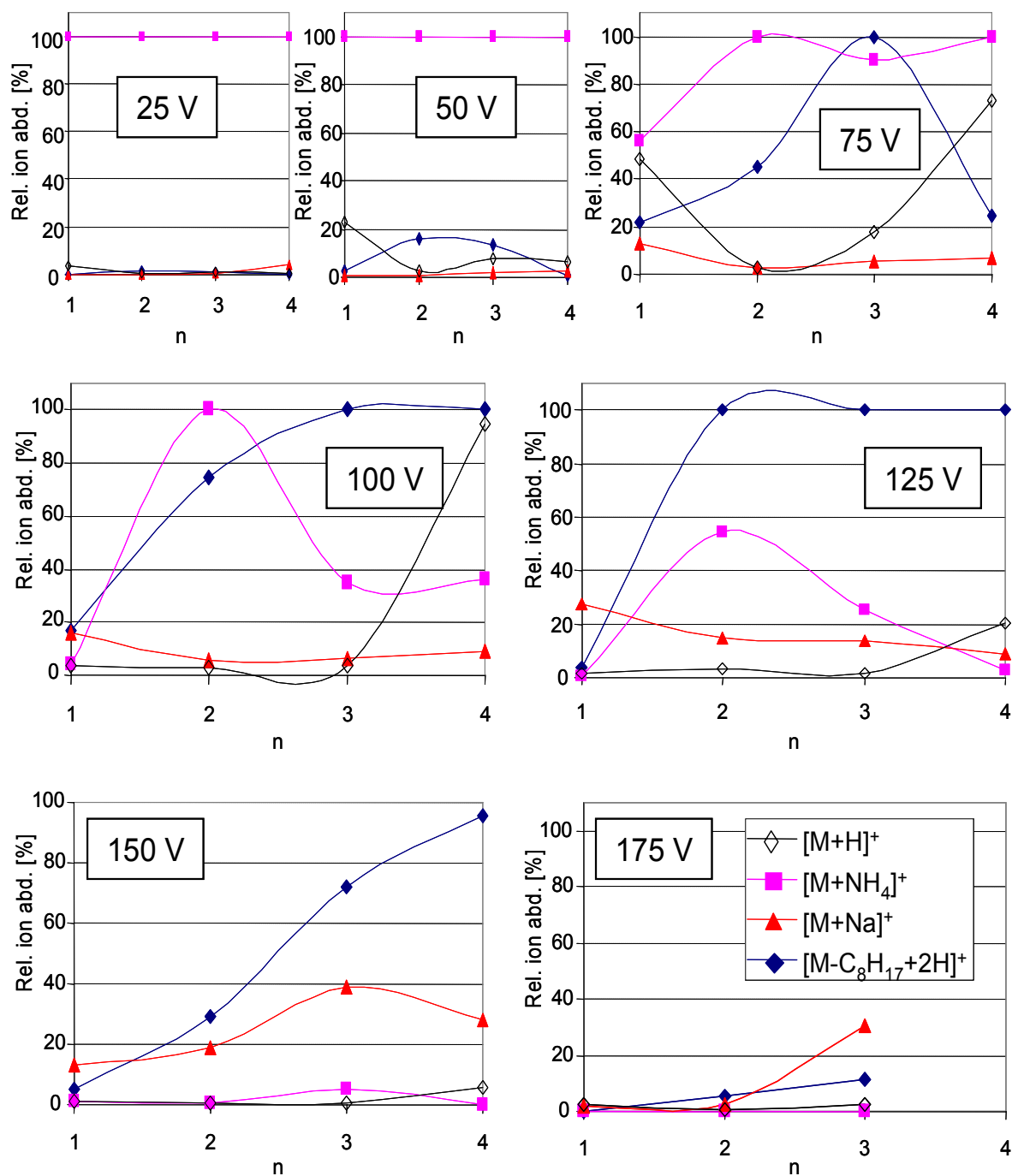


Figure 6.7: Breakdown curves overlaying the $[M+H]^+$, $[M+NH_4]^+$, $[M+Na]^+$ and $[M-C_8H_{17}+2H]^+$ ions at varying fragment voltage and individual n -value for TX-15.

for all oligomers. As the fragmentor voltage is raised going from 50 V to 125 V, the $[M+NH_4]^+$ adducts of $n=1$, $n=3$ and $n=4$ begin to decline and fall off significantly at 100 V. However, $[M+NH_4]^+$ adduct of $n=2$ was still observed with considerable abundance. The fragment ion $[M-C_8H_{17}+2H]^+$ begins to form at 50 V, then generally forms for longer n value as the fragmentor voltage is increased. At 125 V, all $[M+NH_4]^+$ adducts fall below 60% abundance, while the fragment ion $[M-C_8H_{17}+2H]^+$ increases in formation to 100% abundance for $n=2-4$. The protonated molecular ion $[M+H]^+$ was formed in high abundance for $n=1$ and $n=4$ at 75 V, and only for $n=4$ at 100 V, but then falls to less than 20% abundance at higher voltage = 125 V.

The sodium adducts $[M+Na]^+$ were generally formed in low abundance (e.g., 20%) in the range of 25 V to 125 V, although the $n=1$ oligomer was observed to form with ~30% abundance at 125 V. Upon increasing fragmentor voltage from 125 V to 150 V, the fragment ion $[M-C_8H_{17}+2H]^+$ begins to decline for shorter chain oligomers (e.g., $n=2-3$), while the longest chain $n=4$ was still formed in high abundance. The sodium adducts $[M+Na]^+$ were formed in overall highest abundance up to 40% for $n=3$ at 150 V, which is higher than as compared to 125 V. The $[M+H]^+$ ion and the $[M+NH_4]^+$ were not observed at 150 V. Finally, at the highest fragment voltage of 175 V, no mentionable ion formation was observed with the exception of $n=3$ $[M+Na]^+$ adduct.

Breakdown Curves of $[M+H]^+$, $[M+NH_4]^+$, $[M+Na]^+$ and $[M-C_8H_{17}+2H]^+$ at Varying Fragment Voltage for TX-45

The ion and fragment formation at varying fragmentor voltage in the range of 25 V to 175 V for TX-45 ($n=2-10$) is shown in Figure 6.8. Similar to TX-15 in Figure 6.7, at lower fragmentor voltage of 25 V, only the $[M+NH_4]^+$ adducts were observed. Increasing the voltage from 25 V to 50 V promotes fragmentation and formation of $[M-C_8H_{17}+2H]^+$ ions for short oligomers $n=2-3$ up to 20% abundance, along with minor formation of the protonated molecular ion $[M+H]^+$ in the range of $n=3-4$. When the fragmentor voltage is raised to 75 V, an increase in the fragmentation of short oligomers occurs as shown by 95% and 75% abundance of the $[M-C_8H_{17}+2H]^+$ ions for $n=2$ and 3, respectively. At the same 75 V, the protonated molecular ion $[M+H]^+$ forms in high abundance for $n=4$ oligomer, although the abundance of the other oligomers was less than 25%. The ammonium adducts were still of maximum abundance, except that the $n=2$ oligomer begins to decline slightly to 95% from 100% abundance. Upon further increase in fragmentor voltage from 75 V to 100 V, the voltage is too large for the $[M+NH_4]^+$ adducts of short oligomers to withstand. Hence, a drop in abundance for $n=2-4$ to less than 60% is observed. At the same time, the increased fragmentation of the octyl chain of $n=2-4$ oligomers occurs as can be seen from 100% formation of $[M-C_8H_{17}+2H]^+$ ions at 100 V. For the longer oligomers $n=5-10$, the $[M+NH_4]^+$ adducts were stable and only $n=5$ oligomer fragmented to form $[M-C_8H_{17}+2H]^+$ ion with increasing abundance from 25% to ~40% upon increasing the voltage from 75 V to 100 V. In addition, note that at 100 V, the $[M+H]^+$ ion exhibited a shift toward longer n value for ion formation as can be seen

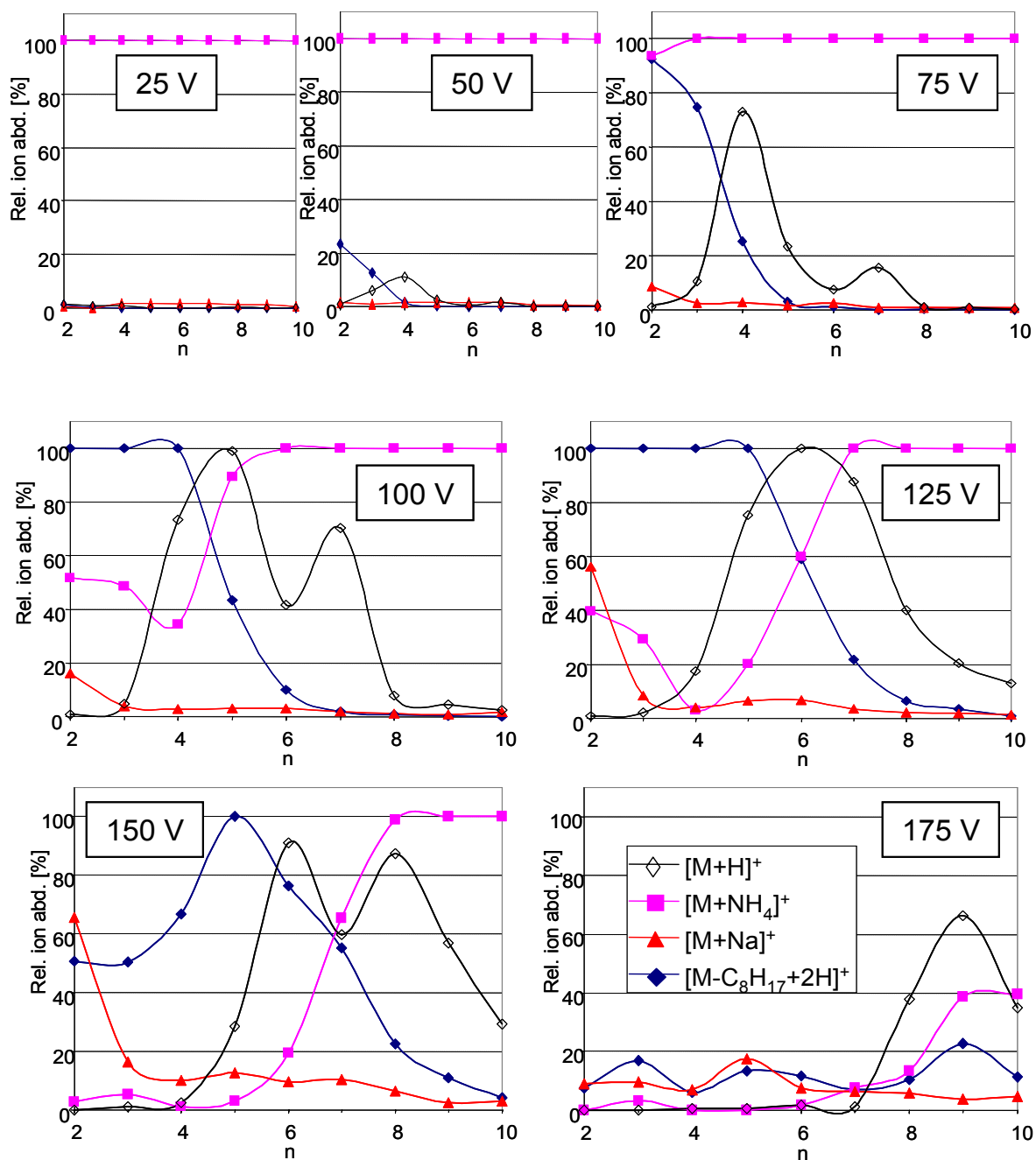


Figure 6.8: Breakdown curves overlaying the $[M+H]^+$, $[M+NH_4]^+$, $[M+Na]^+$ and $[M-C_8H_{17}+2H]^+$ ions at varying fragment voltage and individual n -value for TX-45.

by comparison to 75 V. While the $n=4$ oligomer $[M+H]^+$ is still formed at $\sim 75\%$, there is a noticeable increase in the formation of $n=5$ $[M+H]^+$ ion which shows 100% formation. The longer chain $n=6-8$ oligomers also formed molecular ions in much higher abundance at 100 V as compared to 75 V.

In general, the $[M+Na]^+$ adducts did not form to any large extent in the range of 25 V to 100 V, although the short chain $n=2$ was observed up to 20% at 100 V. When the fragmentor voltage is raised even higher to 125 V, fragmentation of short to mid chainlength oligomers up to $n=5$ is observed as shown by $[M-C_8H_{17}+2H]^+$ formation with 100% abundance. Meanwhile, the ammonium adduct formation decreases for short chain oligomers, and most interestingly the $n=4$ oligomer shows less $[M+NH_4]^+$ formation as compared to $n=2-3$ and $n=5-10$. Only the longer chain oligomers (e.g., $n=7-10$) $[M+NH_4]^+$ adducts were observed to withstand fragmentor voltage applied at 125 V. For the molecular ion $[M+H]^+$ formation at 125 V, the oligomer with highest abundance exhibited a shift from $n=5$ to $n=6$ which is a consistent trend shown before going from shorter to longer chain oligomers. Furthermore, no drop in $[M+H]^+$ formation was observed for $n=6$ as shown before at 75 V and 100 V. Lastly, the $[M+Na]^+$ adducts at 125 V increased to 60% for $n=2$, and very minor formation less than 10% abundance was seen for longer chainlength in the range of $n=3-7$.

Upon increasing the fragmentor voltage from 125 V to 150 V, the $[M+NH_4]^+$ ions for short to mid-chain oligomers in the range of $n=2-5$ are not formed which is consistent with the trend described above. However, at this higher voltage (150 V), even the fragment ions $[M-C_8H_{17}+2H]^+$ fall off in abundance for shorter chains $n=2-4$ (e.g., 50-

70% abundance), and only the $n=5$ oligomer formed at maximum 100% abundance then decline for $n>5$. For the protonated molecular $[M+H]^+$ ion at 150 V, the highest abundance was still observed for $n=6$, although a drop of 10% from 100-90% was observed. The $[M+H]^+$ ions for longer chain oligomers (e.g., $n=8-10$) were formed in higher abundance, however, no distinct shift in n value for highest abundance was observed as seen at lower voltages. The trend in sodium adduct $[M+Na]^+$ formation was similar to 125 V except an increase of approximately 5% abundance was observed for all oligomers. Finally, at the highest fragmentor voltage 175 V, only $[M+H]^+$ ions and $[M+NH_4]^+$ adducts for the longest chain oligomers ($n=8-10$) was observed with significant abundances. An additional correlation of the n value at which the ammonium adduct $[M+NH_4]^+$ trendline crosses the fragmentation $[M-C_8H_{17}+2H]^+$ trendline can be observed. For example, at 100 V the crossover n value is located at $n=5$, at 125 V the crossover point is at $n=6$, at 150 V $n=7$, at 175 V $n=8$, and at 200 V $n=9$.

Breakdown Curves of $[M+H]^+$, $[M+NH_4]^+$, $[M+Na]^+$ and $[M-C_8H_{17}+2H]^+$ at Varying Fragment Voltage for TX-100

The breakdown plots of ion and adduct formation as a function of varying fragmentor voltage for TX-100 nonionic surfactant are shown in Figure 6.9. A range of 25 V to 200 V was studied for TX-100 oligomeric chainlength in the range of $n=3$ to

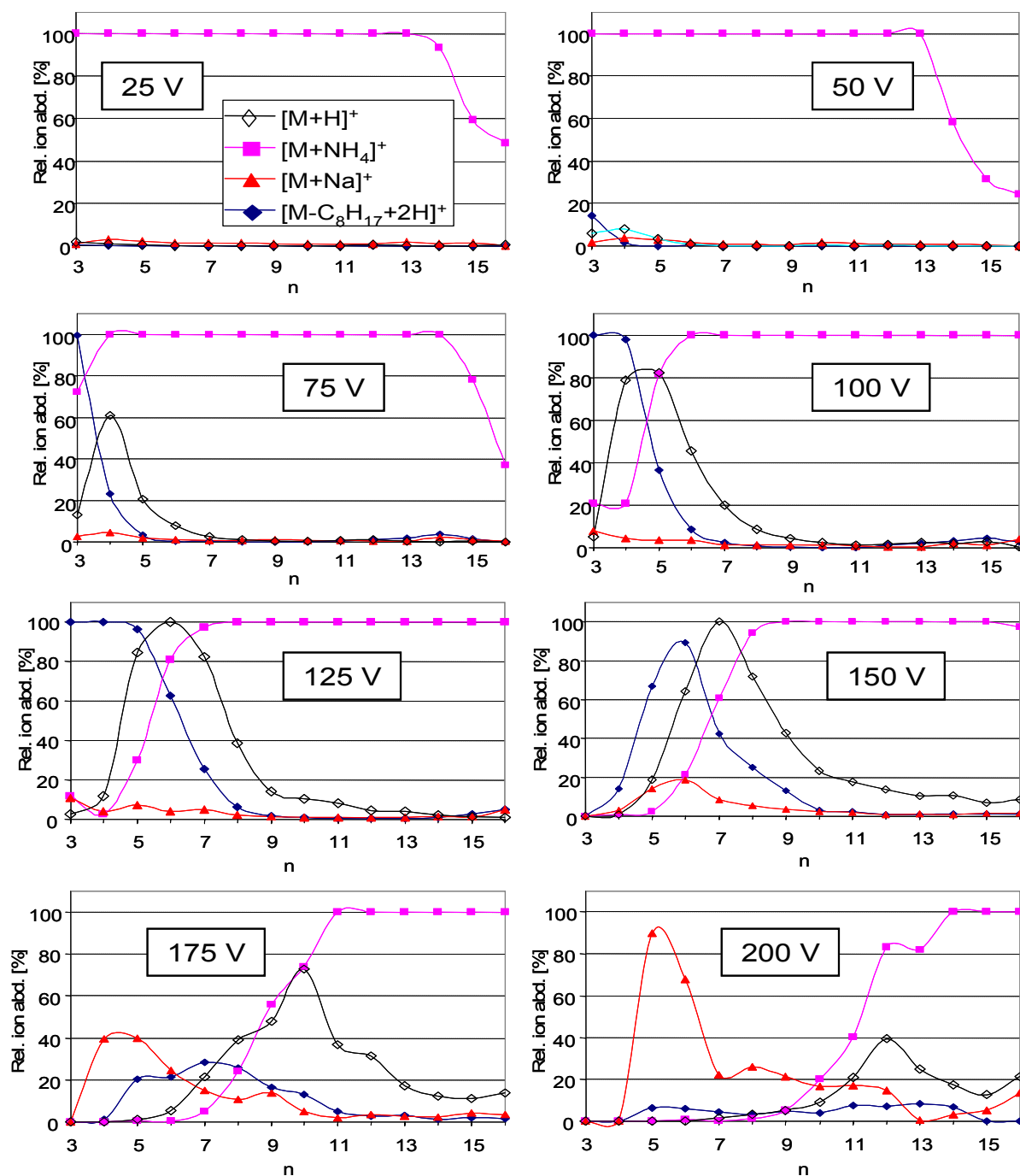


Figure 6.9: Breakdown curves overlaying the $[M+H]^+$, $[M+NH_4]^+$, $[M+Na]^+$ and $[M-C_8H_{17}+2H]^+$ ions at varying fragment voltage and individual n-value for TX-100.

$n=16$. As discussed earlier for TX-15 and TX-45, only the ammonium adducts are formed at low fragmentor voltage of 25 V. However, for TX-100 which contains more ethoxylate groups than TX-15 and TX-45, the longer oligomers (e.g., $n=13-16$) are formed in lower abundance ($\sim 40\%$ for $n=16$) than the shorter ones (e.g., $n=3-13$). When the voltage is increased from 25 V to 50 V the fragment ion $[M-C_8H_{17}+2H]^+$ and protonated molecular ion $[M+H]^+$ are formed in very low abundance (e.g., 10-15%) for short chain $n=3-4$. In addition, the ammonium adducts were not formed for long chain oligomers $n=14-16$. At 75 V, the pattern appears very similar to that obtained for TX-45 at 75 V. This voltage supplies high enough energy to begin breaking the octyl chain of $n=3-4$ oligomers to form fragment ions $[M-C_8H_{17}+2H]^+$ at approximately 100% and 25% abundance, respectively. The formation of $[M+H]^+$ ion for $n=4$ oligomers was observed up to 60% abundance and $n=5$ up to 20%, as well a decline in ammonium adduct formation for $n=3$ oligomer down to 80% from 100%. These patterns become more pronounced upon increasing the voltage to 100 V.

As the fragmentor voltage is increased from 100 V to 125 V, the most abundant $[M+H]^+$ ion shifts again to longer oligomeric chainlength going from $n=5$ (100 V) to $n=6$ (125 V). In addition, the $n=3-4$ shorter oligomers decrease in abundance compared to lower fragmentor voltage. The abundance of $[M+H]^+$ for mid chainlength oligomers with $n=7-9$ also increase formation at 125 V as compared to 100 V. The ammonium adducts $[M+NH_4]^+$ for oligomers $n=3-6$ start to lose abundance while at the same time these oligomers also form $[M-C_8H_{17}+2H]^+$ ions. No mentionable sodium adduct $[M+Na]^+$ formation was observed at 125 V. At larger fragmentor voltage of 150 V, the ammonium

adducts $[M+NH_4]^+$ continue to shift toward longer n -value. For example $n \geq 9$ oligomers were formed at 100% abundance at 150 V whereas at 125 V $n \geq 8$ were formed at 100% abundance. The fragment ions $[M-C_8H_{17}+2H]^+$ for shorter chain $n=3-6$ that formed in high abundance at 125 V were found to decline at 150 V. Most interestingly, the shift for $[M+H]^+$ was observed going from maximum abundance for $n=6$ at 125 V to $n=7$ at 150 V. Lastly, the sodium adducts $[M+Na]^+$ of some of the oligomers (e.g., $n=5$ and 6) increase in abundance but only as high as 20%. Further increase in fragmentor voltage from 150 V to 175 V showed that only the $[M+NH_4]^+$ for longer chain $n=11-16$ and $[M+H]^+$ for $n=7-16$ were able to withstand this higher voltage. The highest abundance of the $[M+H]^+$ ion at 175 V was formed by the $n=10$ oligomer, which is an increase of 3 ethoxylate groups (i.e., n values) as compared to 150 V where the highest $[M+H]^+$ ion was formed at $n=7$ oligomer. This is a different trend compared to lower voltage where the shift in n values was only one ethoxylate group. Note that at ≥ 175 V, the fragment ions $[M-C_8H_{17}+2H]^+$ were not formed greater than 30% abundance, and the $[M+Na]^+$ showed significant increase in formation for shorter oligomers ($n=4-5$). Moreover, no ion or adduct was observed for the shortest oligomer $n=3$ at 175 V.

At the highest fragmentor voltage of 200 V, the ammonium adducts $[M+NH_4]^+$ continue to drop in abundance for short to mid-length oligomers $n=3-13$, and only the longest chains $n=14-16$ were observed at 100% abundance. The $[M+H]^+$ dropped in abundance from 75% at 175 V to 40% at 200 V. In addition, a shift of two n values was observed for the highest $[M+H]^+$ ion going from $n=10$ at 175 V to $n=12$ at 200 V. Similar to 175 V, no ion or adduct formation was observed for $n=3$ oligomer at 200 V. Finally,

the n value at which the ions overlaps (crossover) for the $[M-C_8H_{17}+2H]^+$ and the $[M+NH_4]^+$ is described. For example, at 75 V the crossover is located at $n=3$, at 100 V $n=5$, 125 V $n=6$, 150 V $n=7$, 175 V $n=8$, and for 200 V $n=9$ which is the same pattern as shown previously for TX-45.

Breakdown Curves of $[M+H]^+$, $[M+NH_4]^+$, $[M+Na]^+$ and $[M-C_8H_{17}+2H]^+$ at Varying Fragment Voltage for TX-165

The trend in ion and adduct formation as a function of varying fragmentor voltage for the longest chain nonionic surfactant TX-165 is shown in Figure 6.10. A range of 25-250 V for $n=6-24$ was investigated. Interestingly, some of the trends illustrated for the previous TX-45 and TX-100 surfactants are exhibited for TX-165. For example, at low fragmentor voltage (e.g., 25 V) the ammonium adducts $[M+NH_4]^+$ are formed in very high abundance (100%) for the short to midlength oligomers (e.g., $n=5-12$). But as was shown previously for TX-100 at 25 V (Figure 6.9), this lower voltage is not capable of providing enough energy to generate long chain $n>13$ adducts $[M+NH_4]^+$. Hence the abundance of these $n>13$ adducts approaches zero at 25 V. For the other ions (e.g., $[M+H]^+$, $[M+Na]^+$ and $[M-C_8H_{17}+2H]^+$), no significant formation was observed until 100 V. At this voltage, the $[M+H]^+$ began to form (i.e., 30% abundance) but only for shorter oligomers $n=6$ and approximately 10% abundance of sodium adducts and fragment ions.

Upon further increase in fragmentor voltage from 100 V to 125 V, the formation of $[M+NH_4]^+$ with 100% abundance continue to extend to larger n -values (e.g., $n=16$ to $n=19$). However, a slight decrease in $[M+NH_4]^+$ abundance for short chain length $n=6$

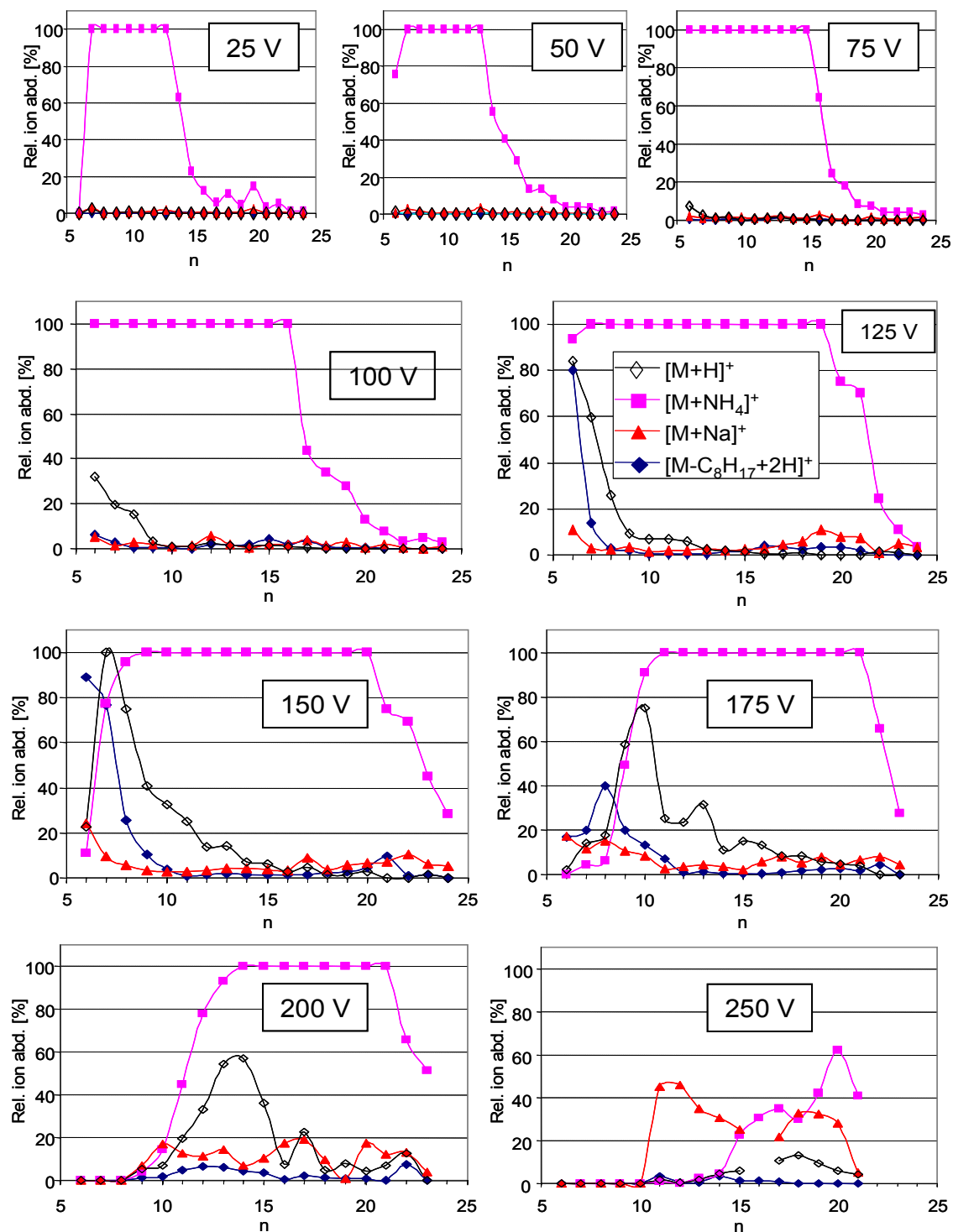


Figure 6.10: Breakdown curves overlaying the $[M+H]^+$, $[M+NH_4]^+$, $[M+Na]^+$ and $[M-C_8H_{17}+2H]^+$ ions at varying fragment voltage and individual n -value for TX-165.

was observed over the same range. Furthermore, at 125 V, the protonated molecular ion $[M+H]^+$ and the fragment ion $[M-C_8H_{17}+2H]^+$, increased significantly for short oligomers $n=6-7$, as well as the sodium adduct for $n=6$ which increased also about 10% abundance. When the fragmentor voltage is raised from 125 V to 150 V, the ammonium adducts $[M+NH_4]^+$ continue to decline for short oligomers $n=6-8$, while at the same time the longer chain oligomers $n=20$ are generated at 100% abundance. The $[M+H]^+$ begins to shift its maximum abundance from $n=6$ at 125 V to $n=7$ at 150 V, and the shorter chain oligomer $n=6$ declined in abundance while the abundance of longer chains $n=7-15$ continue to increase. In addition, the abundance of $[M-C_8H_{17}+2H]^+$ and the $[M+Na]^+$ continue to improve formation for shorter chainlength $n=6-9$ oligomers at 150 V.

Raising the fragmentor voltage from 150 V to 175 V continues to shift ammonium adduct formation from $n=20$ to $n=21$, while the abundance of short to midlength oligomers decrease. The protonated molecular ion shifts its maximum abundance from $n=7$ at 150 V to $n=10$ at 175 V, and in general the oligomers closest to the highest abundant oligomer also increase in abundance. However, the $[M+H]^+$ of shorter chainlength oligomers ($n=6-8$) were observed to decrease. The fragment ions $[M-C_8H_{17}+2H]^+$ were no longer able to withstand higher fragmentor voltage, indicated by much lower abundance down to 40% at 175 V from 90% at 150 V. Sodium adducts $[M+Na]^+$ continued to slightly increase for short chain oligomers $n=6-10$.

At 200 V, the abundance of ammonium adducts $[M+NH_4]^+$ decrease for $n<14$, and increase formation of $n=21$. The $[M+H]^+$ shifts its maximum abundance to $n=14$ although the overall abundance fell to only 60%. The $[M-C_8H_{17}+2H]^+$ was barely

observed as the sodium adducts continue to gradually increase. At the highest voltage of 250 V, only the higher oligomers of TX-165 form $[M+Na]^+$ and $[M+NH_4]^+$ adducts in significant abundance compared to the adducts of short chain oligomers which were not readily formed at this high voltage. Finally, the crossover point for $[M+NH_4]^+$ and $[M-C_8H_{17}+2H]^+$ ions was only observed at 150 V and 175 V for $n=7$ and 9, respectively.

CONCLUSIONS

Overall, upon variation in fragmentor voltage, the mass spectra for TX-series nonionic surfactants was comprised of the protonated molecular ion, ammonium and sodium adducts, and a fragment ion corresponding to the loss of the octyl chain. For one representative surfactant TX-45, the individual mass spectra showed that additional m/z corresponding to fragments due to loss of ethoxylate groups, loss of both octyl chain and ethoxylate groups, ethoxylate groups, and small fragments ions were also observed. This was followed by the breakdown plot analysis of the four major ions.

For the protonated molecular ion $[M+H]^+$, a bell shaped curve on the breakdown plot was observed for all surfactants. The abundances of the $[M+H]^+$ ions of long chain oligomers grow while the abundances of $[M+H]^+$ ions of shorter chain oligomers decrease with fragmentor voltage increasing up to 175 V or 200 V when protonated molecular ions of short chain oligomers vanishes from the spectra. Although the shortest chain TX-15 surfactant demonstrated irregular $[M+H]^+$ ion formation (i.e., $n=4$ most abundant), the other surfactants showed highest abundance of $[M+H]^+$ at varying voltages. For example, TX-45 showed highest abundance of $[M+H]^+$ ion for $n=5$ and $n=6$ at 100 V and 125 V, respectively. For TX-100 $n=6$ $[M+H]^+$ ion was highest at 125 V along with $n=7$ at 150 V whereas for TX-165 $n=7$ was most abundant at 150 V.

For ammonium adducts $[M+NH_4]^+$, a backwards “S” shaped curve was observed in most cases on the breakdown plots. For the shorter chainlength TX-15 and TX-45, the shorter n values formed $[M+NH_4]^+$ ions in maximum abundance at lower fragmentor voltages in the range 25-50 V. For the same two TX-series surfactants, as the voltage was

raised, the ammonium adducts formation declined then fell to zero percent at high voltage. On the other hand, the longer chain surfactants TX-100 and TX-165, the shorter n -values oligomers were also fully adducted or formed at low fragmentor voltage. However, at low fragmentor voltage the longer n value oligomers were formed $[M+NH_4]^+$ in lower abundance and also exhibited an interesting U-shaped ionization pattern on the breakdown plots. At higher fragmentor voltage, the longer n values were fully ammonium adducted in the range of 150-175 but then the abundances fell off in formation in the range of 200-250 V.

The formation of sodium adducts $[M+Na]^+$ were observed for all surfactants at higher fragmentation voltage only. The most abundant adducts were observed for TX-15 $n=3$ at 150 V, for TX-45 $n=6$ at 200 V, for TX-100 $n=5$ at 200 V, and for TX-165 $n=12$ at 250 V.

Similar to the protonated molecular ions, the formation of fragmentation ions $[M-C_8H_{17}+2H]^+$, also showed a bell shaped curve was observed on the breakdown plots. As the fragmentor voltage was sequentially raised, the fragmentation of longer n value oligomers was observed. For TX-15, the range of $n=2-4$ showed significant fragmentation in the range of 75-125 V. For TX-45 and TX-100, a large extent of fragmentation was observed for $n=2-5$ oligomers in the range of 75-150 V for TX-45, and in the range of 75-125 V for TX-100. Finally for TX-165, only a relatively small amount of fragmentation was observed for $n=6-7$ oligomers in the range of 125 to 150 V.

When the four ions were overlaid as a function of varying fragmentor voltage for individual n -values, the shortest surfactant TX-15 demonstrated significant formation of

ammonium adducts and $[M-C_8H_{17}+2H]^+$ in the range of 25-150 V whereas sodium adducts forms in some abundance only at 125 V or 150 V. For TX-45 and TX-100 surfactants, two trends were considered to be most interesting. First, the crossover pattern for the $[M+NH_4]^+$ and $[M-C_8H_{17}+2H]^+$ ions was found to shift to increasing n values upon raising the fragmentor voltage. This was most pronounced for TX-45 and TX-100 surfactants. For example, in the case of TX-100, the crossover point of $[M-C_8H_{17}+2H]^+$ and $[M+NH_4]^+$ goes from $n=5$ at 100 V, to $n=6$ at 125 V, $n=7$ at 150 V, $n=8$ at 175 V and finally $n=9$ at 200 V. Second, the maximum abundance of the protonated molecular ions behaved in a similar fashion showing different maximum abundance at different fragmentor voltages and shifting to higher n values as the fragmentor voltage was increased.

In summary, this work has demonstrated the ability of IS-CID for control and manipulation of the mass spectral pattern of TX-series nonionic surfactants. This can be important for future work utilizing more sensitive single ion monitoring where the selection of the appropriate and highest abundant ions at respective fragmentor voltages utilizing is required.

ACKNOWLEDGMENTS

This work was supported by a grant from the National Institute of Health (Grant No. 62314-02) and funding from Solvay Pharmaceuticals (Marietta, GA, USA).

References:

- (1) Knepper, T.P., Barceló, B., de Voogt, P. (Eds.), Knepper, T.P. and Berna, J.L. in
Analysis and Fate of Surfactants in the Aquatic Environment, Elsevier, Amsterdam
2003, Ch. 2, p.128.
- (2) Hunt, D.F., Shabanowitz, J., Harvey, T.M., Coates, M. *Anal. Chem.* **1985**, 57, 525.
- (3) Johnson, J., Yost, R. *Anal. Chem.* **1985**, 57, 758A.
- (4) Ogura, I., DuVal, D.L., Kawakami, S., Miyajima, K. *J. Am. Oil Chem. Soc.* **1996**,
73, 137.
- (5) Petrovic, M., Barceló, D. *J. Mass Spectrom.* **2001**, 36, 1173.
- (6) Ding, W.H., Wu, C.Y. *Rapid Commun. Mass Spectrom.* **2001**, 15, 2193.
- (7) Vanhoenacker, G., Sandra, P. *J. Chromatogr. A* **2005**, 1082, 193.
- (8) Sparham, C.J., Bromilow, I.D., Dean, J.R. *J. Chromatogr. A* **2005**, 1062: 39.
- (9) Jonkers, N., Govers, H., de Voogt, P. *Anal. Chim. Acta* **2005**, 531, 217.
- (10) Cantero, M., Rubio, S., Pérez-Bendito, D. *J. Chromatogr. A* **2005**, 1067, 161.
- (11) Cantero, M., Rubio, S., Pérez-Bendito, D. *J. Chromatogr. A* 2004; **1046**: 147.
- (12) Jahnke, A., Gandrass, J., Ruck, W. *J. Chromatogr. A* **2004**, 1035, 115.
- (13) Shao, B., Hu, J., Yang, M. *J. Chromatogr. A* **2002**, 950, 167.
- (14) Levine, L.H., Garland, J.L., Johnson, J.V. *Anal. Chem.* **2002**, 74, 2064.
- (15) Espejo, R., Valter, K., Simona, M., Janin, Y., Arrizabalaga, P. *J. Chromatogr. A*
2002, 976, 335.
- (16) Krogh, K.A., Verjup, K.V., Mogensen, B.B., Halling-Sørensen, B. *J. Chromatogr.*
A **2002**, 957, 45.

- (17) Petrovic, M., Diez, A., Ventura, F., Barceló, D. *Anal. Chem.* **2001**, 73, 5886.
- (18) Petrovic, M., Barceló, D. *J. Mass Spectrom.* **2001**, 36, 1173.
- (19) Ferguson, P.L., Iden, C.R., Brownawell, B.J. *J. Chromatogr. A* **2001**, 938, 79.
- (20) Castillo, M., Riu, J., Ventura, F., Boleda, R., Scheduling, R., Schröder, H.Fr,
Nistor, C., Émneus, J., Eichorn, P., Knepper, Th.P., Jonkers, C.C.A., de Voogt, P.,
González-Mazo, E., León, V.M., Barceló, D. *J. Chromatogr. A* **2000**, 889, 195.
- (21) Shang, D.Y., Ikonomou, M.G., Macdonald, R.W. *J. Chromatogr. A* **1999**, 849,
467.
- (22) Kamiyusuki, T., Monde, T., Nemoto, F., Konakahara, T., Takahashi, Y. *J.*
Chromatogr. A **1999**, 852, 475.
- (23) Scullion, S.D., Clench, M.R., Cooke, M., Ashcroft, A.E. *J. Chromatogr. A*
1996, 733, 207.
- (24) Pashynska, V.A., Kosevich, M.V., Van den Heuvel, H., Claeys, M. *Rapid Commun.*
Mass Spectrom. **2006**, 20, 755.
- (25) Kubwabo, C., Vais, N., Benoit, F.M. *Rapid Commun. Mass Spectrom.* **2005**, 19,
597.
- (26) Harrison, A.G., *Rapid Commun. Mass Spectrom.* **1999**, 13, 1663.
- (27) Yan, Z., Caldwell, G.W., Jones, W.J., Masucci, J.A. *Rapid Commun. Mass*
Spectrom. **2003**, 17, 1433.
- (28) Tian, Q., Christine, J.G., Schwartz, J. j. *Mass Spectrom.* **2003**, 38, 990.
- (29) Makowiecki, J., Tolonen, A., Uusitalo, J., Jalonen, J. *Rapid Commun. Mass*
Spectrom. **2001**, 15, 1506.

(30) Norton, D., Zheng, J., Danielson, N.D., Shamsi, S.A. *Anal. Chem.* **2005**, 77, 6874.

(31) Norton, D., Shamsi, S.A. *Anal. Chem.* submitted May **2007**.

Chapter 7:
Packed Column Capillary Electrochromatography (CEC)
and CEC-MS Using a Lithocholic Acid Stationary Phase

Abstract

The preparation and characterization of a novel lithocholic acid (LCA) based liquid crystalline stationary phase (LCP-SP) suitable for application in packed column capillary electrochromatography (CEC) is described. For the attachment of LCA to bare silica, the LCA was first converted to chloroformate (LCA-CF) functionality followed by reaction of LCA-CF with the terminal amino group of modified aminopropyl silica prepared in our laboratory. The extent of these reactions were assessed using ^1H -NMR, ^{13}C -NMR and elemental analysis. This is followed by application of the new LCA stationary phase for separation of β -blockers, phenylethylamines (PEAs), polyaromatic hydrocarbons (PAHs) and polychlorinated biphenyls (PCBs). The most suitable mobile phase operating conditions were determined experimentally to be lower pH in the range of pH=3.0-4.5 along with higher organic (acetonitrile) content 85% (v/v). Utilizing these conditions, a comparison of the chromatographic ability of the aminopropyl silica intermediate to the LCA bonded phase was conducted. The results showed that improved selectivity for all test analytes was achieved using the LCA bonded phase. For example, the CEC-mass spectrometry (MS) of β -blockers demonstrated that the LCA bonded phase provides separation of 6 out of 7 β -blockers, whereas the aminopropyl phase provides 4 peaks of several co-eluting β -blockers. For the CEC-MS analysis of PEAs, the LCA bonded phase showed improved resolution and different selectivity as compared to the aminopropyl phase. An evaluation of the trend in retention for PEAs on both phases suggested that the PEAs were retained based on varying degree of hydroxyl substitution around the aromatic ring. In addition, the several PEAs were found to fragment in the electrospray

(ESI) either by loss of an alkyl group and/or by loss of hydroxyl group to form H₂O. Finally, the new LCA bonded phase was also found capable of significantly higher separation selectivity for PAHs and PCBs as compared to the aminopropyl silica.

Introduction

Materials that display structures which are intermediate between the three dimensional ordered crystalline state and the disordered or isotropic liquid state are known as liquid crystals. Liquid crystalline stationary phases (LC-SP) are widely used as a separation material in gas chromatography (GC) and have been around for over 40 years.¹ In addition, LC-SP have shown applications in supercritical fluid chromatography (SFC)^{2,3} and high performance liquid chromatography (HPLC).⁴⁻¹⁰ However, in comparison to GC, the use of LC-SP in HPLC and SFC is less prevalent. The LC-SPs in GC are often physically coated on the inner wall of the capillary, whereas in HPLC the LCP are chemically bonded in order to withstand the high pressure and increased solubilizing capability of the mobile phase. In addition, the use of much lower temperature in HPLC compared to GC may provide different orientation and chemical property of the LCP which results in different chromatographic selectivity. An advantage of LC-SP over traditional reversed phase (e.g., C₁₈ bonded phase) in HPLC is that LC-SP offer separations based upon unique selectivity. This is due in part to interesting morphological properties resulting from the rod-like shape and ordered arrangement of the LC-SP molecule.¹¹ Currently, some applications of chemically bonded LC-SP in HPLC include polyaromatic hydrocarbons (PAH),^{4,6,7,9} fullerenes,⁵ dipeptides,⁴ carotenoids⁵ and steroids.⁹ Therefore, the exploration of LCP stationary phase for use in LC and similar chromatographic techniques is growing in popularity.

A complimentary technique to HPLC that combines the use of LC retention along with capillary electrophoresis (CE) separations based upon mass to charge ratio is capillary electrochromatography (CEC). One of the advantages of CEC is the use of small internal diameter fused silica capillary (i.e., 75 μm) which permits separations under a wide variety of operating modes. For example, the capillary can be either packed with stationary phase, chemically modified in situ, or simply coated to provide several approaches to challenging analytical separations. Logically, the transition of LC-SP from LC and GC to its use in CEC is an exciting new area that until recently has not received much attention. To date, the most popular approach for application of LC-SP in CEC entails etching the inner wall of the capillary followed by chemical modification of the open tubular capillary surface (OTCEC).¹² Moreover, the use of LC-SP using cholesterol as the stationary phase in OTCEC has been applied for separations of peptides, mixtures of proteins, pyrimidine/purine bases, metabolic compounds including serotonin, and other basic molecules.¹³⁻¹⁷ Although cholesterol has been applied in OTCEC, currently there are no reports for the use of this biological ligand in packed column CEC. This is contrary to HPLC where several reports of cholesterol bonded to aminopropyl silica are described.¹⁸⁻²⁰

In this work, we describe the synthesis of a charged LCP which is a cholesterol based lithocholic acid (LCA) attached to aminopropyl silica for its possible use as a separation media in packed column CEC. A characterization of the reactions using several physiochemical techniques including nuclear magnetic resonance spectroscopy, and elemental analysis is presented. This is followed by comparison to non liquid

crystal phase (i.e., aminopropyl silica) for separation of β -blockers, phenylethylamines (PEAs), PAHs and polychlorinated biphenyls (PCBs). To our knowledge, this is the first report of LCP applied to packed column CEC and CEC coupled to mass spectrometry (MS).

EXPERIMENTAL SECTION

Reagents and Chemicals. The 300 Å, 5 μ m particle size Kromasil silica was obtained from Akzo Nobel (Illinois, USA). 3-aminopropyltriethoxysilane (99%), toluene (anhydrous, 99%), pyridine (99.8%), lithocholic acid (99%), morpholine (99%), sodium sulfate (99%) were purchased from Sigma (St. Louis, MO, USA). Triphosgene was obtained from Aldrich (Milwaukee, WI, USA). The HPLC grade solvents such as dichloromethane (CH_2Cl_2), methanol (MeOH), and acetonitrile (ACN) were purchased from Burdick and Jackson (Muskegon, MI, USA). The β -blockers (Figure 7.1) atenolol, metoprolol, pindolol, oxprenolol, alprenolol, propranolol, and talinolol were obtained as racemic mixtures from Sigma. The PEAs (Figure 7.2) ephedrine, octopamine, epinephrine, pseudoephedrine, synephrine, isoproterenol, norephedrine, norphenylephrine, norepinephrine, and terbutaline were also purchased from Sigma. The PAH mixture (PNA-550JM) (Figure 7.3) and PCB mixture (PCB525-1JM) (Table 7.1) were obtained from ChemService (West Chester, PA, USA). For spiking studies, the individual PAH [dibenzanthracene, fluorine, anthracene, chrysene, phenanthrene, fluoranthene, acenaphthylene, benzo[k] fluoranthene, benzo[ghi] perylene, pyrene, 1,2-

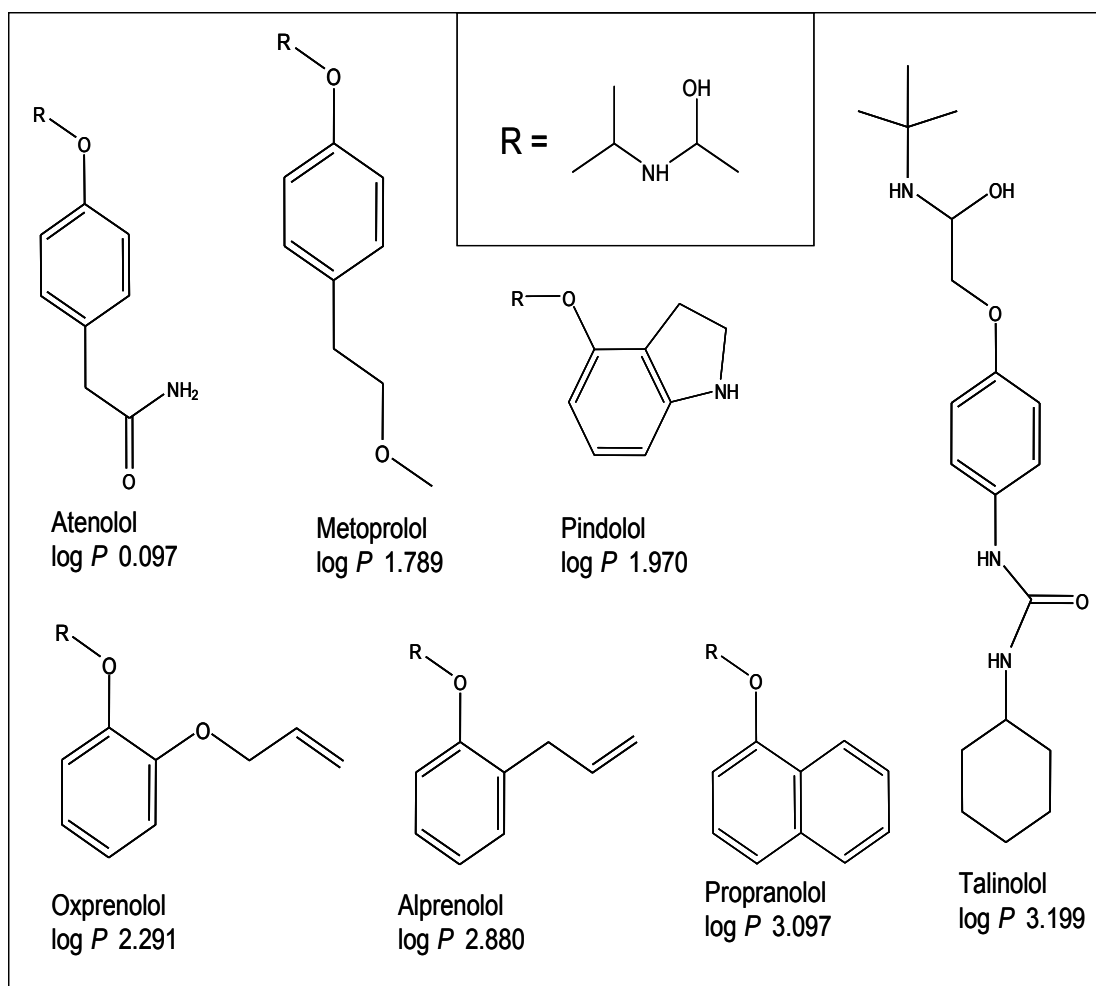


Figure 7.1: Chemical structure of the β -blockers.

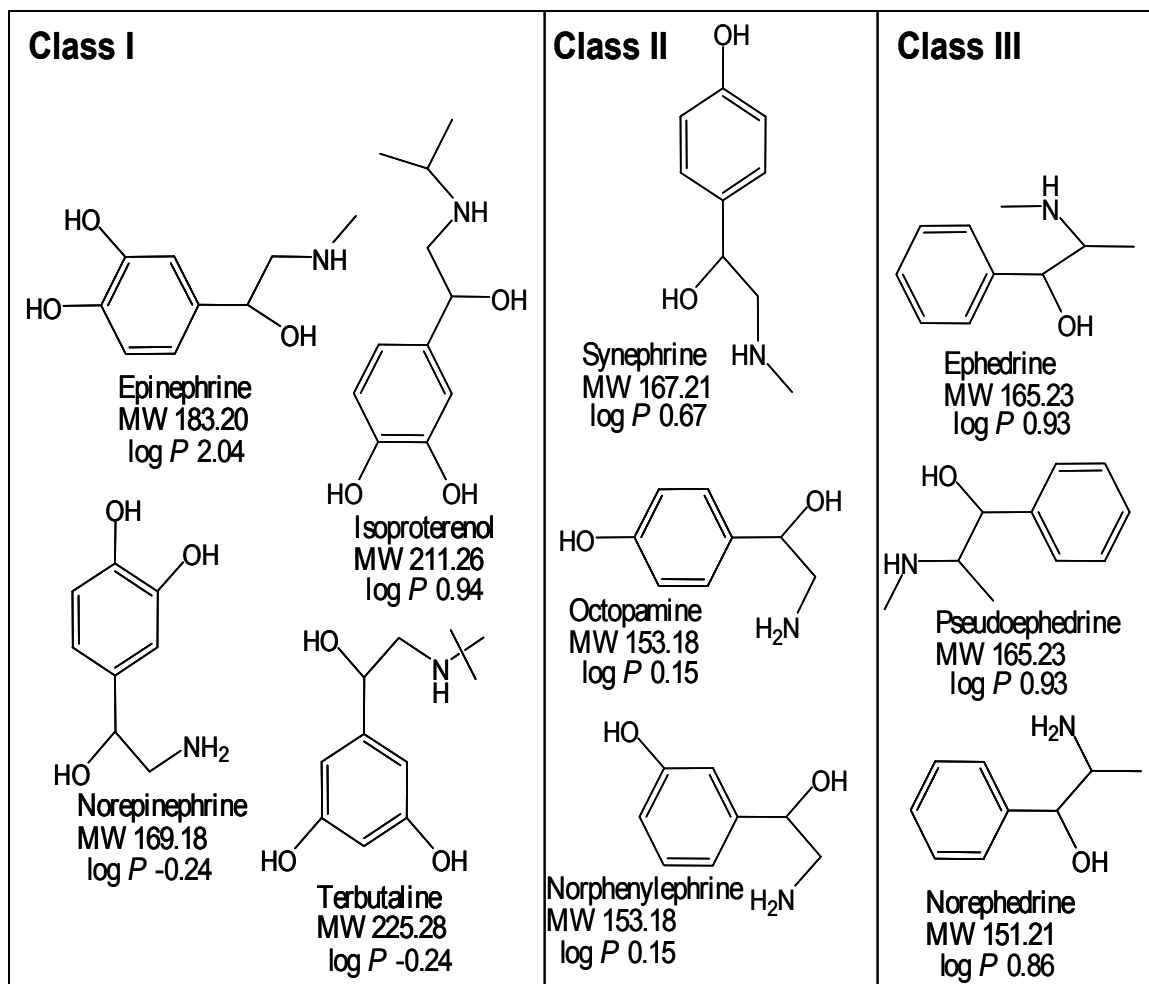


Figure 7.2: Chemical structure of the PEAs with varying degree of hydroxyl substitution around the aromatic ring. Class I has 2 –OH groups, Class II has 1 –OH group, and Class III has no –OH substitution.

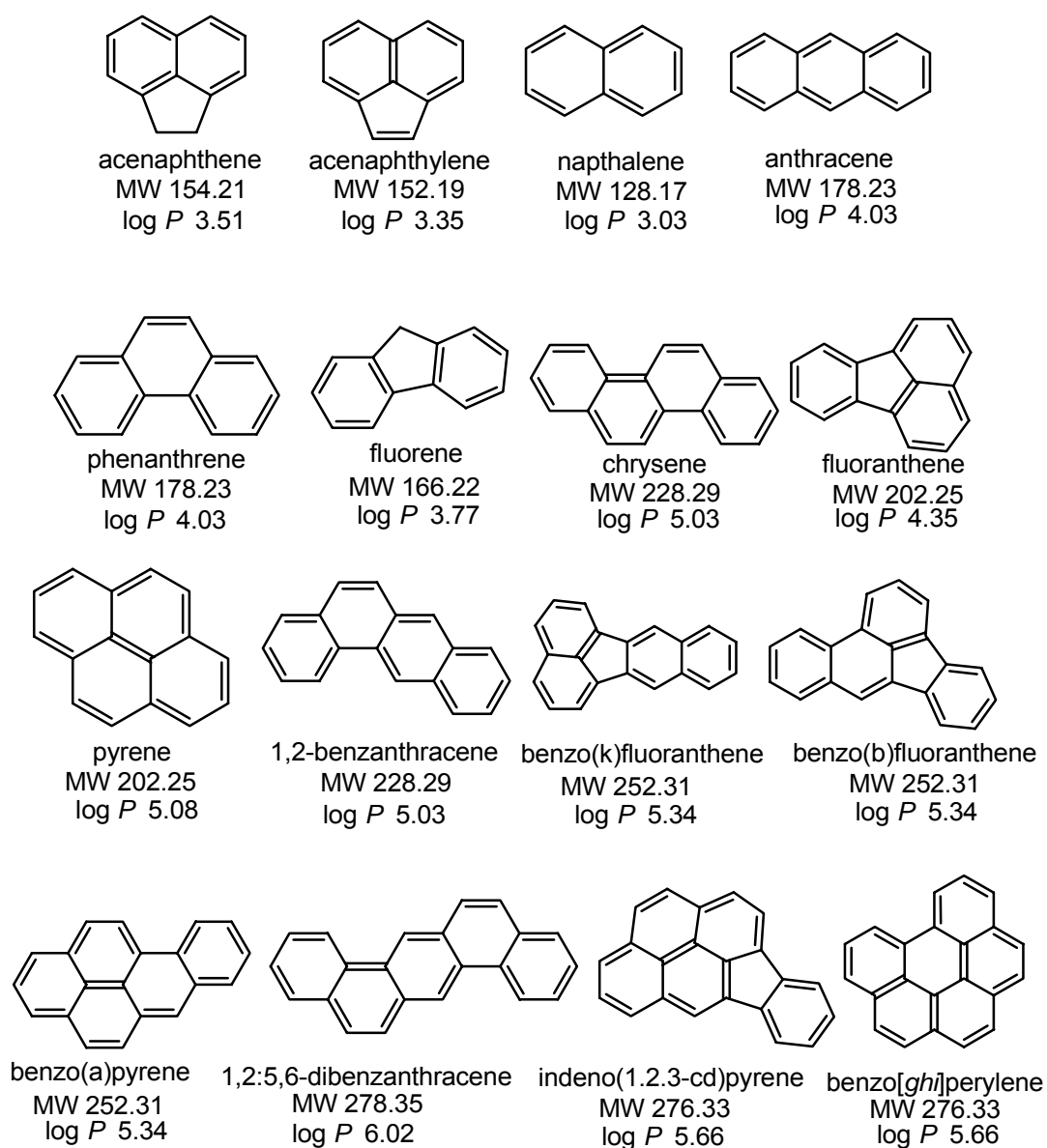
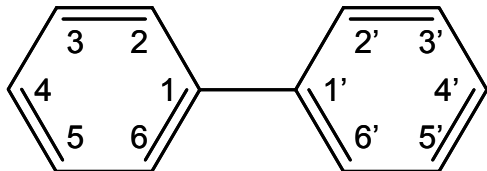


Figure 7.3: Chemical structures of the PAH along with the log *P* value.

benzanthracene, benzo[a] pyrene, naphthalene, benzo[b] fluoranthene, indeno (1.2.3-c.d) pyrene, and acenaphthene] were all obtained from Sigma. Similarly, the individual PCBs [2 chlorobiphenyl, 2.4.5-trichlorobiphenyl, 2.2'.4.4'-tetrachlorobiphenyl, 2.3-dichlorobiphenyl, 2.2'-3.3'-4.4'-6-heptachlorobiphenyl, 2'-4.4'5.6'-hexachlorobiphenyl, 2.2'-3'-4.6-pentachlorobiphenyl, and 2.2'.3.3'4.5'6.6'-octachlorobiphenyl] (Table 7.1) were purchased from ChemService.

Table 7.1: List of PCBs used and their log *P*



IUPAC Name	log <i>P</i>
2 Chlorobiphenyl	4.57
2.3-Dichlorobiphenyl	4.83
2.4'.5-Trichlorobiphenyl	5.38
2.2'.4.4'-Tetrachlorobiphenyl	5.94
2.2'-3'-4.6-Pentachlorobiphenyl	6.50
2.2'.4.4'.5.6'-Hexachlorobiphenyl	7.06
2.2'.3.3'4.4'.6-Heptachlorobiphenyl	7.62
2.2'-3.3'4.5'6.6'-Octachlorobiphenyl	8.17

Synthesis of the LCA Stationary Phase. Preparation of Aminopropyl Silica. A 1.00 g sample of previously dried 300 Å, 5 µm particle size Kromasil silica was weighed into a 250 mL round bottom (RB) flask. Toluene (50 mL) was added to the RB flask, then set up into an oil bath using clamp and holders, and placed onto medium stirring (e.g., #5) using a medium size stir bar. Next, 3-aminopropyltriethoxysilane (3 mL) was added to the flask. A reflux condenser was then attached to the RB flask using a clamp to hold in place. This mixture was allowed to react overnight while maintaining temperature at 100°C. Following 12 h of reaction, the mixture was cooled to room temperature then suction filtered using a Pall FP-200 filter (0.2 µm, 47 mm part no. 66477). The product was washed with 300 mL MeOH, 300 mL deionized H₂O, and finally 300 mL MeOH. The ¹³C-NMR resonance data shown in Figure 7.4 shows that three peaks in the range of 0-50 ppm correspond to the propyl alkyl chain of the aminopropyl silica.

Synthesis of Lithocholic Acid Chloroformate (1). Lithocholic acid (20 g) was placed in a 500 mL RB flask. After adding 300 mL CH₂Cl₂, the reaction mixture was stirred for 10 min followed by sonication for 2 min to disperse any large aggregates of LCA. Separately, 4 mL of pyridine was added to a small extraction funnel along with 100 mL of CH₂Cl₂. Next, 5.3 g (0.018 mol) of triphosgene was added to the LCA solution contained in the RB flask. The pyridine in CH₂Cl₂ was then slowly added dropwise to the RB flask in order to neutralize any HCl produced. Finally, the contents of the RB flask was refluxed and stirred for 96 hrs. A resulting clear mixture was observed within 30 min

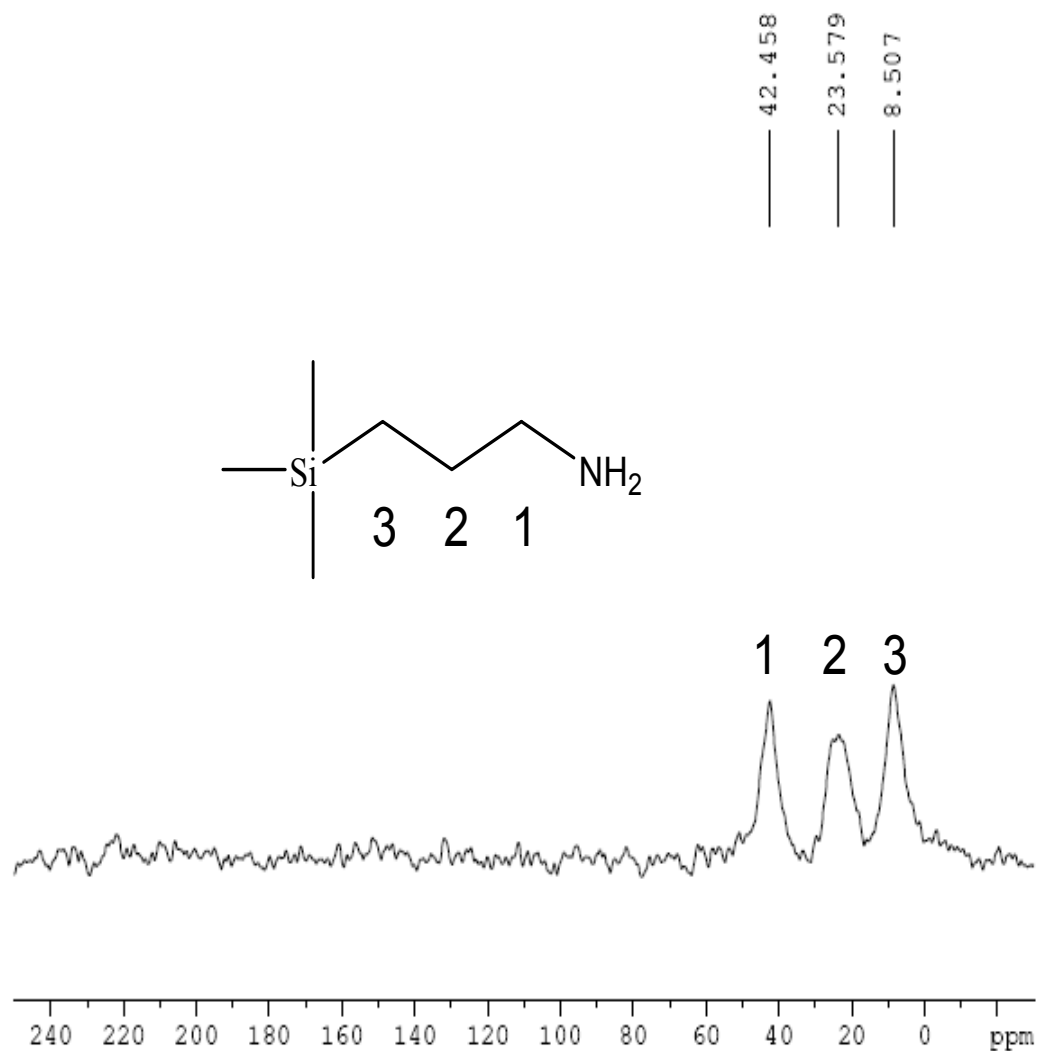
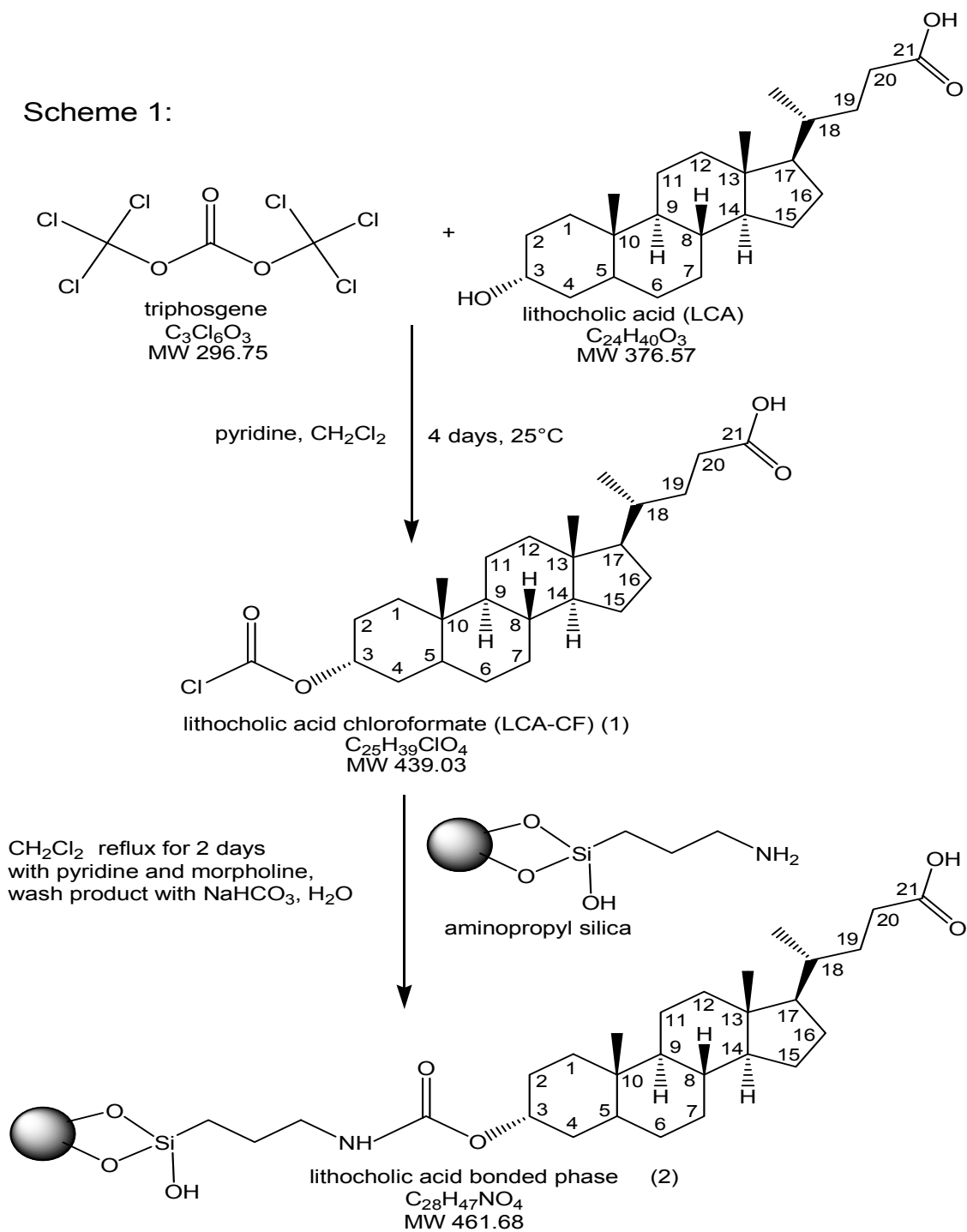


Figure 7.4: Carbon-13 CP-MAS NMR spectrum of the aminopropyl bonded silica intermediate. Instrumentation: Bruker DSX400 solid state NMR spectrometer. Conditions: Data were recorded using a operating at a ^1H frequency of 400 MHz. ^{13}C solid state NMR spectra were recorded using the CP-MAS technique. The 90 degree pulse length was 5 μs . The length of the contact pulse was 1 ms, and high power ^1H decoupling was utilized during the acquisition of the FID. The spinning frequency was 10 kHz. 10,000- 20,000 averages were recorded in order to obtain spectra with sufficient signal to noise ratio.

Scheme 1:



Synthetic scheme for attachment of lithocholic Acid (LCA) to aminopropyl silica. First step involves the conversion of LCA to LCA-chloroformate (1), followed by attachment to aminopropyl silica to yield LCA bonded phase (2).

of reaction time. After 96 hrs, ~100 mL of H₂O was added to RB flask and stirred for 1 hr to dissolve all excess pyridinium chloride formed during the reaction. The mixture was next transferred to a large extraction funnel and the bottom CH₂Cl₂ layer containing product was extracted while discarding the upper H₂O layer. The extraction procedure was then repeated in order to ensure that all excess pyridinium chloride was removed. To the CH₂Cl₂ containing product, sodium sulfate was added to in order to absorb any remaining H₂O. The CH₂Cl₂ was then poured off into a beaker being sure to avoid collection of sodium sulfate. Finally, the CH₂Cl₂ was roto-evaporated to remove solvent. The resulting solid product (1) appeared yellow to white in color. ¹H-NMR was used to characterize the conversion of LCA to LCA-CF. At 400 MHz using CDCl₃ as background solvent, the multiplet at ~3.5 ppm shows downfield shift to ~4.8 ppm (Figure 7.5). Therefore, partial conversion of LCA to LCA-CF was achieved due to presence of LCA starting material (multiplet resonances at 3.5 ppm) along with an additional multiplet at 4.8 ppm due to LCA-CF product.

Attachment of Lithocholic Acid-Chloroformate to Aminopropyl Silica (2).

Aminopropyl silica (800 mg) was placed into a 250 mL RB flask along with excess (3 g) LCA-CF (1). Next, 300 mL of CH₂Cl₂ was added to disperse the contents. Morpholine (5 mL) was added as an activator and the mixture was then refluxed at 70°C overnight for 12 h with slow stirring to avoid damage to the crystalline particles. After 12 h, the temperature of the oil bath was allowed to cool in order to avoid breathing CH₂Cl₂ vapor upon removal of the RB flask from the reflux condenser. The resulting white product (2)

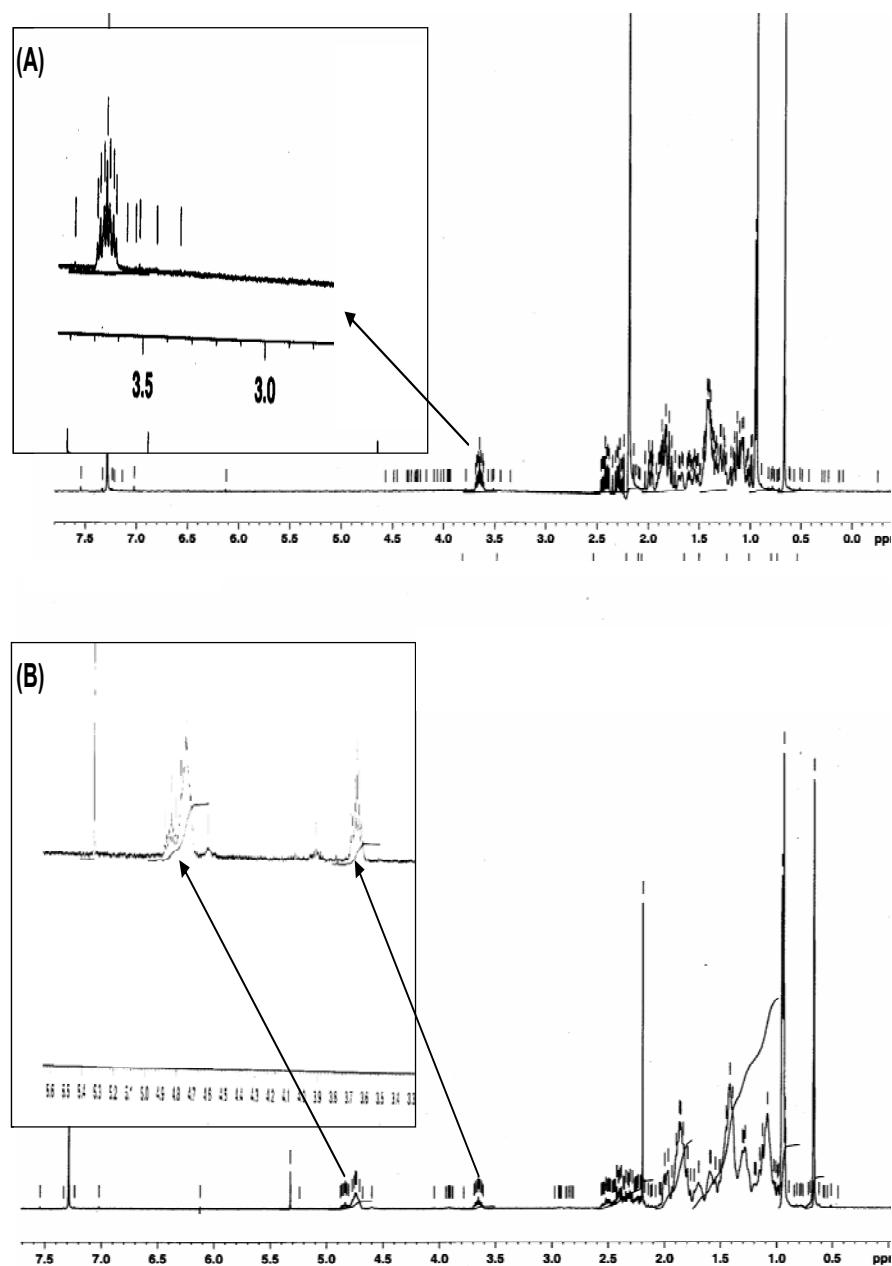


Figure 7.5: ^1H -NMR comparison of the (A) LCA and the (B) LCA following conversion to the chloroformate. Instrumentation: 400 MHz Varian NMR. Conditions: Sample in CDCl_3 .

was suction filtered (Buchner) and washed with H₂O. Next, CH₂Cl₂ was used to rinse away any unreacted LCA-CF. Finally, the product was washed with HPLC grade MeOH.

The product was characterized using solid state ¹³C-NMR at 400 MHz and cross polarization-magic angle spinning (CP-MAS) technique. Chemical shifts corresponding to the cyclic ring network at 9.1, 20.6, 26.0, 33.7, 41.7, 56.0, 66.0, and 72.1 ppm were observed as well as 176.1 ppm for the terminal carboxylic acid (Figure 7.6). The LCA chloroformate carbonyl carbon attached to –NH group of the amino silica showed a chemical shift at 157.0 ppm.

Column Packing Procedure. The CEC-UV columns were packed according to our previously published procedure.²¹ Briefly, slurry was prepared using ACN followed by sonication for 45 min. Next, fused silica capillary (75 μm ID, 362 μm OD) obtained from Polymicro Technologies Inc. (Phoenix, AZ, USA) was packed to 30 cm utilizing 300 bar as previously described.²¹ The internally tapered CEC-MS columns were fabricated and packed according to our previously published method.²²

Buffer and Sample Preparation. The CEC running buffer was prepared using concentrated 100 mM NH₄OAc adjusted to the appropriate pH using HOAc. An appropriate aliquot of stock solution was then combined with ACN, triply deionized H₂O and TEA using volumetric pipettes, followed by 25 min sonication, filtering using 0.45 μm PTFE membrane syringe filter and finally degassing for 10 min. The mixture of seven β-

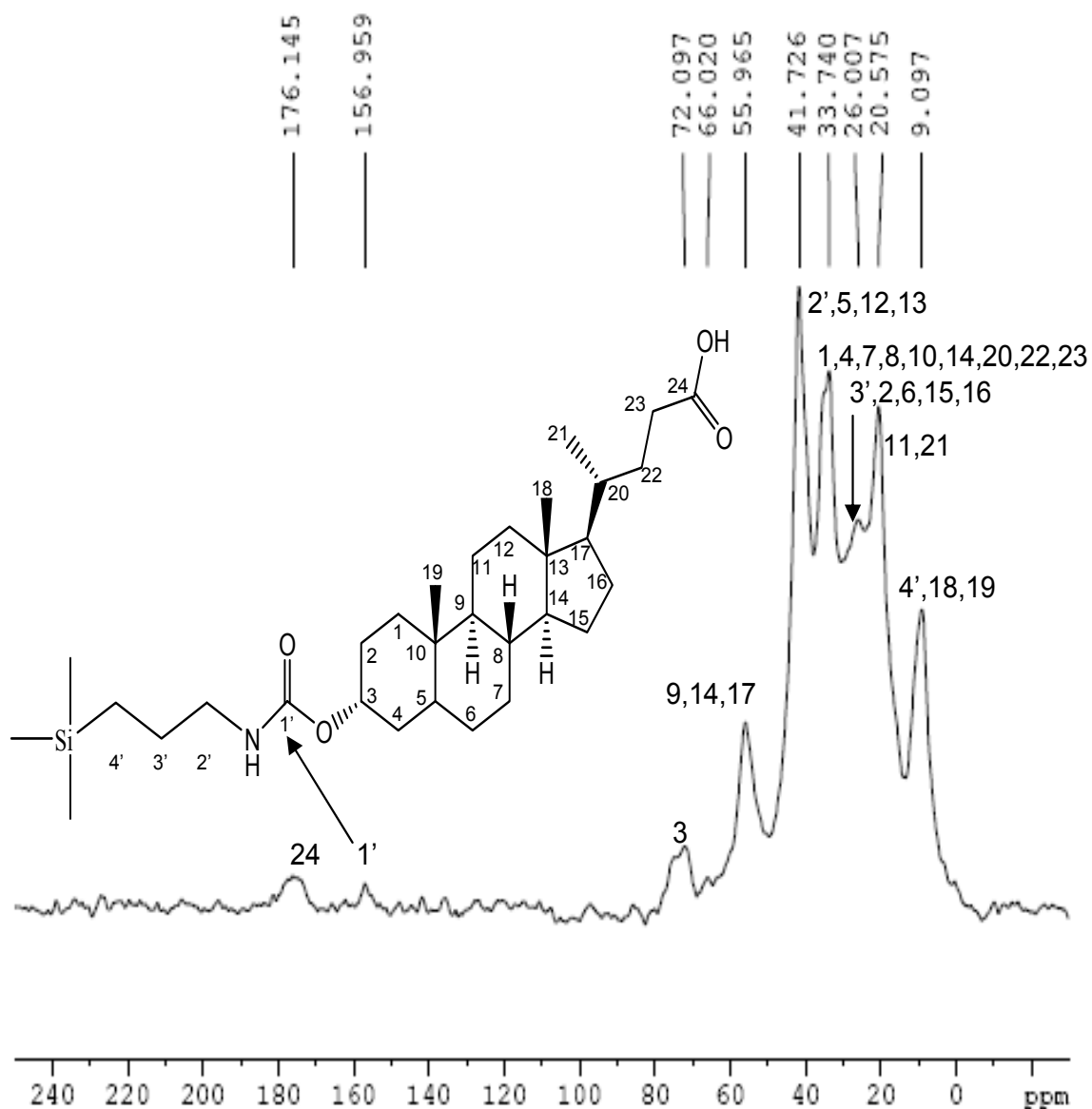


Figure 7.6: Carbon-13 CP-MAS NMR spectrum of the LCA bonded phase. Instrumentation and conditions are same as Figure 7.4. Peaks observed at 176 and 157 ppm in the LCA spectra occur at about 10 kHz from peaks in the aliphatic region. It was confirmed that these peaks are “true peaks” and not spinning sidebands by recording an additional spectrum with a spinning speed of 8 kHz, which look essentially identical to the spectrum recorded with a spinning speed of 10 kHz.

blockers was prepared by taking 100 μL of each analyte dissolved in MeOH (1 mg/mL), followed by addition of 100 μL running buffer. A mixture of ten PEAs was prepared in the same manner. The 16 PAH mixture (200 $\mu\text{g/mL}$ in ACN) and the PCB mixture (500 $\mu\text{g/mL}$ in acetone) were diluted three fold using running buffer prior to analysis. For identification of the PAH elution order, 100 μL of stock 16 PAH mixture was added to 25 μL of individual PAHs (dissolved at 3 mg/mL ACN) followed lastly by addition of 25 μL running buffer. Similarly, the elution order of PCBs was determined by spiking 25 μL individual PCB (dissolved at 500 $\mu\text{g/mL}$ in acetone) to 100 μL stock solution of 8 PCB mixture plus the addition of 25 μL running buffer.

CEC Instrumentation. All CEC-UV experiments were performed on an Agilent HP^{3D}CE system (Agilent Technologies, Palo Alto, CA) using 214 and 254 nm detection. For CEC-ESI-MS instrumentation, all experiments were performed on an Agilent HP^{3D}CE which was interfaced to an Agilent 1100 series MSD quadrupole mass spectrometer equipped with a CE-MS adaptor kit and a sprayer kit. Sheath liquid was delivered by an Agilent 1100 series HPLC pump equipped with a 1/100 split flow. The Chemstation software (v. 10.02) was used for data processing.

RESULTS AND DISCUSSION

The characterization of the bonding reactions using ^1H -NMR, elemental analysis, IR, and ^{13}C -NMR is first presented. The conversion of LCA to LCA-CF is described, followed next by attachment of propyl amine to bare silica, then lastly the attachment of LCA-CF to the modified aminopropyl silica. Finally, the LCA bonded stationary phase and the aminopropyl silica phases were packed in a capillary and compared for the separation of several different classes of positively charged and neutral compounds.

Characterization of the Lithocholic Acid Chloroformate. Lithocholic acid was first converted to the chloroformate. The ^1H -NMR of the LCA and the LCA following conversion to the chloroformate were compared. Figure 7.5A shows that the starting material LCA exhibits a multiplet for the ring protons at position 3 around 3.5 ppm. This is slightly downfield from the Chemdraw estimation of 3.1 ppm. Following the conversion of LCA to chloroformate at ring position 3, Figure 7.5B shows that a downfield shift to 4.8 ppm is observed for the multiplet which is slightly downfield from the Chemdraw estimation of 3.9 ppm. This suggests that the reaction of LCA to LCA-CF was successful.

Characterization of Aminopropyl Silica and Lithocholic Acid Bonded Phase. Elemental analysis of two prepared batches of aminopropyl silica and one batch of

bonded LCA phase were compared. Table 7.2 shows the percent by weight composition of C, H and N for the three materials. The effect of adding more (3 mL) or less (1 mL) volume of silane reagent during the preparation of aminopropyl silica (section 2.2.1) showed little to no effective difference as can be seen by the similarity in %C, %H and %N for batch 1 and batch 2. Following the bonding of LCA-CF to the aminopropyl silica, the elemental analysis showed significantly more C and H by weight percent. As expected, the N content remained fairly constant. Therefore, the increase in %C and %H suggests that the attachment of LCA-CF to aminopropyl silica was indeed achieved.

Table 7.2: Elemental analysis of the aminopropyl silica intermediate and the LCA bonded phase

Kromasil Si-C3-NH ₂ Batch 1 (more NH ₂ silane added)	
C	2.06
H	0.50
N	0.69
Kromasil Si-C3-NH ₂ Batch 2 (less NH ₂ silane added)	
C	1.98
H	0.48
N	0.65
Kromasil Si-C3-NH-LCA	
C	5.75
H	0.98
N	0.61

a) C,H,N elemental analyses are percent by weight.

Next, the infrared (IR) spectroscopy data were collected using GSU Perkin Elmer Spectrum One (Figure 7.7). The IR spectra of the bare silica, attachment of aminopropyl group to bare silica, and finally the attachment of LCA-CF to aminopropyl silica showed no significant differences of the bonds IR in the region of 450 to 4000 cm^{-1} . Therefore, IR was not found to be sensitive enough to identify any characteristic differences between these phases.

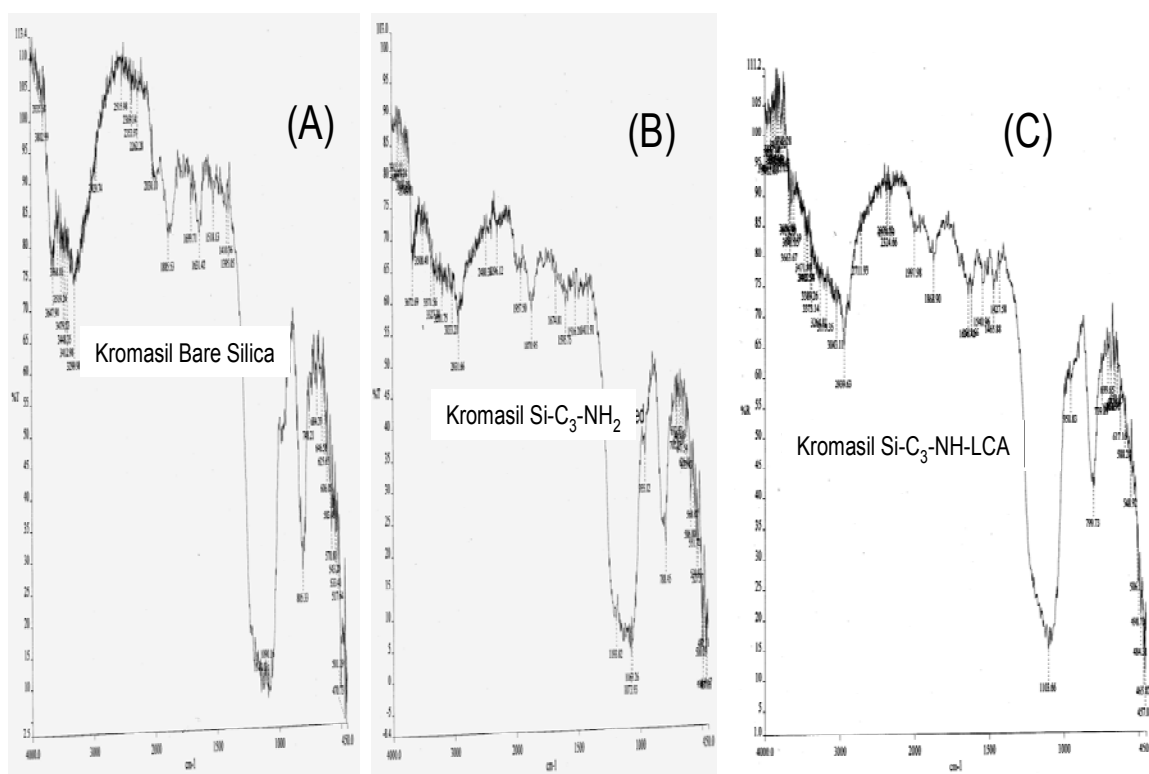


Figure 7.7: IR comparison of the (a) Kromasil 300Å bare silica, (b) Kromasil 300Å bare silica following reaction with aminopropyl silane, (c) attachment of LCA-CF to $\text{Si-C}_3\text{-NH}_2$. Instrumentation: GSU Spectrum One. Conditions: KBr was used as the background.

The solid state ^{13}C -NMR spectra of the aminopropyl silica (Figure 7.4) versus aminopropyl bonded silica bonded to LCA-CF (Figure 7.6) were compared. For the aminopropyl silica, Figure 7.4 shows that 3 peaks corresponding to the chemical shift of the propyl ^{13}C carbon chain which were observed in the range of 8-43 ppm. From the Chemdraw predicted ^{13}C -NMR spectra (not shown), the experimental chemical shift of these carbon atoms agrees nicely with the predicted chemical shift of 9.7, 31.4, and 45.2 ppm for C1, C2, and C3 respectively. In comparison, the ^{13}C -NMR spectra for the LCA bonded phase shown in Figure 7.6 is much more complex. From the peak assignment obtained using Chemdraw predicted ^{13}C -NMR spectra, the chemical shift in the range of 0-80 ppm can be attributed mainly from the extensive cyclic ring carbons which are not present in the spectra of the aminopropyl silica. In addition, the extent of bonding was determined by analysis of the chemical shift of the carbonyl carbon attached to position 3 of the steroid. A small but distinct peak at 156.959 ppm (Figure 7.6) indicates successful bonding. Note that this peak at 156.959 ppm was not observed in the spectra of the aminopropyl silica. Moreover, this is also a larger downfield chemical shift compared to the chemical shift for LCA-CF observed at 150.8 ppm for C-3 using the Chemdraw predicted ^{13}C -NMR spectra (not shown). Finally, a comparison of the obtained bonded phase spectra to the literature cholesteric phase shows several similar resonances in the region of 0-80 ppm representing the chemical shifts of the cyclic ring carbons, as well as the resonance at 155 ppm representing the carbonyl carbon attached at position 3 of the steroid molecule.¹⁹

Although the elemental analysis data and the ^{13}C -NMR data suggested that the bonding of LCA-CF to the aminopropyl silica was successful, alternatively, a comparison of the chromatographic separating ability of these two phases was conducted in order to further distinguish between the two materials. First, the capability of both phases for CEC-MS separation of cationic compounds (seven β -blockers and ten PEAs) was performed. Investigation of the most suitable operating conditions showed that a mobile phase containing 85/15 ACN/10mM NH_4OAc , pH 3, 0.05% TEA could be utilized for the separation of β -blockers and PEAs. Next, the CEC-MS separation of ten PEAs was compared on the two phases utilizing aforementioned mobile phase. This is followed by the CEC-UV analysis of neutral compounds (PAHs and PCBs). Finally, data and comments on the electroosmotic flow (EOF) profile using thiourea as a dead time marker run under various mobile phase conditions are presented.

CEC-MS of β -Blockers. For CEC-MS separation of seven β blockers, Figure 7.8 shows the comparison between the LCA bonded phase (Figure 7.8A) and the aminopropyl silica (Figure 7.8B). The results of the study demonstrate that the LCA bonded phase provides six peaks for separation of 6 out of 7 β -blockers, whereas the aminopropyl phase provides 4 peaks of several co-eluting β -blockers. From the extract ion chromatograms (EIC) shown inset of Figure 7.8 (A-B), the peak identification was assigned as shown in the caption. Overall, the LCA bonded phase was more capable of separating several peak pairs. For example, atenolol/talinolol were baseline resolved whereas propranolol/metoprolol were partially resolved with LCA phases. On the other hand,

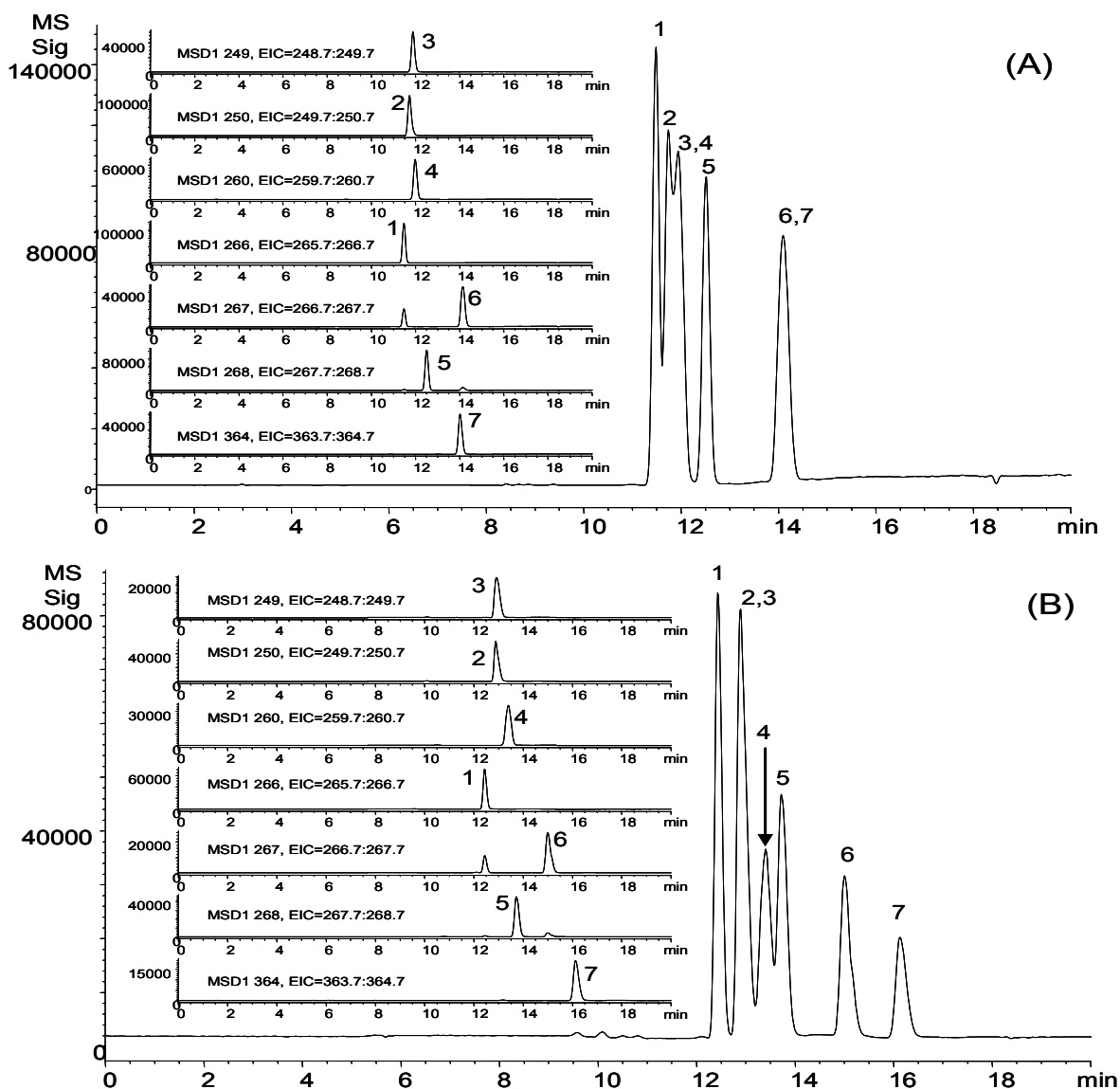


Figure 7.8: CEC-MS Comparison of (A) Kromasil Si-C₃-NH₂ to (B) Kromasil Si-C₃-NH-LCA for separation of 7 component β -blockers. Conditions: Packed bed 25 cm, total length 58 cm, Buffer, 85/15 ACN/10mM NH₄OAc, pH 3, 0.05% TEA. Sheath liquid: 70/30 MeOH/10 mM NH₄OAc delivered at 500 μ l/min. ESI spray chamber: drying gas flow rate 6 L/min, nebulizer pressure 5 psi, drying gas temp. 200°C, Vcap 2700 V, Fragment V 80, CEC 12 kV runs, 4 kV 4 sec injection. Analytes 1 mg/mL in MeOH, injection sample 80/20 analyte/running buffer. Peak identification: 1=oxprenolol, 2= alprenolol, 3=pindolol, 4=propranolol, 5=metoprolol, 6=atenolol, 7=talinolol. The inset provides the EIC for each m/z monitored.

these two peak pairs co-eluted with aminopropyl silica phase. Overall, it can be concluded that the selectivity of β -blockers on the LCA bonded phase is higher than that of the aminopropyl phase.

In order to comment on the trend in elution order shown in Figure 7.8A, for each β blocker the mass (m), charge (z), charge to mass (z/m) ratio and the $\log P$ were listed as a function of elution order as shown in Table 7.3. With the exception of oxprenolol and atenolol, the β -blockers generally follow elution based upon decreasing z/m ratio. No mentionable correlation between $\log P$ and elution order was observed with the exception of talinolol ($\log P=3.20$) which eluted last and had the highest $\log P$ value.

Table 7.3: Elution order, mass (m), charge (z), z/m ratio and $\log P$ of the 7 β -blockers.

Compound	Elution Order	MW	Charge (z) (pH3)	z/m	$\log P$
(Si-C₃-NH-LCA)					
oxprenolol	1	265	+1	.0038	2.29
alprenolol	2	249	+1	.0040	2.88
pindolol	3	248	+1	.0040	1.97
propranolol	4	259	+1	.0039	3.10
metoprolol	5	267	+1	.0037	1.79
atenolol	6	266	+1	.0038	0.10
talinolol	7	363	+1	.0028	3.20

The additional on-line CEC-MS characterization of the LCA bonded phase and the aminopropyl silica utilizing mobile phase conditions of Figure 7.8 (A-B) was conducted by analysis of a neutral marker and also comparison of the operating current on the two phases. Thiourea was chosen as the dead time or neutral marker as this compound was expected to be neutral at pH 3 (pKa of thiourea is 1.44 ± 0.5 , Science Finder Scholar, v.2002). The operating current in μA can provide insight of the flow of ions inside the packed CEC column. If the current profile is different for two phases run under the same operating conditions (i.e., packed bed length and mobile phase composition), it can be reasonable to state that the two materials are structurally different. The results of the study can be seen in Figure 7.9 (A-B). First, an analysis of the current profile (Figure 7.9A) taken from the chromatograms of Figure 8 shows that the LCA bonded phase has higher operating current of 11 μA as compared to the aminopropyl silica phase current of 9 μA . A comparison of the thiourea dead time marker shown in Figure 7.9B shows that the retention on the LCA bonded phase was 42 min as compared to 28 min on the aminopropyl phase. As thiourea is effectively neutral at pH 3, the longer retention of thiourea can be attributed to slower EOF on the LCA bonded phase. Therefore, it can be concluded that the surface property of the two phases are different and suggest that bonding of the LCA did in fact occur.

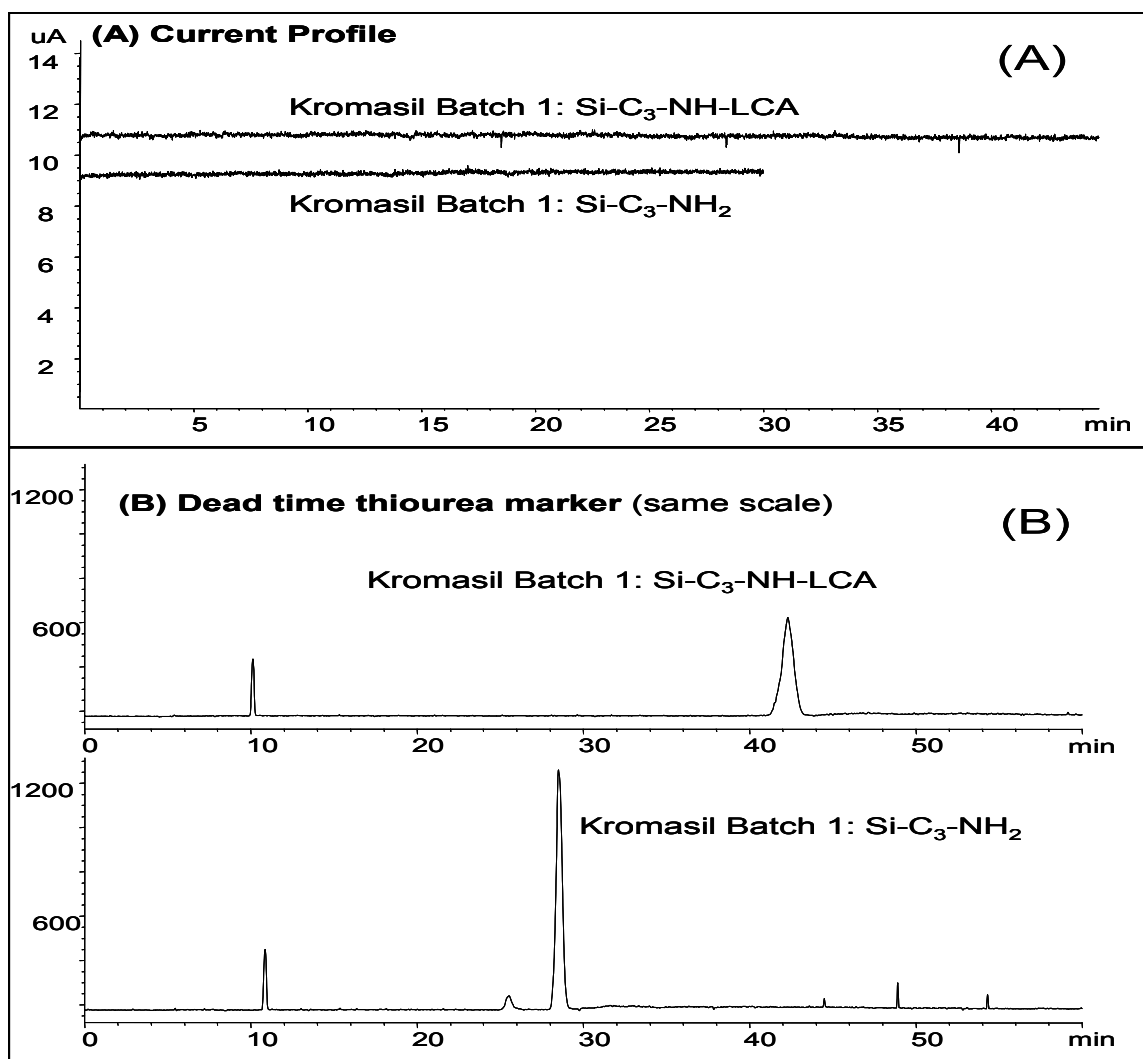


Figure 7.9: CEC-MS Comparison of Kromasil $\text{Si-C}_3\text{-NH-LCA}$ to Kromasil $\text{Si-C}_3\text{-NH}_2$ for (A) comparison of the current profile and (B) comparison of the thiourea dead time marker. Conditions are the same as Figure 7.8.

CEC-MS of Phenylethylamines. Next, the CEC-MS capability of the bonded phase for separation of a series of structurally similar PEAs was assessed. A comparison of the separation on the aminopropyl silica versus the LCA bonded phase is shown in Figure 7.10A-B respectively. The results show that both stationary phases were able to separate 9 out of 10 PEAs within 18 mins. However, several noticeable differences in separation selectivity were observed. For example, reversal of elution order was seen for terbutaline and epinephrine on the two phases. In order to verify the elution order of the PEAs, the EIC for each m/z (shown as inset in Figure 7.10 A-B) was compared to the retention time of each PEA run individually on a much longer packed bed. For this experiment, the results of running individual PEA on the LCA bonded phase are shown in Figure 7.11. From a comparison of the elution trend for each compound run individually (Figure 7.11) to the EIC of the LCA bonded phase (Figure 7.10 inset B), it was determined that the presence of multiple peak in several EIC channels resulted from the fragmentation of several PEA molecules. In general, the PEA fragment in the ESI source either by loss of an alkyl group or by loss of hydroxyl group, or both. In this manner, the multiple peaks (a-o) in the EIC channel were assigned as shown in the Figure 7.10 caption. Overall, at least three PEAs (isoproterenol, terbutaline, norepinephrine) were found to produce fragment ions with same m/z ($m/z=152$) as shown in Figure 7.12 A-B. First, the PEA containing a primary amine such as norepinephrine (Figure 7.12 A) were found to fragment at the hydroxyl group to form a di-cationic species. This is followed by abstraction of the amino proton (acidic conditions, pH 3.0) by the negatively charged hydroxide group to form H_2O , leaving a

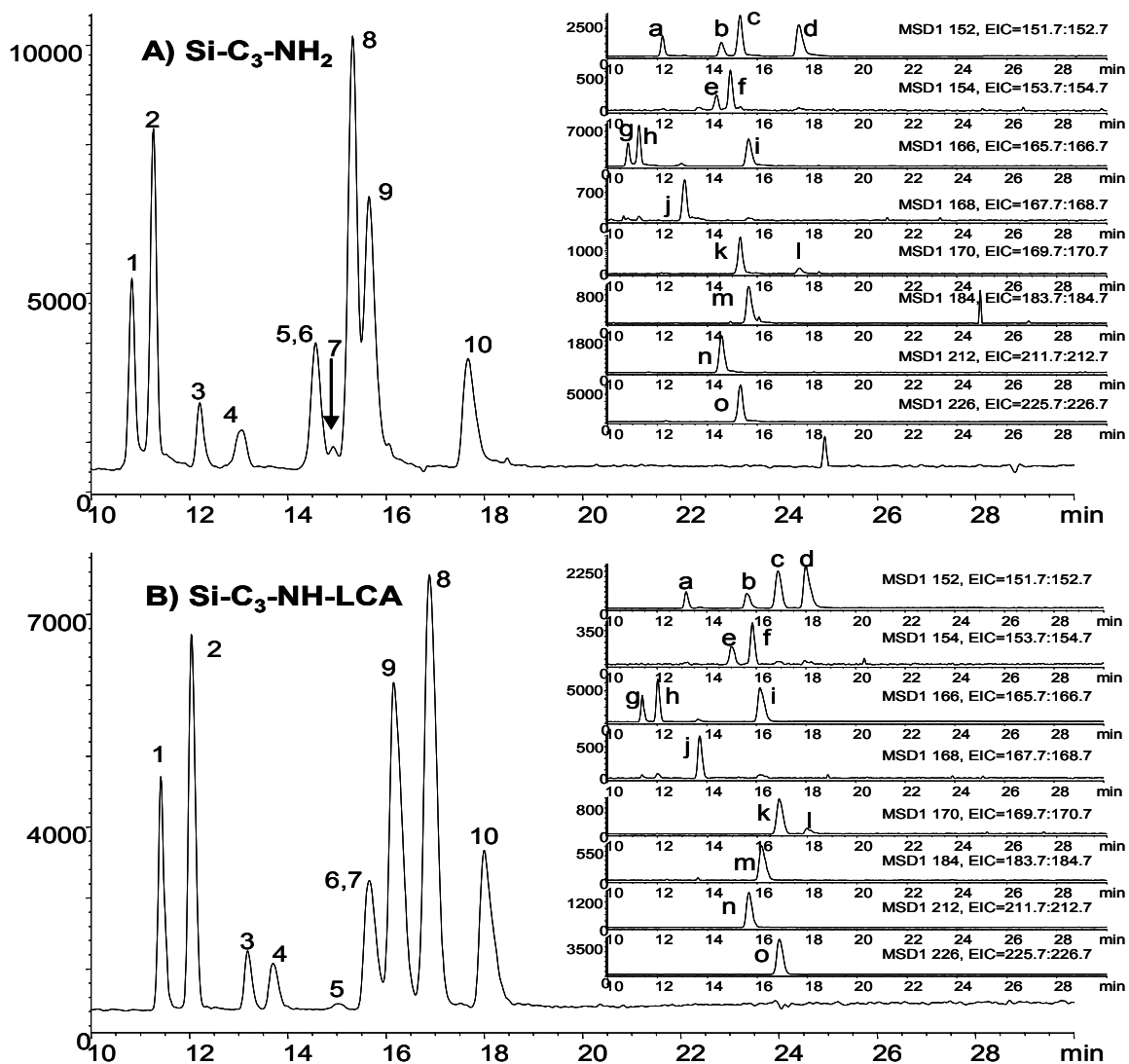


Figure 7.10: Separation of a mixture of ten PEAs compounds on the (A) aminopropyl silica and (B) LCA bonded phase. Conditions are same as Figure 7.8. The protonated molecular ion $[M+H]^+$ was monitored for all analytes. Peak identification; 1=pseudoephedrine; 2=ephedrine; 3=norephedrine; 4=synephrine; 5=octopamine; 6=isoproterenol; 7=norphenylephrine; 8=terbutaline; 9=epinephrine, 10=norepinephrine. The inset provides the EIC for each m/z monitored, for both A) and B) a: [norephedrine $M+H]^+$, b: [isoproterenol $M+H-C_3H_8O]^+$, c: [terbutaline $M+H-C_4H_{10}O]^+$, d: [norepinephrine $M+H-H_2O]^+$, e: [octopamine $M+H]^+$, f: [norphenylephrine $M+H]^+$, g: [pseudoephedrine $M+H]^+$, h: [ephedrine $M+H]^+$, i: [epinephrine $M+H-H_2O]^+$, j: [synephrine $M+H]^+$, k: [terbutaline $M+H-C_4H_8]^+$, l: [norepinephrine $M+H]^+$, m: [epinephrine $M+H]^+$, n: [isoproterenol $M+H]^+$, o: [terbutaline $M+H]^+$. Packed bed lengths 25 cm, total length 60 cm.

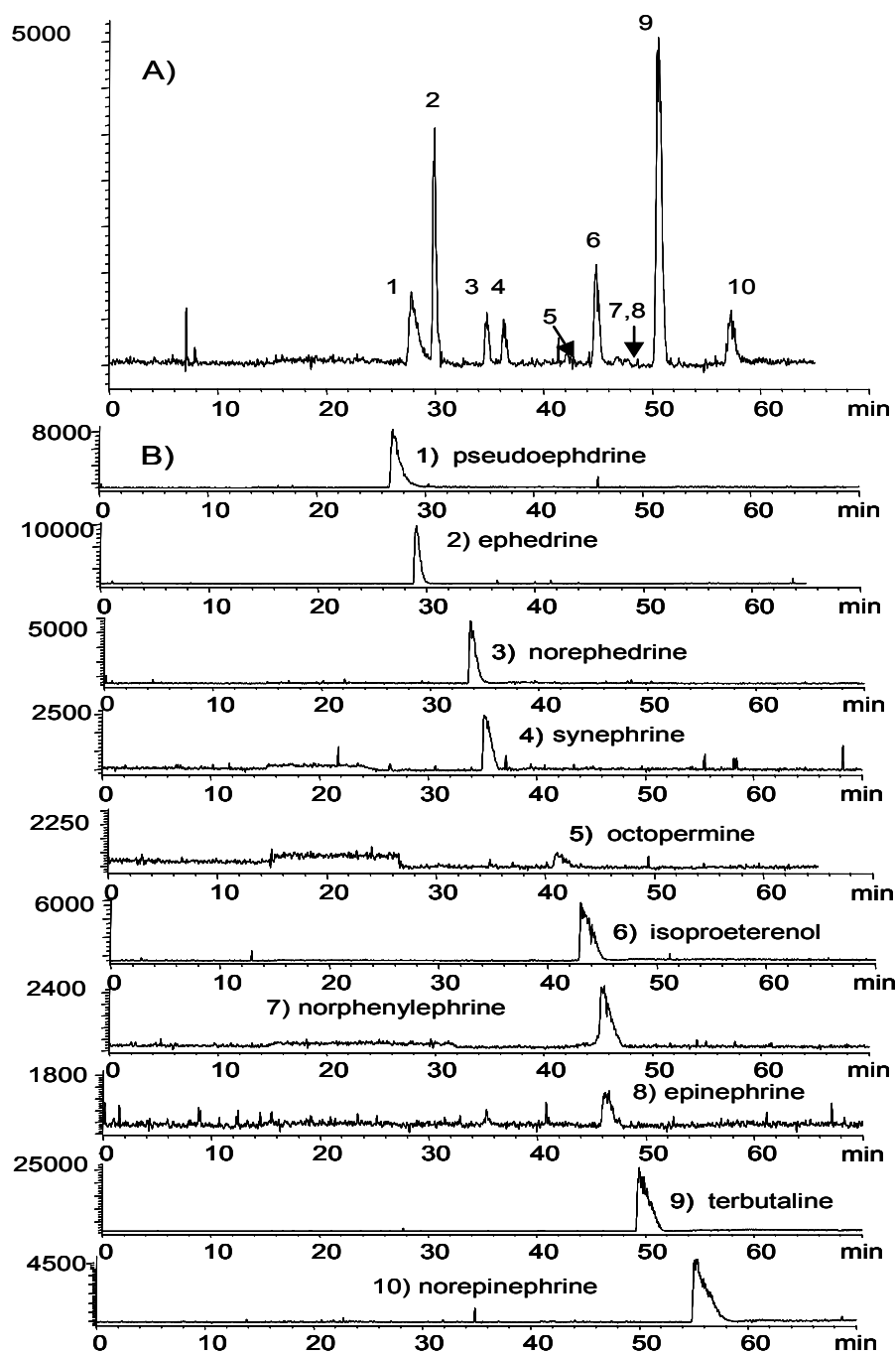
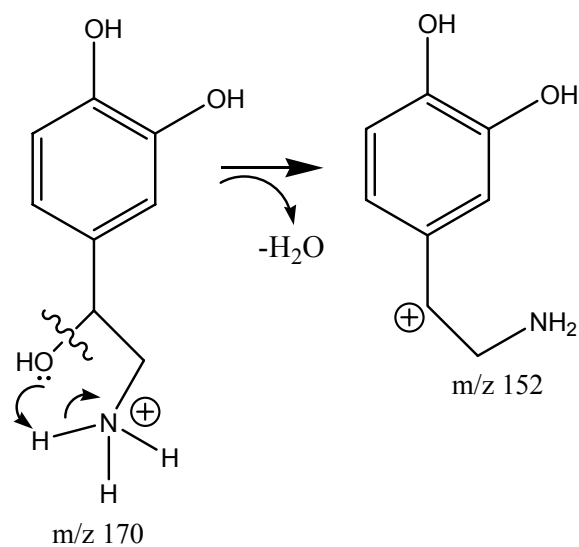


Figure 7.11: Separation of a mixture of ten PEA compounds on the LCA bonded phase using a longer packed bed length of 55 cm. All other conditions are same as Figure 7.10.

A) norepinephrine



B) terbutaline

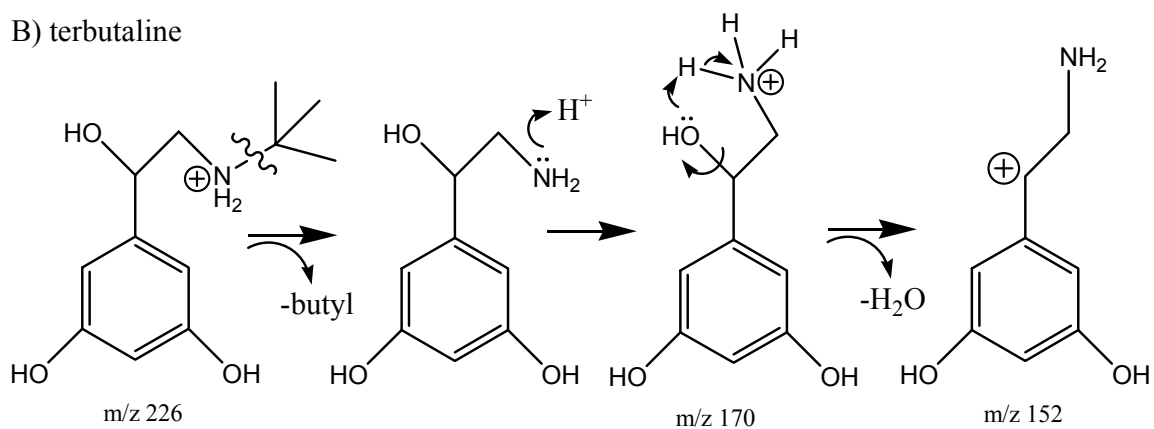


Figure 7.12: Proposed fragmentation pathway of PEAs, A) norepinephrine by loss of H_2O , and B) terbutaline by loss of isobutyl alkyl group followed by loss of H_2O .

neutral amine plus a positive charge at the site of hydroxyl abstraction.

The second fragmentation pattern observed for terbutaline (Figure 7.12B) follows a somewhat similar pattern to norepinephrine. The molecule was found to first fragment at the isobutyl position, followed next by the loss of hydroxyl group to form H₂O as previously shown for norepinephrine. Isoproterenol which is structurally similar to terbutaline was observed to fragment in the same fashion except for the loss of isopropyl group in the first step. Following the determination of the elution order, the trend in elution was evaluated considering the molecular weight (MW), charge (z) at pH 3, charge/mass (z/m) ratio, log P, and finally the class as shown in Table 7.4.

Table 7.4: Elution order, mass (m), charge (z), z/m ratio and log P of the PEAs.

Compound	Elution Order (Si-C ₃ -NH ₂) (Si-C ₃ -NH-LCA)		MW	Charge (z) (pH3)	z/m	log P	Class ^a
pseudoephedrine	1	1	165.23	+1	.0061	0.93	III
ephedrine	2	2	165.23	+1	.0061	0.93	III
norephedrine	3	3	151.21	+1	.0066	0.86	III
synephrine	4	4	167.21	+1	.0060	0.67	II
octopamine	5	6	153.18	+1	.0065	0.15	II
isoproterenol	6	5	211.26	+1	.0047	0.94	I
norphenylephrine	7	9	153.18	+1	.0065	0.15	II
epinephrine	8,9	7,8	183.20	+1	.0054	2.04	I
terbutaline	8,9	7,8	225.28	+1	.0044	-	I
norepinephrine	10	10	169.18	+1	.0059	-0.24	I

a) See Figure 7.2.

A consideration of z/m and $\log P$ showed no correlation with the elution order on either phase. Alternatively, the class or degree of hydroxyl group substitution around the aromatic ring was found to compare well with retention of the PEAs. For the aminopropyl (Si-C₃-NH₂) phase, the separation can be attributed to hydrophobic interactions between the propyl group of the stationary phase and the short chain alkyl group of the PEAs. In addition, the amine group of this phase can hydrogen bond with the neutral alcohol groups of the PEAs. Therefore, the early eluting PEA follows elution relative to substitution of hydroxyl groups around the aromatic ring. Increasing the number of hydroxyl groups permits increased hydrogen bonding between the analyte and the protonated amine of the aminopropyl stationary phase. For example, pseudoephedrine, ephedrine and norephedrine (class III) have no hydroxyl substituent on the ring and eluted first (Table 7.4). The remaining PEAs containing one (e.g., class II, octopamine, synephrine, norphenylephrine) and two hydroxyl substituent (e.g., class I, isoproterenol, epinephrine, norepinephrine, terbutaline) on the ring eluted second and third respectively with the exception of isoproterenol and norphenylephrine. This general trend in elution order based on class I-III PEAs was also found to hold true for the LCA bonded phase. This suggests that some unbonded propylamine still exist on the LCA bonded phase. Another possibility is that the hydroxyl group on the aromatic ring of the PEA hydrogen bonds with the carboxylic site of the LCA stationary phase. Moreover, the differences in elution order for later eluting PEAs (e.g., class I and class II) suggests that these PEA actually interact with the LCA bonded phase in a different manner than the aminopropyl phase. For example, octopamine (peak 5) was able to be

resolved from isoproterenol (peak 6) on the LCA bonded phase whereas these compounds co-eluted on the aminopropyl phase. In contrast, norphenylephrine (peak 7) was able to be separated from isoproterenol on the aminopropyl phase, which co-eluted on the LCA bonded phase. Most interestingly, the elution order of terbutaline and epinephrine was reversed between the two stationary phases. The different positioning of the hydroxyl groups on the ring most likely provides varying steric interactions that contribute to this separation. Overall, it can be concluded that for the separation of class II and class III PEAs, the LCA bonded phase provides somewhat improved separation with different selectivity for several PEAs as compared to the aminopropyl phase.

CEC-UV of PAHs. The capability of the LCA bonded phase for CEC-UV separation of the 16 PAH test mixture was next evaluated. Initially, a study of mobile phase ACN content was conducted. It was determined that the LCA bonded phase was not well suited to run at lower ACN (i.e., 65% ACN) using 15 mM NH_4OAc at pH 5.0 (data not shown). However, the phase was well suited to be run under higher ACN content using conditions of 85%ACN, which were therefore utilized for optimizing the mobile phase pH. The results of the study are presented in Figure 7.13 and is discussed below. As shown in Figure 7.13, a lower pH of 3 provided longer analysis time (e.g., 80 min) along with broader peak shapes. The longer retention times can be attributed to the increased ionic strength from addition of HOAc used to lower the pH of the NH_4OAc buffer. Furthermore, increased viscosity along with decrease in the electrical double layer results in the longer retention shown above. At higher pH 4.0 and 4.5 little difference between

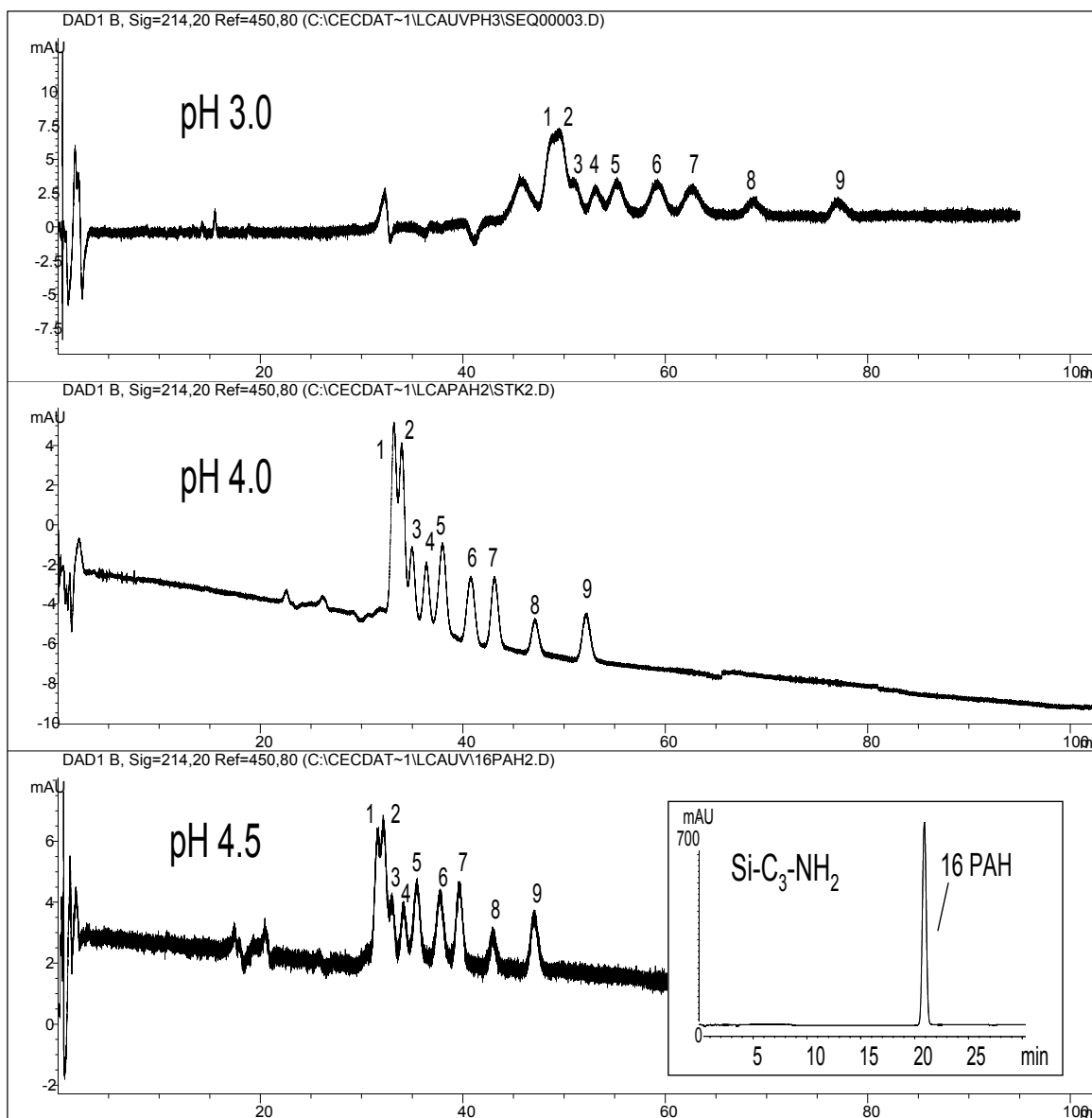


Figure 7.13: Variation of the mobile phase pH for separation of 16 PAH test mixture on the LCA bonded phase. The inset shows the same separation achieved at pH 4.5 using the aminopropyl silica phase. Conditions: 85/15 ACN/15 mM NH₄OAc, packed length 30 cm, 10 kV runs, 10 kV 18 sec injection. Analytes 1mg/mL in 85% ACN, injection sample 85/15 analyte/running buffer Peak identification: peak 1=acenaphthylene; peak 2=naphthalene, acenaphthene, peak 3=phenanthrene; peak 4=fluoranthene; anthracene, fluorene; peak 5=chrysene, pyrene, 1,2-benzanthracene; peak 6=benzo[k]fluoranthene, benzo(b)fluoranthene; peak 7=1,2:5,6-ibenzanthracene; benzo[a]pyrene; peak 8=indeno(1.2.3-cd)pyrene; peak 9=benzo[ghi]perylene.

the two separations is observed. The weaker ionic strength of the mobile phase at pH 4.5 results in faster analysis time although the resolution between the first two peaks is diminished. Interestingly, the same separation at pH 4.5 using the aminopropyl silica phase (shown inset of Figure 7.13) provided a single peak with no resolution of PAH. Overall, a pH 4.0 was chosen as the optimized mobile phase pH. Next, a spiking study for determination of the elution order of the 16 PAH mixture was conducted. From the results of the spiking study, separation of three representative mixtures of PAH clearly demonstrate the ability of the LCA stationary phase for baseline separation of PAH differing in number of aromatic rings as shown in Figure 7.14. From Figure 7.14, the elution order was evaluated for insight into the molecular recognition properties of the LCA bonded phase. The $\log P$ of the PAH along with elution order are shown in Table 7.5. A comparison of the $\log P$ with elution order showed that the PAH follow a typical reversed phase retention mechanism on the LCA bonded phase based upon increasing carbon number or hydrophobicity as supported by increasing retention with increase in $\log P$.

CEC-UV of PCBs. Following analysis of PAH, the capability of the LCA bonded phase for separation of a series of polychlorinated biphenyls (PCBs) was assessed. Similar to the study of PAHs, the PCBs were run at low (e.g., 65%) and high content (85%) of ACN. The results of the study were found to be the same as for PAH, in that the LCA bonded phase was not well suited for operating conditions at 65% ACN. The results showed that only one peak was observed at 65% ACN. Similarly, a variation in

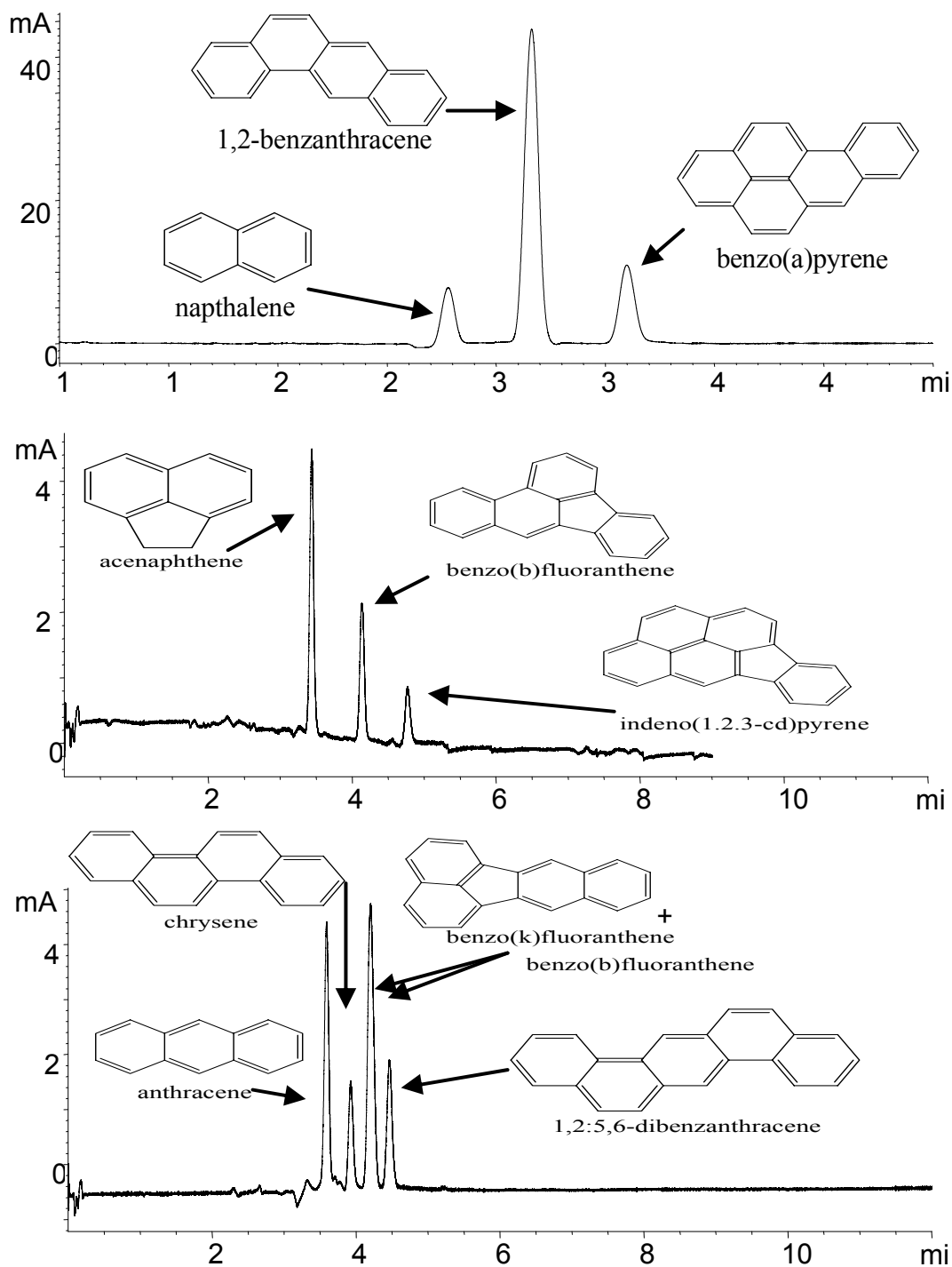


Figure 7.14: Separation of different PAH on the LCA bonded phase. Conditions are the same as Figure 7.14 except for the mobile phase pH = 4.

Table 7.5: Elution order and log *P* of the PAH test mixtures run on the LCA bonded phase.

Compound	Elution order	Log <i>P</i>
acenaphthene	1	3.51
benzo(b)fluoranthene	2	5.34
indeno(1,2,3-cd)pyrene	3	5.66
anthracene	1	4.03
chrysene	2	5.03
benzo(k)fluoranthene	3	5.34
benzo(b)fluoranthene	3	5.34
1,2:5,6-dibenzanthracene	4	6.02

the mobile phase pH in the range of pH 3-5 was evaluated as shown in Figure 7.15.

Overall, pH 4.0 was found to be a good compromise between resolution and analysis time, as shown by the degree of separation of the early eluting PCBs. A comparison of the separation of 8 PCBs on the LCA bonded phase versus the aminopropyl silica (Figure 7.15 inset, both run at pH 4.5) showed that the aminopropyl silica was not able to resolve any PCBs, as can be seen by all 8 PCBs co-eluting as one peak.

Next, the spiking experiment for determination of the elution order was conducted. A representative chromatogram presenting a good separating capability of the LCA bonded phase for PCBs is presented in Figure 7.16. From analysis of Figure 7.16, the elution order of the PCB on the bonded phase generally follows increasing chlorine substituent group on the biphenyl ring. This trend follows an increase in hydrophobic nature of the analyte which is a similar trend observed for PAHs (Figure 7.15) and as shown in our previous work utilizing micellar electrokinetic chromatography (MEKC).^{23,24}

EOF Marker in CEC-MS and CEC-UV. Finally, the elution trend of the neutral marker (thiourea) at different mobile phase conditions for CEC-MS and CEC-UV is provided. These data can lend to some useful insights regarding the EOF and overall

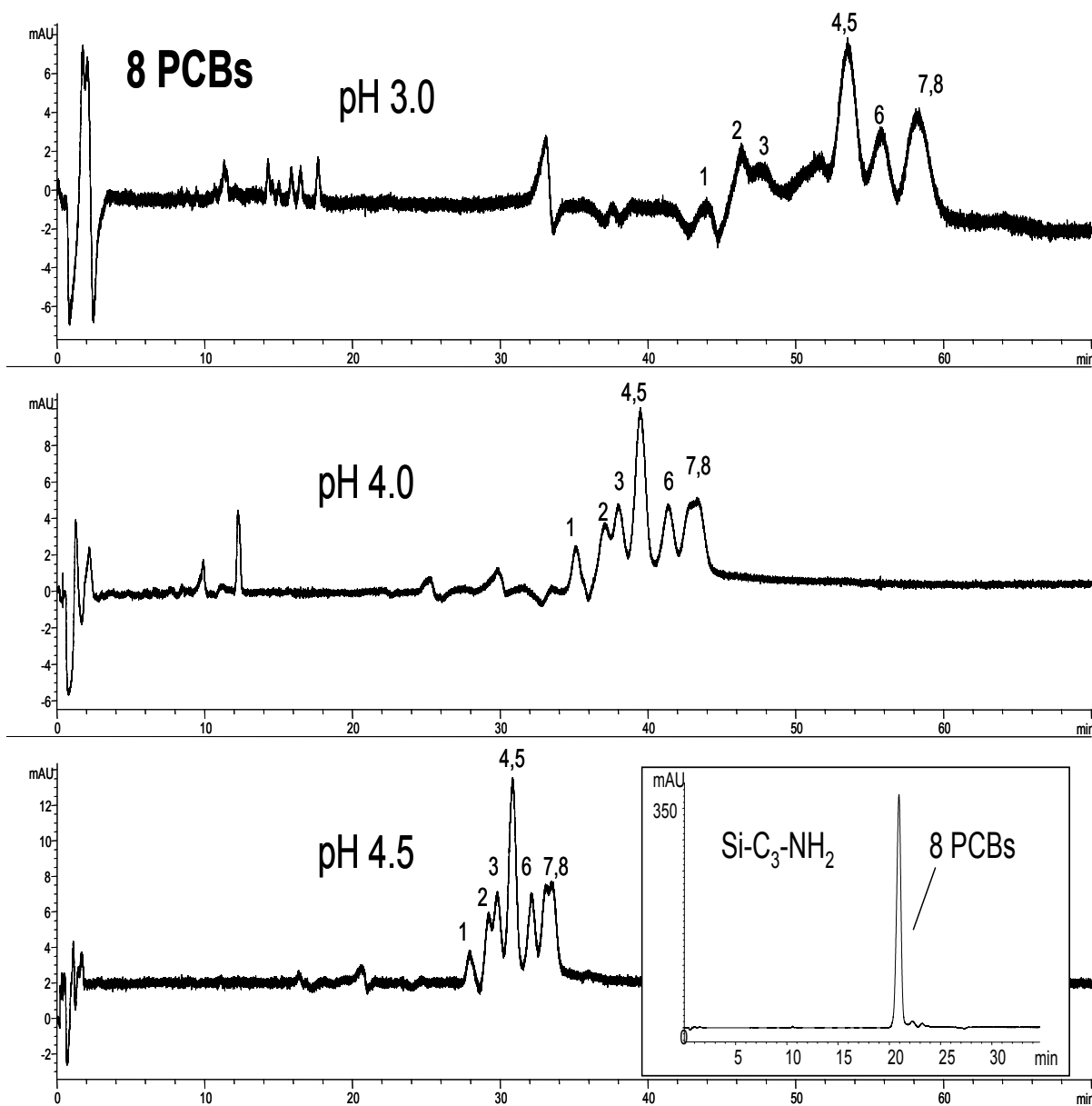


Figure 7.15. Variation in mobile phase pH in the range of pH 3.0-4.5 for analysis of 8 component PCB mixture on the LCA bonded phase. The inset shows the same separation at pH 4.5 on the aminopropyl silica phase. Conditions are same as Figure 7.14. Peak identification: peak 1=2 chlorobiphenyl; peak 2=2,3-dichlorobiphenyl; peak 3=2,4',5-trichlorobiphenyl; peak 4,5=2,2',4,4'-tetrachlorobiphenyl, 2,2'-3'-4,6-pentachlorobiphenyl; peak 6=2,2',4,4',5,6'-hexachlorobiphenyl; peak 7,8=2',3,3',4,4',6-heptachlorobiphenyl, 2,2'-3,3',4,5',6,6'-octachlorobiphenyl.

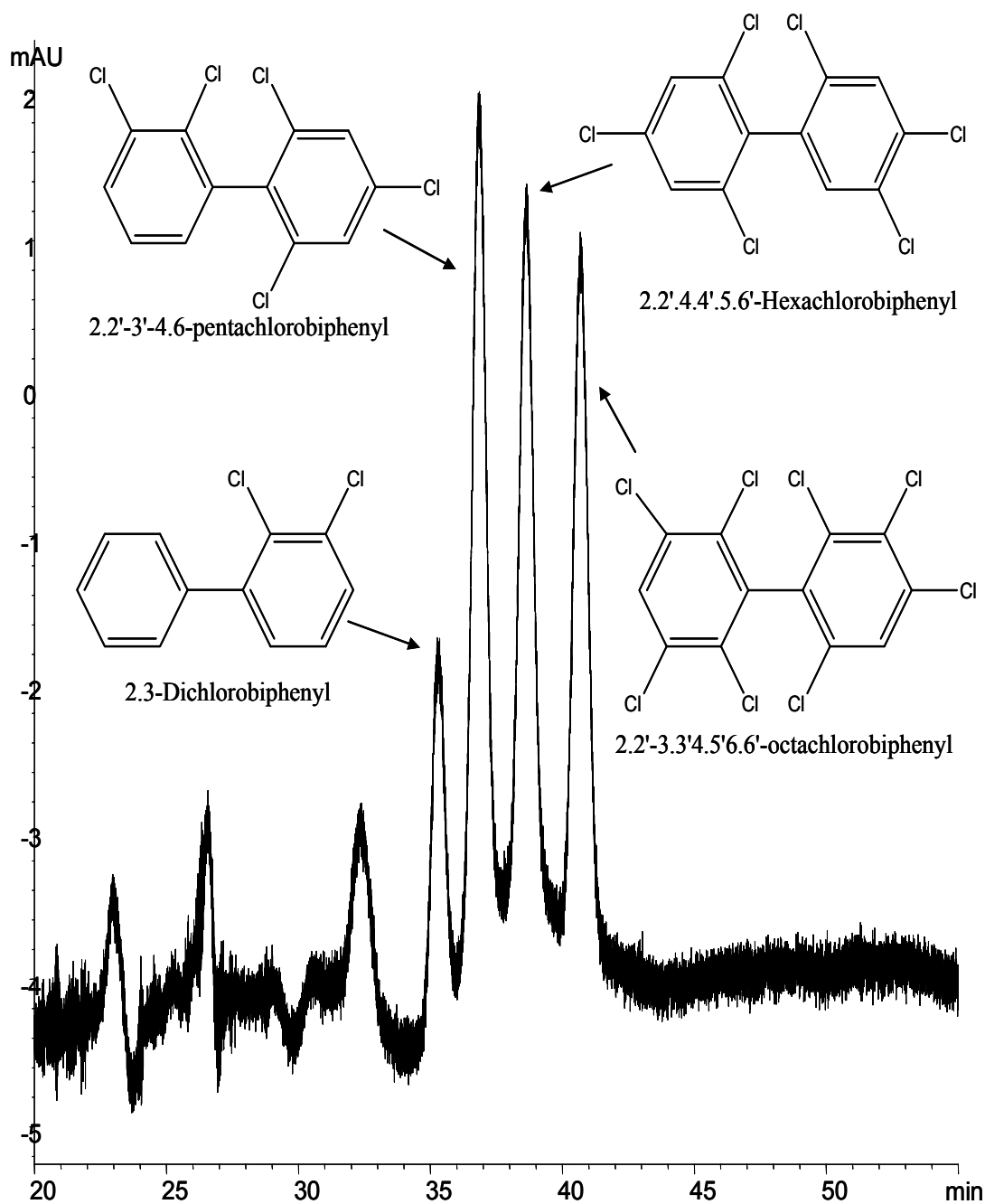


Figure 7.16: Separation of 4 PCB mixture on the LCA bonded phase. Conditions are the same as Figure 7.15.

allow conclusion for the most suitable operating conditions of the LCA bonded phase. The CEC-MS data of thiourea is presented in Figure 7.17. Mobile phase conditions varying the percentage of ACN are compared. A comparison between the aminopropyl phase and the LCA phase at 70% ACN content shown in Figure 7.17 A-B shows that the retention of thiourea is significantly longer on the LCA phase (108 min) as compared to amino phase (54 min). Furthermore, this composition of 70% ACN provides poor peak efficiency of thiourea indicated by its wide peak base. Therefore this mobile phase composition is concluded to be not suitable operating conditions which is consistent with the analysis of PAH and PCB at 65% ACN which also provided poor analysis. Next, a comparison of the two phases was conducted at higher organic composition of 85% ACN. A similar trend to 65% ACN was observed, whereupon the propyl amine phase showed shorter retention (29 min, Figure 7.17 C) vs. the LCA phase (42 min, Figure 7.17D). The peak shapes and efficiencies were dramatically enhanced on both phases compared to lower ACN content. Furthermore, the decreased retention at 85% ACN as compared to 65% ACN along with higher efficiency suggests that 85% ACN is a much better operating condition. Lastly, the LCA bonded phase was run at 90% ACN (Figure 7.17 E) which continued to decrease the retention. Therefore, two conclusions can be reached. First, a comparison of the thiourea retention time for different operating ACN conditions between the two phases showed that slower EOF was always observed on the LCA phase. Second, the retention time for thiourea on both phases decreased with increase in ACN which is consistent with change in dielectric constant/viscosity ratio and reversed phase retention mechanism.

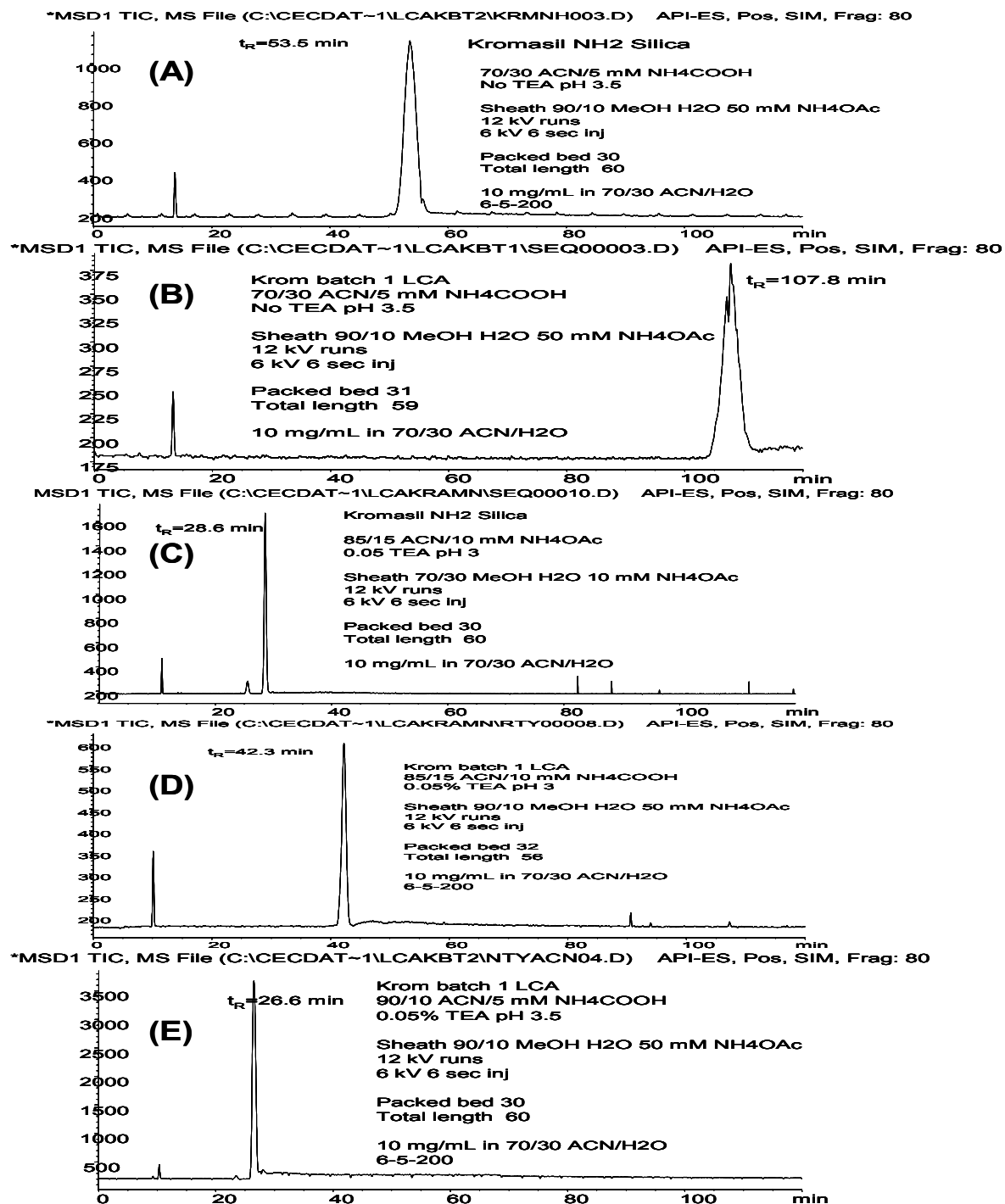


Figure 7.17: CEC-MS trend of thiourea used as a dead time marker for propyl amine silica compared to the LCA bonded phase. Conditions are as shown on the Figure.

Next, the CEC-UV trend in thiourea retention time is summarized in Figure 7.18 which compares the change in pH range 3.0-4.5 using optimum 85% ACN for the LCA bonded phase. One comparison to amino propyl silica is described. A direct comparison at pH 4.5 between the LCA phase (Figure 7.18 A) and the amino phase (Figure 7.18 B) again shows that the thiourea marker is shorter retained on the amino phase (26 min) as compared to the bonded phase (34 min). This data supports differences between the two materials. The trend of increasing retention time is illustrated in Figure 7.18 A,C,D which clearly shows that the EOF marker slows down with decreasing pH. Two conclusions can be reached. First, decreased EOF at low pH is consistent with the theory. In addition, increasing ionic strength with added HOAc for pH adjustment also slows down the EOF and alternately affects the thickness of the electrical double layer. Second, the useful operating range illustrated in this Figure is below the pKa of the carboxylic acid group of the LCA ($pK_a = 4.76 \pm 0.10$, SciFinder Scholar 2007). Hence, very low EOF is generated when the LCA phase is uncharged at low pH.

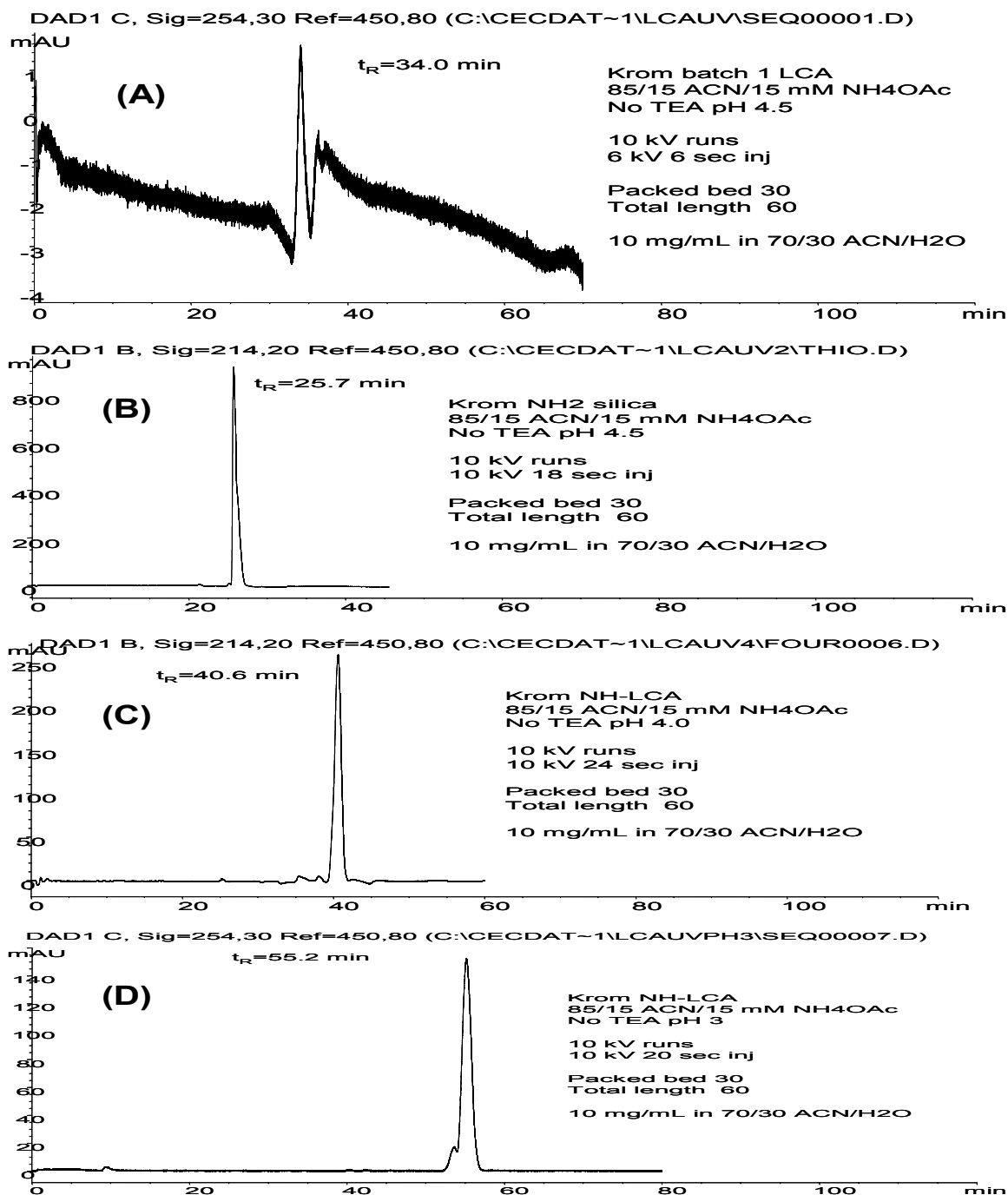


Figure 7.18: CEC-UV trend of thiourea used as a dead time marker for propyl amine silica compared to the LCA bonded phase. Conditions are as shown on the Figure.

CONCLUSIONS

This work has described the preparation and characterization of a LCA stationary phase suitable for application in packed column CEC-MS and CEC-UV. The LCA ligand was first converted to chloroformate followed by attachment to aminopropyl silica. Reaction of the LCA to chloroformate was confirmed via ^1H -NMR while the attachment of the LCA chloroformate to the modified silica was assessed using elemental analysis, IR, and finally ^{13}C -NMR. The elemental analysis comparing aminopropyl silica to the LCA bonded phase showed significantly more carbon and hydrogen on the LCA bonded phase although the nitrogen content remained constant. IR analysis of stationary phases was found to be inconclusive for the determination of structural differences between the two phases. Lastly, the ^{13}C -NMR comparison of the two phases showed significant differences in peak resonances suggesting that the surface property of the two phases were different. For example, ^{13}C -NMR peak observed at 157 ppm suggested that the LCA ligand was in fact bonded to the aminopropyl silica. Next, CEC-MS and CEC-UV were used to compare the two phases whereupon the LCA phase showed distinct differences in separating capability and EOF profile compared to the aminopropyl silica phase. The capability of the LCA phase for applications in CEC-MS and CEC-UV was assessed utilizing several mixtures of cationic and neutral compounds important for pharmaceuticals and environmental industry. First, the analysis for small charged molecules including β -blockers and PEAs by CEC-MS showed that the LCA bonded phase exhibited higher selectivity compared to the aminopropyl silica phase. For the analysis of neutral, more hydrophobic

molecules such as PAH and PCB, the LCA bonded phase demonstrated superior separation power compared to aminopropyl silica phase with a typical reversed phase retention mechanism. A comparison of EOF trend between the two phases under the same conditions showed that the thiourea marker was shorter retained on the amino phase (26 min) as compared to the bonded phase (34 min). Overall, the optimized mobile conditions were determined to be pH 4.0, 85% ACN, 15 mM NH₄OAc. In summary, this work is the first report of LCA bonded liquid crystalline phase suitable for packed column CEC-MS and CEC-UV applications.

ACKNOWLEDGMENTS

This project was supported by National Institute of Health (Grant No. GM 62314-02) and Solvay Pharmaceuticals (Marietta, GA). The authors would like to thank Dr. Asad Rizvi and Dr. Brian Crow for their participation in this project. Also, thanks to Dr. Johannes Leisen at Georgia Tech for ¹³C-NMR characterization of the stationary phases.

References:

- (1) Witkiewicz, Z., Oszczudlowski, J., Repelewicz, M. *J. Chromatogr. A* **2005**, *1062*, 155.
- (2) Rokushika, S., Naikwadi, K.P., Jadhau, A.L., Hatano, H. *Chromatographia* **1986**, *22*, 209.
- (3) Lufter, D.R., Novotny, M. *J. Phys. Chem.* **1990**, *94*, 3161.
- (4) Gritti, F., Félix, G. *Chromatographia* **2002**, *55*, 523.
- (5) Gritti, F., Terrien, I., Menu, S., Dufourc, E.J., Félix, G., Achard, M.-F., Hardouin, F. *J. Chromatogr. A* **2001**, *922*, 37.
- (6) Gritti, F., Félix, G., Achard, M.-F., Hardouin, F. *J. Chromatogr. A* **2001**, *922*, 51.
- (7) Gritti, F., Félix, G., Achard, M.-F., Hardouin, F. *J. Chromatogr. A* **2000**, *897*, 131.
- (8) Al-Haj, M.A., Haber, P., Kaliszan, R., Buszewski, B., Jezierska, M., Chilmonzyk, Z. *J. Pharm and Biomed Analysis* **1998**, *18*, 721.
- (9) Pesek, J.J., Matyska, M.T., Dawson, G.B., Wilsdorf, A., Marc, P., Padki, M., *J. Chromatogr. A* **2003**, *986*, 253.
- (10) Buszewski, B., Jezierska, M., Welniak, M., Berek, D. *J. High Resol. Chromatogr.* **1998**, *21*, 267.
- (11) Ferroukhi, O., Guermouche, S., Sebih, S., Guermouche, M.H., P. Berdagué, Bayle, J.P. *J. Chromatogr. A* **2002**, *971*, 87.
- (12) Dawson, G.B., Matyska, M.T., Pesek, J.J., Seipert, R.R. *J. Chromatogr.*

- A **2004**, 1047, 299.
- (13) Matyska, M.T., Pesek, J.J., I-Chen Chen, J., Boysen, R.I., Hearn, M.T.W. *Chromatographia* **2005**, 61, 351.
- (14) Pesek, J.J., Matyska, M.T., Dawson, G.B., I-Chen Chen, J., Boysen, R.I., Hearn, M.T.W. *Electrophoresis* **2004**, 25, 1211.
- (15) Matyska, M.T., Pesek, J.J., Boysen, R.I., Hearn, M.T.W. *J. Chromatogr. A* **2001**, 924, 211.
- (16) Matyska, M.T., Pesek, J.J., Boysen, R.I., Hearn, M.T.W. *Anal Chem* **2001**, 73, 5116.
- (17) Matyska, M.T., Pesek, J.J., Katrekar, A. *Anal Chem* 1999, 71, 5508.
- (18) Buszewski, B., Jezierska-Świtala, M., Kowalska, S. *J Chromatogr. B* **2003**, 792, 279.
- (19) Buszewski, B., Jezierska, M., Welniak, M., Kaliszan, R. *J Chromatogr. A* **1999**, 845, 433.
- (20) Delaurent, C., Tomao, V., Siouffi, A.M. *Chromatographia* 1997, 45, 355.
- (21) Norton, D., Shamsi, S.A. *Electrophoresis* **2004**, 25, 586.
- (22) Norton, D., Zheng, J., Shamsi, S.A., Danielson, N.D. *Anal Chem* **2005**, 77, 6874.
- (23) Edwards, S.H., Shamsi, S.A. *Electrophoresis* **2002**, 23, 1320.
- (24) Edwards, S.H., Shamsi, S.A. *J. Chromatogr. A* **2000**, 903, 227.